

Benoît Lorentz

An approach to investigate surface roughness influence on non-lubricated and lubricated contacts by means of the finite element analysis

Ein Ansatz zur Untersuchung der Oberflächenrauheitinflüsse bei geschmierten und trockenen Kontakten mittels der Finite Elemente Methode

Band 63

Systeme ■ Methoden ■ Prozesse

Benoît Lorentz

**An approach to investigate surface roughness
influence on non-lubricated and lubricated contacts by
means of the finite element analysis**

Ein Ansatz zur Untersuchung der
Oberflächenrauheitseinflüsse bei geschmierten und
trockenen Kontakten mittels der Finite Elemente
Methode

Copyright: IPEK ▪ Institut für Produktentwicklung, 2013
Karlsruher Institut für Technologie (KIT)
Universität des Landes Baden-Württemberg und
nationales Forschungszentrum in der Helmholtz-Gemeinschaft
Alle Rechte vorbehalten

Satz: Benoît Lorentz

ISSN 1615-8113

An approach to investigate surface roughness influence on non-lubricated and lubricated contacts by means of the finite element analysis

Zur Erlangung des akademischen Grades

Doktor der Ingenieurwissenschaften

der Fakultät für Maschinenbau

Karlsruher Institut für Technologie (KIT)

genehmigte

Dissertation

von

Dipl.-Ing. Benoît Lorentz

aus Obernai / Frankreich

Tag der mündlichen Prüfung:

28. Mai 2013

Hauptreferent:

o. Prof. Dr.-Ing. Dr. h.c. A. Albers

Korreferent:

Prof. Dr.-Ing. habil. G. Knoll

Vorwort des Herausgebers

Wissen ist einer der entscheidenden Faktoren in den Volkswirtschaften unserer Zeit. Der Unternehmenserfolg wird in der Zukunft mehr denn je davon abhängen, wie schnell ein Unternehmen neues Wissen aufnehmen, zugänglich machen und verwerten kann. Die Aufgabe eines Universitätsinstitutes ist es, hier einen wesentlichen Beitrag zu leisten. In den Forschungsarbeiten wird ständig Wissen generiert. Dieses kann aber nur wirksam und für die Gemeinschaft nutzbar werden, wenn es in geeigneter Form kommuniziert wird. Diese Schriftenreihe dient als eine Plattform zum Transfer und macht damit das Wissenspotential aus aktuellen Forschungsarbeiten am IPEK – Institut für Produktentwicklung Karlsruhe (ehemals: Institut für Maschinenkonstruktionslehre und Kraftfahrzeugbau) verfügbar.

Die Forschungsfelder des Institutes sind die methodische Entwicklung und das Entwicklungsmanagement, die rechnergestützte Optimierung von hochbelasteten Strukturen und Systemen, die Antriebstechnik mit einem Schwerpunkt auf den Gebieten Antriebsstrang-Engineering und Tribologie von Lager- und Funktionsreibsystemen, die Mikrosystemtechnik mit dem Focus auf die zugehörigen Entwicklungsprozesse sowie die Mechatronik. Die Forschungsberichte werden aus allen diesen Gebieten Beiträge zur wissenschaftlichen Fortentwicklung des Wissens und der zugehörigen Anwendung – sowohl den auf diesen Gebieten tätigen Forschern als auch ganz besonders der anwendenden Industrie – zur Verfügung stellen. Ziel ist es, qualifizierte Beiträge zum Produktentwicklungsprozess zu leisten.

Albert Albers

Vorwort zu Band 63

Die Tribologie ist ein zentrales Feld in der Produktentwicklung technischer Systeme. Tribologische Fragestellungen treten in mannigfacher Form auf. Insbesondere in den zwei großen Gruppen der Gleitsysteme, bei denen die Hauptzielrichtung eine Reibungsreduzierung bei relativ bewegten Wirkflächen ist und der zweiten großen Klasse der Friktionssysteme, bei denen die im Wirkflächenpaar auftretende Reibung systematisch für die Funktionserfüllung genutzt wird, sind von zentraler Bedeutung in modernen technischen Systemen. Aspekte, wie die Steigerung der Leistungsdichte, aber auch die Verbesserung der Energieeffizienz ergeben sowohl für die Gleitsysteme als auch für die Friktionssysteme entsprechend hohe Anforderungen an deren Weiterentwicklung. Um hier gezielt neue Innovationspotenziale zu gewinnen, sind verstärkte und tiefer gehende Analysen des tribologischen Systems erforderlich, aus denen dann mit neuen Ansätzen die Modellbildung so verfeinert werden kann, dass relevante Aspekte von vorne herein in die Synthese und Analyse von Tribosystemen integriert werden können. Hier haben sich, insbesondere durch die Weiterentwicklung der Rechnerstechniken, in den letzten Jahren ganz neue Möglichkeiten ergeben. Während über lange Zeit in der praktischen Produktentwicklung die Synthese von tribologischen Systemen im Wesentlichen auf empirischen, experimentellen Vorgehensweisen und Ansätzen beruhte, wird es durch die höheren Rechenleistungen moderner Computersysteme in den letzten Jahren zunehmend möglich, auch strukturiert physikalische Effekte durch Modellbildung zu beschreiben und zu erfassen. Ein wichtiger Aspekt in tribologischen Systemen ist dabei der Einfluss der Rauigkeiten der Wirkflächen in ihrem Zusammenwirken im Wirkflächenpaar. Die Berücksichtigung der Rauigkeiten in ihrer Wechselwirkung mit dem tribologischen System für Friktionssysteme ist bisher überhaupt nicht gelöst. Bei Gleitsystemen, insbesondere bei den Gleitlagern, aber auch im Gebiet der Wälzlager, erfolgt zunehmend eine Berücksichtigung des Rauigkeitseinflusses durch Integration in die beschreibenden Differenzialgleichungssysteme, wobei auch hier sehr häufig noch Hilfsgrößen, die im Wesentlichen auch über eine Parameteranpassung bestimmt werden, die Vorgehensweise dominieren. An dieser Stelle setzt die Arbeit von Herrn Dr.-Ing. Benoît Lorentz an. Er hat sich zum Ziel gesetzt, die Potenziale moderner Simulationsmethoden zu Nutzen um den Einfluss von Rauigkeiten, sowohl in ungeschmierten trockenlaufenden Systemen als auch in geschmierten Systemen, besser zu erfassen, in Modelle abzubilden und daraus Ansätze für eine Verbesserung der Synthese technischer Systeme abzuleiten. Das grundlegende Ziel der Forschungsarbeiten von Herrn Dr.-Ing. Benoît Lorentz ist es, die Simulation des Einflusses von Oberflächenrauigkeiten auf das Reibungsverhalten von geschmierten

und ungeschmierten Wirkkontakten mit numerischen Methoden zu untersuchen. Das daraus abgeleitete Zielsystem seiner Arbeit beinhaltet damit die Berücksichtigung der Parameter Material, Eigenschaften, elastische und plastische Materialeigenschaften, Rauheit – beschrieben durch entsprechende Rauheitsparameter, die Herstellverfahren sowie die Betriebsbedingungen. Als wesentliche Schritte der Forschungsarbeiten definiert Herr Dr.-Ing. Benoît Lorentz die Mikromodellbildung und -analyse, die Modellverifikation, dann die Validierung des Verfahrens über eine Parameterstudie und eine Ausweitung der Mikrobetrachtung auf der Ebene der Skalen der Rauigkeiten hin in die makroskopische Skala der betrachteten technischen Systeme. Die Arbeit leistet einen hervorragenden Beitrag zum besseren Verständnis tribologischer Systeme und zeigt auch Wege auf, wie in der praktischen Produktentwicklung diese neuen Möglichkeiten erfolgreich genutzt werden können. Die Arbeit ist sicher Ausgangspunkt weiterer grundlegender Forschungsarbeiten in der Zukunft.

Albert Albers

Kurzfassung

Die Tribologie war und ist auch heute noch ein wesentliches Forschungsfeld der Energieeffizienz mechatronischer Systeme. Vor diesem Hintergrund werden in der vorliegenden Arbeit Einflüsse der Oberflächentopographie auf das Reibverhalten tribologischer Systeme untersucht. Hierzu werden überwiegend Modelle auf der Mikroebene gebildet – sowohl bei trockenlaufenden als auch geschmierten tribologischen Systemen. Zur Kontaktmodellierung wird die Finite-Elemente-Methode eingesetzt, wobei für beide Kontaktarten das Adhäsionsmodell von Bowden und Tabor genutzt wird. Modelle von nicht-geschmierten Kontakten werden mittels „Ball-on-Disk“-Versuche validiert, wohingegen Modelle von geschmierten Kontakten rein numerisch verifiziert werden.

Kern dieser Arbeit ist die numerische Modellierung von Mischreibungseffekten, die eine Kombination von Festkörper-Festkörper- und Fluid-Festkörper-Kontakten aufweisen. Die Modellierung erfolgt durch Anwendung eines neuen Ansatzes zur Fluid-Struktur Kopplung, der „Coupled-Eulerian-Lagrangian“-Methode.

Der in dieser Arbeit entwickelte Ansatz basiert auf einer ausführlichen, methodischen Analyse des tribologischen Systems, wobei insbesondere die multiskalige Validierungsumgebung „X-in-the-Loop“ und der „Contact-and-Channel“-Ansatz genutzt werden. Auf dieser Grundlage wird ein Untersuchungs-Rahmenwerk gebildet, das den Schwerpunkt auf die Modellbildung des mikroskopischen Mischreibungsmodells inkl. der zu treffenden Annahmen und zu verwendenden Randbedingungen legt. Auf dieser Basis erfolgt eine erste Validierung des Ansatzes nach Bowden und Tabor, indem das verwendete Adhäsionsmodell anhand des trockenlaufenden mikroskopischen Kontaktmodells mit Prüfstandversuche abgeglichen wird. Hierdurch kann die Hypothese bestätigt werden, dass in Modellen trockenlaufender Kontakte die Normalkomponente der Adhäsionskraft vernachlässigt werden kann. Da eine analoge Validierung des nasslaufenden Kontaktmodells im vorliegenden Fall physikalisch nicht möglich ist, wird das Mischreibungsmodell numerisch verifiziert.

Anschließend wird eine Parameterstudie durchgeführt, die die Einflüsse unterschiedlicher Parametern auf den Reibwert untersucht. Eine anschließende Sensitivitätsanalyse zeigt, dass im Wesentlichen die Bearbeitungsrichtung des Fertigungsprozesses und der R_p Wert das Reibverhalten beeinflussen.

Als letzter Schritt wird ein Vorgehen skizziert, das die Übertragung der Ergebnisse von der mikroskopischen auf die makroskopische Ebene erlaubt. Hiermit kann die Wirkung der Oberflächenrauheit auf das dynamische Verhalten eines tribologischen Systems untersucht werden.

Abstract

Tribology remains an essential research area according to energy efficiency. On this account, present work focuses on the investigation of surface roughness on lubricated and non-lubricated contacts in existing systems such as clutches or journal bearings. This task is achieved numerically by means of the finite element method. For both contact types, the adhesion model of Bowden and Tabor was used. A validation took place for the non-lubricated contacts whereas a numerical verification has been done for the lubricated contacts.

Main challenge remaining in present work was the simulation of mixed lubrication in a whole model. The combination of both contact types, solid-solid and fluid-solid which are changing during the sliding phase can be modeled using a novel approach called Coupled Eulerian Lagrangian method.

Whole work bases on a methodical based approach: typical system design approach have been used in order to define which part of a given system has to be investigated. A direct consequence was the use of a multiscale approach called "X-in-the-Loop".

Present thesis develops the analysis framework, and sets the focus on the microscopic mixed lubrication model development, boundary conditions to be applied and which assumptions have been met during the modeling. A validation of the Bowden and Tabor theory has also been done in comparing numerical results of the non-lubricated version of the model with real ball-on-disk experimental tests. This allowed arguing the assumption by not taking into account normal adhesion component in the non-lubricated model. As a consequence, same assumption has been chosen for the lubricated model which can unfortunately not be validated by similar experimental tests. On this account, verification has been done to check the convergence of the microscopic mixed lubrication model on both the normal and tangential contact force components.

Parameter study done for the mixed lubrication model displayed the contact stresses as well as contact temperatures. It also enabled it to check which of the varied parameters had the most influence on the friction behavior itself. It has been shown that machining has the most impact: machining direction as well as the R_p value of surfaces.

A last part exposes the transposition of the results calculated at the microscopic scale into the macroscopic scale. This has been done with non-lubricated surfaces in order to give an overview on the machining impact on the dynamical behavior of macroscopic systems.

Acknowledgment

I would like to thank all people who contributed to the achievement of this dissertation. I wish to sincerely apologize to those I have forgotten to mention. Foremost, I would like to thank my doctoral advisor, Professor Albert Albers, for his interest and counseling during my graduate work, and more generally for giving me the opportunity to work on this challenging project. I am also grateful to Professor Gunter Knoll who accepted the second examination of my thesis and for his support in our common project.

My gratitude goes to my actual and formal colleagues from the research group CAE/Optimization who always took time for fruitful discussions and offered me the best working atmosphere.

My profound thanks go to my colleagues of the Institute of Product Development (IPEK) for their open-mindedness. Among them, I am particularly grateful to Dr. Wolfgang Burger and Johannes Bernhardt who always supported my work during the five years of common work. I also thank my colleagues responsible for administrative issues during my work at the institute as well as Daniele Savio for his inputs for the dissertation. I am also grateful to Dr. Hartmut Hetzler and Benedikt Wiegert from the Institute of Technical Mechanics for their contribution to my work.

Apart from my colleagues, a very special thank-you goes to my life partner, Irène Sacksteder, for her continuous encouragement in this long-term project. The support of my brother Vincent was really appreciated as well as his precious advice. Despite the distance, my family and my partner's family were always present for me, therefore I wanted to express my warmest thank to them.

Benoît Lorentz

“Le plus dangereux conseiller, c'est l'amour-propre.”

Napoléon Bonaparte

*“Man muß mit den richtigen Leuten zusammenarbeiten, sie achten und motivieren.
Dauerhafter Erfolg ist nur im Team möglich“*

Klaus Steilmann

“Difficulties are the salt of life”

Robert Baden-Powell

Contents

- Contents.....XIX**
- SymbolXXIII**
- AbbreviationXXVI**

- 1 Introduction 1**
 - 1.1 Context.....1
 - 1.2 Motivation.....2
 - 1.3 Outline.....4

- 2 Fundamentals and State of the Art 5**
 - 2.1 Methods for System Analyses.....5
 - 2.1.1 Structured Analysis Design Technique (SADT).....6
 - 2.1.2 Principle of the Contact and Channel Approach (C&C²-A).....7
 - 2.1.3 Application and Advantages of both Methods8
 - 2.2 Technical Surfaces.....10
 - 2.2.1 Signal Composition of a Technical Surface.....10
 - 2.2.2 Statistical Characterization of Technical Surfaces13
 - 2.2.3 Frequency Analysis of the Surface Characteristic.....16
 - 2.2.4 Generation of Rough Surface Profiles.....16
 - 2.2.5 Fractal Description.....17
 - 2.2.6 Wavelet Description of Technical Surfaces18
 - 2.3 Structural Mechanics and Material Science18
 - 2.3.1 Basics: Movement Description19
 - 2.3.2 Description of the Solid Deformation Parts Submitted to Friction.....20
 - 2.3.3 Thermal Properties of the Solids21
 - 2.3.4 Wear Phenomena Occurring in Tribological Systems22
 - 2.3.5 Failure and Damage Models used for Wear Modeling in Contacts24
 - 2.4 Solid-Solid Interaction and Adhesion26
 - 2.4.1 Description of the Adhesion Phenomenon26
 - 2.4.2 Tangential Component28
 - 2.4.3 Normal Component28
 - 2.4.4 Hysteresis Phenomenon30
 - 2.5 Fluid Mechanics Theory30
 - 2.5.1 Theoretical Background.....31
 - 2.5.2 Fluid Compressibility, Newtonian fluid and Thermal Effects.....32
 - 2.5.3 Fluid Flow and Viscosity Relationships33
 - 2.5.4 Thin Film Theory: Elastohydrodynamic (EHL).....34

2.5.5	Impact of the Surface Roughness on the Fluid Friction.....	36
2.6	Numerical Methods used in Tribology	37
2.6.1	Methods used for Spatial and Temporal Discretization	38
2.6.2	Multibody Dynamics Simulations	41
2.6.3	Contact Modeling.....	42
2.6.4	Methods Application	44
2.7	Fluid Structure Coupling in Numerical Methods	44
2.7.1	Conventional CFD FSI-Coupling	44
2.7.2	Mesh Distortion Management.....	45
2.7.3	Thermal Exchange Between Fluid and Structure	48
2.8	Design of Experiments (DoE) and Use in Numerical Simulations	50
2.8.1	Full Factorial Method	50
2.8.2	Fractional Factorials	51
2.8.3	Screening Experiments	51
2.8.4	Response Surface Method (RSM).....	51
2.8.5	Selecting a DoE Strategy	53
2.9	State of the Art: Experimental Investigations in Tribological Systems.....	53
2.9.1	Investigation on Pin-On-Disk Devices Type	54
2.9.2	Investigation of Clutch Systems	54
2.9.3	Investigation of Journal Bearings	55
2.10	State of the Art: Numerical Investigation in Tribology	56
2.10.1	Non-lubricated Contacts	56
2.10.2	Mixed Lubricated Contacts	57
2.10.3	Multi-Level Modeling in Tribology	59
3	Research Objectives	61
3.1	Potential Issuing from the State of the Art.....	61
3.2	Establishment of the Target System	62
4	Analysis Framework	63
4.1	Demonstrator Definition.....	63
4.1.1	Classification of Tribological Systems (Tribo-System)	63
4.1.2	Identification of the System Functions by Means of System Design Methods SADT and C&C ² -A	64
4.1.3	Identification of the Function to be investigated	68
4.2	Definition of Investigation Steps to Reach Objectives	73
4.2.1	Demonstrators Functions Leading to Theoretical Models	73
4.2.2	Working Conditions and Investigation Steps	74
4.2.3	Experimental Device Required for the Verification	75

4.3	Main Assumptions used for the Microscopic Model Implementation.....	76
5	Numerical Model at the Microscopic Scale	77
5.1	Discretization of the Rough Surfaces	77
5.1.1	Signal Treatment to Characterize the Surfaces.....	77
5.1.2	Importation of the Surfaces into a Commercial Finite Elements Software .	81
5.2	Establishment of Operating Conditions for the Lubricated Micro Model.....	83
5.2.1	Operating Conditions for Lubricated Demonstrators	83
5.2.2	Boundary Conditions Calculated in Linear Bearings	83
5.2.3	Boundary Conditions Calculated in Journal Bearings	86
5.3	Microscopic Model Taking into Account Lubricant	89
5.3.1	Two-Dimensional Model	89
5.3.2	Applied Boundary Conditions	90
5.3.3	Material Model	91
5.3.4	Contact Definitions	93
5.3.5	Model Extension into three Dimensions and Model Generation Process...	94
5.4	Microscopic Model of Dry Friction	97
6	First Steps for the Micro-Models Verification	101
6.1	Demonstrator for Dry Running Model.....	101
6.2	Convergence Verification and Validation of the Dry Running Model.....	104
6.2.1	Shear stress	104
6.2.2	Friction.....	105
6.2.3	Validation of the Dry Running Model with the Ball-On-Disk Experiment ..	106
6.3	Convergence of the Mixed Lubrication Model	107
6.3.1	Convergence Study on Fluid Mesh	107
6.3.2	Impact of Solid Element Size on Normal Load	109
6.4	Comparison of CFD and CEL for Full Hydrodynamic Conditions.....	110
6.5	Impact of the Boundary Conditions	112
6.5.1	Pressure	112
6.5.2	Loading Velocity	115
6.5.3	Model Height	116
6.6	Summary	117
7	Results and Investigations on the Micro Scale for Lubricated Conditions	119
7.1	Influence of the Fluid Viscosity on the Friction Behavior.....	119
7.2	Impact of Solid Properties on Friction.....	120
7.2.1	Impact of Temperature on Solid Properties and Friction Coefficients	120
7.2.2	Impact of Elastic Modulus and Yield Strength on Friction	121

7.3	Impact of Loads and Sliding Velocity Applied on the Friction Coefficient.....	124
7.3.1	Normal Load	124
7.3.2	Sliding Velocity	126
7.4	Influence of the Surface Machining	128
7.4.1	Impact of Machining Type	128
7.4.2	Machining Directions	132
7.4.3	Impact of Roughness on Contact Temperature.....	136
7.5	Classification of the Most Influencing Parameters.....	139
7.5.1	Classification of Roughness Parameters on Friction.....	139
7.5.2	Classification of the Operating Conditions.....	143
7.5.3	Summary of Parameters Impact on Friction Behavior	146
8	Extension of the Investigations to the Macroscopic Scale	147
8.1	Demonstrator of the Tribological System	147
8.2	Extension to the Macroscopic Scale: Macro-Model.....	148
8.3	Establishment of the Frictional Rule at the Microscopic Scale	149
9	Conclusion and Outlook	153
9.1	Synthesis of the Results.....	153
9.2	Discussion of the Method	154
9.3	Future Development and Requirements	155
10	References	157

Symbol

$\dot{\nabla}$	-	Differenced nabla operator
$\pm, ^2$ and c	-	Empiric coefficients used in viscosity calculation
'	-	Empiric parameter
"	-	Grüneisen ratio
3_i	J	Surface energy of solid i
"	Hz	Frequency
•	-	Deformation
μ_e	-	Yield strain
—	Pa·s	Dynamic viscosity
„	rad	Angular position of the journal bearing
» _s	mm	Wavelength for the roughness filter
» _c	mm	Wavelength for the waviness filter
» _f	mm	Wavelength for the primer profile filter
»	W/m/K	Thermal conductivity
»	-	Elasticity parameter for adhesion theory
», $\frac{1}{4}$	-	Lamé parameters
μ	-	Friction coefficient
μ	-	Tabor parameter
\dot{A}	kg/m ³	Mass density
\tilde{A}^2	-	Variance
\tilde{A}	Pa	Stress
\tilde{A}_{crit}	Pa	Yield strength
\ddot{A}	Pa	Contact shear stress
\ddot{A}_{crit}	Pa	Critical shear stress
\ddot{A}	Pa	Fluid shear
A	-	Amplitude
A	mm ²	Contact surface area

B	mm	Pad bearing length
C_P	J/g·K	Specific heat capacity
c	mm	Bearing clearance
c_0	m/s	Sound velocity in the lubricant
D	-	Fractal dimension
d	mm	Hydraulic diameter
E	Pa	Elasticity modulus
E^*	-	Reduces elasticity modulus
e	mm	Eccentricity
e	J/kg	Energy per unit of mass
F_N	N	Normal force
F_T	N	Tangential force
\vec{f}	N/kg	Force per mass applied to a fluid volume
G	-	Characteristic length
H_{\min}, H_{\max}	mm	Minimal and maximal pad bearing height
H	-	Hamaker constant
h	W/m ²	Convection coefficient
h	mm	Lubricant film thickness
K	-	Kurtosis
K_{IC}	Pa \sqrt{m}	Toughness
L	mm	Bearing length
L_e	mm	Characteristic length
l	mm	Contact sliding way
ln	mm	Length of a measured profile
m	μm	Mean value of a profile topography
P_i, P_o	Pa	Inlet, resp. outlet pressure
p	Pa	Pressure
Q	J	Contact heat generation
\vec{q}	J/m ² /s	Heat flux lost due to convection

R	μm	Asperity radius
R_a	μm	Average roughness
R_e	-	Reynolds value
R_e	Pa	Yield strength
R_k	μm	Difference between maximum and minimum of the supporting surface
R_p	μm	Maximal roughness peak
R_q	μm	Quadratic mean value
R_t	μm	Amplitude between maximal and minimal profile height
r	$\text{J}/\text{m}^3/\text{s}$	Radiation heat lost per unit of volume
r_{tip}	mm	Radius of the sensing device
r_0	μm	Distance between two atoms
$S(\acute{E})$	W/Hz	Spectral power density
S_k	-	Skewness
s	-	Slope of the curve u_s-u_p
T	$^{\circ}\text{C}$	Temperature
t	s	Time
u_0	m/s	Sliding wall velocity
u_A, u_B	mm	Sliding positions
u_s	m/s	Shock velocity
u_p	m/s	Particle velocity
$v_E(M,t)$	m/s	Eulerian velocity
$v_L(M,t)$	m/s	Lagrangian velocity
w	J	Surface energy
X	mm^2/s	Thermal diffusivity
$z(x)$	μm	Profile

Abbreviation

IPEK	Institute of Product Engineering
KIT	Karlsruhe Institute of Technology
UK	United Kingdom
iPeM	integrated Product engineering Model
FSI	Fluid-Structure-Interaction
CPU	Central Processing Unit
DoE	Design of Experiment
SADT	Structured analysis design technique
C&C ² -A	Contact and Channel Approach
WS	Working surface
WSP	Working surface Pair
CSS	Contact and Channel Support
C	Connector
GPS	Geometrical Product Specification
DIN	Deutsches Institut für Normung (German institute of normalization)
R	Roughness
W	Waviness
P	Primer profile
CAE	Computer Aided Engineering
HOT	Hurst Orientation Transform
PIFS	Partitioned Iterated Function System
VCCT	Virtual crack closure technique
DMT	Derjagin, Muller, Toropov adhesion model
JKR	Johnson, Kendall, Robertson adhesion model
MD	Molecular dynamic
RICC	Roughness-induced crack closure
PICC	Plasticity-induced crack closure
VOF	Volume of Fluid method
ALE	Arbitrary Lagrangian Eulerian method
CEL	Coupled Eulerian Lagrangian method
CFD	Computational Fluid Dynamics
EHL/EHD	Elastohydrodynamic Lubrication / Elastohydrodynamics
RSM	Response Surface Method

CCD	Central Composite Design
CVT	Continuously variable torque
CCC	Centrale composite Design Circumscribed
CCI	Centrale composite Design Inscribed
CCF	Centrale composite Design Face centered
AFM	Atom Force Microscopy
FIB	Focused Ion Beam
TEM	Transmission Electron Microscopy
RNT	Radio-Nuclide-Technique
XiL	X-in-the-Loop analysis technique
DoF	Degree of Freedom
IGES	Initial Graphics Exchange Specification
STEP	STandard for the Exchange of Product Model Data
FVA	Forschungsvereinigung Antriebstechnik
FVM	Finite volume method
ILS	Intelligent Lifting System
MBS	Multi-Body System

1 Introduction

1.1 Context

Mobil systems and mobility engineering represents a central competence area of the Karlsruhe Institute of Technology (KIT). Especially in this area, a major research field “powertrain systems” has been established at the Institute of Product Engineering of Karlsruhe (IPEK). This field includes whole system chain going from engine output (dual masse flywheel) until the wheels of any vehicle. Engine system is here not taken under focus in-house. In order to be able to support partners in designing and improving new powertrain systems, different phenomena occurring in powertrain systems have to be mastered. As a consequence, such phenomena have to be described by physical models. Moreover, each interacting phenomenon needs to be modeled and taken into account during the designing phase. On this account, a second major field of the modeling methods of systems and systems’ design is also established at the same institute. Practically, this second research activity consists in developing different investigation Methods and Processes applied to the engineering process of any System in order to increase manufacturing quality and velocity.

Present work uses a friction system (clutch) present in the powertrain chain as demonstrator and presents an approach on how modeling tribological behavior of contacts occurring in this type of system. This topic is fully belonging to tribology which takes its origin from both Greek terms “Tribos” and “Logos” meaning literally surface interactions science.¹ Tribological phenomena are described by means of many parts of fundamental sciences such as solid and fluid mechanics, thermodynamics, material science, rheology or reliability and impact highly energy efficiency of mechanical systems.

Although this research field has been named quite recently in 1966 by the UK Department of Education and Science, scientists were working in such problematics for a long time (since the 17th century). First theoretical investigation in tribology began with studies on contact mechanics, achieved by Hertz² at the end of the 19th century after numerous observations mainly stated by Coulomb, Boussinesq or da Vinci. Since then, several models were developed, based on preceding work in order to evaluate their window of validity. In a context of constant environmental and

¹ Dowson (1979)

² Hertz (1881)

economic costs increasing, energy saving becomes even more important. Thus, this is the reason why present work aims at decreasing engineering costs and designing time, by considering only tribological aspects, a choice motivated in the next section (1.2). On this account, the content of present study focuses on tribological phenomena occurring between two rough or profiled surfaces in dry contact on the one hand and mixed lubricated conditions on the other hand.

1.2 Motivation

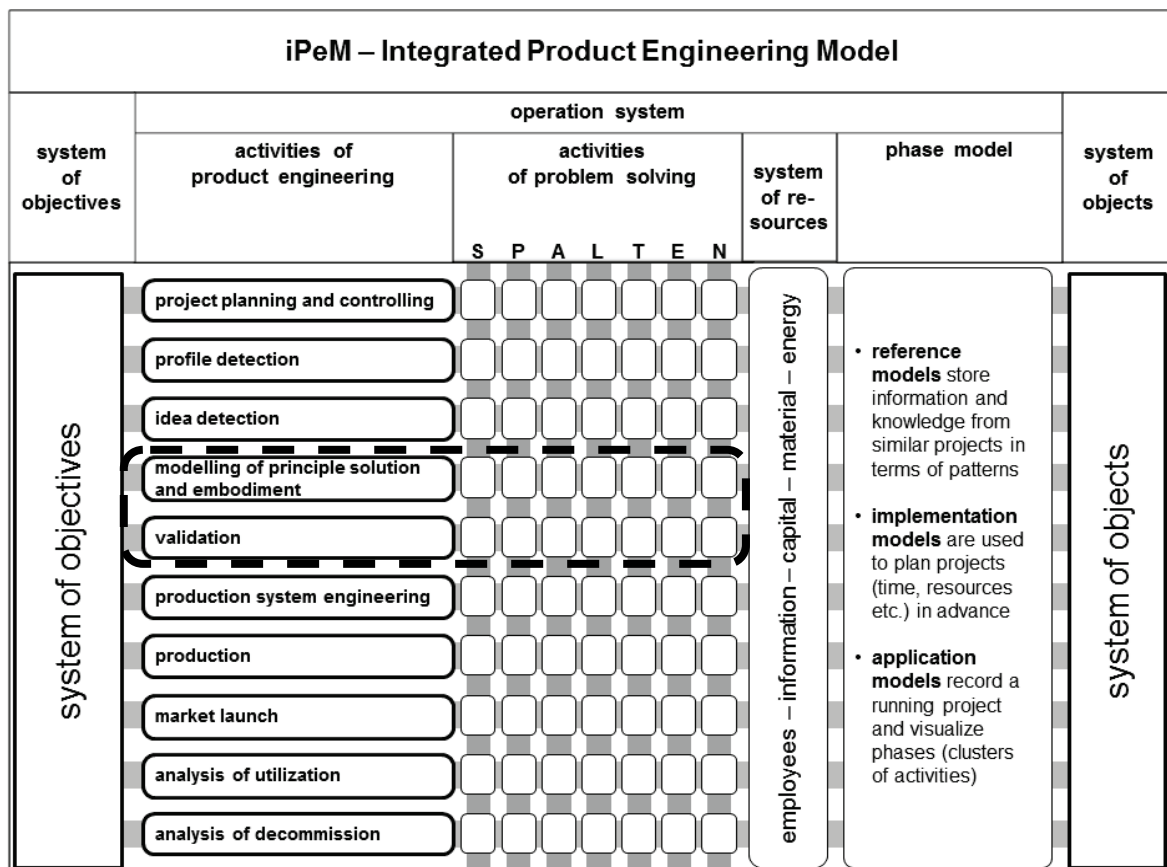


Figure 1.1: Integration of the work into the iPeM³

Main reason why only tribological phenomena is considered remains in its impact on energy saving. Friction losses, occurring in any mechanical systems are responsible for up to 10 % loss of the overall worldwide produced energy.⁴ Knowledge of the different occurring friction phenomena has to be increased for the dry tribo-systems and respectively for lubricated tribo-systems. This is achieved through the development of different theoretical models that need to be taken into account in the

³ Albers / Braun (2011)

⁴ Gras (2009)

early phase of the Integrated Product Engineering Model (iPeM) developed at the IPEK and composed of many iterative steps displayed on Figure 1.1.

The iPeM, described by Albers and Braun,⁴ consists in identifying how the designer has to proceed from the system of objective (product ideas) to the system of objects (product). The concept of the present work is to be able to deliver tribological models to support the designer in the conception of tribological systems. The integration of these theoretical models mainly takes place in two activities: modeling of principle solution and embodiment and validation

These models reproduce the behavior of any demonstrator in which the investigated phenomenon is occurring. In the frame of this work, these demonstrators are typically tribological systems (also called tribo-systems) which can be classified in two categories:

- Friction systems: in which the friction itself is the main function of the system
- Bearing systems: in which the friction is a "noise" function

The same type of phenomenon can occur in both classes, but in the first one, the function has to be optimized to reach the wanted dynamical behavior, whereas friction needs to be minimized in the other class.

Present work focuses on the investigation of tribo-systems taking into account effects only observable at the microscopic scale. Generally, two parallel streams are followed to achieve such analyses. First approach used considered being the nearest to the reality was the experimental one as it enables measurements on real prototypes. Nevertheless this approach requires huge resources, a further argument for increasing investigation efficiency.

Parallel stream takes into consideration mathematical models reproducing phenomena present in investigated systems. The main advantage of this method was the short time spending and costs. The disadvantage of this way of investigation resides in the difficulty to solve the mathematical problem and to get reliable, accurate and valid results. The first limitation gets even smaller since high computer resources are available whereas the second one often needs the building of physical prototype.

The theoretical models developed in this thesis are principally based on numerical approaches using different simulation tools, mainly based on the finite elements method coupling fluid and solid mechanics. In order to take into account adhesion and surface roughness, investigations related to these aspects are necessary to be done preliminarily at the micro scale. After verification, output data are directly integrated into models that have a higher scale in order to deliver the complete system's behavior.

Using numerical way cannot be avoided as experimentations are nowadays approaching their scale limits. They need to be completed with so called numerical models especially for the characterization and description of phenomena occurring at the micro- and resp. nanoscale. These numerical models need to be developed at different scales going from nano to macroscale. In order to simulate the behavior of a whole product, the required coupling of different scales is a big challenge considering the discontinuities existing between different scales. Present study focuses at the macroscopic and microscopic scale. First scale is used to model a whole system's behavior whereas the second one is used to calculate a locale friction law used afterwards in the macroscopic model. Nanomodels are not used in this work, as the thesis-framework would be too large.

The analysis of tribo-systems is set on the running regimes that are leading to system failure: dry-running and mixed lubrication. The last lubrication regime consists in having a discontinuity in the lubricant film laying between both sliding solids. The need to identify the concerned phenomenon on how to influence it is real and has to be done in an early phase of the product development process for a costs reasons. Next part exposed a procedure to purchase the fixed goal.

1.3 Outline

The first part of this report deals with the basics and extensive state of the art combining several research fields used to solve the previous described problem. Beginning with the simulation ways used for modeling surface roughness, the report develops the principles of structural resp. fluid mechanics. Next part concerns the coupling way between both theories. At last, adhesion theory is exposed as well as the measuring facilities used for the experimental verification. Chapter 3 defines main objectives of the work as well as the procedure used to reach them.

Chapter 4 sets the global analysis framework, the used demonstrator and numerical methods taken for the investigations. Chapter 5 describes the dry friction and mixed lubrication model development at the microscopic scale, their corresponding boundary conditions and the data treatments necessary to use real rough surfaces in the numerical model. Chapter 6 states the verification of the micromodels with corresponding experimental setup.

Chapter 7 exposes the parameter study, related to the impact of different parameters on the friction. A macromodel is then built in chapter 8 in which the results issuing from the micro scale are imported. Last chapter summarizes results and evaluates the potential of the developed method. The report ends with an outlook providing the tasks needed to purchase investigations.

2 Fundamentals and State of the Art

Composed of ten parts, this chapter provides an overview of each component to be used in investigation of mixed lubrication, starting with system analysis method up to different numerical and experimental methods, statistical design of experimental investigations. First of all, methodology is required to analyze a system and be able to determine which component of a tribological system is responsible for a given function (mainly friction force transmission). This part is followed by several techniques related to the way of characterizing surfaces' roughness of tribological systems. This is especially required to establish a relationship between roughness and friction behavior.

In a next step, mechanical laws describing phenomena occurring in tribological contacts are presented. This is followed by adhesion theory – main phenomena happening in such working conditions – which has to be used in this kind of investigations. For lubricated contact, fluid mechanics theories are also displayed, to describe lubricant flows. Then, as the present work is based on numerical investigations, available methods are presented and classified in order to be selected regarding their application. Also here, a special case is treating fluid-structure-interactions (FSI) modeling techniques.

Due to the requirement of high CPU resources, number of calculation has to be limited. This implies using design of experiment (DoE) techniques, based on statistical approaches. These techniques are displayed in the eighth subsection and are issuing on experimental techniques. This procedure is necessary to validate numerical models. Finally, last part treats the research activities done in present field of research, identifying which domain has to be deepened.

2.1 Methods for System Analyses

An essential aspect within the product engineering process is to improve a product's function. This can be optimally achieved after a system analysis. Two methods are used for this purpose and explained in next paragraphs.

2.1.1 Structured Analysis Design Technique (SADT)

The SADT is copyrighted since 1977 by both software companies SofTech (USA) and IGL Technologie (France). A technique developed by the software engineers in order to keep an overview of the design of their software was generalized to any kind of industrial application to increase the maintainability of a developed system or product. A major aspect of this method is, that it enables to define communication standards between product users and designers. The technique is defined by 7 fundamentals⁵:

- SADT model is context dependent
- The analysis is hierarchic, downward, modular and structured
- SADT tells where the method is efficient and not how the method realizes the “where”
- SADT models both the objects and events achieved by the objects
- SADT is a semi-formal language
- SADT improves team work
- SADT obligates the documentation of the system

The principle of the method is to identify the function of any complex existing system as displayed in Figure 2.1. This method can be used in different analysis levels, going from the whole product until its smallest components (see Figure 2.2). Nevertheless, this method does not enable a concrete visualization of a system. On this account, another method can be used to help the designer to understand the function that has to be transformed into a product.

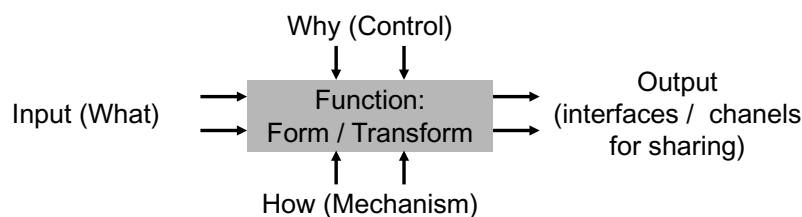
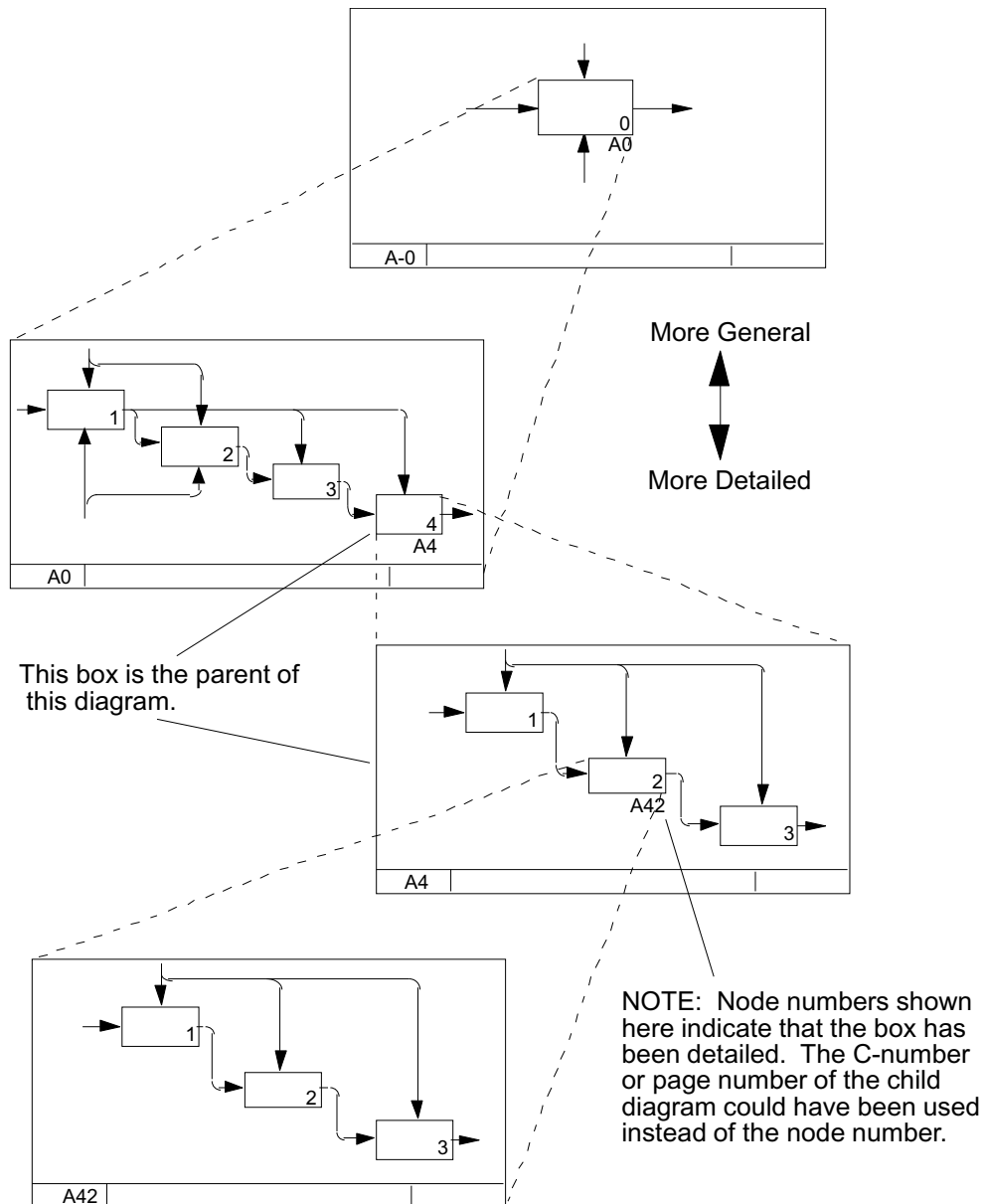


Figure 2.1: SADT principles⁶

⁵ Sadeg (1996)

⁶ Ross (1985)

Figure 2.2: Example of multilevel SADT⁷

2.1.2 Principle of the Contact and Channel Approach (C&C²-A)

The generalized Contact and Channel Approach displayed in Figure 2.3 is based on the following hypothesis: each system can be described as a blackbox with following inputs: "Information", "Stuff" and "Energy".

By using this approach, any tribological system (blackbox on Figure 2.3) can be separated into subsystem themselves decomposed into smaller subsystems, etc. To achieve any system description, four main tools are available and visualizable on Figure 2.4:

⁷ Federal Information Processing Standards Publications (1993)

- Working Surface (WS): boundary of any element of the concerned system (solid, liquid, gas or field)
- Working Surface Pairs (WSP): combining of two working surface between whom information, mater and energy can be transmitted
- Channel and Support Structure (CSS): element of solid, fluid, gas or field which is contained between two WSP and which transmits information, mater and energy from one side to the other
- Connector (C): entity representing the environment and symbolizing the boundary conditions of a system

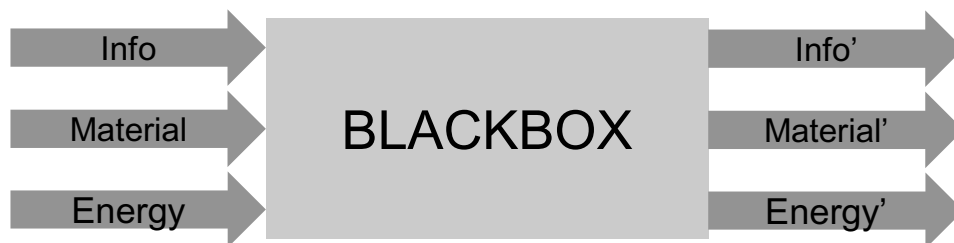


Figure 2.3: Generalized description of any technical systems⁸

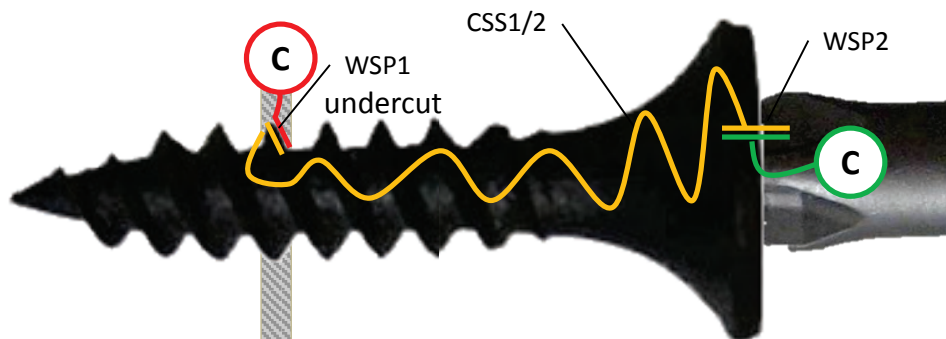


Figure 2.4: C&C²-A model⁹

2.1.3 Application and Advantages of both Methods

The differences between the two design methods – SADT and C&C²-A – are displayed in the following table (Table 2.1):

⁸ Ropohl (2009)

⁹ Albers / Braun / et al. (2011)

Table 2.1: differences between SADT and C&C²-A

TASK	SADT	C&C²-A
System analysis (multiscale analysis)	Yes	Yes
Function description	Yes	Yes
Overlapping with the design	No	Yes
Normalized visualization of the analysis	Yes	No
Flexible	No	Yes
Possibility to visualize the interfaces between functions	No	Yes
Dissociation between the implementation and controlling of the function	Yes	No

To conclude, some advantages of the C&C²-A towards the SADT resides in a better possibility to identify potential problems. In the case of the C&C²-A, the understanding of a complex system is improved by the visualization: the modeling method can be superposed to an existing technical drawing of a specific system in order to visualize it. As a consequence, the overall readability of the system is improved. Moreover, a better flexibility and interface visualization allows to say that the C&C²-A should be combined with the SADT. Main reason for that resides in combining both advantages: a good readability for the designer, a good system description for the system's engineer. Additionally, it offers a normalized modeling design and a better dissociation of the controlling and implementation of the function.

Describing a system is from high interest in multiscale modeling of tribological phenomena, as they are observed at the macro scale but may issue from localized processes established at the micro scale. These same phenomena follow laws that are completely different from them observed at the macro scale. After defining functions of a given tribo-system, characterization technique of surface roughness existing in these systems is required to parameterize rough solids. Next subsection displays different methods to assess such a characterization.

2.2 Technical Surfaces

In macroscopic models, each surface is usually assumed to be flat but the reality is different and tribological behavior strongly depends on surface manufacturing. Such surfaces can be measured by means of optical facilities, delivering a 3-dimensional scatterplot of the surface.

2.2.1 Signal Composition of a Technical Surface

The three-dimensional profile of the solid is described through different normalized measurement.¹⁰ Geometrical Product Specification (GPS) applied in 1998 created the norm for the classification of surface roughness: each rough surface can be separated into different profile classes depending on the wavelength of the measure. The first four presented surfaces are measurable with conventional sensing or optical devices (see Figure 2.5 and Table 2.2):

- Form profile
- Waviness profile
- Roughness profile
- Atomistic roughness

where the second atomistic roughness can only be measured with x-rays or optical devices such as scanning electron microscopes to determine

- Crystal structure of the surface
- Atomic structure

Analyses done in this work take place on different scales. As a consequence and for reasons explained in chapter 4, different profile resolutions need to be taken into account:

- Macro scale: form profile
- Meso-scale: waviness profiles
- Micro scale: roughness profile

In order to characterize these different “roughness classes”, different filters are necessary. Low pass filters are used for the form profile, whereas high-pass filters are used for the roughness profile. Waviness profile is calculated using a bandpass filter. An example of wavelengths is given on the diagram on Figure 2.5 where X

¹⁰ DIN EN ISO 4288 (1998)

stands for the profile length and Y for the percentage of the signal passing through the respective filter.

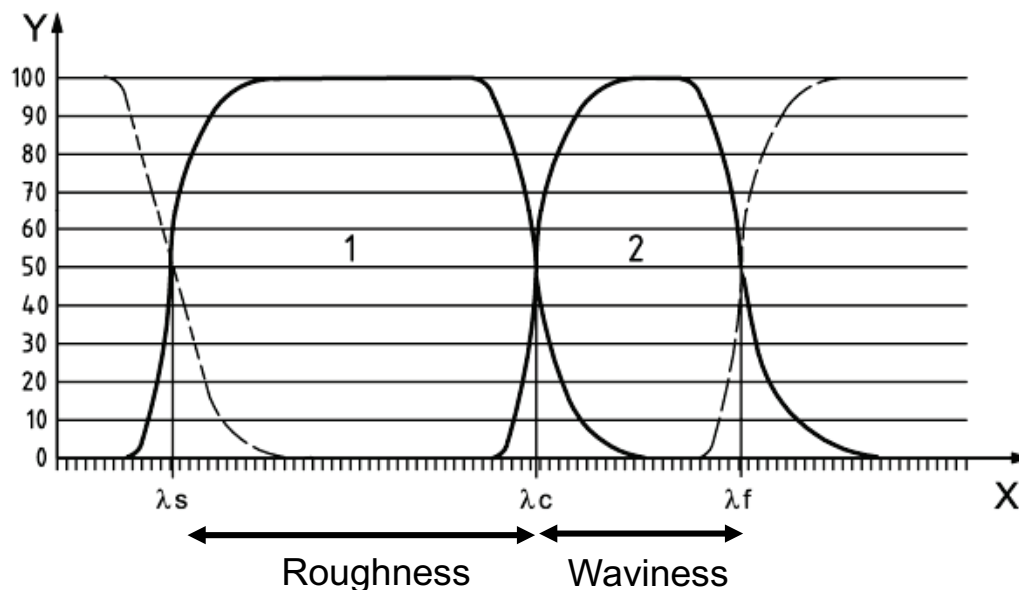


Figure 2.5: Wavelength of the waviness and roughness profiles¹¹

Waviness and roughness are dissociated from the primary profile through the primary filter with wavelength λ_f and roughness filter λ_c which are defined according to DIN ISO 12085¹² (see Table 2.2).

Table 2.2: Determination of the wavelength to separate the waviness from the profile¹²

λ_c (mm)	λ_f (mm)	ln (mm)
0.02	0.1	0.64
0.1	0.5	3.2
0.5	2.5	16
2.5	12.5	80

Then, length ln is set in DIN ISO 13565-1.¹³ If both parameters λ_c and λ_f are unknown, λ_c can be linked to the length ln according to Table 2.3.

¹¹ DIN EN ISO 4287 (2009)

¹² DIN EN ISO 12085 (2002)

¹³ DIN EN ISO 13565-1 (1998)

Table 2.3: Relation between λ_c and ln ¹³ in mm

λ_c	ln
0.8	4
2.5	12.5

A further filter λ_s needs to be used to separate roughness from the waviness¹⁴ (see Table 2.4). According to DIN 4287¹¹ norm, three wavelengths are describing the limit of each profile: λ_s , λ_c and λ_f , respectively for lower limit of roughness, limit between roughness and waviness and between waviness and primary profile (see Figure 2.5).

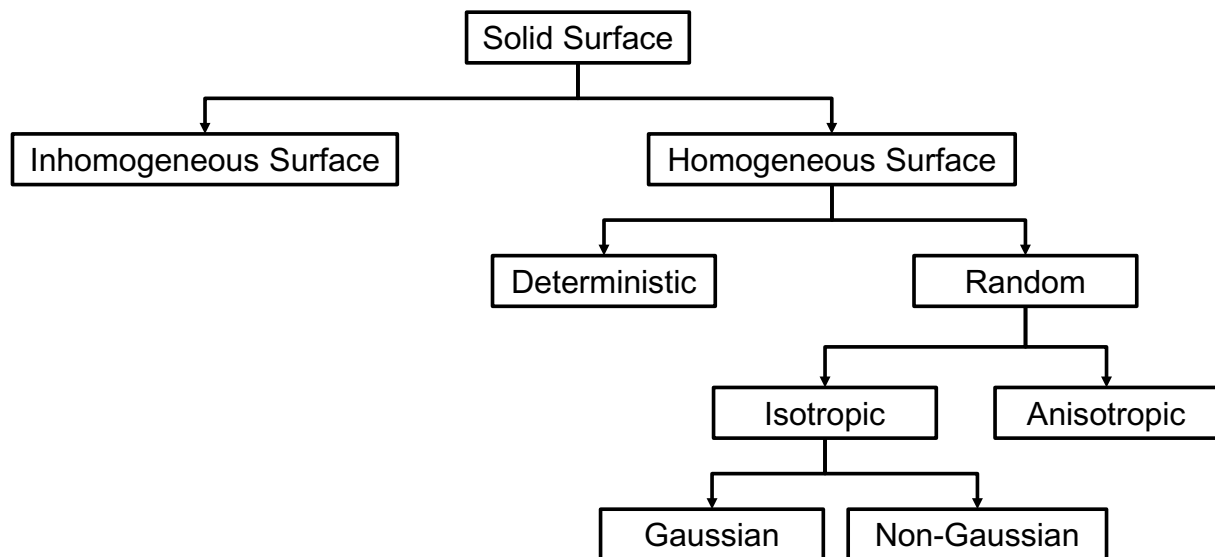
Table 2.4: Relationship between λ_c and λ_s ¹⁴

λ_c (mm)	λ_s (μm)	λ_c/λ_s	r_{tip} maximal value (μm)	Profile maximum (μm)
0.08	2.5	30	2	0.5
0.25	2.5	100	2	0.5
0.8	2.5	300	2	0.5
2.5	8	300	5	1.5
8	25	300	10	5

Technical surfaces can be classified into different kinds of categories as displayed in Figure 2.6.¹⁵ Extreme finishing processes (with only one or extreme numerous cutting points) are categorized as anisotropic or isotropic- non-Gaussian surfaces. This corresponds to turning, shaping and milling. On the contrary, finishing governed by random processes is leading to Gaussian distributed surfaces corresponding more to milling. The characterization diagram is displayed in the next paragraph.

¹⁴ DIN EN ISO 3274 (1997)

¹⁵ Bhushan (2002)

Figure 2.6: Categories of technical surfaces¹⁵

2.2.2 Statistical Characterization of Technical Surfaces

Each of enounced technical surface's profile is characterized through a letter (P for primary profile, W for the waviness and R for the roughness) following parameters:

- Vertical parameters: maximal peak height (index p), maximal valley depth (v), profile amplitude (t), average of the profile (a) and mean square of roughness profile (q), skewness (sk), stepness (ku) or kurtosis (K)
- Horizontal parameters: mean period width (Sm) and peak number (Pc)

Vertical parameters are the most conventional ones used to define a technical surface and especially these (s. Figure 2.7):

- m : mean value of the signal

$$m = \frac{1}{L} \int_0^L z(x) \cdot dx \quad (2.1)$$

- R_p : maximal peak of the signal

$$R_p = \max(z(x)) - m \quad (2.2)$$

- R_a : mean value of the profile from the mean line

$$R_a = \frac{1}{L} \int_0^L |z(x) - m| \cdot dx \quad (2.3)$$

- R_q : quadratic mean value

$$R_q = \left[\frac{1}{L} \cdot \int_0^L (z(x))^2 \cdot dx \right]^{1/2} \quad (2.4)$$

- R_t : maximal amplitude of the profile

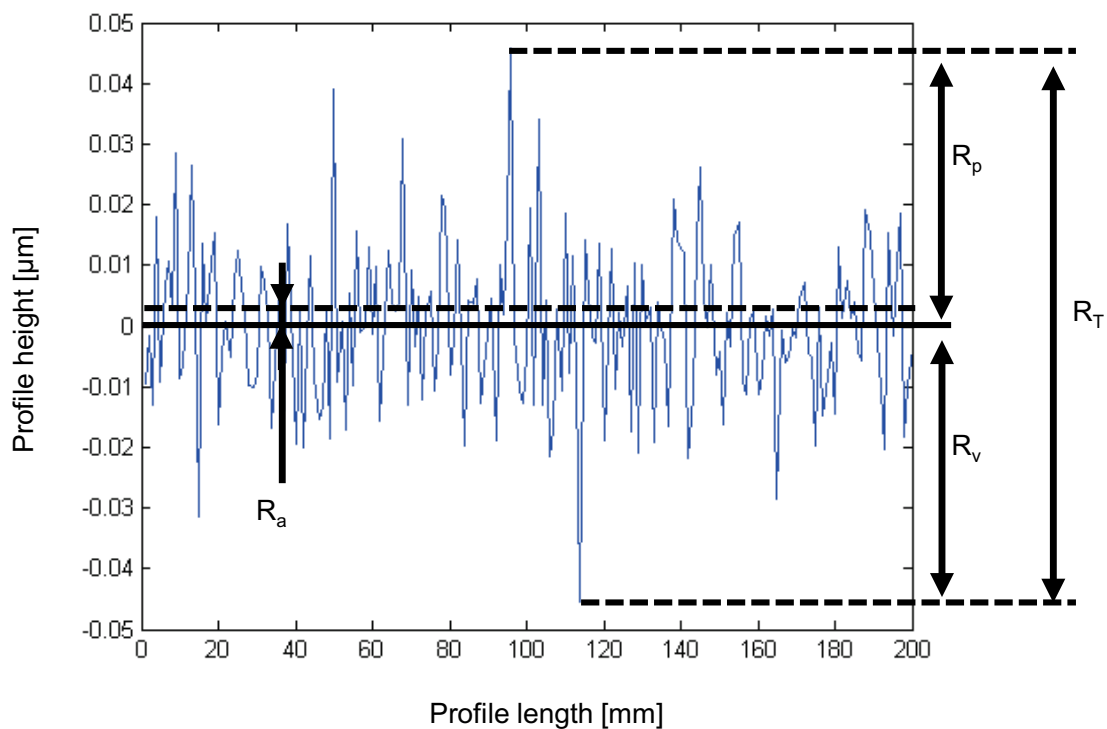


Figure 2.7: Main parameters for the roughness description

Further characteristics reside in the use of the Abbott-Firestone curve to define the material ratio of the technical surface. Figure 2.8 shows a rough surface which can be characterized by a primary profile shown in Figure 2.7.

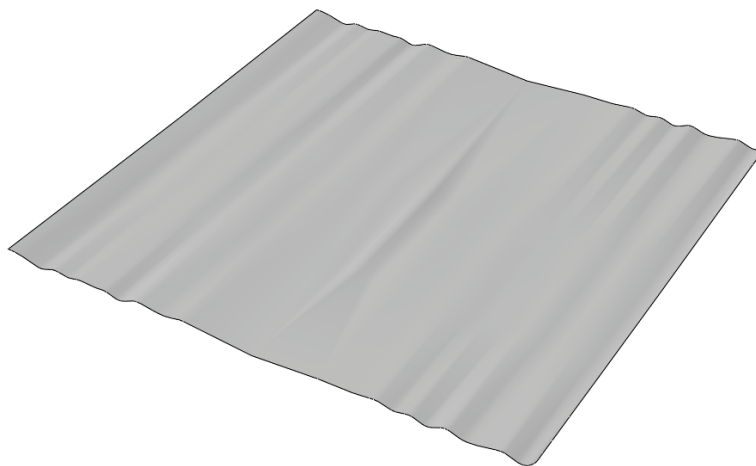


Figure 2.8: Corresponding rough profile

Different profiles can have the same roughness, thus Abbott and Firestone¹⁶ establish a rule which determines the effective load surface (see Figure 2.9). The concept consists in the calculation of the lowest tangent of the curve in order to determine the average roughness range of the supporting surface (R_k).

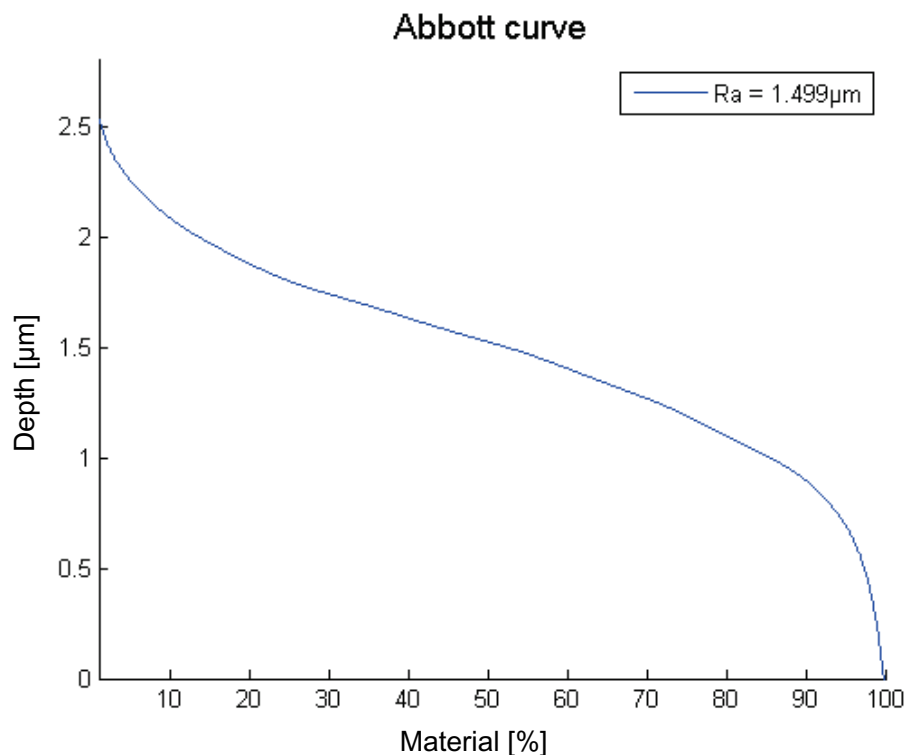


Figure 2.9: Corresponding Abbott-Firestone curve of displayed technical surface

Both last statistical parameters, skewness and kurtosis are defined as follow and used to determine the type of surface (Gaussian or not). The skewness

$$Sk = \frac{1}{\sigma^3 \cdot L} \cdot \int_0^L (z(x) - m)^3 \cdot dx \quad (2.5)$$

and the kurtosis

$$K = \frac{1}{\sigma^4 \cdot L} \cdot \int_0^L (z(x) - m)^4 \cdot dx \quad (2.6)$$

are normalized with the variance

$$\sigma^2 = \frac{1}{L} \cdot \int_0^L (z(x) - m)^2 \cdot dx \quad (2.7)$$

¹⁶ Abbott / Firestone (1933)

All these parameters are the most often used for industrial applications as they are normalized. However, these are not sufficient to characterize completely the surface topography and correlate it with the tribological behavior as they do not take into account the spatial characteristics. It does not give an overview with enough details about the behavior of rough profiles:

- periodical or aperiodic profile
- the amplitude corresponding to the profiles

The use of frequency analyses contribute to a better characterization and thus enables a frequency description of profile's signals through the combination of correlation functions as well as Fourier analyses. Autocorrelation delivers dominant signal periods of a periodical signal submitted to high noise effects whereas a Fourier analysis gives the dominant frequencies of a signal.

2.2.3 Frequency Analysis of the Surface Characteristic

This technique consists in decomposing the measured signal into a frequency vector by means of a Fast Fourier Transform to get the number of dominant frequencies.¹⁷ However, main limitation resides in the difficulty to deliver scale independent results as the measuring facility has its own acquisition resolution. Furthermore, no special information – where peaks are occurring – is delivered but the occurrence of the rough motif in form of a frequency f , amplitude A and phase \mathcal{A}

2.2.4 Generation of Rough Surface Profiles

As measuring surfaces profile costs a lot of time, surface profiles can be generated using numerical methods which are then imported into used Computational Aided Engineering (CAE) software. The so called surface generation process was implemented by Nowicki¹⁸ in order to reduce time spent in measuring real rough surfaces. This process is able to generate a three dimensional spline by means of an optimizing process.

Usually based on deterministic approaches, the characterization of the rough surface begins with its discretization. One generation method, developed by Patir¹⁹ and based on Gaussian surfaces, used correlation functions. Bakolas²⁰ extended this approach with more efficient numerical approaches: roughness and waviness were taken into account through their decomposition in the frequencies domain. Cai and

¹⁷ Peng / Kirk (1997), Dong et al. (1994)

¹⁸ Nowicki (2008)

¹⁹ Patir (1978)

²⁰ Bakolas (2003)

Bushan²¹ used this approach for concrete applications especially for investigations of lubricated surfaces at the microscopic scale.

From the different methods used for characterizing surfaces the frequency approach was retained there. Signals frequency spectrums can be described through a vector composed of amplitudes and phases of each signal. A database composed of amplitudes and phases was used as base for rough surface generation.

Last step consists in generating rough surfaces by means of a sensitivity based optimization getting previous database as input. This delivers new profiles which are compared with real measured surfaces giving defining if generated profile was near enough to real ones.

Once the artificial surface is generated, it has to be imported into numerical software. Two ways are possible for that, generating a mesh with the spline on the one hand or generating a solid body using a neutral file format so that no specific software is required for the importation. The first solution was chosen due to its ability to mesh it from different ways but is software dependent. No program is available to generate such files for the wanted structures, for that reason an appropriate tool needs to be developed.

2.2.5 Fractal Description

In addition with preceding characterization methods, the fractal method allows characterizing technical surfaces without being influenced by the scale. They are also mainly used to characterize the order of the profile. Majumdar²² stated that Weierstrasse-Mandelbrot function is adapted for this purpose through following form:

$$z(x) = G^{(D-1)} \sum_{n=n_1}^{\infty} \frac{\cos(2\pi\gamma^n x)}{\gamma^{(2-D)n}} \quad (2.8)$$

where the characteristic length G of the surface and the fractal dimension D ($1 < D < 2$) are calculating using the power spectrum

$$S(\omega) = \frac{G^{2(D-1)}}{2\ln(\gamma)} \frac{1}{\omega^{(5-2D)}} \quad (2.9)$$

of the z function²³. ω corresponds to the frequency. Its range goes from the sampling length up to the high limit defined by the frequency of the measuring instrument. To

²¹ Cai / Bhushan (2006)

²² Majumdar / Bhushan (1990)

²³ Berry / Lewis (1980)

deliver both fractal parameters a correlation is done with the usual power spectrum density calculated from the Fourier Transform.

The parameter β defines the density of the spectrum and the relative phase of the spectral modes²², n_1 the lowest frequency of the spectrum ($\beta^{n_1} = 1/L$, L the sampling length). β^n represents the n frequency mode ($\beta^n = 1/\lambda_n$).

The presented method is adapted for isotropic-gaussian surfaces, and that is why Hurst Orientation Transform (HOT) was created.²⁴ Nevertheless, this last created method was insufficient, and finally induced the development of the Partitioned Iterated Function System (PIFS) to describe three dimensional topographies into simple mathematical rules²⁵ in order to classify the surfaces into different groups. The combination of the fractal method with the wavelet method can be useful for multi-level characterizations.

2.2.6 Wavelet Description of Technical Surfaces

As the Fourier Transform, wavelets enable the decomposition of a signal into frequency components but also in different scales. First used in biomechanics,²⁶ this method separates, even though with some difficulties,²⁴ the signal into form, waviness and roughness but always in a given scale.

In combination with the fractal description, the scale independent method, wavelet extends the investigation to a given scale, so that the surface can be characterized at different scales. Methods combining both description techniques are developed, a surface is broken down into different scales with wavelets technique and then the fractals are applied to describe the topography.²⁷

After using surface characterization, interactions between rough surfaces are treated. On this account, next subsection displays background of solid mechanics as well as material sciences.

2.3 Structural Mechanics and Material Science

First theoretical part of lubricated tribological systems is related to structural mechanics. This part is determinant in tribological investigations as interactions between solids and the material behavior itself are described by solid mechanics and material sciences theories. First basics concerns movement and trajectory descriptions and are displayed in next paragraph.

²⁴ Podsiadlo / Stachowiak (1998)

²⁵ Podsiadlo / Stachowiak (2000), Stachowiak / Podsiadlo (1999)

²⁶ Jiang et al. (1999)

²⁷ Podsiadlo / Stachowiak (2002)

2.3.1 Basics: Movement Description

Principles of solid mechanics are found in continuous mechanics laws and especially the equation of motion of a continuous domain. Two descriptions are possible for that, the Lagrangian equation of movement considering a point M of the continuous domain (solid for example) moving from a time t_0 and place M_0 to time t and M :

$$M = f_{t_0,t}(M_0, t) \quad (2.10)$$

The other motion description is the so called Euler description considers a point M belonging to a fixed domain and crossed by a material flow. This point called “observation” point gives the velocity vector field from each material particle crossing this point. The vector field is displayed:

$$\vec{V} = \vec{V}_E(M, t) \quad (2.11)$$

Main difference between both approaches is that the Lagrangian gives the trajectory of a particle and the Eulerian one gives the velocity field of a particle. To determine the Lagrangian Velocity of the particle V_L equation (2.10) is derivated:

$$\vec{V}_L = \frac{df_{t_0,t}(M_0, t)}{dt} \quad (2.12)$$

Moreover, getting particle trajectories through the Eulerian description needs solve following differential equation:

$$\frac{d\vec{M}(t)}{dt} = \vec{V}_E(M, t) \quad (2.13)$$

where $M(t_0) = M_0$. Solving of this equation gives the Lagrangian description (s. equation (2.10)).

Both the Euler and Lagrange approaches are adapted for different investigation cases. On the other hand, the Lagrangian description is well adapted for describing solid motions because of the small relative displacement of each solid’s point. On the other hand, a fluid flow can be described easier through the Eulerian approach as it directly gives a velocity field vector from the particle crossing a defined domain. Following subchapters are based on the Lagrangian description as they focus on solid deformations.

2.3.2 Description of the Solid Deformation Parts Submitted to Friction

Whole purchased investigations are based on structural mechanics laws starting from the simple case of elastic behavior up to cases where solids get plastic deformations. These deformations μ have a relationship with the constraint \tilde{A} issuing from applied load on the structure. The relation is depending on the wanted characteristics of the system and for strict elastic deformations generalized Hooke's law can be applied:

$$\sigma = E \cdot \varepsilon \quad (2.14)$$

where E represents the Young's modulus. Usually taking into account only elasticity is sufficient to determine if a structure will resist to the applied load or not. In tribology, for a question of accuracy, this assumption cannot be assumed anymore.

Elastic and plastic deformations lead to hysteresis effects, which imply energy loss. To be able to calculate these different contributions, following methods can be taken into account, as presented in the work of Nowicki.¹⁸

Plasticity needs to be modeled, to deliver information of deformation and new profile topographies. Several plasticity models were developed for isotropic materials: the ideal, fragile and ductile damage models for that purpose. The simplest plastic model, ideal plasticity assumes a constant stress until the yield strength of the material is reached. Conventional structural steels can have a behavior near the ideal plasticity.²⁸ More realistic models used for metals and also implemented in numerical solution can be listed as follows:

- Ideal plastic: can be used in cases of ductile materials where the stress does not increase significantly after yield limit
- Rate-dependent yield: "is needed to define a material's yield behavior accurately when the yield strength depends on the rate of straining and the anticipated strain rates are significant"²⁹
- Anisotropic yield/creep: is mainly used for anisotropic materials
- Johnson-Cook plasticity: is the most accurate plasticity model for isotropic ductile materials combining hardening law to plastic deformations

The damage models are handled in the next subsection. From the presented plastic models, the ideal one is not adapted to simulate tribological deformations, as for the

²⁸ Vanlaere et al. (2004)

²⁹ Simulia (2011)

used materials, plastic properties are directly influencing the friction coefficient calculation. This coefficient is defined here as a division of tangential load by normal load.

Thus an experimental tensile test delivering strain-stress curve needs to be used in order to keep an acceptable quality of the results. Other parameters such as elasticity modulus and shear stress are also dependent on the temperature present in contact interfaces. Investigations established by Merchant³⁰ showed that the hardness of the steel has an exponential relationship towards temperature

$$H = A_2 \cdot e^{-B_2 \cdot T} \quad (2.15)$$

with H the hardness A_2 and B_2 two constants. The Hardness characterizing the plasticity of the material for indentation processes is also temperature dependent as displayed on Figure 2.10 in which

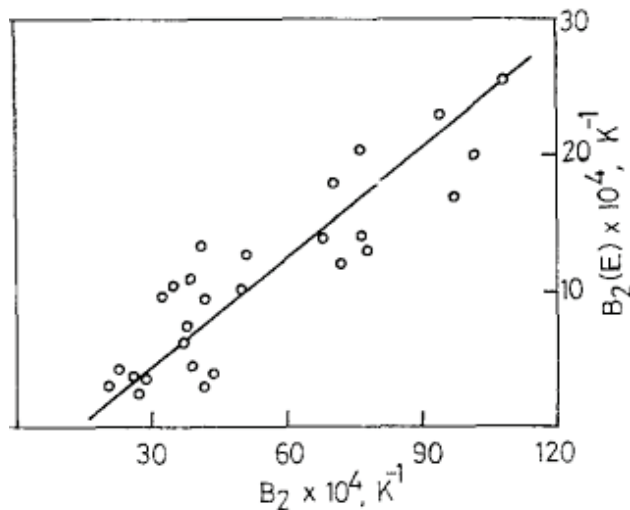


Figure 2.10: Relationship between softening parameters (B_2) of elastic modulus and hardness³⁰

Hardness and Young's modulus are both decreasing with rising temperatures. This fact has an impact on the friction force for solid-solid contact. Temperature cannot be neglected, as elastic modulus can be divided through a factor two for temperatures rising of 150°C.

2.3.3 Thermal Properties of the Solids

Explained in last paragraph, heat occurring in tribological contacts has impact on the solid's mechanical properties:

³⁰ Merchant et al. (1973)

- Elasticity modulus
- Yield stress
- Heat conductivity
- Heat capacity
- Density
- Thermal dilatation

The heat Q occurring in contacts can be described with following formula

$$Q = \tau \cdot A \cdot l \quad (2.16)$$

where Q represents the dissipated energy, \dot{A} the critical shear stress in the contact interface. A represents the contact area whereas l is the sliding distance. The temperature T at time t and place r can be calculated as follows

$$T(r, t) = \frac{Q}{8 \cdot \rho \cdot C_p \cdot (\pi \cdot \kappa \cdot t)^{3/2}} e^{-\frac{r^2}{4 \cdot \kappa \cdot t}} \quad (2.17)$$

with

$$\kappa = \frac{\lambda}{\rho \cdot C_p} \quad (2.18)$$

where the thermal conductivity symbol is represented by λ , ρ is the material density and C_p the heat capacity. These heat effects do also influence fluid properties as presented in the next section and so impact the friction (see chapter 2.5).

2.3.4 Wear Phenomena Occurring in Tribological Systems

In tribological contacts, different types of wear phenomena are occurring, they are classified in the Table 2.5.

Table 2.5: Wear phenomena classification for conventional structural steels³¹

Wear process	Damage process	Relative importance (Economical importance)	Wear quantity
Adhesion	Material transfer – microscopic links	15 %	10-2 mm per year
Abrasion	Wear particles, wear lines	50 %	10 mm per year
Erosion	Impacts, Cavities	8 %	1 mm per year
Deformation	Cracks, Impacts		No material dis- placed to the systems' outside
Contact fatigue (Sliding, Rolling or Fretting)	Cracks, delamination, oxidation	8 %	–
Corrosion	Corrosion films, particles, oxydes	5 %	–

These wear phenomena can be observed in different charging types as displayed in Table 2.6. From all the wear processes, abrasion, adhesion and deformation have the highest occurrence and economic impact. On this account main damage processes present in these wear phenomena are described in the next subsection in more details. Adhesion is treated in a separate section, as the mechanisms are more complex and impacting directly the friction coefficient.

³¹ Eyre (1979)

Table 2.6: Wear process in function of the load type⁴

Interaction type	Load type	Wear process
Solid-Solid	Sliding	Adhesion, Abrasion
	Rolling	Contact fatigue
	Impact	Deformation, Crack
	Oscillation	Fretting, Adhesion, Abrasion, Corrosion
Fluid-Solid	Flowing	Cavitation, Erosion
Fluid + Particles-Solid	Flowing	Erosion

2.3.5 Failure and Damage Models used for Wear Modeling in Contacts

Abrasion can be defined as material deformation occurring between two solids in relative sliding³². Contrary to adhesion, no chemical link between both solids is taken into account. Typically, two types of abrasive wear can occur:

- abrasion when the hardest body is initiating cracks on asperity contacts due to high asperity-asperity contact pressures³³
- abrasion when the abrasive body issues from mixing between external bodies (wear particles, lubricants, dirt...), also called third body³⁴

Different investigations were performed to simulate this phenomenon with a view to predict the wear during a turning process.³⁵ Furthermore, statistical simulation tools were developed for two bodies³⁶ and three body abrasive phenomena.³⁷ Abrasion

³² Khruschov (1974)

³³ Wang / Hsu (1998)

³⁴ Nikas (2012)

³⁵ Attanasio et al. (2008), Attanasio et al. (2011)

³⁶ De Pellegrin / Stachowiak (2004)

³⁷ Jhurani / Higgs (2010)

during grinding machining was also simulated by Zhang et al.³⁸ In this case, phenomenon was simulated using the smoothed particle hydrodynamic (SPH) method. Other macroscopical methods were used to model wear phenomena, like the Archard model used to calculate the wear in composite multi-disk clutches³⁹ or the Finnie⁴⁰ methods.

Abrasion, which usually takes place between hard and soft materials in frictional contact or when hard grains from a given metal are in contact with softer grains,⁴¹ issues from the shearing of two asperities as displayed in Figure 2.11.



Figure 2.11: Abrasive wear:⁴² shear stress (left), plastic deformation (right)

Abrasion and further wear processes can be decomposed into several damage processes themselves listed as follows:

- Strain hardening phenomenon
- Viscous damage (flowing)
- Viscous crack
- Brittle crack

Depending on the material type, abrasion and other types of wear processes can be subject to effects such as hardening, corrosion and heat generation. The worse type of damage is the crack initiation, as it directly leads to the creation of small wear particles that may themselves also initiate wear. Such cracks can be modeled using the finite element method, based on different criterions such as:

- Critical stress intensity factor (K_{IC})
- Contour integral (VCCT)
- Max Displacement
- Critical stress

³⁸ Zhang et al. (2011)

³⁹ Zhao et al. (2009)

⁴⁰ Finnie (1965)

⁴¹ Khruschov (1974)

⁴² Ayel (1974)

An application of this modeling realized by Kamp et al.⁴³ Crack growth simulated by means of the finite element method and taking into account surface roughness were both considered there. The same type of investigations was made before with artificial rough profiles.⁴⁴ Further numerical and analytical models were made to analyze the influence of RICC and PICC effects during overloads by considering crack modes I and II.⁴⁵ Usual damage models used for ductile material are based on the Johnson-Cook model⁴⁶ but this is not a part from present work.

2.4 Solid-Solid Interaction and Adhesion

In mixed lubricated systems, taking into account adhesion effects is inevitable. This phenomenon induces adhesive wear and initiates friction forces. In the macro scale, such phenomenon does not need to be investigated locally because the Coulomb principle is valid. Following paragraphs go on the different components of adhesion forces and describe the theory used to define them. In the present work the friction coefficient is defined as follows:

$$\mu = \frac{\iint \tau \cdot dA}{\iint p \cdot dA} \quad (2.19)$$

The integral of contact shear \dot{A} over the whole contact area A is divided by the contact pressure p integral.

2.4.1 Description of the Adhesion Phenomenon

Adhesion forces can be defined using the principle of the Van der Waals forces, issuing of intermolecular attraction forces. These can be separated into three main components: tangential, normal and hysteresis components, as explained in next three subsections.⁴⁷

⁴³ Kamp et al. (2004)

⁴⁴ Parry et al. (2000)

⁴⁵ Singh et al. (2006a), (2006b)

⁴⁶ Johnson / Cook (1985)

⁴⁷ Broster et al. (1974)

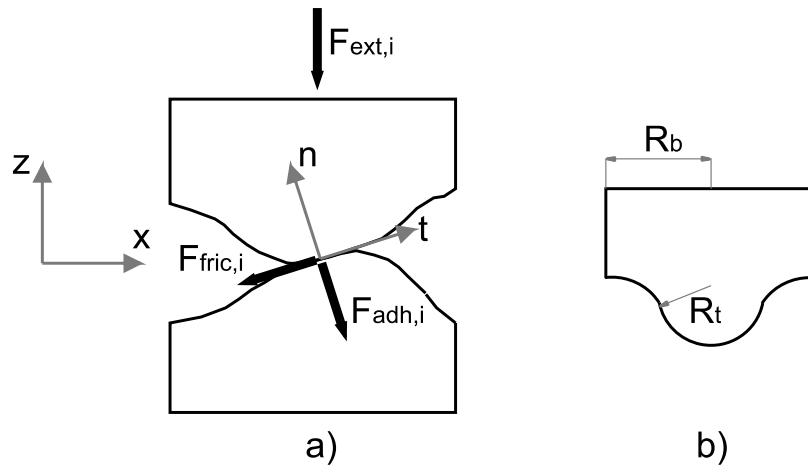


Figure 2.12: Van der Waals forces between two solid bodies (a) depending on the radius of the asperity peak (b)⁴⁸

Adhesion effects are based on electromagnetic attraction effect present between two molecules. Based on the Lennard-Jones potential theory, the attraction is present for a maximal intermolecular distance of r_0 (s. Figure 2.13).

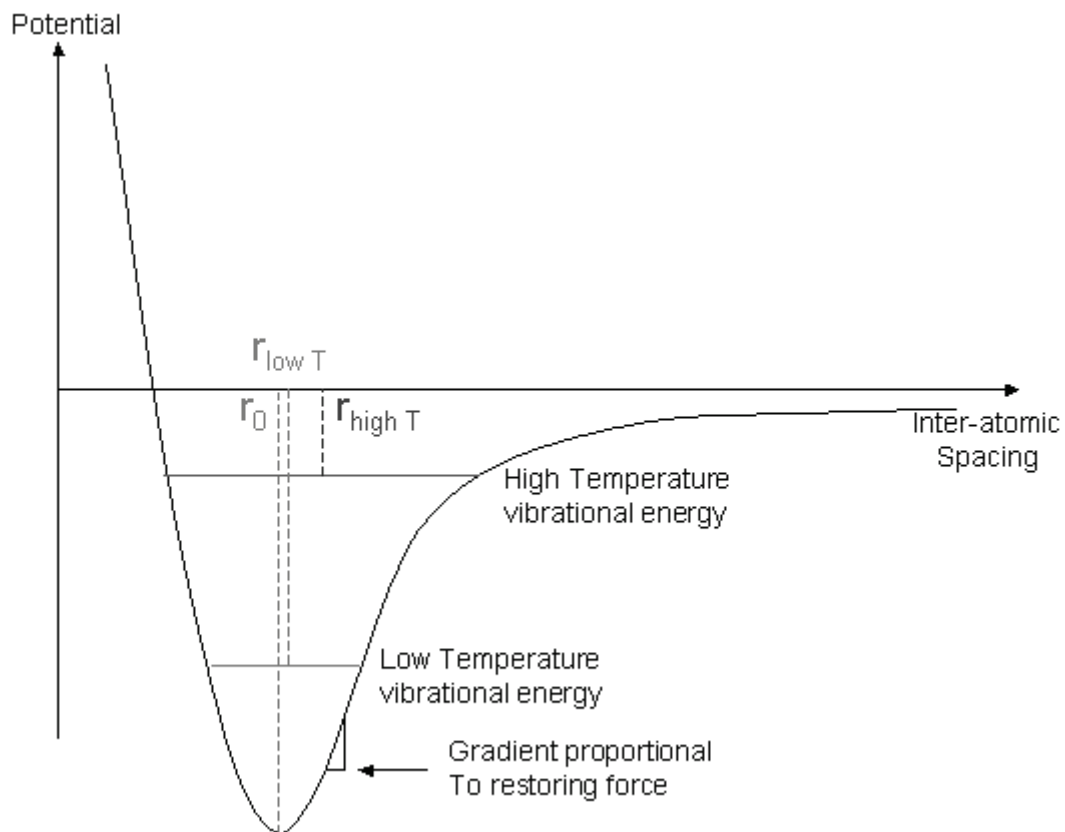


Figure 2.13: Lennard-Jones potential⁴⁹

⁴⁸ Savio (2010)

⁴⁹ DoITPoMS - TLP Library The Stiffness of Rubber - Lennard-Jones potential (n.d.)

Beyond this distance, no attraction is present between two atoms and adhesion effects can be neglected. An important aspect concerns the quality of considered surfaces. For corroded or lubricated surfaces, adhesive attraction has less influence than for optimal surface (ideal cleaned non-lubricated surfaces).

2.4.2 Tangential Component

The tangential component has the most important influence on friction resistance forces. Basically, when a tangential force is applied on the upper body (s. Figure 4.10), a shear stress is resulting at the interface of both solids. The whole force is transmitted to the lower body until a limit is reached. This limit was identified and described by Bowden and Tabor⁵⁰ to be a critical shear stress value $\tilde{\sigma}_{crit}$ corresponding to following criterion

$$\tau_{crit} = \max(\tau_{crit1}, \tau_{crit2}) \quad (2.20)$$

where $\tilde{\sigma}_{crit1}$ corresponds to the maximal shear stress of the first material and $\tilde{\sigma}_{crit2}$ to the second material. These parameters are calculated from the next Bowden's study where $\tilde{\sigma}_{crit}$ can be related to yield stress $\tilde{\sigma}_{crit}$ by means of following relation:

$$\tau_{crit} = \frac{\sigma_{crit}}{\sqrt{3}} \quad (2.21)$$

The assumption made by Bowden and Tabor was that maximal yield stress is reached at the contact place between both bodies. Actually, this boundary zone is more complex and can be composed of oxide, dirt or lubricant layers.

This boundary zone is important as lubricated systems boundary layers are covered with dirt, corrosion and lubricant layers. This makes the evaluation of friction critical shear ratio complex. Major part of this work does not consider the tribochemical effects present in these zones and considers that the sliding of both solids happens at their ideal contact interface.

2.4.3 Normal Component

The normal component is also influencing the behavior of tribosystems. It rises the forces needed for initiating the sliding of both solids and can lead to wear particle arrachement. Different models are used to describe this component and compare it to the hertzian theory. Basically, adhesion theory reposes on the Dupré equation⁵¹

⁵⁰ Bowden / Tabor (1950)

⁵¹ Straffelini (2001)

$$W = \gamma_1 + \gamma_2 - \gamma_{12} \quad (2.22)$$

with γ_1 and γ_2 representing the surface energy of respective solids in contact and γ_{12} the interface energy between both solids. If two solids are the same, this value remains zero. The determination of the surface energy is done with the Hamaker constant H in Joules⁵²

$$\gamma = \frac{H}{24\pi r_0^2} \quad (2.23)$$

where r_0 represents the distance between two atoms (see Lennard-Jones potential on Figure 2.13). H depends on the surface cleanness and corroded surfaces can have a constant 10 times smaller than in cleaned conditions. For lubricated surfaces, the Hamaker constant need to be adapted

$$H = \left(\sqrt{H_{\text{Solid1}}} - \sqrt{H_{\text{Lubricant}}} \right) \cdot \left(\sqrt{H_{\text{Solid2}}} - \sqrt{H_{\text{Lubricant}}} \right) \quad (2.24)$$

whereas this constant varies from 300 until 500 zJ for metals. For lubricated surfaces, it decreases nearly to 50 zJ. Based on this energy theory, different models were established, depending from different parameters, such as surface energy, the asperity radius and normal load⁵³ as presented on Figure 2.14.

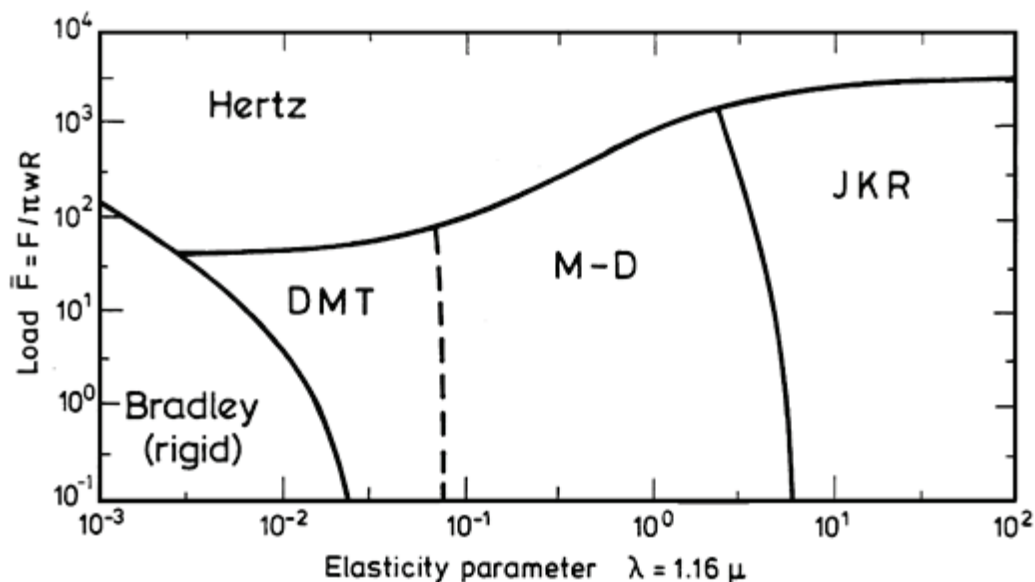


Figure 2.14: Adhesion model in function elasticity and load parameters

⁵² Butt et al. (2003)

⁵³ Johnson (1998)

The parameter λ is calculated with the reduced elasticity modulus E^* , asperity radius R , r_0 and surface energy w :

$$\lambda = 1.16 \cdot \mu = 1.16 \cdot \frac{R \cdot w^2}{E^{*2} \cdot r_0^3} \quad (2.25)$$

The parameter μ is called Tabor parameter. As the asperity radii from turned, grinded, milled and lapped surfaces are considered to be established between 10 and 200 μm ,⁵⁴ μ belongs to the interval [0.21, 0.57]. These parameters have a high impact in determining which adhesion model can be used for the normal load. Among three adhesion components, normal and tangential loads are the most important. The third aspect, hysteresis is treated in the next subsection.

2.4.4 Hysteresis Phenomenon

Until now, the adhesion effects were treated as fully reversible phenomenon. Nevertheless, adhesive forces generate damages, changes in the boundary layer through tribochemical processes and leading to energy loss.⁵⁵ Last mostly used adhesion models – DMT and JKR – models are quite different for determining the dissipated energy. Wang et al. measured this dissipated energy⁵⁶ by means of molecular dynamics (MD) models and stated that adhesion hysteresis becomes higher for decreasing Tabor parameter. Adhesion takes an essential part of the tribological behavior. Another essential phenomenon is the abrasion, which is most present at the contact beginning or run-in phase is not calculated yet in discrete models.

Previous theoretical parts treated solid mechanics, a part of each non- and lubricated tribological system. Following structural mechanics part, next subsection presents fluid mechanics necessary to describe lubricant flow.

2.5 Fluid Mechanics Theory

The second essential part in tribology concerns fluid mechanics, describing the behavior of the lubricant present between two solids. This part takes into account the description of laminar and turbulent flows, but no shear damages when the film thickness becomes too thin or cavitation effects.

⁵⁴ Robbe-Valloire (2001)

⁵⁵ Rimai et al. (1995)

⁵⁶ Wang et al. (2012)

2.5.1 Theoretical Background

For the models taking into account fluid lubrication, basics on fluid mechanics are necessary to explain occurring phenomena. Fluid mechanics is also modeled with the continuous mechanic approach and considered as a viscous structure. Claude Navier and George Gabriel Stokes described fluid movement using the three following equations:

$$\frac{\partial \rho}{\partial t} + \vec{\nabla} \cdot (\rho \vec{v}) = 0 \quad (2.26)$$

corresponding to the mass conservation,

$$\frac{\partial (\rho \vec{v})}{\partial t} + \vec{\nabla} \cdot (\rho \vec{v} \otimes \vec{v}) = -\vec{\nabla} \rho + \vec{\nabla} \cdot \vec{\tau} + \rho \vec{f} \quad (2.27)$$

corresponding to the momentum equation and

$$\frac{\partial (\rho e)}{\partial t} + \vec{\nabla} \cdot [(\rho e + p) \vec{v}] = \vec{\nabla} \cdot (\vec{\tau} \cdot \vec{v}) + p \vec{f} \cdot \vec{v} - \vec{\nabla} \cdot \vec{q} + r \quad (2.28)$$

as energetic sight.

Formal enounced Navier-Stokes equations are leading to Reynolds generalized equations, considering flat surfaces, and laminar flow:

$$\begin{aligned} & \frac{\partial}{\partial x} \left(\frac{\rho h^3}{12\eta} \frac{\partial p}{\partial x} \right) + \frac{\partial}{\partial y} \left(\frac{\rho h^3}{12\eta} \frac{\partial p}{\partial y} \right) \\ &= \frac{\partial}{\partial x} \left[\frac{\rho h (u_a + u_b)}{2} \right] + \frac{\partial}{\partial x} \left[\frac{\rho h (u_a + u_b)}{2} \right] \\ &+ \rho \left[(w_a - w_b) - u_a \frac{\partial h}{\partial x} - v_a \frac{\partial h}{\partial y} \right] + h \frac{\partial \rho}{\partial t} \end{aligned} \quad (2.29)$$

This generalized Reynolds equation provides the relationship between lubricant film thickness and pressure. Consequently this is used for solving complex problems through the use of numerical software. However, simplified boundary conditions are required in order to solve it numerically. Typical two-dimensional problem of the “wedge effect” leads to following equation simplification:

$$\frac{dp}{dx} = 6 \cdot \eta_0 \cdot u_0 \left(\frac{h - h_m}{h^3} \right) \quad (2.30)$$

where p is the pressure, η_0 dynamic viscosity, h the lubricant film thickness, h_m maximal lubricant film thickness and u_0 the sliding velocity. Pressure field is displayed on Figure 2.15

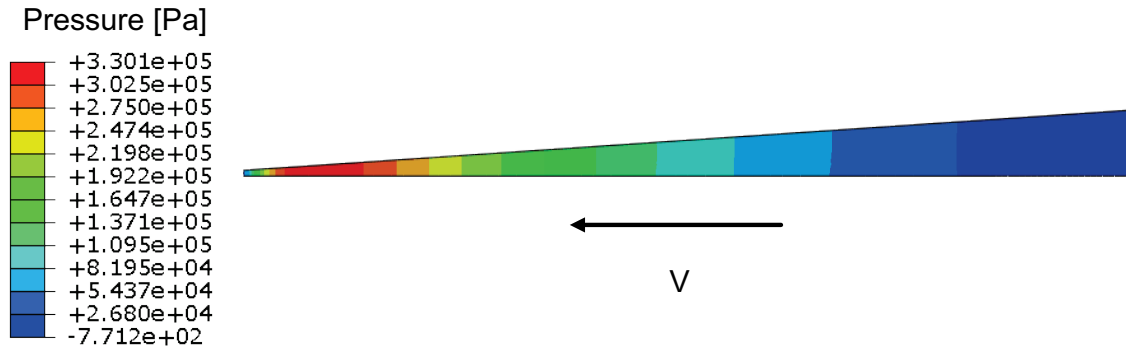


Figure 2.15: Hydrodynamic pressure distribution in a pad bearing

2.5.2 Fluid Compressibility, Newtonian fluid and Thermal Effects

One property of the fluid concerns its compressibility, and conventional lubricants are considered as incompressible. Nevertheless, when high pressure is applied to them, a non-neglectable compression phenomenon is observed. This is the case for liquids and also concerns the gases which are much more sensitive to such compressibility phenomena. This elastic behavior is important if small fluid films are investigated as it could lead to film break. The relationship between fluid volume and temperature can be described as follows:

$$V_m = C_1 + C_2 \cdot T + C_3 \cdot T^2 - C_4 \cdot p - C_5 \cdot p \cdot T \quad (2.31)$$

using five empirical constants C_1 to C_5 , the fluid temperature T and pressure p . V_m represents the molar volume. An additional fluid property concerns its relationship between resulting shear stress and velocity observed in the fluid. When this relationship is linear, the fluid follows the Newtonian rule and the fluid is called Newtonian Fluid and described by the Newton-Navier's law:

$$\tau = \eta \cdot \frac{dv}{dz} \quad (2.32)$$

where τ represents the shear stress, η the dynamic viscosity and $\frac{dv}{dz}$ the velocity evolution. Presented models (s. chapter 4) are based on two lubricated sliding

surfaces. Solid sliding is initiating a lubricant flow between both surfaces, leading to appearing fluid shear and pressure.

A further important parameter concerns the thermal behavior of fluids. They are affected as all other materials by radiation and conduction effects. In addition to this, convection phenomena are present and have quite often the most important influence on the fluid temperature. For the tribological effects studied in present work, thin films imply to investigate the influence of both conduction and convection effects. Conduction is described through next equation and consists in energy flow through contact:

$$Q = -\lambda \cdot (T_f - T_i) \quad (2.33)$$

where T_f and T_i represent final and initial temperatures respectively. Q is the energy exchange whereas λ is the conduction factor. On the other the convection as a quite similar relationship but the energy transfer is realized through the fluid molecule movements:

$$Q = h \cdot (T_f - T_i) \quad (2.34)$$

where the only difference from equation (2.33) concerns the convective constant h .

2.5.3 Fluid Flow and Viscosity Relationships

Two regimes are present in fluid flows, the laminar and turbulent. These regimes are strongly influenced by the characteristic hydraulic length L_h , the dynamic viscosity η , the density ρ and fluid velocity v as shown through following expression:

$$R_e = \frac{\rho v d}{\eta} \quad (2.35)$$

R_e is called Reynolds number and determines which regime is observed in the fluid domain. For high values (> 3000) the regime is turbulent whereas for low values (< 2000) the regime is laminar (also called Stokes flow). Domains present between both enounced Reynolds values, the regime is called transient regime but flow is considered as laminar.

Fluid velocity is directly linked to the hydraulic diameter and does not really vary during the sliding process. The dynamic viscosity encountered in elasto-hydrodynamic domains can vary through different occurring pressures and temperatures. That is one reason why laminar flow predominates in such conditions.

The pressure dependence of the dynamic viscosity was observed by Barus⁵⁷ and can be described by using following relation:

$$\eta(p) = \eta_0 \cdot e^{\alpha p} \quad (2.36)$$

where η_0 is the dynamic viscosity when the fluid is at room pressure (10^5 Pa) and p is the pressure of the new condition. The coefficient α is an empiric constant calculated through experimental tests.

This law highlights the increasing viscosity for rising pressures. This is explained through a closer gap between molecules. As a consequence higher forces are required to initiate any movement, an effect transduced with a higher viscosity.

A comparable relationship is observed with the temperature, influencing on the other way on the viscosity. Not less than twelve relationships were established, based on the investigation of Seeton.⁵⁸ For low temperature ranges, the most accurate according to Crouch and Cameron⁵⁹ is the Vogel equation

$$\eta(T) = a \cdot e^{\beta(T-c)} \quad (2.37)$$

where η is the viscosity at the temperature T . The coefficient a , β and c are formal constants established experimentally.

2.5.4 Thin Film Theory: Elastohydrodynamic (EHL)

Concerning thin fluid films, a difficulty occurs when the Reynolds equation (2.29) trends to lead to infinite pressures. That means that for mixed lubrication and EHL methods need correction factor also called flow factor¹⁵ to deliver acceptable outputs.

Elastohydrodynamic concerns hydrodynamic lubrication regimes where the lubricant film is contained between 0.025 and 5 μm . Basically, EHL represent cases where structure deformation is no negligible compared to film thickness. This lubrication domain corresponds to the transition from a conventional hydrodynamic regime to the mixed lubrication as shown on Figure 2.16.

⁵⁷ Dowson / Higginson (1977)

⁵⁸ Seeton (2006)

⁵⁹ Crouch / Cameron (1961)

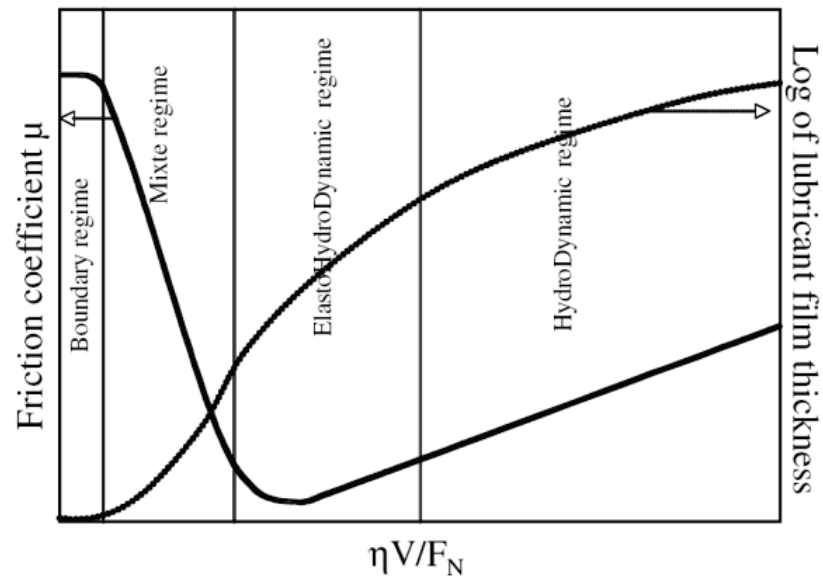


Figure 2.16: Stribeck diagram illustrating lubrication regimes of bush bearings⁶⁰

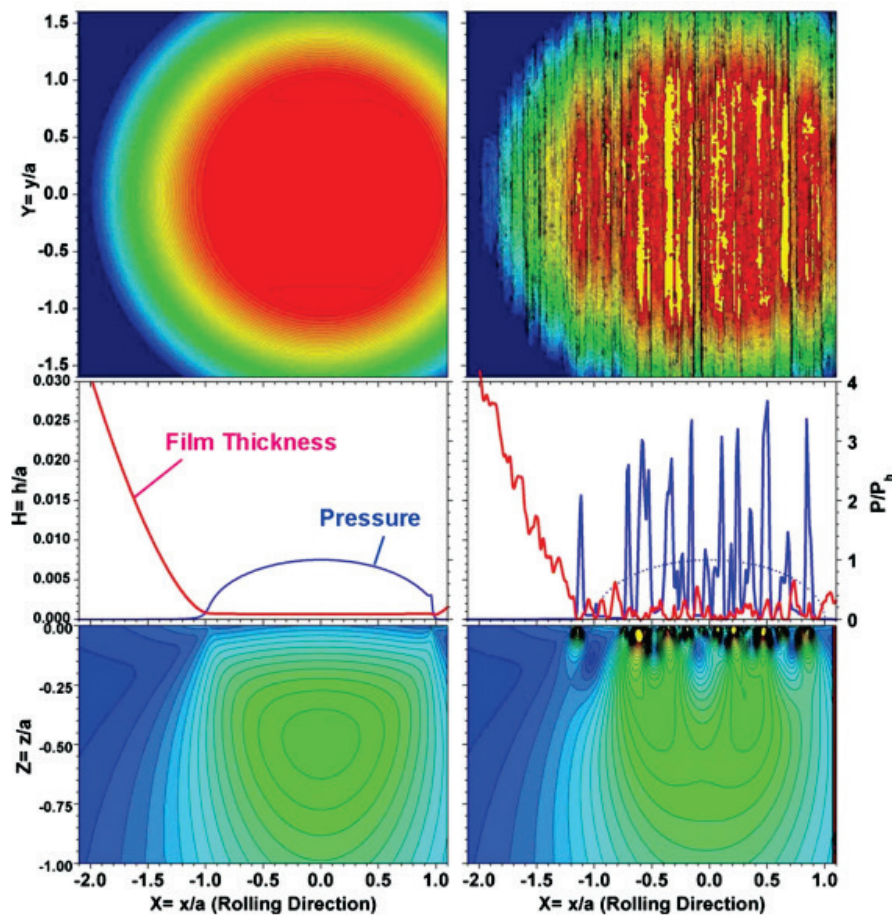


Figure 2.17: EHL pressure profile and dimensionless lubricant film thickness with smooth surfaces (left) and rough surfaces (right)⁶¹

⁶⁰ Mansot et al. (2009)

⁶¹ Ren et al. (2010)

Greenwood⁶² was a pioneer in the EHL domain and was the first scientist who coupled Reynolds and elastic deformation equations. Theoretical models were developed later on by Hamrock and Dowson⁶³ for applications such as rolling elements (bush or rolling bearings) with point or line contacts.

Typical EHL pressure and film thickness are plotted in Figure 2.17 for point contacts and steel-steel material pairings. In last work, investigations were made with smooth and rough surfaces. The pressure height can reach 4 GPa with a peak at the outlet of the fluid because the film thickness is at its minimum at this place. These analyses do not take into account surface roughness when fluid film breaks are occurring.

2.5.5 Impact of the Surface Roughness on the Fluid Friction

Generalized Reynolds equation is valid for flat and parallel surfaces, implying that roughness has a non-negligible impact on the fluid flow conditions. The equation becomes false whether the roughness slope is too large in comparison with the film thickness. The ratio h/\tilde{A} determines if the equation is valid or not. h represents the film thickness whereas \tilde{A} is the composite standard derivation of surface height. In the case of a ratio larger than six, the equation is considered as false.⁶⁴

In such conditions, Cheng and Patir⁶⁵ have developed a flow model, an approach that takes into account surfaces' roughness with additional factors used in the Reynolds equation for analytical models. Nevertheless these so called flow factors were calculated by means of static numerical simulation based on random generated rough surfaces⁶⁶ (s. Figure 2.18)

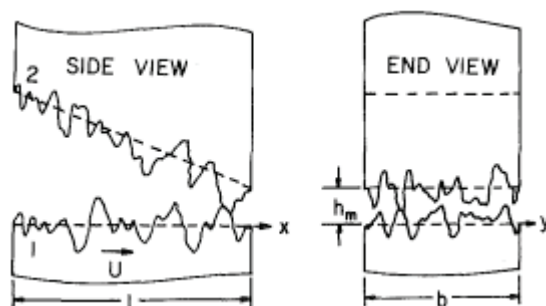


Figure 2.18: Model including roughness in hydrodynamic systems⁶⁶

This highlights the potential residing in the development of a three dimensional model in which the real roughness is taken into account for quantifying the phenomenon occurring in the contact.

⁶² Greenwood (1972)

⁶³ Hamrock / Dowson (1975)

⁶⁴ Bhushan (2002) pp. 499

⁶⁵ Patir / Cheng (1978)

⁶⁶ Patir / Cheng (1979)

One further problem consists in having cavitation effects. This typical effect is caused by rough profiles initiating low pressure fields or pressure loss as displayed on Figure 2.19.

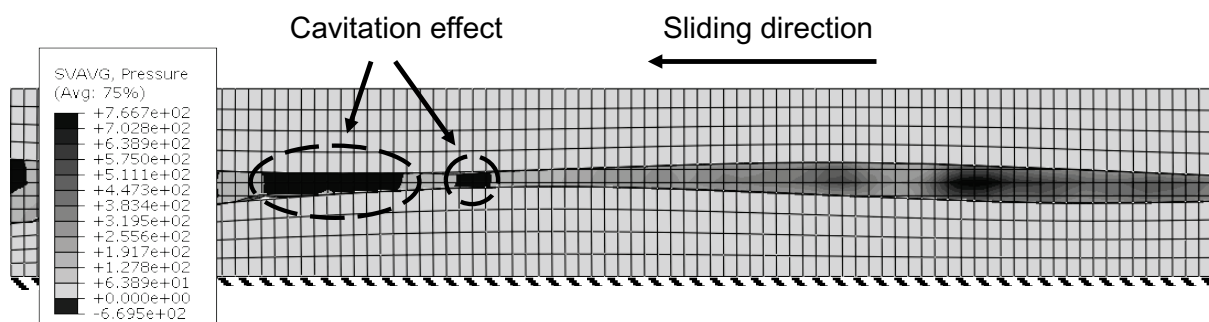


Figure 2.19: Pressure field (in MPa) of the fluid separating two rough surfaces

Cavitation consists in having gas bubbles into the lubricant leading to hardly unknown effects: they may induce higher pressure forces or lower ones. These gas bubbles can appear on the one hand in case of brutal pressure loss, or in case of multiple fluid phases present in the investigated system. Taking in account such effects increases highly the complexity of the model as it finally leads to a multi-phase modeling. On this account, current assumption is to neglect cavitation effect as they are less important in comparison with previous effects.⁶⁷ The next subsection displays which numerical methods can be used to solve complex problems of fluid structure interactions, taking into account the most relevant parameters.

Theories treated until now have to be implemented in order to solve complex problems. On this account, following section describes ways how to solve theoretical problems by means of numerical schemes.

2.6 Numerical Methods used in Tribology

In order to predict and describe tribological behavior of any system, models need to be implemented. Once these are implemented into physical and mathematical models, numerical methods can be needed to solve them. In the present work, models are mainly described by means of complex and numerous non-linear partial differential equations. The solutions are mostly unknown, which is to discretize the problem. As a consequence, two possibilities exist to verify if the mathematical model deliver a realistic solution:

⁶⁷ Tzeng / Saibel (1967)

- Validation with a real valid experimental model
- Check the convergence of the model

2.6.1 Methods used for Spatial and Temporal Discretization

In order to solve cited equations of structural and fluid mechanics, three main methods are available.⁶⁸ Table 2.7 summarizes the advantage and inconvenient for each method:

- The finite Difference Method

The finite difference method consists in approaching differential equations displayed in sections 2.3 and 2.3.5 with Taylor developments using directly the definition of the limit calculation. Main issue related to this method is the difficulty to manage complex boundary condition and especially Newmann type. Furthermore, the method is limited to simple geometries. The only advantage of this method is its calculation efficiency.

- The finite Volume Method (FVM)

For the finite volume approach, boundary mesh motion is described by means of the lagrangian equation of motion. This formulation consists in discretizing a fluid domain into mesh composed of elements. Then with equations of continuity at their bordure, equations enounced below are solved used the finite volume method for at each point called node of the concerned element. The fluid flow description is achieved by means of the eulerian equation of motion.

As enounced in chapter 2.3.5, this method is used in most of the Computational Fluid Dynamics – CFD – programs due to the solving efficiency. One disadvantage is the difficulty of managing fluid mesh topology changes occurring in the model and leading to the use of the finite element method.

The finite volume method consists in solving the conservative equations in using elementary volume of the investigated volume. Well adapted for linear fluid simulations, the limit resides in the stability and convergence in case of high non-linearities. For this reason the finite element method is used for structural mechanics where geometries are more complex and deformable.

- The finite Element Method (FEM)

A more CPU intensive method also used in structural mechanics can be used for solving the same systems of equations. With this approach two formulations are possible, the Lagrangian and the Eulerian. The first one consists in discretizing directly an existing fluid part whereas the second one consists in discretizing a

⁶⁸ Goncalvès (2005)

domain and afterwards define which element is initially defined as material and which not. This approach is mostly used for applications with high deformations such as high plastic deformations. The advantages of both methods will be discussed in the next section (see 2.7) where contact algorithms are discussed.

Table 2.7: Advantage and inconvenient of each resolution method

Method	Advantage	Inconvenient
Finite difference method	<ul style="list-style-type: none"> • Efficient calculation time 	<ul style="list-style-type: none"> • Only possible for simple geometries • Inadequate for Neumann boundary conditions
Finite volume method	<ul style="list-style-type: none"> • Complex geometries can be handled • Possibility to handle Neumann boundary conditions • Efficient computational time compared to FEM 	<ul style="list-style-type: none"> • Less theoretical results on convergence behavior
Finite element method	<ul style="list-style-type: none"> • Complex geometries • Numerous results on convergence 	<ul style="list-style-type: none"> • Huge computer resources required

Each listed method can solve given equations by means of two main numerical schemes called explicit and implicit. When taking an example of thermal calculation, first method solves spatial and temporal sight

$$\frac{\partial T}{\partial t} = \alpha \frac{\partial^2 T}{\partial x^2} \quad (2.38)$$

where both parts can be displayed

$$\left(\frac{\partial T}{\partial t} \right)_i^{n+1} = \frac{T_i^{n+1} - T_i^n}{\Delta t} \quad (2.39)$$

and

$$\left(\frac{\partial^2 T}{\partial x^2}\right)_i^{n+1} = \frac{T_{i+1}^{n+1} - 2T_i^{n+1} + T_{i-1}^{n+1}}{\Delta x^2} \quad (2.40)$$

resulting to

$$T_i^{n+1} = \lambda T_{i-1}^n + (1 - 2\lambda)T_i^n + \lambda T_{i+1}^n \quad (2.41)$$

defining » as $\alpha \frac{\Delta t}{\Delta x^2}$. The Implicit scheme, bases on the Newmark theory⁶⁹, extended by Hilber, Hughes and Taylor (HHT),⁷⁰ explained using following differential equation results to:

$$(1 + 2\lambda)T_i^{n+1} - \lambda(T_{i-1}^{n+1} + T_{i+1}^{n+1}) = T_i^n \quad (2.42)$$

This underlines the problem of the matrix inversion in order to get T^{N+1} . As a consequence, if studied geometries imply a high number of degrees of freedom (DoF), the investigations will be highly inefficient, especially for a high number of iterations (high non-linearities) implying to inverse the stiffness matrix for each iteration. In such cases, the use of the explicit scheme will be more appropriate, as it offers also better abilities to parallelize the calculation.

Nevertheless, the explicit scheme becomes obsolete if the investigation time of the analysis becomes too high or if the element characteristic length L_e becomes too small. To avoid last case, elements should have a large characteristic length as the convergence criterion depends highly on this parameter as displayed in next equation

$$\Delta t = \text{MIN} \left(L_e \sqrt{\frac{\rho}{\lambda + 2\mu}} \right) \quad (2.43)$$

where » and μ represents the Lamé coefficients and ρ the material density. Explicit solving is also not well adapted for quasi-static analyses (necessity to compute the transient and static domain). Next table (see Table 2.8) summarizes the optimal use of both integration schemes.

⁶⁹ Newmark (1959)

⁷⁰ Hilber et al. (1977)

Table 2.8: Application of the implicit and explicit schemes for the FEM

Integration scheme	Advantages	Inconvenient
Implicit	<ul style="list-style-type: none"> • Possibility to achieve quasi-static analyses • Possibility to solve non-linear problems • Method always stable: convergence is always reached 	<ul style="list-style-type: none"> • Computational time depending on the stiffness matrix • High time increments lead to high number of iteration to reach equilibrium • Convergence not always reached • Not adapted for quasi-static analyses
Explicit	<ul style="list-style-type: none"> • Possibility to model huge non-linearities • Better ability to model huge system (no matrix inversion required) 	<ul style="list-style-type: none"> • Time increment dependent from mesh elements and material density

2.6.2 Multibody Dynamics Simulations

Multibody systems (MBS) are mostly simulated by using rigid bodies. This implies that the degrees of freedom or applied forces can be restrained to the points where there are connections between solids. Used to describe whole systems, this step is one of the last of the simulation process used in the product engineering process. Such simulations are, if they do not get appropriate boundary conditions, not precise enough to quantify the behavior of a product. This is firstly due to the flexibility present in real systems and to the impossibility of taking into account material damping.

Taking into account flexibility is since 5 years possible through the use of modal description of a meshed body. To achieve this, a previous modal analysis of the flexible body has to be realized in order to calculate their eigenfrequencies and eigenmodes⁷¹. The limitation of this method is that it can only be applied with linear

⁷¹ Bosseler et al. (2009)

deformation (only elastic deformation). For the last reasons and for accurate descriptions of complex or detailed tribological problems, this approach may not be the appropriate one.

2.6.3 Contact Modeling

Contact definition, one of the most important techniques used in the present work can be achieved through different algorithms for the normal contact behavior.⁷² They are all displayed in Table 2.9. Two classes are defined, the softened and hard contact. Only available for implicit solving, the softened contact way allows the contact to increase the convergence whereas the hard contact is increasing the CPU-efficiency. Different softened formulations are available but not treated here:

- linear formulation
- tabular formulation
- geometric scaling (active for after overclosure)
- exponential law

These algorithms influence the precision of the contact parameters, the convergence and consequently the computing time. This finally implies the contact definition to be set up to optimize the simulation time in function of the needed quality of the results. Contact definitions are from high interest in tribological investigations as they are responsible of the whole system's behavior. The goal is not to have a too high penetration depth when contact occurs in order to keep an acceptable precision. For this reason a hard contact is adapted.

Tangential behavior is also important as it manages the friction behavior of the studied system. Two possibilities are used to initiate sliding between two bodies in contact:

- Define a sliding coefficient μ giving a relationship between normal and tangential load
- Define a critical shear stress factor \dot{A}_{crit} giving the limit for the sliding initiation

Both criterions lead to a constant limit for the sliding initiation. The advantage of the second criterion compared to the constant sliding coefficient is that the normal load has also an influence on the critical shear stress initiation meaning that the resulting calculated friction coefficient is not constant.

⁷² Dassault-Simulia (2011a)

Table 2.9: Normal contact models used in conventional hard contact

Contact algorithm	Advantage	Inconvenient
Penalty method	CPU-Time	Accuracy
Lagrange method	Contact error Convergence	CPU-Time
Augmented-Lagrange method	Contact accuracy	Convergence CPU-Time
Rough contact	Convergence CPU-Time	Not tangential displacement possible
No separation	Convergence CPU-Time	No separation or relative movement possible

A next essential parameter for contact precision is the contact surface definition. Three variants are available ranked from the less up to the most precise type:

- Node to surface
- Points to surface
- Surface to surface

The surface to surface contact is the most accurate variant which leads to the lowest overlapping and penetration. There are further contacting possibilities between rigid and flexible bodies but are not treated here.

For tribological contacts, multi-physical problem are also encountered in contacts, such as thermal exchange (conduction and convection) or heat generation. For these types of interactions, no complex algorithms are used, a definition on the part of frictional energy converted into heat has to be defined. There is also the parameter heat proportion between the contacting parameters

For the thermal exchanges, convection in form of film conditions and convection coefficient are to be defined. The contact conduction has also to be defined in accordance with the literature and contacting solids.

2.6.4 Methods Application

The available CPU technology enables nowadays solving tasks having a high level of complexity and keeps an acceptable precision. Preceding equations are implemented in existing commercial software (ANSYS CFX, Abaqus CFD, COMSOL, ...) and solved using two previously presented approaches. Most of the time, the finite volume method is used for a reason of lower level of calculation time. But for more complex problems, especially non-linear ones, the finite element method is used. These are mainly present in contact simulations. A mixed lubricated system beholds the particularity of having contact status that are continuously changing between both solids and also between fluid and solid. As a consequence, conventional EHD modeling which is normally not a problem for the finite volume method as long as the fluid domain remains continuous is submitted to discontinuities of the fluid mesh, a problem which cannot be managed by the usual meshing method. The reason resides in the high non-linearities requiring the use of explicit resolution schemes and different strategies to keep good results unless high potential of mesh distortion. Next part gives an overview on the different fluid structure coupling methods as well as the management of the mesh deformations.

Solving a problem numerically has been explained here, schemes working for fluid mechanics on the one hand and for solid mechanics on the other hand. Nevertheless, numerical difficulties remain if fluid-structure couplings are required; next part treats and explains potential couplings being used for this.

2.7 Fluid Structure Coupling in Numerical Methods

Coupling fluid and structure domains are always a big challenge if the deformations need to be taken into account. Occurring difficulties are introduced by the different observation ways of the investigated entities: the fluid is described using the Eulerian method whereas the solid is described by Lagrange parameters. As a consequence, for mixed lubricated systems, three meshes are interacting: one fluid mesh and two solid meshes.

2.7.1 Conventional CFD FSI-Coupling

Conventional CFD methods couple fluid and solid meshes together at their boundary nodes leading to the continuity of the transmitted force. This coupling began with a one way method consisting in transmitting the fluid pressure to the structure but no answer from the structure was taken into account. Benra compared both coupling

way to quantify the differences in results and computing time.⁷³ When the deformations do not impact too highly the fluid flow, a one-way coupling can be used as the computing time gain is of more than 50% comparison of the two-way computing time.

For complex tribological problems taking into account lubricant flows, a two-way coupling is required as the structure deformation can change significantly the fluid flow.

This allows a better precision due to the concordance of both fluid and solid boundary conditions. At each node the force can be transmitted from the fluid to the solid and inversement. Three coupling algorithms can be used for that, the iterative quasi-direct and the direct resolution.⁷⁴ Due to high computational costs, equations are mostly solved iteratively. Furthermore, this “strong coupling way” leads more easily to convergence as it is more stable.⁷⁵

In mixed lubricated systems, both bodies surrounding the lubricant are in relative motions. Since the meshes are connected this movement will lead to fluid mesh distortions and consequently to numerical error. To limit this effect, different approaches were developed two of them are explained in next subsection.

2.7.2 Mesh Distortion Management

Two streams can be used from the available approaches to override the difficulty of large deformations. The first one consists in having a direct coupling of fluid and structure mesh. As a consequence the fluid mesh is moving and following the structure. In this case, adapting the mesh quality is required to keep acceptable results during the calculation. This is done when adaptive meshing tools are used. The most well none method bases on the studies of Hirt⁷⁶ and called Arbitrary-Lagrangian-Eulerian Method (ALE). It consists in having a mesh distortion control which takes the decision when a remeshing phase is required.

After first applications to high structural deformations, ALE formulation was used to manage fluid mesh distortion for typical FSI.⁷⁷ Also used for compressible fluid dynamics.⁷⁸ This formulation delivers realistic results, especially for biphasic FSI like sloshing analyses.⁷⁹ This remeshing uses the boundary nodes that are kept and

⁷³ Benra et al. (2011)

⁷⁴ Tezduyar et al. (2006)

⁷⁵ Hübner et al. (2010), Schäfer et al. (2008)

⁷⁶ Hirt (1971)

⁷⁷ Donea et al. (1982)

⁷⁸ Kcharik et al. (2007)

⁷⁹ Ozdemir et al. (2009)

generates a fully new mesh in the volume as displayed in Figure 2.20. This method can also be combined to refinement rules being defined by the user, in order to reduce the element size at critical places where accuracy is required.⁸⁰

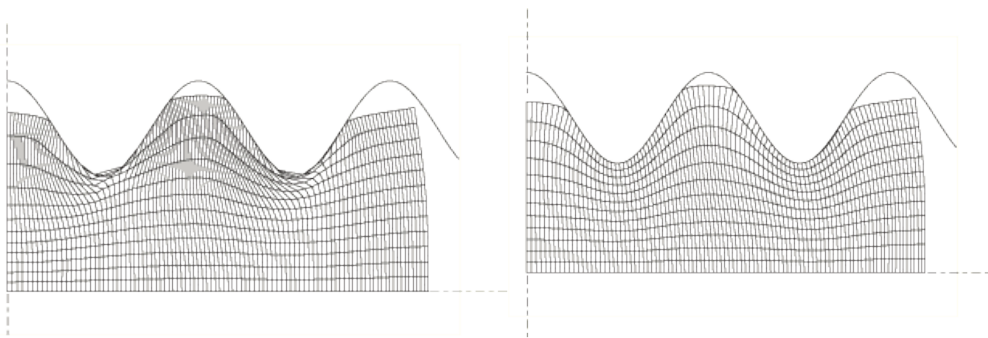


Figure 2.20: Without remeshing (right) and with the remeshing algorithm (left)⁸¹

Using only the ALE formulation, Nowicki⁸² modeled mixed lubricated systems but was confronted to the problem of fluid domain separation. Especially this case cannot be modeled directly with ALE method, as the fluid domain cannot get new discontinuities: for instance, a full hydrodynamic condition cannot be replaced with a solid-solid interaction.

On this account, new approaches were implemented, from them the fully Eulerian approach, the coupled Eulerian-Lagrangian Method. Vanloon⁸³ compared different methods for such problems and concluded that this method was not adapted for high deformations like those observed in mixed lubrication.

In order to overcome these limitations, previous approach was used and firstly applied on airbags opening simulation.⁸⁴ This method was also adapted to parachute simulation by Wang,⁸⁵ showing that such high non-linear problems can be modeled using this approach as well as huge fluid domain deformations.

Principle of this method bases on the volume of fluid (VOF) theory⁸⁶ and on the Eulerian description. A static mesh (Eulerian body) is used to model the fluid whereas a conventional Lagrangian mesh discretizes both bodies. The particularity of this mesh is that, only one Eulerian mesh allows defining different material properties. No node displacement is calculated even though material flow through the

⁸⁰ Garcia et al. (1999)

⁸¹ Dassault-Simulia (2011a)

⁸² Nowicki (2008)

⁸³ Vanloon et al. (2007)

⁸⁴ Moatamedi et al. (2006)

⁸⁵ Wang et al. (2008)

⁸⁶ Hirt / Nichols (1981)

element. Difference between a conventional fluid mesh (also Eulerian mesh) is that the Eulerian mesh is not connected to the Lagrangian one. The contact takes place between the “material” of the Eulerian mesh and the solid mesh as exposed on Figure 2.21. Blue elements represent fluid elements whereas red ones are void.

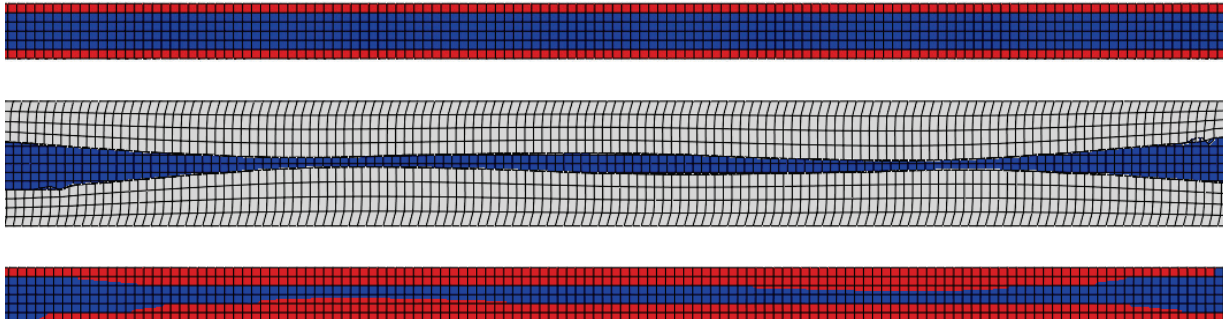


Figure 2.21: Initial state of the contact (on the top)⁸⁷

Method’s principle is that the material is defined in the Eulerian mesh also modeled by a Lagrangian mesh (in the background) which is remapped at every increment on the Eulerian explaining why this method is also called Coupled-Eulerian-Lagrangian method. The contact definition is based on a material criterion at each of the solid node as shown on Figure 2.22.

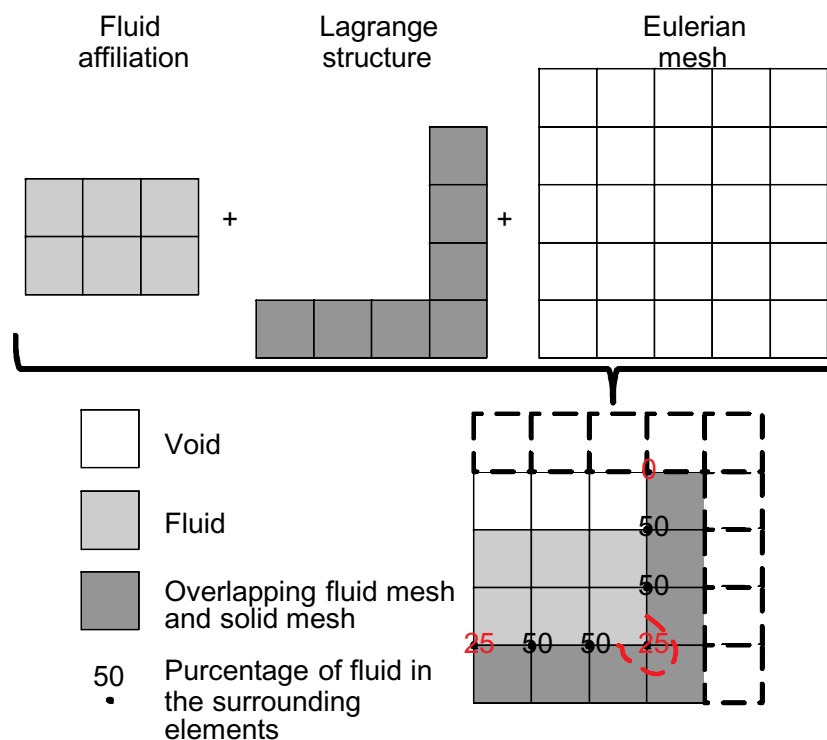


Figure 2.22: Contact definition of the CEL method⁸⁸

⁸⁷ Albers / Lorentz (2011)

⁸⁸ Albers / Lorentz (2012)

The criterion defining when a contact occurs depends on the surrounding elements of each solid node. If more than 50% of material is around this node, a contact occurs between the fluid and the solid. Last illustration highlights the problem of fluid penetration which takes place when only one full element surrounds a node, in case of angled edges.

2.7.3 Thermal Exchange Between Fluid and Structure

Thermal coupling between fluid (see 2.5.2) and solids (2.3.3) is displayed here. Thermal exchange is essential for the determination of friction behavior. This is not a problem in conventional CFD analyses,⁸⁹ as the fluid mesh is directly linked with the solid mesh. That means that the thermal coupling can be achieved like mechanical coupling. Some applications were done in the research field of bearings, where the temperature field was calculated.⁹⁰ Nevertheless, thermal flow such as conduction or convection need to be analyzed to decide which or if both have to be modeled. This is dependent of the average film thickness, the ratio between conducted heat and convected heat can be calculated. For line contacts, the conduction heat is expressed

$$Q_{cond} = \int_0^L \lambda \cdot \frac{\Delta T}{l} \cdot \frac{x}{h} dx \quad (2.44)$$

» representing the conductivity of the lubricant, T the temperature rise, l the width of the contact, h the hydrodynamic film thickness and x the length position. At the same time, convection heat is described

$$Q_{conv} = \frac{U \cdot h \cdot \rho}{2} \cdot C_p \cdot \frac{\Delta T}{2} \quad (2.45)$$

where U is the surface velocity, ρ the lubricant density and C_p the specific heat of the lubricant. Consequently, the ration conduction/convection can be expressed as follows

$$\frac{Q_{cond}}{Q_{conv}} = \left(\frac{\lambda}{\rho \cdot C_p} \right) \cdot \frac{2l}{U \cdot h^3} \quad (2.46)$$

with the lubricant diffusivity ζ

⁸⁹ Redlich (2002), Knoll et al. (2000)

⁹⁰ Jackson / Green (2008)

$$X = \frac{\lambda}{\rho \cdot C_p} \quad (2.47)$$

This underlines the impact of the lubricant film thickness has the most impact on the ratio, followed by the contact length and all other parameters having the same weight. This is highly dependent of the lubricant film thickness. The so called heat generation (highest contact temperatures) occurring in EHL are calculated by means of the friction energy dissipated in the contact

$$Q = \mu \cdot F_N \cdot |U_A - U_B| \quad (2.48)$$

with Q the generated heat, F_N the normal load and μ the EHD friction coefficient. This hydrodynamic friction can be calculated with following formula

$$\mu = \frac{\iint_S \tau \cdot dx \cdot dy}{\iint_S p \cdot dx \cdot dy} \quad (2.49)$$

p representing the fluid pressure and \dot{A} the lubricant shear at the contact surface. A part of the friction generated heat is transferred through conduction and another part through convection. The temperature rise can then be calculated based on the energy equation (see both equations 2.36 and 2.37). These simulations are possible using CFD programs as the temperature rise occurs in the simulation time window.

On the contrary, the CEL method, which does not couple both meshes, has also very short investigation time due to the explicit solving⁹¹ and does not have the thermal coupling implemented. The reason is that low investigation time decreases the interest of taking into account transient thermal exchange between fluid and structure as well as in the fluid itself. The reason for that is that these exchanges are principally longer than the time window used for explicit investigations. On this account, this limitation has to be investigated.

Nevertheless, for mixed lubrication phenomena additional thermal energy coming from the solid-solid friction needs to be taken into account. This shows the necessity to implement this coupling to estimate the real lubricant temperature as well as the flash temperatures. In order to analyze impacts coming from different parameters, and for a question of high computational time, model calculation need to be reduced.

⁹¹ Albers / Lorentz (2010c)

This can be done by means of statistical approaches, as displayed in next subsection.

2.8 Design of Experiments (DoE) and Use in Numerical Simulations

Statistical approaches are used to support numerical and experimental investigations of system's models. This is due to the huge investigation time sometimes required for both techniques. As a result, only a small number of measuring/calculation points are needed to describe a complete testing window in which the models are valid. To achieve an efficient parametric study, a design of experiment (DoE) is needed.

The design of experiment method consists in establishing test plans (numerical or experimental or both) in order to minimize the quantity of tests to be done and so the costs by identifying which is the relevance of varied parameters. The principle of this structured and organized method bases on several algorithms listed in the next subsections.

2.8.1 Full Factorial Method

The method consists in taking the considerate most important parameters of the system and analyzes their impact on the variable which is analyzed. For instance, three factors (average roughness R_a , sliding velocity V_s , and film thickness h) and their impact on the maximal contact pressure p can be considered. For a two level scheme, two experimental measure points per factor, 2^3 combinations are possible and the pressure can be expressed as follows⁹²

$$\begin{aligned} p(\beta, R_a, V_s, h) = & \beta_0 + \beta_1 \cdot R_a + \beta_2 \cdot V_s + \beta_3 \cdot h + \beta_{12} \cdot R_a \cdot V_s \\ & + \beta_{13} \cdot R_a \cdot h + \beta_{23} \cdot V_s \cdot h + \beta_{123} \cdot R_a \cdot V_s \cdot h \end{aligned} \quad (2.50)$$

Principle of the full factorial method is to define the eight coefficients ² which establish the relationship between the pressure and all three factors. For this, each factor is normalized, taking -1 for its minimum and +1 for the maximum. Finally, a system of eight equations is solved. The following step is to classify the factors through their importance. A two-level design expresses only linear relationships between the response and factors. On this account, to have a quadratic relationship, a three-level design is required. The general rule is that the polynomial degree of the relation is one layer inferior as the design level.

⁹² Institute SAS (2005)

Getting the same conclusion without this method would need much more experimentation as more than two measurements would be required per factor.⁹³

2.8.2 Fractional Factorials

This method is a reduction of the full factorial. The motivation to use this type of scheme resides in the limitation of run achievement. The concept is here to use only a fraction of the runs established in a full factorial scheme.

The determination of the fraction to use is highly dependent on the interactions between factors as well as reliability of the runs themselves.⁹⁴ The extent of fractionation has to be decided in function of interactions between factors and reliability. For instance, if the fractionation is of 1/2, for three factors and a two-levels factorial design, the number of runs will be of 2^{3-1} and so four trials are required instead of eight.

2.8.3 Screening Experiments

A further step in the runs reduction is the so called screening concept. In this model, it is assumed that all interactions between the factors are irrelevant. Developed by Plackett and Burman,⁹⁵ this method was extended by Taguchi in order to take into account two way interactions at the same time. For instance, instead of doing 2^{11} runs with a conventional two-level full factorial scheme with 11 factors, this method will take only 12 runs. Nevertheless, this method is only adapted for case in which the main effects are not numerous.

2.8.4 Response Surface Method (RSM)

Well adapted, because it leads to a good visualization, to study the impact of two factors on the response, this method is also adapted for a higher number of factors. A response surface is concretely a polynomial function determined after one or more full-factorial runs. This polynomial function establishes a relationship between the response and the varied factors as shown on Figure 2.23.⁹⁶

⁹³ Leslabay (2009)

⁹⁴ NIST (2012)

⁹⁵ Plackett / Burman (1946)

⁹⁶ Lin / Chou (2002)

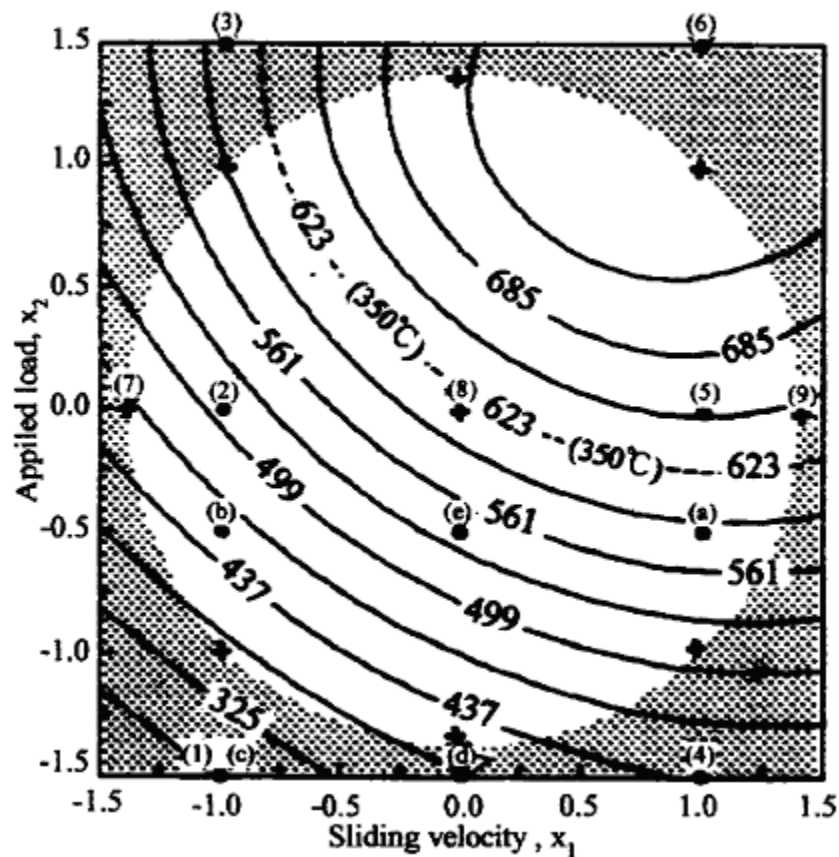


Figure 2.23: example of response surface

Last figure showed the variation of contact temperature displaying the response, in function of the sliding velocity and applied load. This method allows a linear, quadratic or cubic description.

Nevertheless, when the factor number and the complexity (when the model is not linear, in most cases) are too high, conventional RSM induces a too high number of runs to be done. On this account, different variants were introduced: central composite design (CCD).⁹⁴

- Circumscribed (CCC): requires 5 levels for each factor
- inscribed (CCI): requires 5 levels for each factor
- face centered (CCF): requires 3 levels for each factor
- Box-Behnken designs: requires 3 levels for each factors

Advantageous to decrease the experimental and numerical costs, the RSM also has limitations such as its sequential costs. Another point concerns its robustness and resistance to noise for the sensitive models, a problem solved by Taguchi.⁹⁷

⁹⁷ Ray (2006)

2.8.5 Selecting a DoE Strategy

The DoE method has to be selected in function of the objectives and input parameters. A summary of the application of previous enounced methods is done in Table 2.10.

Table 2.10: Design selection strategy⁹⁴

Number of factors	Comparative objective	Screening objective	Response surface objective
1	1-factor completely randomized design	–	–
2-4	Randomized design	block Full or fractional factorial	Central composite or Box-Behnken
5 or more	Randomized design	block Fractional factorial or Plackett-Burman	Screen first to reduce number of factors

Generally, in case of high number of factors, it is better to begin with a screening operation of the experimental/numerical setup, to reduce the number of irrelevant number of factors.⁹⁸

After the description of methods and tools to be used in theoretical mixed lubrication analyses, a validation part is exposed in next subsection, explaining how experimental devices can contribute to these investigations.

2.9 State of the Art: Experimental Investigations in Tribological Systems

Investigations achieved to correlate surface topography with the friction behavior are presented in this subsection. Different scales were used, going from the macroscopic scale until the nano scale, using atomic force microscopy (AFM), focused ion beam (FIB) and transmission electron microscopy (TEM) in order to define the crystal and chemical composition of the contact layers.⁹⁹

⁹⁸ Resource Engineering Inc. (n.d.)

⁹⁹ Reichelt et al. (2006)

2.9.1 Investigation on Pin-On-Disk Devices Type

Usual device in tribology is the tribometer pin on disc, with which a contact states between a pin (different profiles type) with a planar surface (rotating disk). Used for non-lubricated and lubricated contacts, it allows mainly simulating sliding contacts.

Kubiak and Mathia¹⁰⁰ investigated the impact of roughness on the contact interfaces in different fretting contacts. Tests were carried out in dry and boundary lubrication regimes. Quadratic response surface were expressed for both regimes. Comparable tests were made with one ceramic (Al_2O_3) and a structural steel, in order to analyze the impact of adhesion on friction force.¹⁰¹ Comparable tests, made by Le et al.,¹⁰² stated experimentally that, when using a typical pin-on-disk facility, that the frictional coefficient between aluminium and steel increases in lubricated conditions with an increasing roughness. The reason was an increasing amount of asperity-asperity contact. Further works tried to correlate the three parameters average roughness R_a , kurtosis R_k and skewness R_{sk} with the friction coefficient of dry and lubricated contacts. This was done by Sedlacek et al.¹⁰³ In his paper they conclude that the friction coefficient of lubricated contacts get higher with increasing kurtosis and skewness, where the skewness has a much higher impact than the kurtosis.

Enounced experimentations are required in order to understand the phenomena happening in different tribological systems, here especially clutch and journal bearings.

2.9.2 Investigation of Clutch Systems

Gao investigated lubricated clutches and the impact of the surface roughness on the friction behavior.¹⁰⁴ She completed the experiment with a numerical model by means of the contact model of Greenwood and Williamson. Wet clutch are also set under investigation by Mäki in his PhD thesis where he concluded on following trends¹⁰⁵:

- Normal load has only a minor effect by conventional working temperatures
- Sliding velocity interferes highly on the transmitted torque
- Torque transmission happens mainly under mixed and boundary lubrication, so that the conventional lubricant properties have no real impact

¹⁰⁰ Kubiak / Mathia (2009)

¹⁰¹ Achanta et al. (2009)

¹⁰² Le et al. (2005)

¹⁰³ Sedlacek et al. (2011)

¹⁰⁴ Gao et al. (2002)

¹⁰⁵ Mäki (2005)

- Temperatures have high impact on the viscosity and so on the friction coefficient

Further statements were made on the useful experimental device to investigate clutch systems: special test rigs are required, as small scale tests are insufficient. Moreover, the three parameters torque capacity T , dynamic friction μ_d and ratio T/μ_d are the most relevant parameters for characterizing the friction properties of the fluid.

Many results such as the impact of the additives on the friction behavior were also found out as well as an evaluation of prediction capacity of a simulation model of clutches.

These kinds of tests are insufficient to fully understand the phenomena happening in the contact, on this account Märklund and Larsson developed an experimental model based on typical pin-on-disk device.¹⁰⁶ This offers the advantage to analyze more locally the friction and contact temperatures. This analysis confirms the trend that the normal load is not affecting highly the friction coefficient. The same scientist team investigated with comparable testing device the impact of the thermal effects on the friction coefficient.¹⁰⁷ They stated that the load is transmitted in a main part through boundary lubricated contacts.

Thermal behavior and cooling abilities of lubricated clutches can be highly improved if the cooling lubricant flow is mastered and measured. This case was investigated in the work of Albers and Bernhardt,¹⁰⁸ where measures were taken with particle image velocimetry devices.¹⁰⁹ They were able to evaluate the lubricant quantity in the cooling cavities of the clutch disks.

2.9.3 Investigation of Journal Bearings

A very typical mechanical element, the journal bearing, is one of the oldest demonstrators taken for investigating lubrication effects. This field recovers the EHL, HD lubrication as well as the boundary lubrication. Conventional facilities used in this field, are the test rigs composed of a shaft and two bearings (ball bearings mostly to limit the friction). To override the problem of friction occurring from the testing rig bearings, Albers et al. developed a testing rig with pneumatic bearings.¹¹⁰ This device enables a more precise way to measure the friction moment of the bearing. The question of energy efficiency was investigated by means of the test rig to optimize the oil flow in function of the loading in order to decrease the friction loss

¹⁰⁶ Märklund / Larsson (2008)

¹⁰⁷ Märklund et al. (2007)

¹⁰⁸ Albers / Bernhardt / et al. (2010)

¹⁰⁹ Hishda / Fujiwara (2003), Zhu et al. (2006), Lee et al. (2008)

¹¹⁰ Albers / Nguyen / et al. (2011)

coming from the lubricant side. Other testing rigs were used to detect mixed lubrication through the analysis of the frequency spectra.¹¹¹ Since the bearing goes from the hydrodynamic regime into the mixed lubrication regime, the frequency spectrum changes: frequencies become higher. A correlation has been done with Radio-Nuclide-Technique (RNT) to state this effect.

After this part on experimental validation, a last part (see next subsection) issues on an overview of whole investigations achieved in the field of numerical investigations of mixed lubrication phenomena. This is completed with the state in simulation of dry contacts, ending with state of multilevel approaches, used in different research fields.

2.10 State of the Art: Numerical Investigation in Tribology

This section gives an overview of the activities in numerical modeling of the surface roughness's impact on the tribological behavior, going from dry and lubricated contacts at the micro scale onto multi-level modeling.

2.10.1 Non-lubricated Contacts

A major part of numerical investigation in tribology concerns the macroscopic scale. In his paper, Wriggers summarize some of the existing frictionless contact formulations used in dry contacts with an example on large deformations.¹¹² Nevertheless contact properties used in these simulations are established at the microscopic scale. For this reason, numerous investigations of rough surfaces working in dry conditions were achieved in different research areas, respectively the brakes¹¹³ rail-wheel contacts,¹¹⁴ metal-forming¹¹⁵ and machining techniques¹¹⁶ as well as sealing technique.¹¹⁷ In this areas, many models were developed but no direct correlation between roughness parameters and friction behavior were stated. Many papers focus on the contact stress and plasticization occurring in the contacts¹¹⁸. Some models were developed to reduce the computing time of the finite element model for investigations determining real contact areas between bodies.¹¹⁹

¹¹¹ Dickerhof (2011)

¹¹² Wriggers (1996)

¹¹³ Dmitriev et al. (2008)

¹¹⁴ Bucher et al. (2006)

¹¹⁵ Leu (2009)

¹¹⁶ Özel et al. (2011)

¹¹⁷ Bielsa et al. (2010)

¹¹⁸ Kogut / Etsion (2004)

¹¹⁹ Yastrebov et al. (2011) ; Sellgren (2003)

All these works did not develop a theory between friction behavior itself and the roughness. They mainly compare the parameter R_p or R_a as these parameters are the most used for the roughness description. First models done by Albers et al.¹²⁰ taking into account adhesion effects (Bowden and Tabor model) showed the impact of the machining direction on the friction coefficient. It cannot be stated that the flatter the surfaces are, the lower the friction coefficient is. It is also dependent on the contact configuration itself, which determines the contact area. The same trend can be stated in lubricated contacts.

Such investigations were extended to take into account wear effects such as abrasion.¹²¹ Wear occurring in brake systems was also set under focus by Dimitrev et al.¹²² as well as Söderberg and Andersson.¹²³ Machining processes are usually simulated by means of the finite element method such as grinding processes.¹²⁴ Cheng used the molecular dynamics method to simulate the cutting process at the nanometric scale.¹²⁵

2.10.2 Mixed Lubricated Contacts

Lubricated line contacts with rough surfaces were investigated numerically by Chang,¹²⁶ with sinusoidal generated profiles. These investigations concerned elastohydrodynamic contacts models. These theories were then developed by Mihailidis¹²⁷ who calculated the friction coefficient of mixed lubricated line contacts. These numerical models were working in a stationary regime, as well as the model of point contact from Redlich.¹²⁸ The reason for that is a huge calculation time necessary to couple fluid and structure equations if time integration is chosen.

As a consequence, similar approaches were impossible to be used at the macroscopic scale. On this account, different solutions were used in parallel to these discretization methods: robust and very useful analytical approaches were developed for journal bearings¹²⁹ based on the Stribeck curve. Other approaches, such as multi-level systems of equations were used by Hu,¹³⁰ but did not allow the same level of

¹²⁰ Albers / Savio / et al. (2010)

¹²¹ Fang et al. (2005)

¹²² Dimitrev et al. (2008)

¹²³ Söderberg / Andersson (2009)

¹²⁴ Aurich et al. (2008)

¹²⁵ Cheng (2003)

¹²⁶ Chang (1995)

¹²⁷ Mihailidis et al. (1999)

¹²⁸ Redlich (2002)

¹²⁹ Andersson et al. (2007)

¹³⁰ Hu / Zhu (2000)

details as conventional CFD or FEM. Whole preceding investigations were not taking into account thermal exchange neither between fluids and solids nor directly inside of the fluids and solids.

Larsson,¹³¹ who used the FEM to model surface roughness at the microscopic scale was able to describe real rough surface but did also not take into account thermal exchanges. At the macroscopic scale only Jackson¹³² took into account thermal effects but this time without modeling any adhesion or roughness characteristics.

On the other hand, parallel to last described investigations, an analysis combining asperity contacts and taking into account thermal effects was achieved by Zhai¹³³ but without impacting the fluid (no thermal coupling with the fluid). This was done by Wiersch¹³⁴ who integrated thermal conditions in elasto-hydrodynamics, meaning coupling fluid structure and thermal behavior. Knoll¹³⁵ and Bartel¹³⁶ also developed similar methods to investigate journal bearings, and based on the flow factor theory¹³⁷ (correction of the Reynolds equation).

Mixed lubrication contacts phenomenon is to be regarded in transient conditions with a relative moving of two rough surfaces. Taking into account this movement is limited in elasto-hydrodynamic simulations as only one asperity is modeled. If not, a relative movement may lead to fluidmesh distortions caused by the movement. For this reason, adaptive and remeshing methods were developed.¹³⁸ Based on such approaches, Albers et al.,¹³⁹ analyzed rough surfaces under mixed lubrication conditions, allowing calculating the part of solid and hydrodynamic friction firstly with ALE approaches. This is only possible when, the fluid flow is not broken, that means, in hydrodynamic conditions.

Then, the use of CEL methods enabled it to overpass fluid mesh distortion limitations,¹⁴⁰ by evaluating in a first step the potential of the method in a two dimensional analysis. Further analyses performed in a three dimensional

¹³¹ Larsson (2009)

¹³² Jackson / Green (2008)

¹³³ Zhai (2001)

¹³⁴ Wiersch (2006)

¹³⁵ Knoll et al. (2007)

¹³⁶ Bartel et al. (2011)

¹³⁷ Almqvist et al. (2011)

¹³⁸ Schäfer et al. (2008)

¹³⁹ Albers / Lorentz / et al. (2010)

¹⁴⁰ Albers / Lorentz (2010a)

configuration, this time in real mixed lubrication conditions, displayed encouraging results.¹⁴¹ Also in this context wear are from a high interest.

Research field of sealing¹⁴² or the medicine technique¹⁴³ are using similar simulation models. Taking into account transient conditions, heat generation and real measured rough surfaces, the models need then to be calculated with different machining conditions and directions.

An essential point of roughness investigations is the usability of the results at the system scale. Often the analyses are done at a microscopic scale and cannot be transmitted to the macroscopic scale used to describe globally its tribological behavior. This shows the necessity to use multilevel modeling techniques, introduced in the next part.

2.10.3 Multi-Level Modeling in Tribology

An “in house” method called x-in-the-loop (XiL) was developed to guaranty a validation framework for powertrain investigation process. Based on this approach, Düser investigated and validated powertrain functions and driver assistance systems.¹⁴⁴ Other works achieved to transmit the experience coming from the microscopic scale onto the macroscopic scale are listed here, showing different approaches used for this matter. The rail/wheel contact is here also set under focus¹⁴⁵ as the movable cellula automata method,¹⁴⁶ used at the nanoscopic scale to determine a friction coefficient between the rail and the wheel. By means of an analytical approach, this friction was established in relation with the normal load, so that a law could be stated and used at the macroscopic scale.

Another approach used by Jackson¹⁴⁷ takes surface roughness at the microscale in order to predict the contact area in function of the load. Based on Fast-Fourier-Tranformée of real measured rough surfaces, he was able to reach the same results than Greenwood and Williamson¹⁴⁸ statistical models in order to determine the plasticization of the machined surfaces. This is achieved in using an iterative process taking into account different type of asperities, identified with their occurring frequency and applying to them corresponding load. As a result different scales are

¹⁴¹ Albers / Lorentz (2010b)

¹⁴² Du (2010) and Debler (2005)

¹⁴³ Barink et al. (2005)

¹⁴⁴ Düser (2010)

¹⁴⁵ Bucher et al. (2006)

¹⁴⁶ Popov / Psakhie (2001)

¹⁴⁷ Jackson / Streator (2006)

¹⁴⁸ Greenwood / Williamson (1966)

covered, from the micro (roughness asperities) to the macroscopic scale (form asperities). This method was also applied to determine adhesion forces in MEMS at different scales.¹⁴⁹

Other approaches consist in mixing continuous and discrete models as the state of the art of third body wear simulation presented by Renouf.¹⁵⁰ Both ways needs to be used, investigations done at the microscopic scale require boundary conditions adapted to the real working conditions. To get realistic boundary conditions, convergence studies have to be conducted. This consists in following an iterative process in giving the output of one model as input for a second model – modeled with the same approach – to check if the whole process is converging.

Further investigations used the response surface method to investigate sealing techniques.¹⁵¹ Using this type of design of experiment (DoE) enables the determination of the relationship between relevant identified parameters.

¹⁴⁹ Jackson (2011)

¹⁵⁰ Renouf et al. (2011)

¹⁵¹ Ledoux et al. (2011)

3 Research Objectives

The state of the art presented in chapter 2 gives an overview of different investigations required to simulate the impact of roughness on friction. This research area combines different parts of physics and mathematics going from the characterization of technical surfaces up to adhesion effects present in the investigated phenomenon.

3.1 Potential Issuing from the State of the Art

The second chapter exposed the state of the art of tribological investigations conducted with rough surfaces running in dry as well as lubricated conditions. From this state of the art, several points can be extended.

First point concerns the simulation of critical lubrication regime of tribological systems: mixed lubrication. The actual state of the art underlines the difficulty to simulate it in a whole finite element model for a question of numerical limitations. Nevertheless this becomes possible with different innovative approaches (CEL approach, CFD and FEM) also used in other research fields, and offers the possibility to increase the degrees of freedom of the actual mixed lubrications models. This methods were never used before for this kind of problematic for the reasons displayed in chapter 2.7.

Another point relates to the characterization of the surface roughness which is necessary to investigate the influence of rough profiles on the friction behavior. The correlation between this profile's property and the friction behavior cannot clearly be distinguished at the microscopic scale. On this account, a study is required to know which ones of the different roughness parameters can be used to deliver a useful relationship between roughness and friction coefficient. This has to be done for dry and lubricated tribological conditions. Additionally, microscopic effects such as adhesion, wear phenomena like abrasion and other plastic deformations, are not taken into account in past mixed lubrication models. The impact of the roughness on the wear and plastic deformation also need to be stated.

Huge challenge of this type of investigations remains the modeling of multiphysics and multiscale problems. Next subsection exposes the procedure to reach the enounced goal as well as the current limitations.

3.2 Establishment of the Target System

Main objective of this work is to develop a numerical approach that can take into account real rough profiles, and simulate the impact of roughness on the tribological behavior of a system. This has to be done for non-lubricated and lubricated surfaces. On this account, tribological behavior is described here according to following criterions: *friction coefficient*, *contact temperatures* and *contact pressures*.

Different parameters having an impact on friction behavior taken into account in present these are listed as follows:

- Material properties (elasticity and plasticity)
- Roughness' parameters (see chapter 2.2)
- Machining type and direction
- Working conditions: sliding velocity, normal load (or oil film thickness)

A further objective is to develop a method that can be adapted for any tribological systems. It also has to transfer information from the microscopic scale into the macroscopic scale, in order to be used for the description of macroscopic tribological systems. To do this, several steps are required, listed below:

- Micro model building and analysis of the function and
- Model verification
- Results and parameter study
- Extension of the investigation to the macroscopic scale

Main reason of this whole investigation process is to enhance the accuracy of the method by increasing the number of parameters being taken into account. It also have to quantify the impacts of different listed interfering parameters. Such investigations are necessary to be carried out at the microscopic scale as the occurring phenomena are not the same as at the macroscopic scale. In this way, the phenomena are described with more details.

Systems set under focus in this work are sliding systems in running-in phases, like journal bearings, or friction systems like continuously variable torque (CVT), clutches and brakes. In this context, use of numerical tools gives here the advantage of investigating phenomena which are not measurable with experimental facilities. Nevertheless, the difficulty is to validate the numerical method, to clearly identify the application window. This whole problematic is developed in the next sections.

4 Analysis Framework

Initial step necessary in any investigation process is to set analysis framework. Which parameters are necessary for the analysis and which are the important boundary conditions to be defined. Demonstrators are defined, setting the bases for developed numerical models.

4.1 Demonstrator Definition

4.1.1 Classification of Tribological Systems (Tribo-System)

Occurring tribo-contacts and tribo-systems can be described using the Contact and Chanel Approach (C&C²-A). Tribo-system can be separated into two categories:

- Friction systems: system in which the function “friction” of the contact WSP accomplishes a main function of the system: transmitting energy, information and material from one working surface onto the other
- Bearing systems: systems where the function “friction” occurring in contact WSP is considered as “noise” for the system’s global function and could so be avoided

Each of these categories can also be separated into two types of friction regime:

- Non-lubricated tribo-systems: composed of two channel and support structures (CSS), and one working surface pair (WSP)
- Ideal lubricated tribo-systems: composed of three channel support structures (CSS) and two working surface pair (WSP), between the lubricant and both solids

An analysis is necessary at different scales to quantify the phenomena occurring in the system. Reason for that is the required level of detail the macroscopic scale is insufficient and does not allow to take each detail into account. On this account, a microscopic scale is necessary to establish friction laws to be used at the macroscopic scale.

Enounced problematic is typical of clutch systems, or journal bearings, and as these “machine components” are investigated at the institute, they are used in this analysis as demonstrators and define consequently the working and boundary conditions of the models.

Moreover, each product aims at realizing at least one function which links input to output parameters. As present work focuses on tribological systems, next subsection

takes the powertrain as demonstrator to establish the function of a clutch and parameters which are characterizing it.

4.1.2 Identification of the System Functions by Means of System Design Methods SADT and C&C²-A

Any system can be defined as enounced in section 2.1.1. To improve their design, functions have to be identified and described. For this reason, SADT and C&C²-A are applied to the system analysis in order to deliver a concrete description of a system and its functions. Both methods are complementary and deliver a full description of the systems functions. As central activity of the IPEK takes part in the development of powertrain technology, the system “car” is the frame of present investigations, as displayed in Figure 4.1.

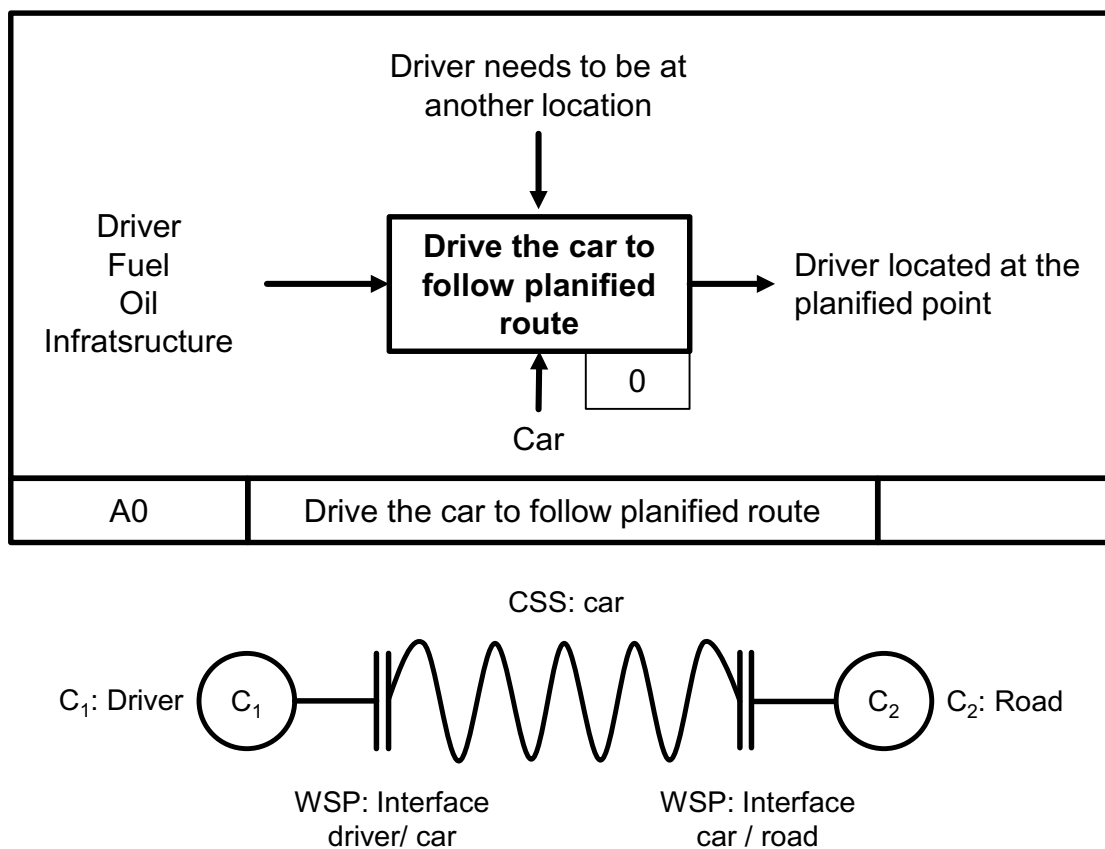


Figure 4.1: Defined car model SADT (on the top) and C&C²-A on the bottom

Applied to this system, main difference between the SADT and the C&C²-A is that the last approach synthezes every parametre in only three entities, 2 connectors

- C₁: driver
- C₂: car

and one working surface pair (WSP) which transmits information from the driver to the car. On the other hand the SADT uses 5 different parameters: input, output,

function, control and system. For a low level of description, the SADT offers a better readability than the C&C²-A. Furthermore, on the contrary to SADT, the second method does not take the function as center of the investigation but the system.

If the investigation level increases, in order to isolate the function “car-driving”, previous enounced differences are different. Characterization of the dynamical behavior of a car in a driving phase gives the engineer the source of noise or vibrations occurring in the car as well as the interactions taking place between the car and the driver. Next figure (Figure 4.2) focuses on the function “car-driving”. It gives an overview of the description and potential of each method to underline the function and system subject to interact in the acceleration phase.

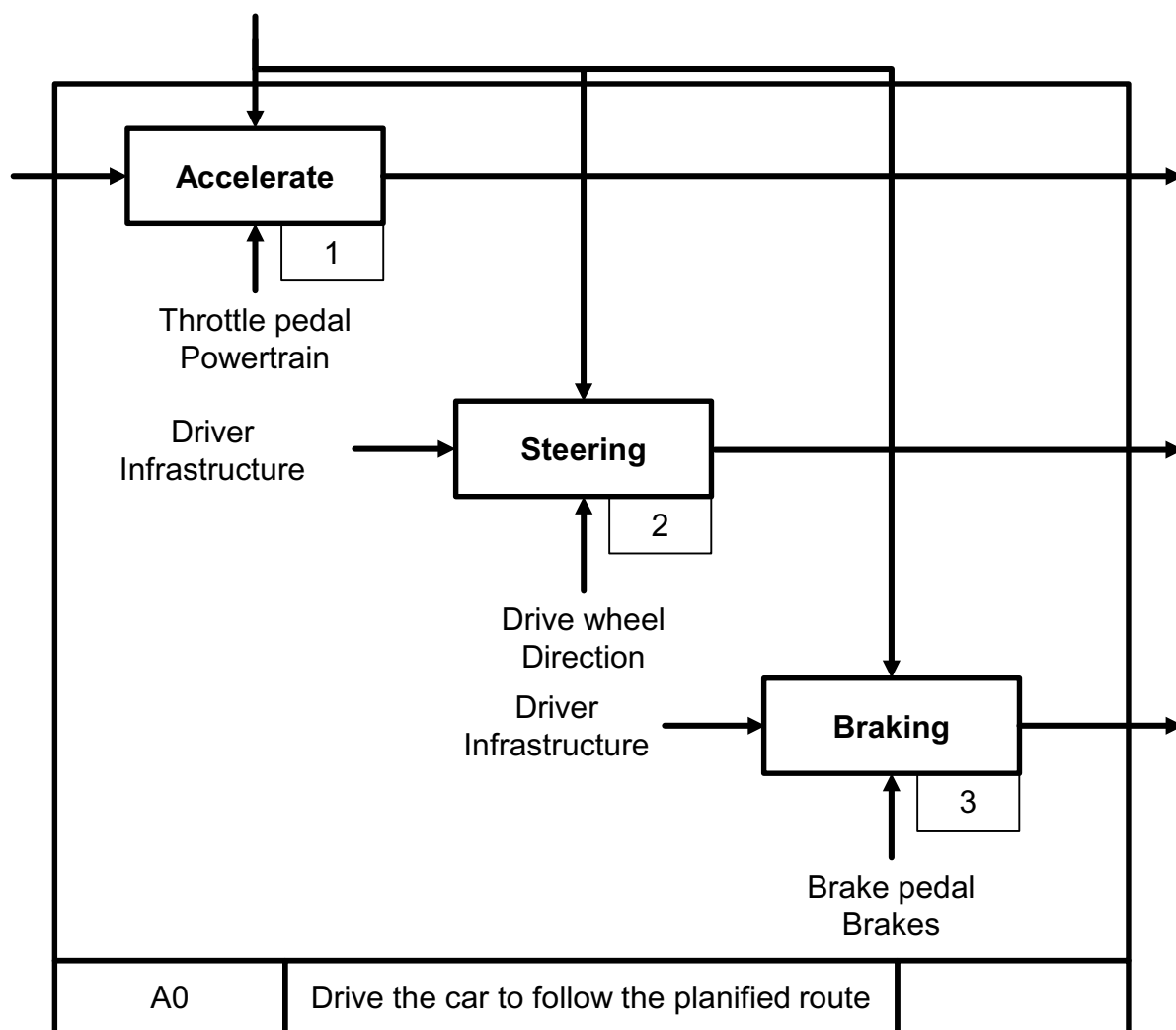


Figure 4.2: Isolation of the function “acceleration”

This diagram shows which element controls the function “acceleration” and which subsystems interacts during the acceleration. Same analysis done with the other method is displayed in Figure 4.3.

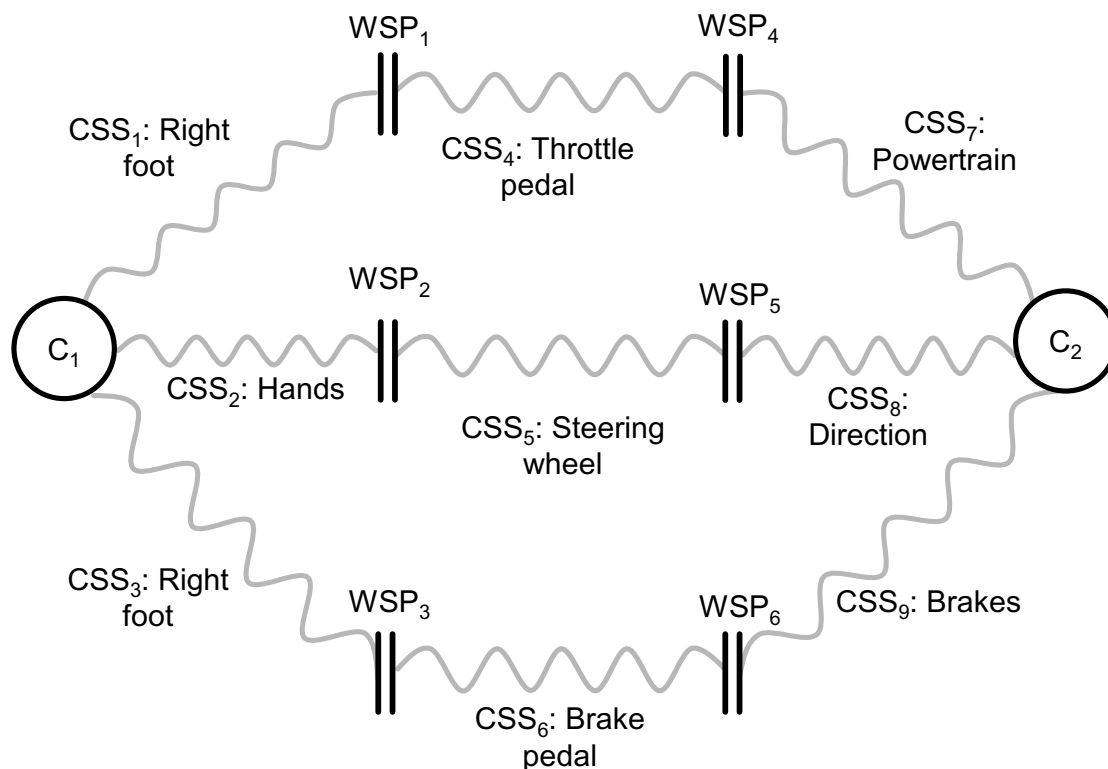


Figure 4.3: Identification of the acceleration phase by means of the C&C²-A

In Figure 4.3, the connectors are the same than those displayed on Figure 4.1, the working surface pairs which transmit “Energy, Information and Material” can be characterized as follows:

- Closed WSP₁: energy transmission through a plan to plan interface (rotational displacement of the throttle pedal)
- Closed WSP₂: energy transmission through a connection line to plan interface (rotational displacement of the steering wheel)
- Closed WSP₃: energy transmission through a plan to plan interface (rotational displacement of the braking pedal)
- WSP₄: information transmission from the throttle pedal to the powertrain
- WSP₅: information transfer from the steering wheel to the wheels
- WSP₆: information transmission from the brake pedal to the brakes

A significant difference between both methods concerns the temporal space: with the C&C²-A, the function can only be achieved if the corresponding WSP is closed whereas SADT describes only a given function and does not take into account other components that do not always participate to the function’s achievement.

Additionally, the analysis is more structured in case of the application of the SADT. However, the interfaces between the different entities are more easily recognizable

with the C&C²-A. Thus, a coupling between both methods can be significantly helpful for complex systems, where interfaces have to be modeled.

After having identified boundaries and sub-systems interacting in the acceleration phase, one can focus on these same parts with a view to analyze the vibration during acceleration. Principal systems are the “powertrain” and the actuator “throttle pedal”. The vibration related phenomena can be induced by three factors or a combination of these factors and external boundaries:

- Driver
- Powertrain
- Throttle pedal

Such interactions can be modeled and are detailed in Figure 4.4, where the complete powertrain chain is displayed. By decomposition into isolated systems, the source of vibration can be identified in an easier way.

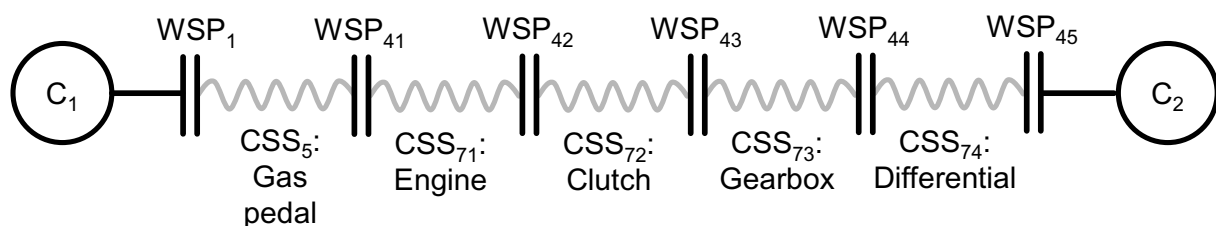


Figure 4.4: Powertrain

C&C²-A displays the component chain of the powertrain. By means of the SADT, each of the components can be described as illustrated in Figure 4.5. A combination of both description approaches offers a better understanding and visualization of the system’s components and functions. The first approach lists the functions, inputs, controlling outputs and controls achieved by each of the subsystem whereas the second approach lists the interface between the subsystems.

From these analyses, the shiftable clutch is the subsystem connects two rotating shafts. Through its function to break up the torque flow, the clutch is also in charge of synchronizing both sides:

- first side: torque origin (Engine)
- second side: torque used for vehicle acceleration (wheels)

Reasons why a clutch is required can be resumed in three points:

- the combustion engine has a small range chart: the maximal torque is available in almost 50% from the rotation window
- a gearbox is required to override the previous problematic

- required torque is too high to shift gears without breaking the torque flow and so guaranties the lifetime of the gearbox

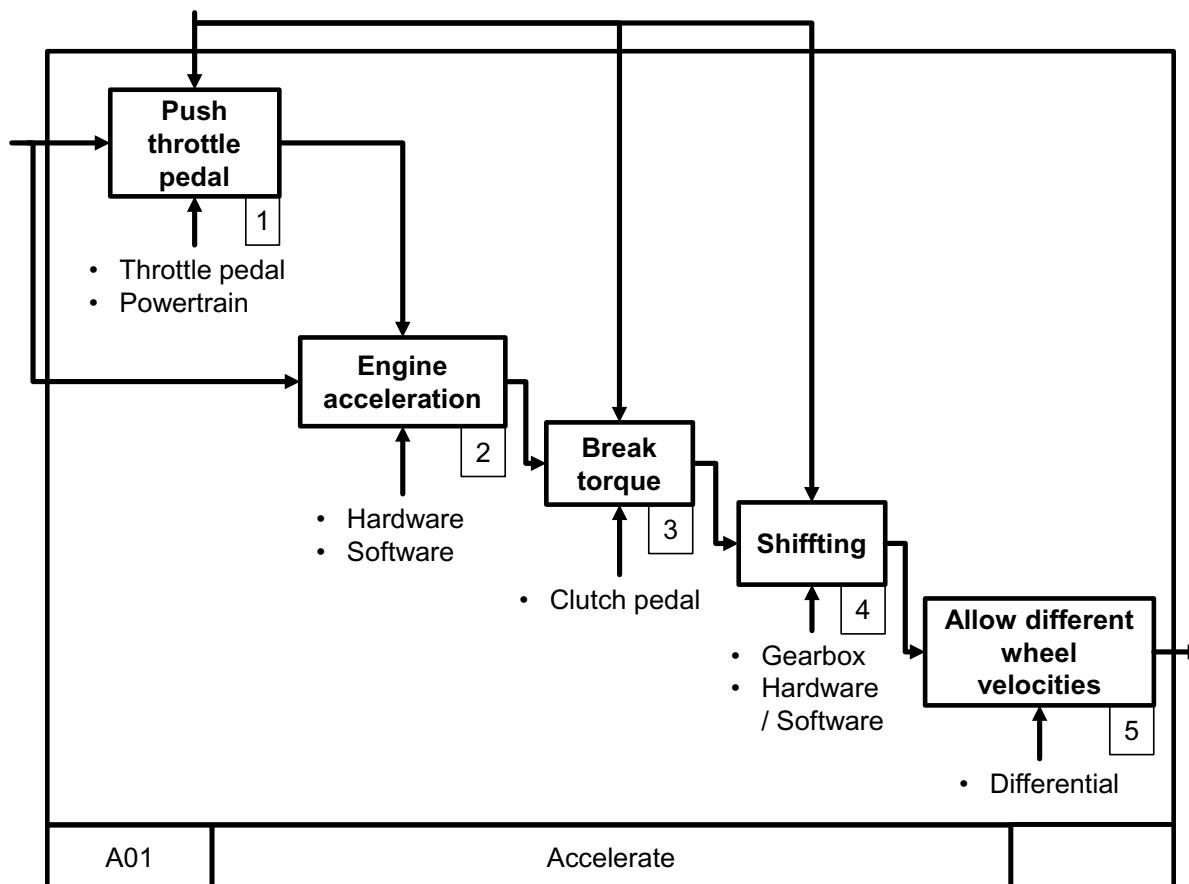


Figure 4.5: SADT of the powertrain in the acceleration phase

Nowadays trend is to have even faster gearboxes and so indirectly and implicitly faster clutches. At the same time, customers are asking for even more shifting comfort. This possibility resides in a special type of clutches: lubricated multi-disk clutches and is detailed in the next subsection.

4.1.3 Identification of the Function to be investigated

Previous enounced clutch system is mostly used in complex and high level products like double clutch or automatic gearboxes. Unlike the second transmission type, first concept enables no torque discontinuity during the shifting phase. Nevertheless some violent impacts are present during the shifting as well as hydrodynamic friction losses. Such phenomena need to be investigated.

Main reason why multi-disk clutches are used is due to their higher power density in comparison with simple disk clutches. This result from the lubrication of the multi-disk clutches: lubricant induces a better cooling and consequently, higher torque can be transmitted for a same disk diameter. On the other hand, dry clutches have better global energy efficiency: less friction losses.

Moreover, such systems are subject to wear phenomena which need also to be analyzed. Using the contact and channel approach, a lubricated multi-disk clutch can be separated into the subsystems and scales by means of the XiL method as listed in Figure 4.6. Next scheme (see Figure 4.6, level 3) sets the different scales required to have a model for a lubricated clutch.

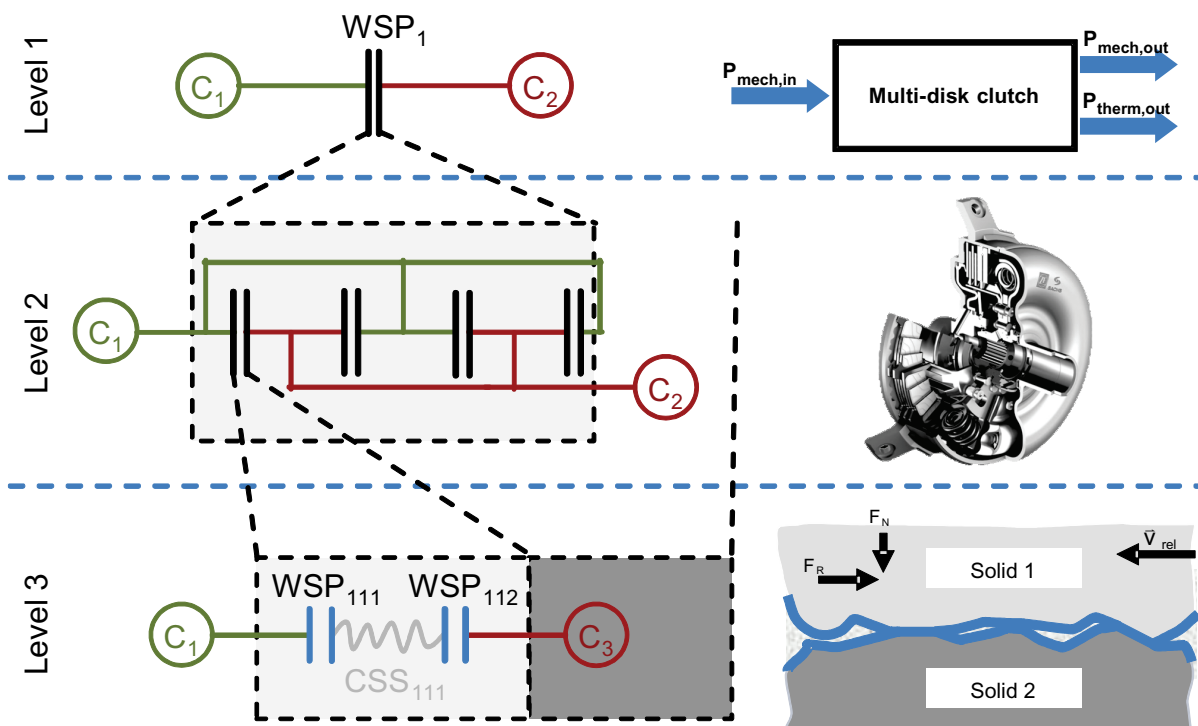


Figure 4.6: Multi-level description of a multi-disk clutch described with the C&C²-A

According to Figure 4.6, a multi-disk clutch can be decomposed into a simple disk-disk contact pairing. In this way, the simulation of phenomena occurring in this contact type can be achieved, Figure 4.7 gives an illustration of contact pairs.

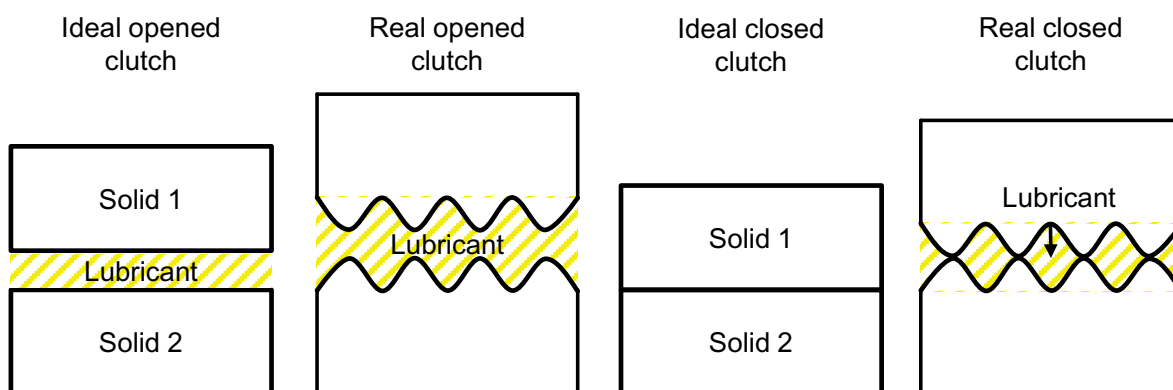


Figure 4.7: Comparison between ideal and real plan-to-plan contact at different scales for lubricated cases

Figure 4.10 underlines the fact that ideal surfaces are not sufficient if a detailed analysis of the contact pairing is required. Mixed lubrication is observed for the real

closed clutch whereas hydrodynamic phenomena are observed for real opened clutches. Both phenomena have an impact on the friction behavior of the concerned systems.

A C&C²-Model built for the interactions taking place at the micro scale allows to get more details. This means that each of the existing WSP can be separated into further WSP and CSS. The analysis displayed in Figure 4.8 goes down to the microscopic scale and is a schematization from Figure 4.7; any tribological system can be schematized as displayed in Figure 4.5.

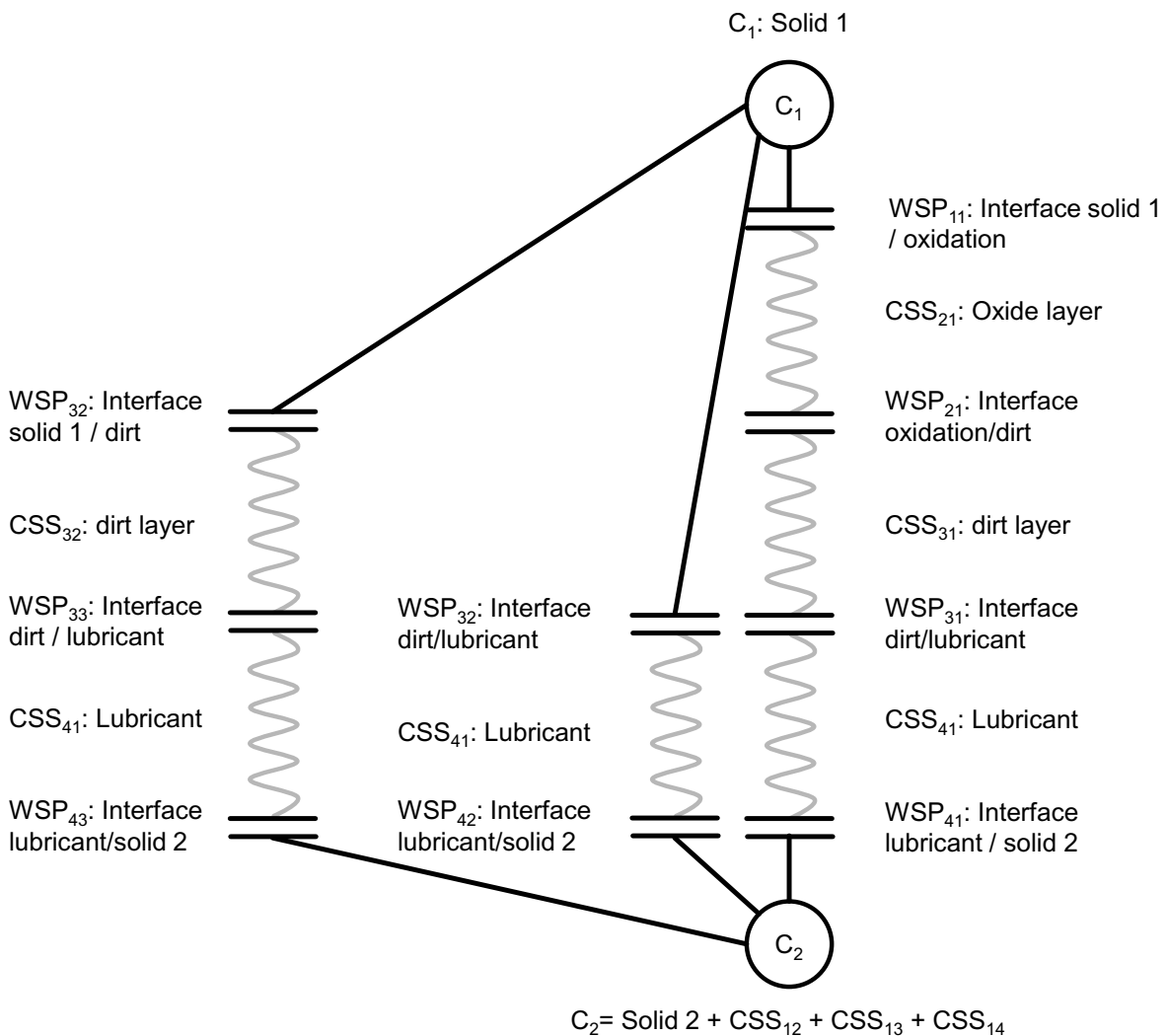


Figure 4.8: Analysis of the tribological lubricated plan to plan contact with the C&C²-A

Case displayed in the last figure puts into relief phenomena occurring in reality and related to lubrication regime in tribological systems. Nevertheless, this implies taking into account, the dirt and oxide layer which are most of the time unknown and playing an essential role at the beginning of the contacting phase. Dry-running tribological systems can be modeled in the same way by only suppressing the lubricant.

Schematization of Figure 4.8 is simplified for technical reasons enounced in section 2.6 and is visible in Figure 4.9. However, as mentioned in subsection 2.5.4, the lubricant does not have the same behavior for different film thickness and pressure. On this account, the channel support structure CSS_{41} needs to be separated in function of the lubricant film thickness as presented on Figure 4.10.

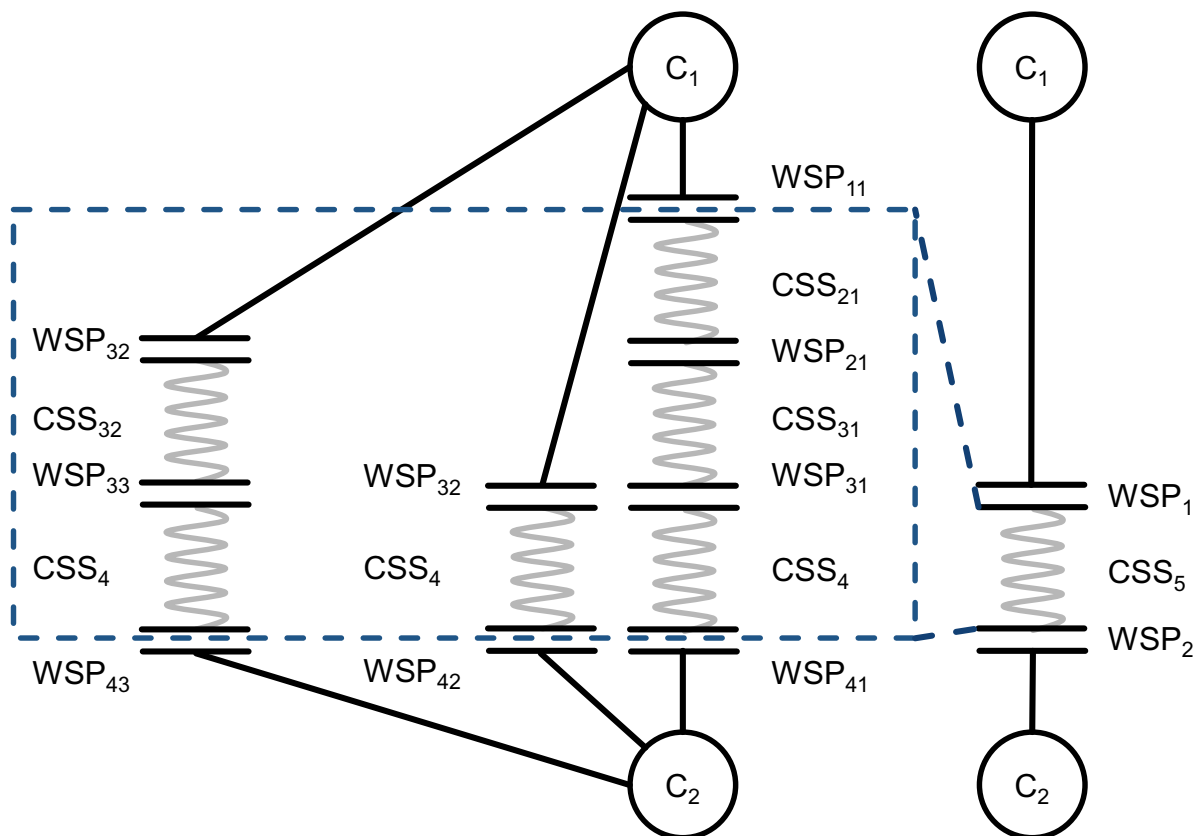


Figure 4.9: Simplification of the tribological problem

These analyses also underline the importance of the surface topography considered for the contact. Contact kinematics occurring in lubricated clutches, is going ideally from the full hydrodynamics into solid-solid contact. The real case displayed in Figure 4.8 shows that the solid-solid contact does not exist in reality: this leads to boundary lubrication. Nevertheless real cases need to be simplified in order to set first bases for a numerical mixed lubrication model. Main assumptions are displayed in next figures, considering, that neither dirt nor oxidation are present on solids. Considering the surface roughness, some contact regions are laying under boundary lubrication and others under hydrodynamic conditions as shown on Figure 4.10.

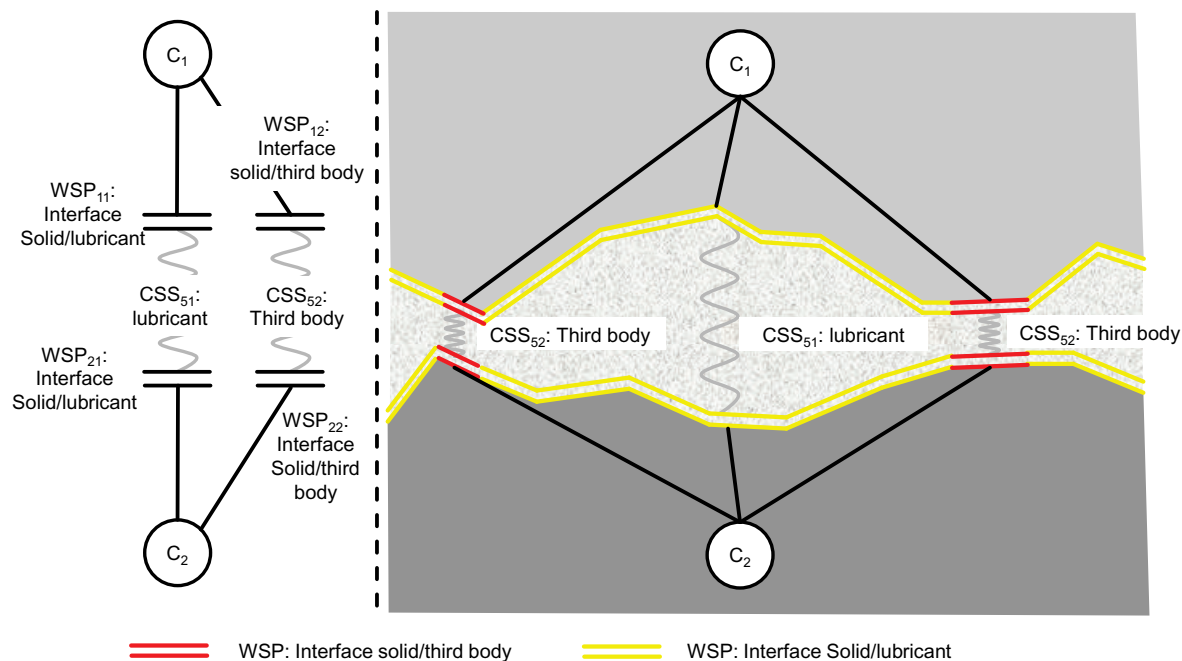


Figure 4.10: C&C-Modell of mixed lubrication

According to Figure 4.10, lubricant channel support structure can be sorted out into two entities:

- lubricant which symbolizes the hydrodynamic regime (CSS_{41}) when the film thickness $h > 0.025 \mu\text{m}$
- the third body which represents the mixture between corrosion, dirt and lubricant (CSS_{42}) when the film thickness $h < 0.025 \mu\text{m}$

The separation of the structure is essential for determination of the third body. Indeed, neither chemical composition nor physical properties are published in the literature. This type of interaction is present in almost every lubricated contact, such as journal bearings (during run-in phase) or lubricated clutches, two active research fields of the institute. Working conditions of both systems are synthesized in the next subsection. The relevant function set under focus in the present work are: “**transmit force**” and “**protect from wear**” in contacts between two clutch disks, running under dry conditions as well as lubricated conditions (see Figure 4.11).

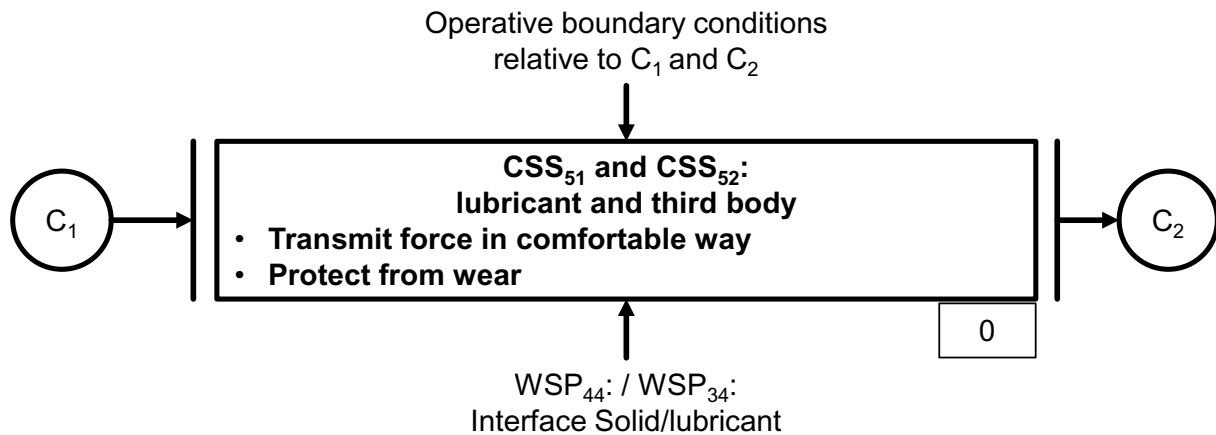


Figure 4.11: Combination of the SADT and C&C²-A for the function description

4.2 Definition of Investigation Steps to Reach Objectives

This part exposes the phases required to build up the model to investigate mixed lubrication phenomena. Related demonstrators analyzed and enounced in the previous subsection and summarized in the next subsection are taken here to isolate functions leading to the definition of the device and methods to be used.

4.2.1 Demonstrators Functions Leading to Theoretical Models

Both functions defined previously are here taken to set the bases of the investigations: transmit forces by means of frictional contacts through lubricant and third body (or only contact bodies for dry conditions) in increasing comfort and wear prevention.

From these functions, the wear prevention and also force transmission are part of journal bearing investigations. In this case, “force transmission” is considered as “perturbation” as it leads to conventional friction loss and so energy waste. The similitude between run-in phases of journal bearing and clutch contacts enables the development of universal investigation method for both types of contacts. To achieve the analysis, different models and scales are required, resulting from the concept presented in Figure 4.6 and displayed on Figure 4.12.

The borders in pointed lines represent the steps required in the global process but are not treated in the present work. The main challenge represents the transfer going from the macroscopic into the microscopic scale. Next subsection enounces the workflow of the different steps needed to build and validate the method.

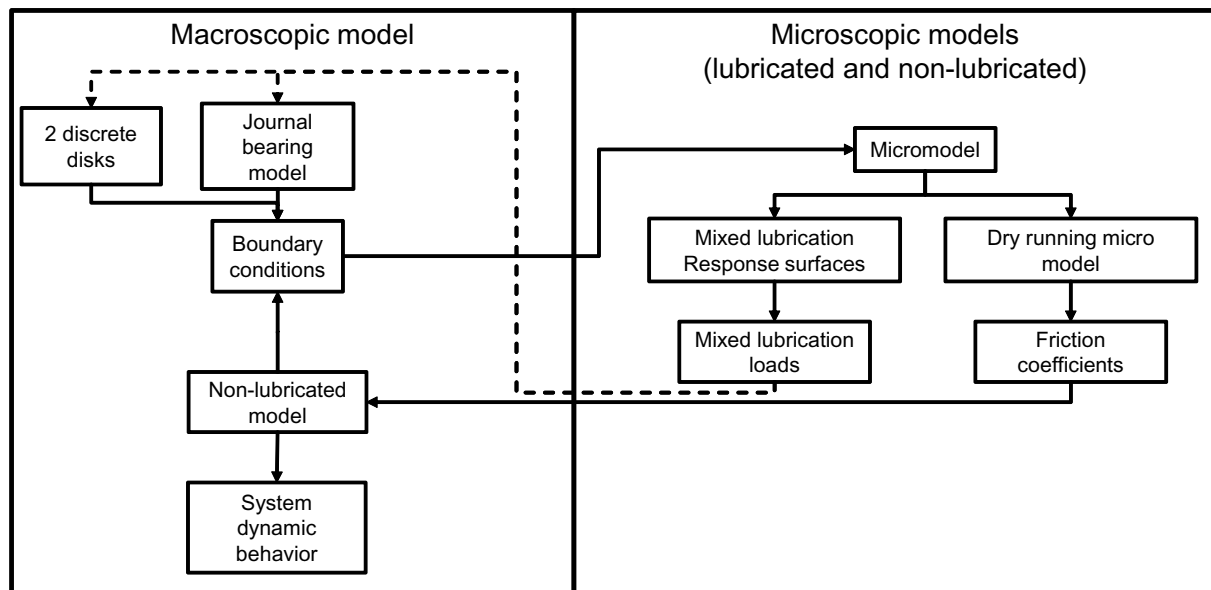


Figure 4.12: Principe of the whole investigation process

4.2.2 Working Conditions and Investigation Steps

For the investigations, two models are developed: the macroscopic model of the given system and a microscopic model whose aim is to deliver mixed lubrication loads for the macroscopic one. As the present work focuses hardly on the microscopic scale, the description begins with it.

Based on numerical methods, principally the finite element method, the microscopic model simulates the contact interactions presented in cited systems (journal bearing and lubricated clutch). This simulation approach consists in taking the CEL method (see section 2.7) allowing high displacement of the solid mesh in contact with the fluid mesh. In this method the contact algorithm is investigated in order to check if its accuracy is sufficient for required investigation.

Using this method a micro-model is developed composed of three dimensional rough technical surfaces measured with laser interferometry technique as in the work achieved by Albers et al. for microstructured electrical connectors.¹⁵² Different profiles are used in order to analyze which influence a specific profile has on the friction behavior. Passed investigations showed that a statistical scheme is specially useful to define a frictional trend.

The parameters taken into account in the microscopic mixed lubrication model are the following:

- Temperature dependence of the plasticity
- Temperature dependence of the elastic modulus
- Temperature and pressure dependence of the lubricant's viscosity

¹⁵² Albers / Martin / et al. (2011)

- Each roughness parameter
- Machining direction
- Fluid pressure
- Surrounding temperature
- Heat generation in the contact interface
- Thermal conductivity
- Sliding velocity
- Average lubricant's film thickness

Working conditions chosen for dry conditions remain the same as those taken for the model taking into account the lubricant. The impact of each of this parameter will be analyzed by means of the micro-model in order to evaluate and reduce the number parameters to be taken into account. For the parameters that have a high impact on the friction behavior, a friction law is established by means of the microscopic model. This friction law establishes the friction coefficient in function of following input parameter: machining parameters and working conditions (load and sliding velocity).

To deliver useful results, the microscopic model requires adapted boundary conditions described in next chapter. A second numerical model uses input of the first model and is developed at the macro scale. Its dimensions are in the order of 100 mm. As the roughness cannot be modeled when structures reach such dimensions, only the waviness is taken into account in the second model. In order to investigate the influence of roughness on real structures, a coupling with the micro-scale is required.

4.2.3 Experimental Device Required for the Verification

For both developed models, experimental tests on real system are required. For the microscopic scale, pin-on-disk tests are achieved whereas on the macroscopic scale real journal bearing are tested in run-in phase in order to compare outgoing results with those resulting from the numerical simulation. This part is of high importance as it is used for the verification of the developed numerical method and models.

Analyzing roughness impacts on dry and mixed lubricated tribological systems at the microscopic scale implies having demonstrators as simple as possible. On this account, the dry model is based on conventional pin on disc tests. This has the advantage to decrease the number of parameters which are interacting on the system and leads consequently to less complex verification. The pin is made of saphir disk (Al_2O_3) whereas the disk is in Titan. Titan is used for its ability to resist against corrosion and for its relative similar behavior compared to steel. The saphir is taken for the same reasons as well as for the low adhesive resistance and also for its hardness and high elastic abilities.

Concerning the lubricated demonstrators, the difficulty to reproduce exactly the pin on disk conditions is caused by the lubricant. Neither the film thickness can be measured nor solid-solid interfaces can be identified. The demonstrator used for the lubricated model is a part of a journal bearing: steel shaft against journal bearing (SiAlSn). This whole presented investigation chain has also some limitations. As different scales are interacting, different assumption required to limit computational costs need to be defined. These are expressed in next section.

4.3 Main Assumptions used for the Microscopic Model Implementation

Developed method is using two numerical models (presented in chapter 5) and two physical models. As a model is a representation of the reality of the pointed phenomena occurring in the system under investigation, each detail is not able to be reproduced by these different models. At the microscopic scale and for the numerical model, following assumptions are met for reasons related to the physics:

- wear phenomena: adhesive, corrosive and erosive wear are not taken into account (occurs mainly for very clean surfaces)
- boundary layers' physical and chemical properties are considered as ideal (no existing possibility to know the composition of boundary layers)
- no direct thermal interactions are taking place between fluid and solid (investigation time too short to take into account thermal exchange between solid and fluid)
- no cavitation effect is taken into account (two phasic model is too complex in this preliminary study)

At the macroscopic scale, the numerical model has following assumptions:

- Constant oil temperature for the lubricated model, constant air temperature for the dry model
- Solid-Solid contact modeled by means of an interpolation function calculated with microscopic models (no exact values)
- No thermal impact on the fluid viscosity: viscosity adapted to a temperature of 90°C
- Use of statistical methods (response surface) to determine shear stress present in the solid-solid interface (exact rule cannot be used)

5 Numerical Model at the Microscopic Scale

Present chapter exposes the method employed to develop the numerical model which takes into account surface roughness of a tribological system. For technical reasons explained in section 2.10.3 the modeling has to take place at the microscopic scale. This enables the calculation of the friction occurring between two rough bodies. Among the existing types of numerical models, discrete numerical models are most adapted as they offer the possibility to take a huge number of degrees of freedom (DoF) into account. On the other hand, computational costs are higher than in other kinds of models. A finite element model is then used in which real rough surfaces are imported and next step consists in applying the real working conditions.

5.1 Discretization of the Rough Surfaces

Surface topography is measured using laser interferometry according to parameters displayed in chapter 2.2.1.

5.1.1 Signal Treatment to Characterize the Surfaces

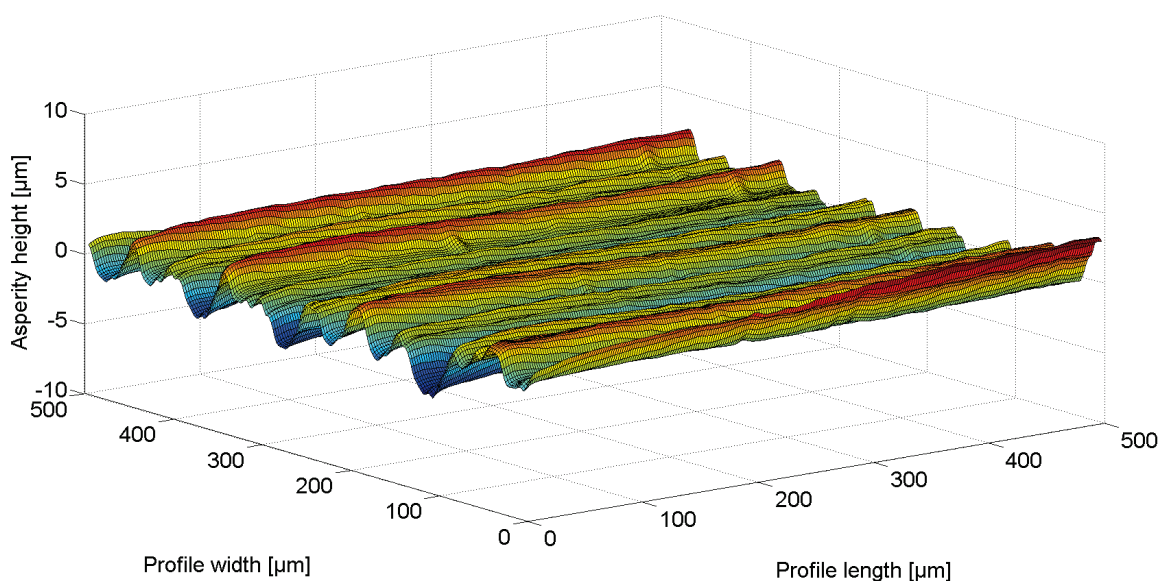


Figure 5.1: Rough profile of a turned surface

In order to measure the roughness of a technical surface, measuring points need to be set according Table 2.2 and Table 2.4: an acquisition takes place each $2\ \mu\text{m}$ for an overall length of $600\ \mu\text{m}$. The measurements are taken by means of an optical device which delivers 3D discrete scatter plot (see Figure 5.1).

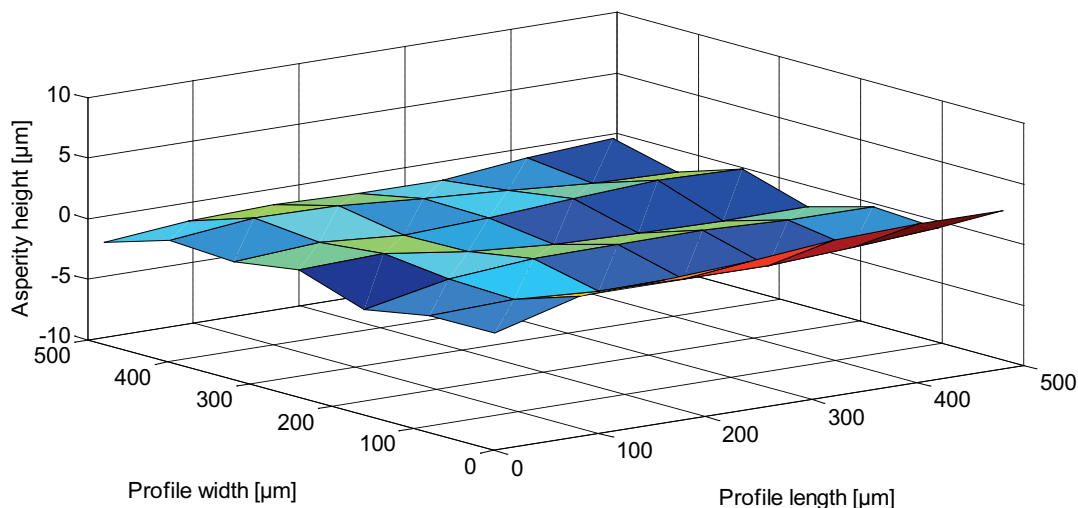


Figure 5.2: Waviness profile of a turned surface

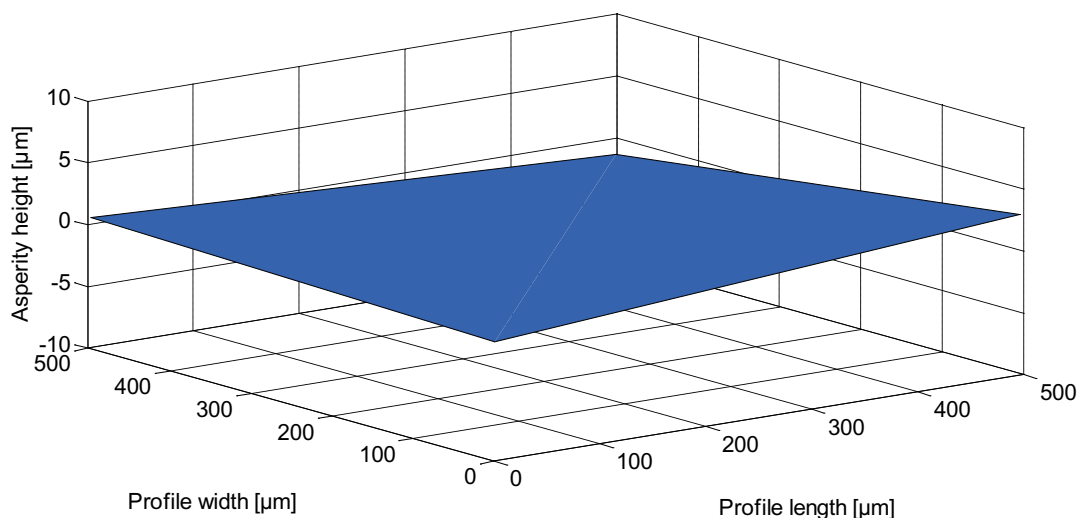


Figure 5.3: Form profile of a turned surface

According the same cited tables issuing from DIN-4287-4288, the topography signals are filtered to separate the roughness from the waviness as well as from the form profile as displayed in the last three figures. Plots underline that details are present online in the roughness profile. Nevertheless, a whole measured profile cannot be taken into account in order to simulate the friction behavior as there are too many degrees of freedom to be modeled. This motivates the necessity of a multiscale investigation. In addition to the spatial characterization, a frequency decomposition of

the profiles is performed by using the Fast Fourier Transform. This decomposition characterizes the profiles with their frequency spectrum as displayed in Figure 5.4.

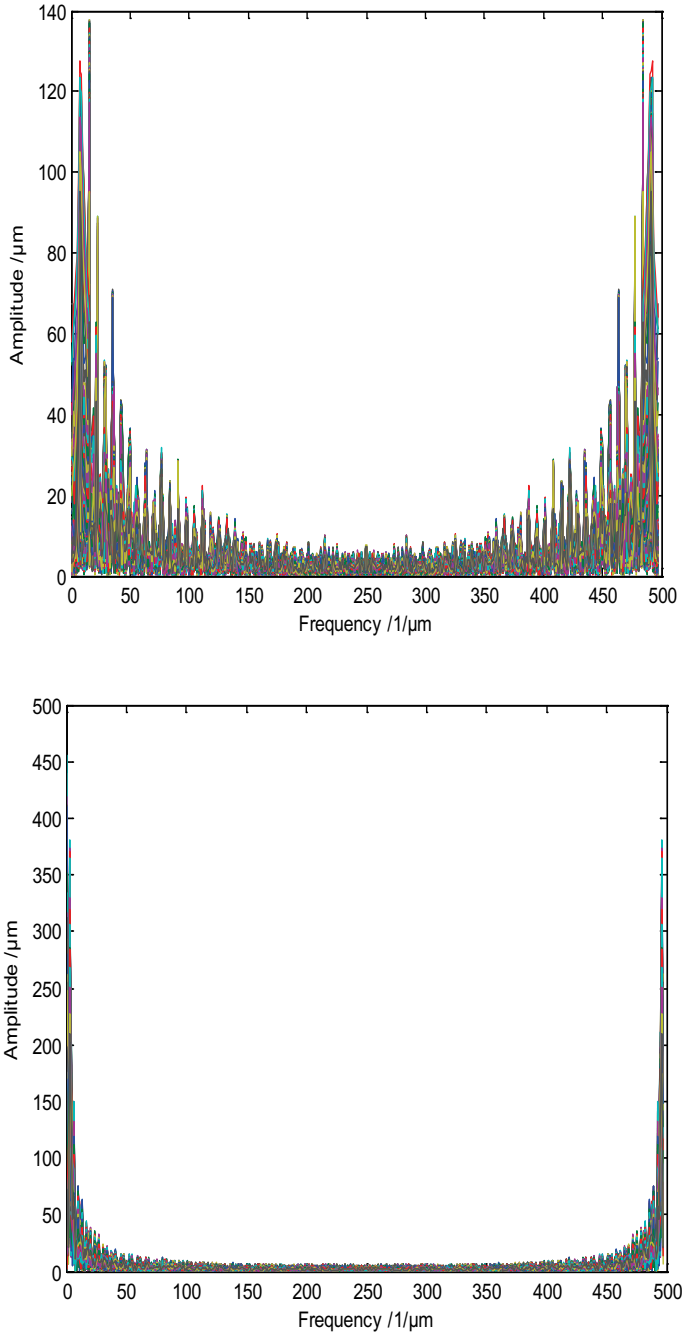


Figure 5.4: Example of a frequency spectrum of a grinded surface (on the left) and a turned surface (on the right)

Last figure shows that the homogeneity of the spectrums highly depends on the machining method used to manufacture the different friction surfaces: the finer the machining is the larger the frequency spectrum is. Table 5.1 represents a classification of the number of relevant frequencies in function of the machining process and also the dispersion of the profile. Four categories of importance related

to the frequencies are considered relatively to the maximal amplitude (the maximum amplitude represents 75-100%).

Table 5.1: Most relevant frequencies for the four machining

Machining	10-25%	25-50%	50-75%	75-100%	Total
Turning	88	16	2	2	108
Grinding	432	114	12	6	564
Milling	350	64	30	10	454
Lapping	3630	390	44	8	4072

Last table displays that the number of different signals is low for single point machining (turning and milling). For multiple points machining (grinding and lapping) a higher number of frequencies is observed. This trend is confirmed by next diagram displaying the dispersion of measured points for different machinings (see Figure 5.5). Topography measurement resolution was the same for each profile.

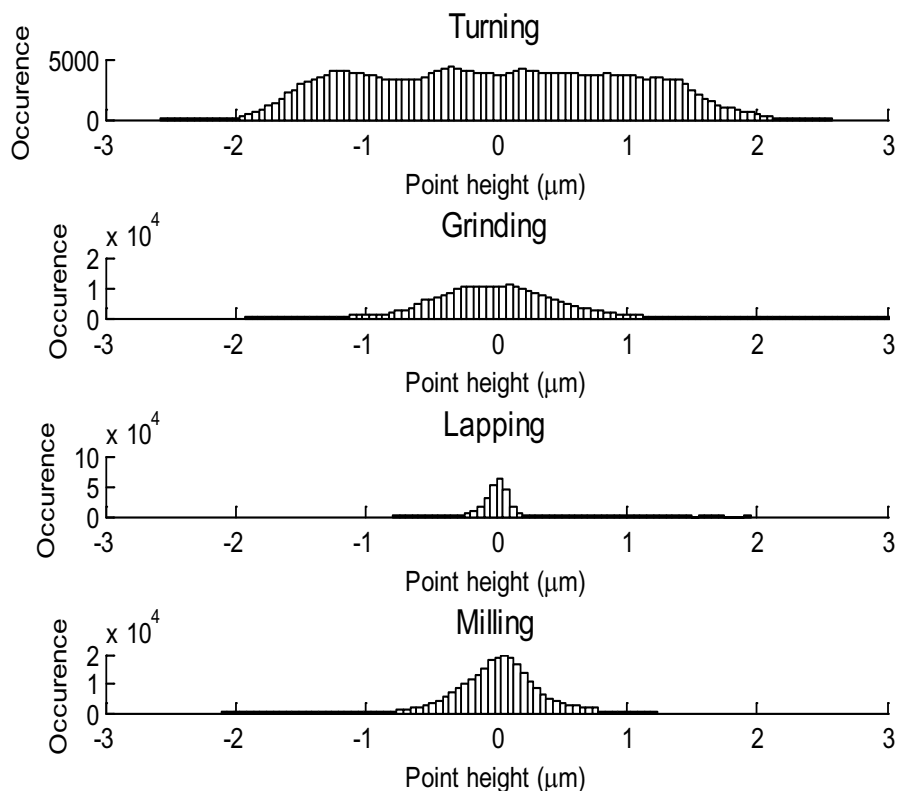


Figure 5.5: z-Coordinate repartition for all four machining types

Although the theme of this thesis belongs to multiscale topics, present approach focuses mainly on the microscopic scale. Next part of the modeling only takes into account two profiles: one single point machining (turned surfaces) and one multiple

point machining (grinding). These so called profiles need then to be imported and integrated into a finite element framework, the step is described in next paragraph.

5.1.2 Importation of the Surfaces into a Commercial Finite Elements Software

Measured topographies can be integrated into any preprocessing tool of finite element software by using on following available methods:

- build directly a mesh of the measured topography
- build a solid of the topography

First solution would be more effective, as a finite element model can be directly generated with an “in-house” written code. Nevertheless, this method is highly dependent from used FE-solver as meshing and input syntax need to be adapted. It would also require the implementation of a meshing algorithm, which is realistic for tetrahedron but not for hexahedron meshing.

Second solution is more flexible, as the output generates a solid which can be imported in any software as the used format is an open one. Next advantage is the flexibility of meshed refinement that can be adapted more efficiently without requiring rebuilding the model. Nevertheless, the available formats have some restrictions:

- only cubic volumes can be represented with rectangular surfaces
- if the number of points is too high, the size of generated files can be too large

Chosen for its flexibility and robustness, second solution is implemented using the software Matlab. Available neutral file formats for the importation of geometries are following ones:

- IGES, Initial Graphics Exchange Specification¹⁵³
- STEP, STandard for the Exchange of Product Model Data¹⁵⁴
- parasolid (binary or ASCII form)
- SAT

Using the IGES format has the advantage that it is fully structured and documented on the contrary to all other formats.

In order to generate such a file, measured or stochastically generated splines are taken as input data. On this account, 3D B-Spline theory is used following the

¹⁵³ IGES/PDES Organization (1996)

¹⁵⁴ Schulze (2006)

process illustrated in Figure 5.6 to generate a continuous surface from the experimental measurements, to finally deliver the IGES files.

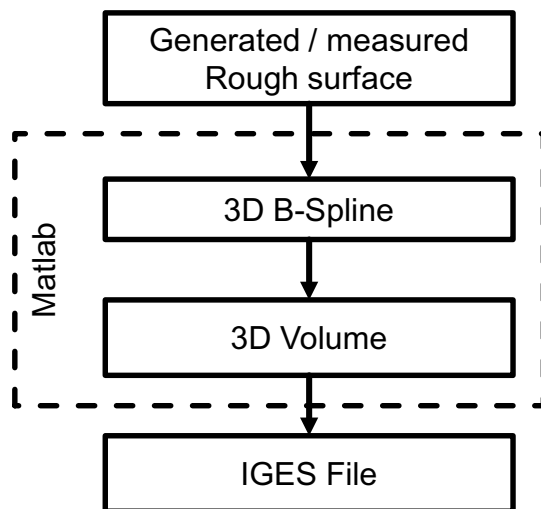


Figure 5.6: Generation process of the IGES Format¹⁵⁵

First step consists in having measure points read into a matrix. IGES format need to have a “cubic” structure, so that a closed volume can be generated through a juxtaposition of 6 surfaces as displayed in Figure 5.7.

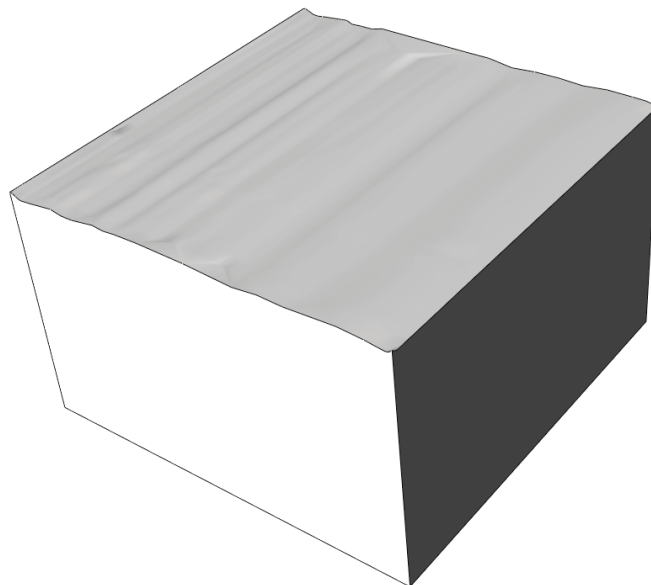


Figure 5.7: Closed IGES volume of a grinded surface

A limitation of this format is the amount of points describing the spline. Usual models are built with 4900 points for surfaces of 140 x 140 μm while measurement resolution is set to 2 μm (in both directions). Generated files get much bigger when measured surfaces increase, so that generating a surface 5 x 5 mm remains impossible.

¹⁵⁵ Savio (2010)

5.2 Establishment of Operating Conditions for the Lubricated Micro Model

Both previously enounced machining processes set the basic characteristics of the model. The machining can be present in both following systems:

- Journal bearing
- Clutch counter plate, clutch lining are assumed to have the same machining

For both systems, boundary conditions need to be calculated roughly at the mesoscopic scale (system level). These are then applied to the microscopic model for their calculation.

5.2.1 Operating Conditions for Lubricated Demonstrators

Both demonstrator characteristics are displayed in Table 5.2. Although the motion of both systems is completely different, occurring phenomena are quite similar at the microscopic scale.

Table 5.2: Working conditions of the journal bearing and wet clutches

Parameter	Journal bearing	Lubricated clutch
Rotation velocity range (rad.s ⁻¹)	0-628	1-838
Inner diameter (mm)	1-62	120
Outer diameter (mm)	–	150
Maximal Sliding velocity (m.s ⁻¹)	39	100
Load (kN)	0,5	5

For both systems, boundary conditions (mainly pressure field) need to be calculated by means of existing analytical models that can be considered as mesoscopic models. In this case, lubrication regime is considered as a full hydrodynamic regime. This step is used to define which assumptions can be met at the microscopic scale for the lubricant on the one hand and for the “assumed” solid-solid interface on the other hand.

5.2.2 Boundary Conditions Calculated in Linear Bearings

Linear bearing and clutch systems can be modeled by means of a same analytical model: typical pad bearing (see Figure 5.8).

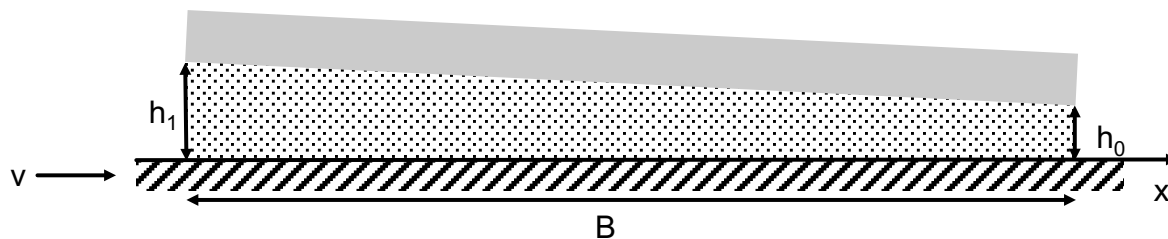


Figure 5.8: Model of the pad bearing

Pressure calculation is done by means of the Reynolds equation linking pressure to lubricant film thickness to sliding velocity:

$$P = \frac{6 \cdot v \cdot \eta \cdot B}{K \cdot H_{\min}} \cdot \left(\frac{-1}{h} + \frac{H_{\min} \cdot (K+1)}{h^2 \cdot (K+2)} + \frac{1}{H_{\min} \cdot (K+2)} \right) \quad (5.1)$$

with

$$K = \frac{H_{\max} - H_{\min}}{H_{\min}} \quad (5.2)$$

and

$$h = H_{\min} \cdot \left(1 + \frac{K \cdot x}{B} \right) \quad (5.3)$$

Table 5.3: Lubricant properties¹⁵⁶

Oil type	FVA 1	FVA 2	FVA 3	FVA 3
Density (15°C) (kg/m ³)	861	870	879	902
Kinematic viscosity (20°C) (mm ² /s)	34	82	-	-
Kinematic viscosity (40°C) (mm ² /s)	15	32	95	480
Kinematic viscosity (100°C) (mm ² /s)	3,36	5,35	10,7	31,5
Density-viscosity constant	0,818	0,815	0,807	0,826

Four different reference oils without additives defined by the German research association of powertrain technology – FVA (Forschungsvereinigung Antriebstechnik)

are used in present investigations¹⁵⁶ and displayed in Table 5.3. Bearing length B is of 10 mm whereas the minimal fluid film thickness H_{min} is of 0,8 μm and H_{max} 1,5 μm . Sliding speed is of 3,5 m/s. Pressure occurring over the whole contact is calculated with previous cited equations and leads to results displayed in Figure 5.9.

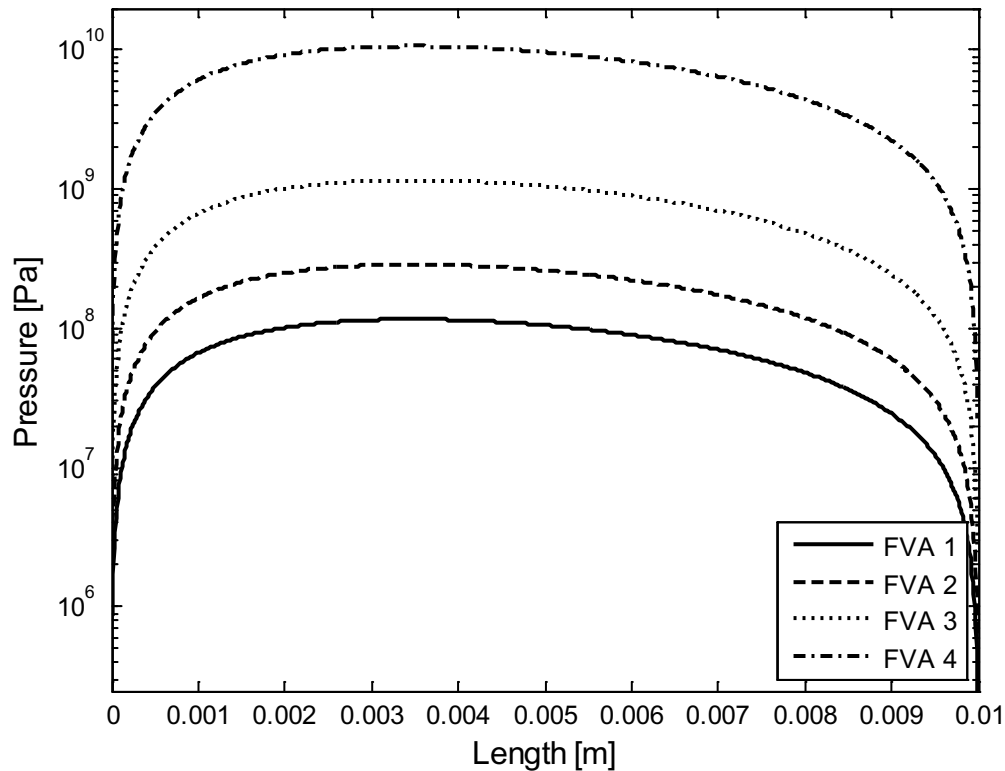


Figure 5.9: Pressure field along the pad bearing for four different lubricants

This pressure profiles corresponds to average pressures and not local pressures. Further investigations are needed when the pressure reaches its maximum. For the FVA1 lubricant, a value of circa 110 MPa is observed. This observation can be easily visualized when extracting a length of 140 μm from last profile. This extraction takes place at the maximal average pressure and is displayed in Figure 5.10. The reason why the lubricant with the lowest viscosity is taken here is to limit frictional energy loss due to lubricant viscosity.

¹⁵⁶ FVA (2003)

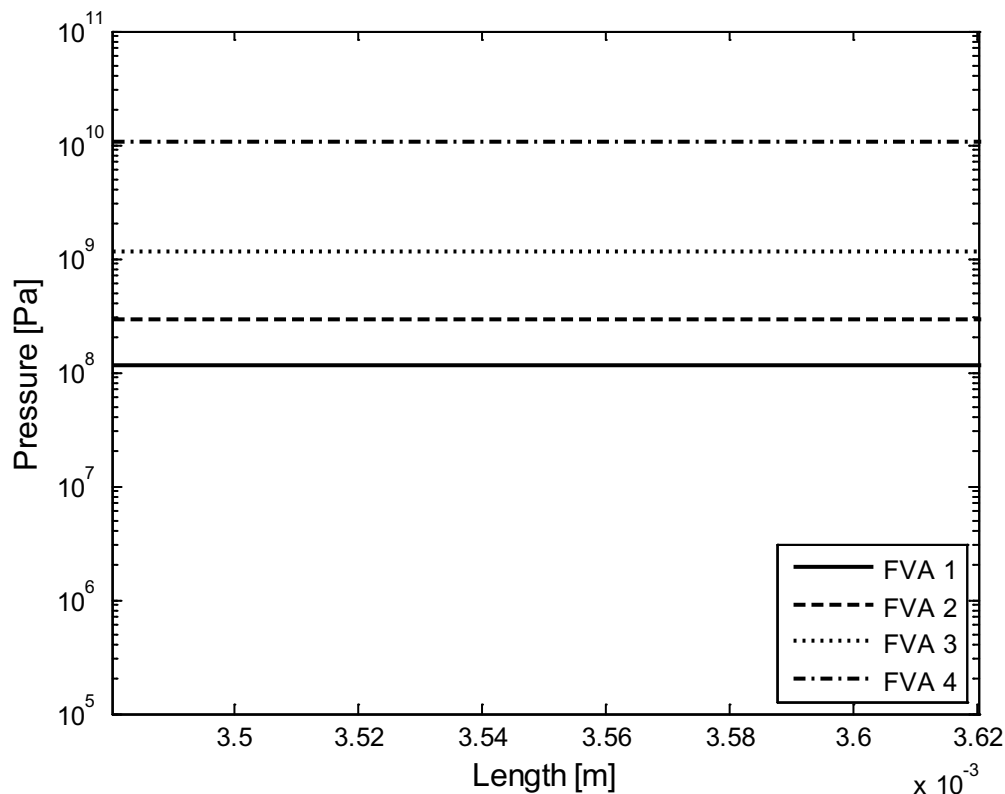


Figure 5.10: Focus on maximum pressure

5.2.3 Boundary Conditions Calculated in Journal Bearings

A modeling approach similar to the one observed for linear bearing can be used for a journal bearing model. An analytical hydrodynamic model can be built based on the same Reynolds equations. Pressure field is also calculated to identify which boundary conditions have to be applied for regimes in which mixed lubrication can occur. As mixed lubrication appears mainly for low sliding velocities, the sliding velocity previously chosen for pad bearings is kept here as working conditions. Two types of journal bearings exist: infinite and short bearing. First type has opened sides whereas long one is considered as closed on boundaries. From the both existing types, a model is here realized for the short one because $L/D < 1/3$. D represents the diameter and L is its width (see Figure 5.11).

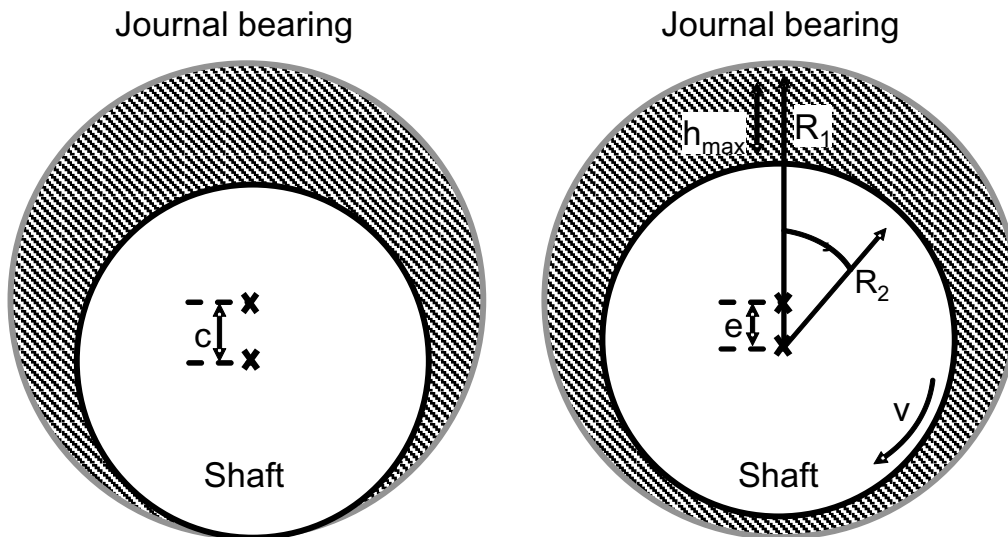


Figure 5.11: Schematization of short journal bearing

Reynolds equation is used to calculate pressure present where the film thickness is the lowest

$$p(\theta) = \frac{3v\eta}{h^3 R} \frac{dh}{d\theta} \left(y^2 - \frac{L^2}{4} \right) \quad (5.4)$$

with v representing the sliding velocity, η the dynamic viscosity adapted with barus law (see chap. 2.5.3), y the width coordinate, R the bearing radius and L the bearing width, and h the film thickness is defined as follows

$$h = c(1 + \varepsilon \cos \theta) \quad (5.5)$$

where c represents the bearing clearance and e the eccentricity. Simulation model calculated with data displayed in Table 5.4, results from pressure boundary conditions displayed in Figure 5.12. Domain between 2.8 and 2.94 mm represents section used for microscopic models. This domain corresponds to the location where average pressure reaches its maximum.

Table 5.4: Journal bearing parameters

Parameter	Journal bearing
Rotation velocity range (RPM)	4800
Diameter (mm)	20
Eccentricity (μm)	1,525
Bearing clearance (μm)	1,55
Length (mm)	20
Oil	FVA 1

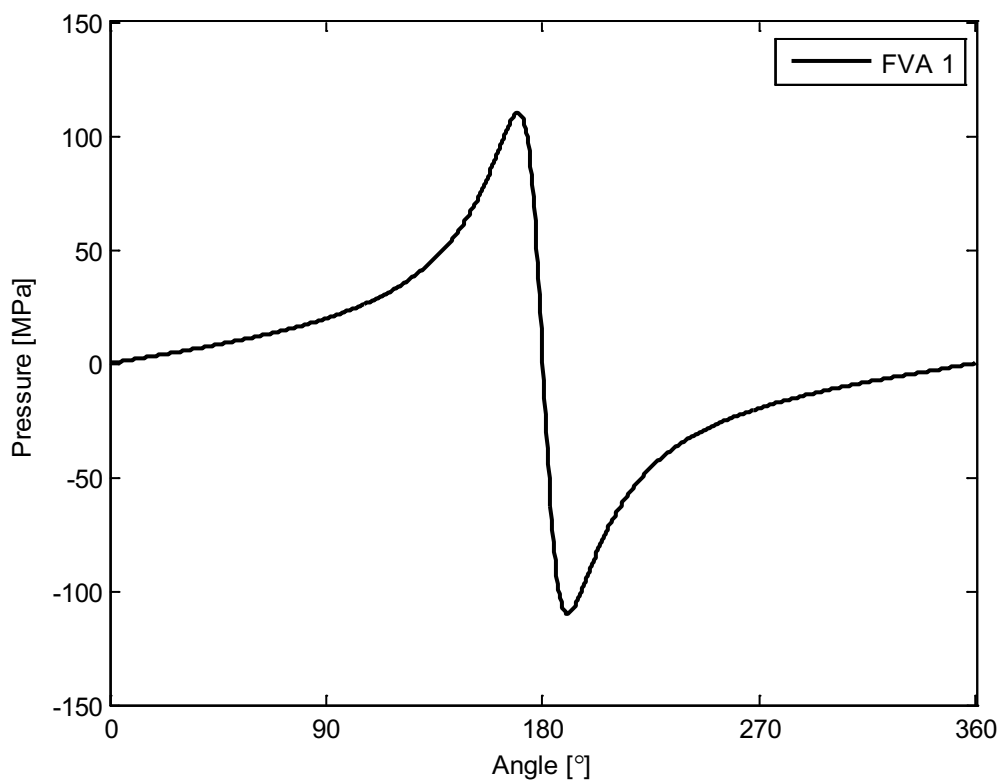


Figure 5.12: Boundary conditions calculated with journal bearings

From a micromechanical point of view, these boundary conditions are similar to those calculated with a pad bearing model. They allow using a unique microscopic model to simulate both system types. Modeling approach is exposed in next subsection.

5.3 Microscopic Model Taking into Account Lubricant

The first modeling step consists in taking simple geometries, as well as minimal boundary conditions to optimize modeling efficiency. On this account, next paragraph treats at first the quasi-2D model used for basic investigations. Then, a 3D extension of the model has been elaborated, taking into account real or generated profiles whose importation process is explained in last subsection.

5.3.1 Two-Dimensional Model

This model is composed of two rough bodies which have both two asperities. This model aims at studying the feasibility of the CEL method in modeling mixed lubrication.

The studied model is composed of three parts: two lagrangian bodies and one eulerian part. Lagrangian bodies are used to model the solid structure whereas the eulerian part is used for the fluid as presented in Figure 5.13.

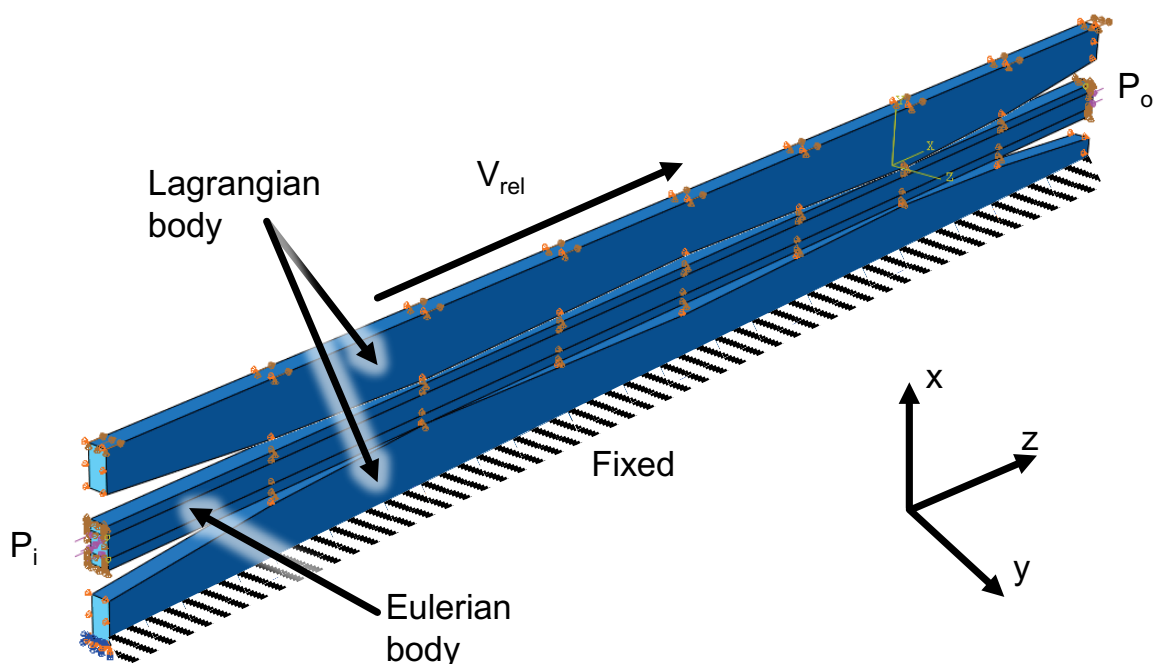


Figure 5.13: Scheme of the two-dimensional model

This model is called two dimensional because no flow is possible in the normal direction (z direction on Figure 5.13). Further reason is that the model has only one layer of elements in the z direction. In order to reproduce real working conditions, different boundary conditions need to be applied onto the model.

5.3.2 Applied Boundary Conditions

As the investigations take place at the micro-scale, the previous announced boundary conditions are applied in order to simulate the conditions present in previous treated tribological systems. For this reason an inlet and respectively one outlet pressure ($P_i = 110$ MPa and $P_o = 109.99$ MPa) are applied on both fluid boundaries as displayed on Figure 5.14. In addition, so called wall conditions need to be applied in the normal direction (z) so that the fluid cannot leave the domain from the side. A next case also needs to be taken into account, it refers to the leakage phenomenon (explained in 2.7.2) occurring when fluid-solid contact has not enough precision. In the present case the upper and lower fluid domain boundaries do not allow any leakage phenomenon.

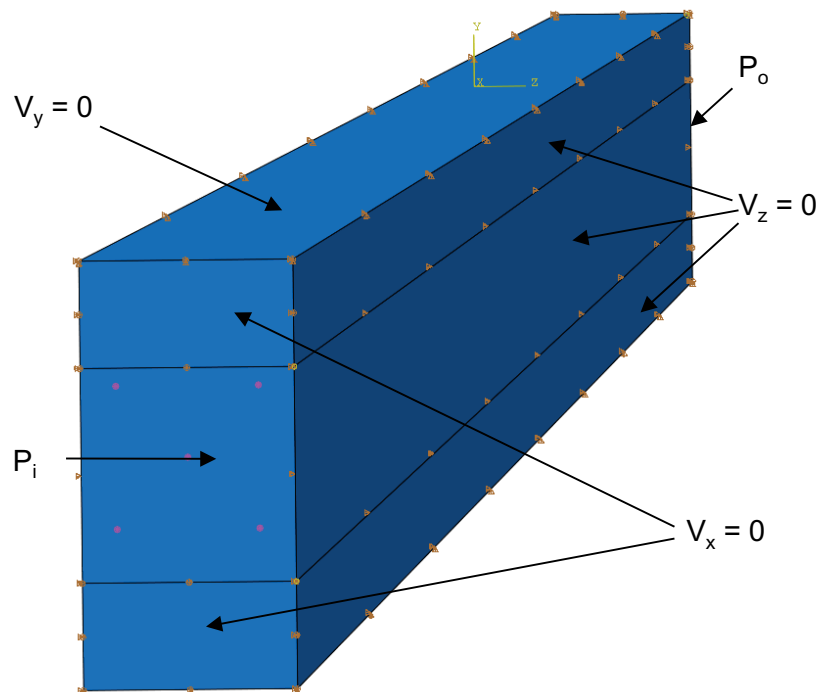


Figure 5.14: Boundary conditions applied to the fluid domain (Eulerian domain)

In order to model an incompressible fluid flow, the coupled-eulerian-lagrangian (CEL) method needs at least having one void subdomain and one filled subdomain. According to this, Figure 5.14 shows how subdomains are defined in the present case: two void domains are present respectively on the top and on the bottom of the fluid subdomain.

A major challenge consists in limiting the meshing refinement as low as possible and limiting at the same time leakage phenomena as solid and fluid meshes are not directly coupled. In addition, fluid pressure boundary conditions have not to be applied too close to the structures in order to avoid leakages and unrealistic solid deformations.

In this preliminary model, no thermal loads are taken into account, as well as no special contact formulation. A friction coefficient of 0.2 has been defined for the solid-solid interaction but was then changed as explained in section 5.3.4. Material properties used in this academic model are the same than those used in the 3D model.

5.3.3 Material Model

Each part needs a material definition. Solid material properties that are listed in Table 5.5 corresponding to an ideal elastic-plastic behavior.

Table 5.5: Relevant solid properties

Symbol	Quantity	Value
ρ	Density	7800 kg/m ³
E	Elastic modulus	210.10 ⁹ Pa
ν	Poisson ratio	0.33
R_e	Yield stress	700.10 ⁶ Pa
μ_e	Yield strain	0.15

Although journal bearing are made of mild materials, developed model assumes using a conventional A514 steel¹⁵⁷ for both contacting solids. Its behavior is an elastic-plastic behavior and has been chosen because it has no special treatment, and has a well-known behavior. Typical strain-stress diagram is displayed on Figure 5.15. Mixed lubrication model uses the same material properties for both contact solids, whereas dry running model uses different materials.

¹⁵⁷ ASTM (2012)

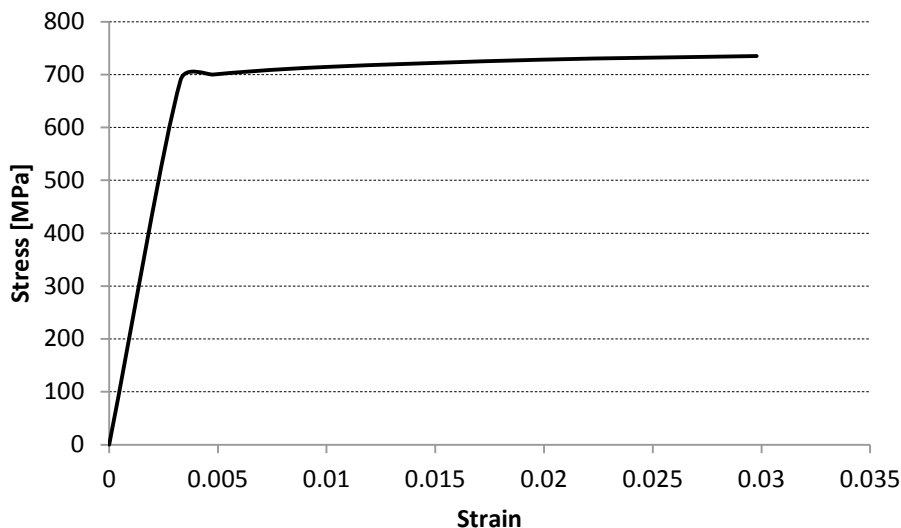


Figure 5.15: Strain-stress curve of the used steel (A514)

After solid properties, fluid properties need to be defined according to the standards displayed in Table 5.3. Mineral oil “FVA1” is used during the development phase but further study will underline the influence of the oil parameters on the tribological behavior. This fluid is assumed to be incompressible and strictly Newtonian. Parameters required for the modeling are listed in the next table (see Table 5.6). Fluid viscosity is adapted by means of the Barus law and sound velocity is calculated by means of the work of Netherwood and Tauber.¹⁵⁸

Table 5.6: Adapted fluid properties

Symbol	Quantity	Value
ρ	Density	880 kg/m ³
μ	Dynamic viscosity	0.088 Pa.s
c_0	Sound velocity	2135 m/s
ν	Grüneisen ratio	0
s	Slope of the $U_s - U_p$ curve	0
h_{oil}	Convection coefficient in the oil	5678 W/m ² K
h_{air}	Convection coefficient in the air	28 W/m ² K

¹⁵⁸ Netherwood / Tauber (1972)

Lubricant flow is supposed to stay laminar and no turbulences are taken into account. Additionally, no cavitation is modeled to simplify the modeling. Moreover, oil is assumed to be incompressible, this explains why Grüneisen ration and slope of the U_s-U_p curve is set to zero. Verification is done in chapter 6.4 by means of a CFD model in order to check the ability to reproduce the pressure field of this kind of contact by means of the CEL approach. In the following of material model definition, contacts are formulated between solid and fluid but also between both solids.

5.3.4 Contact Definitions

Contacts are modeled by means of the general contact algorithm present in FEA software Abaqus (Dassault Systems). This software allows several interaction types to be combined. Fluid-solid contacts are taken into account using the CEL method (see chap. 2.7.2). Fluid-solid interface is assumed to be a pure “no slip” contact, so that no relative displacement occurs between fluid and solid at their boundaries. This type of flow is also called Couette flow.

Second interface – solid-solid contact – is modeled with two components: normal and tangential forces. Normal components are managed through hard contact conditions whereas tangential component is modeled by the Bowden-Tabor model (see. 2.4.2). The reasons for this are detailed in the diploma thesis from Savio,⁴⁸ explaining that normal pressure is high enough so that normal adhesion component can be neglected. The implementation of the model bases on the principle displayed on Figure 5.16.

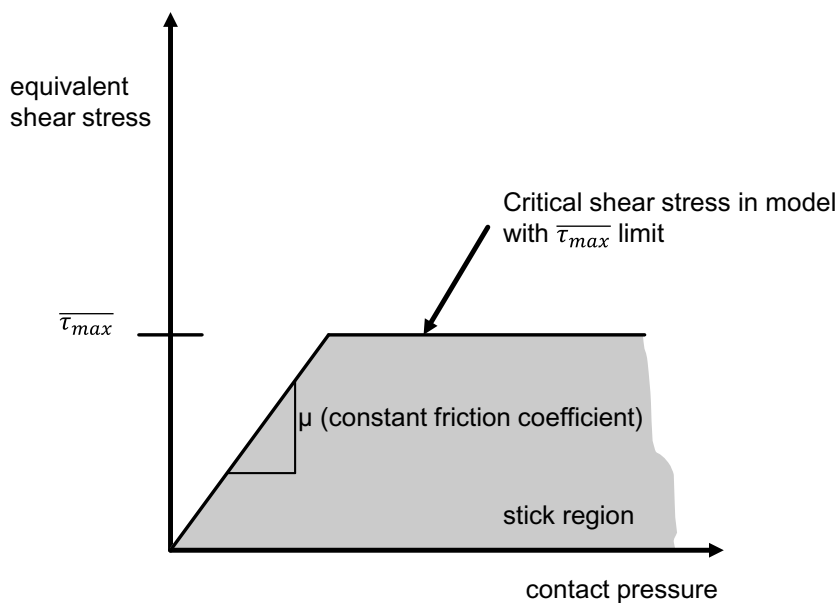


Figure 5.16: Calculation of the friction coefficient¹⁵⁹

¹⁵⁹ Dassault-Simulia (2011b)

Main advantage in using this friction theory towards the use of conventional friction coefficients is that normal load is also taken into account in the calculation of friction coefficient. Nevertheless, instead of defining a friction coefficient, the user has to set a critical shear stress which is responsible for the sliding initiation.

5.3.5 Model Extension into three Dimensions and Model Generation Process

One limitation of the two dimensional model is the fact that for mixed lubrication, no flow is really taking place because the locations where solid-solid contact occurs break the fluid flow which implies a higher pressure between the asperities, as the fluid is blocked between them. As a consequence, investigations are extended into three dimensions in order to take into account real three dimensional topographies. For that, the same boundary conditions as for the two dimensional model are applied.

Once used rough solids are generated, 3D-model is developed using an automatized python program. It aims at controlling whole process, from rough surfaces importation up to application of boundary conditions and input file generation (see Figure 5.17). Main reason to automatize this process is to avoid errors and reduce modeling time as modeling process requires lot of time.

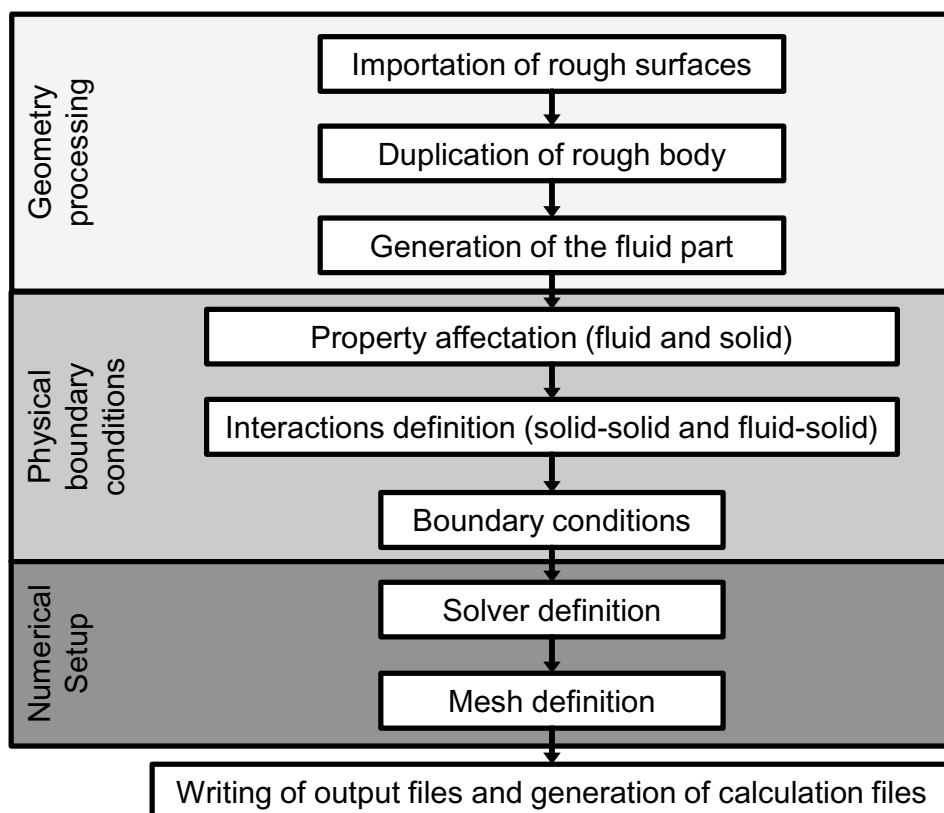


Figure 5.17: Model generation process

Modeling process is separated into three main phases: geometry processing, physical boundary conditions and numerical setup. This step consists in importing IGES geometry files generated with Matlab scripts into finite element software. To build a complete model, imported body is duplicated to build a complete model composed of two contacting bodies. Then the duplicated body needs to be positioned in order to setup different roughness orientations. Additionally, fluid part is generated, following procedure of Figure 5.18. This task consists in defining a volume where fluid is defined at initial state.

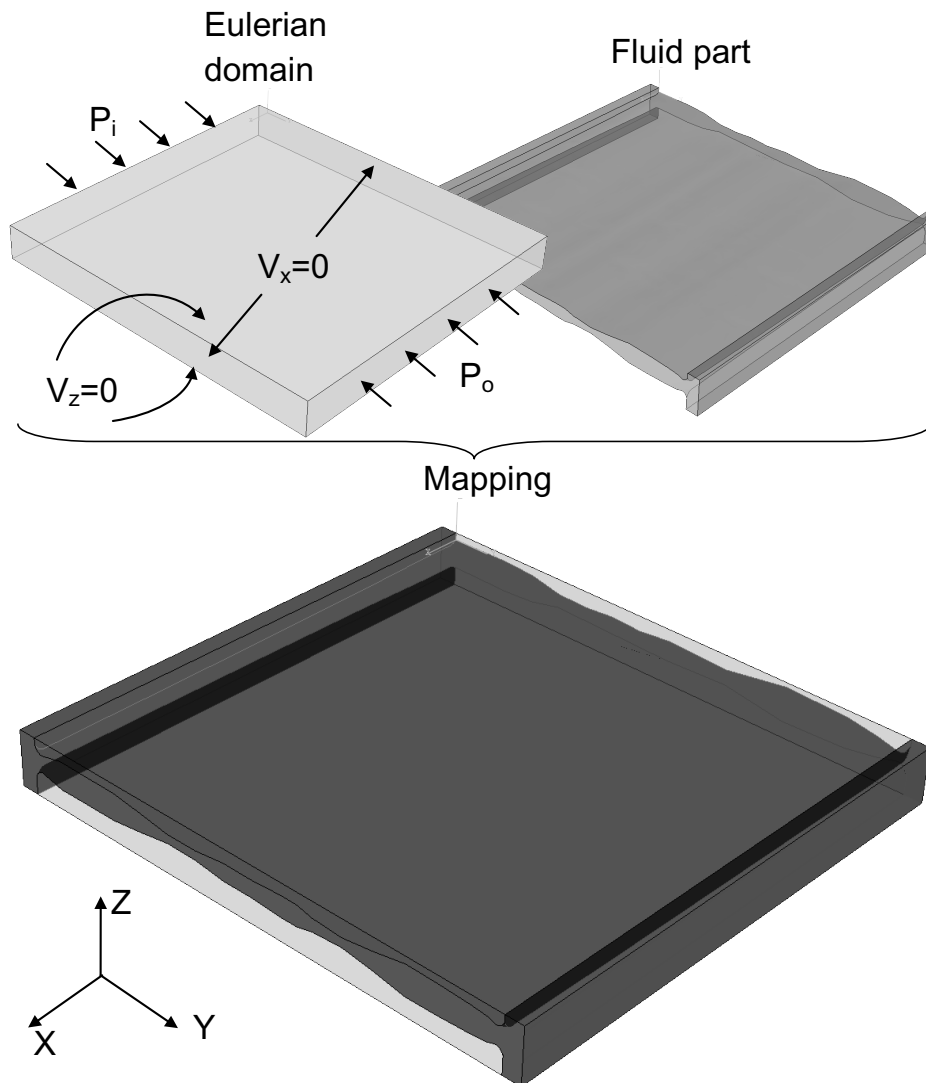


Figure 5.18: Building up of fluid domain

This consists in intersecting the Eulerian domain and both rough bodies in order to generate the so called initial fluid topology. Once this part is created, a mapping of the fluid part is executed on Eulerian domain. This step corresponds to the material initialization necessary when using the CEL method. Last step consists in applying of the working boundary conditions. Total number of built models is 45, taking into

account two different machining types, three machining orientations and five different profiles from each machining type.

- Physical boundary conditions

In this part, material properties displayed in Table 5.5 and Table 5.6 are selected for both the solids and the lubricant. Further essential boundaries concern setup of fluid-solid and solid-solid interactions managed through a fortran routine. Heat generation occurring in the contact is taken into account, in accordance with equation 2.48. Generated heat is considered to propagate equally into both solids. Load conditions are then applied for parameter variation: three different film thicknesses and three sliding velocities. Thermal loads are also implemented but not varied in the different studied models. Only convection phenomena are taken into account in modeling thermal exchange between lubricant and solid. Heat flux coming from air convection is also taken into account to simulate cooling of both bodies. Whole applied boundary conditions are summarized on Figure 5.19. Last step of the application of physical boundary conditions remains in configuring mesh and solving parameters.

- Numerical setup

This part consists in establishing mesh setup such as element type and length as well as the solver to be used. CEL imposes the use of explicit solving scheme as it was foreseen for modeling of high non-linear problems, which is also the case here (high contact non-linearity due to the opening and closing). Consequently, only quadratic tetrahedrons or linear tetrahedrons are available for solving. An essential limitation of explicit solving concerns its dependence on element characteristic length. When element lengths are too small, critical increment size is too small, this finally leads to huge CPU time. In present case, characteristic length is of 4 μm for solids and 2.5 μm for fluid mesh meshed with specific hexahedrons (only eulerian element available). Figure 5.19 shows how the three dimensional model is built up using three of the presented 5.1.1: grinded and turned surfaces.

Whole investigation is achieved by using a four step process in order to optimize the overall CPU efficiency:

- Load application
- Load stabilization
- Application of the relative motion
- Quasi-static regime for the parameter variation

Next subsection concerns the development of the dry friction model, which is less complex than the lubricated one and which uses the same modeling approach. This dry model was mainly developed to validate the solid-solid contact model for the

lubricated model but also to establish boundary condition for a further macroscopic model. This dry model offers the possibility to be compared with information resulting from real experimentations of ball-on-disc tribometer developed in next chapter.

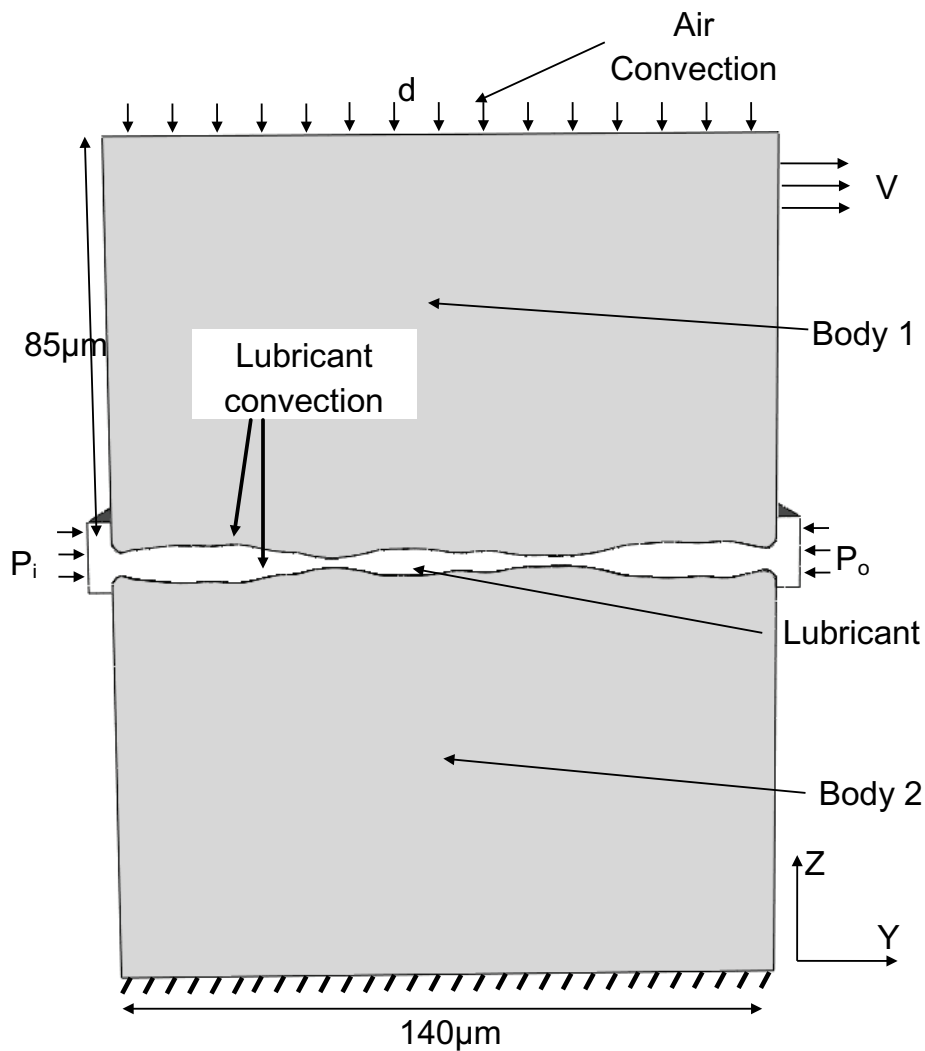


Figure 5.19: Three dimensional model

5.4 Microscopic Model of Dry Friction

A part of present work consists in analyzing impact of roughness on friction behavior of dry running systems. This case considers four machining types: grinding, milling, lapping and turning. Model was essentially built by Savio based on the lubricated model as showed on Figure 5.20.

Motivation for this model is to check if Bowden and Tabor theory used to model solid-solid contact is precise enough or if more details need to be taken into account. It is also used to set boundary condition in form of friction coefficients for a further macroscopic model exposed in chapter 8. The motivation of that is to show the

importance of establishing preliminarily a frictional law at lower scales that can be used in real systems. This avoids a lot of approximations when using arbitrary random friction coefficients.

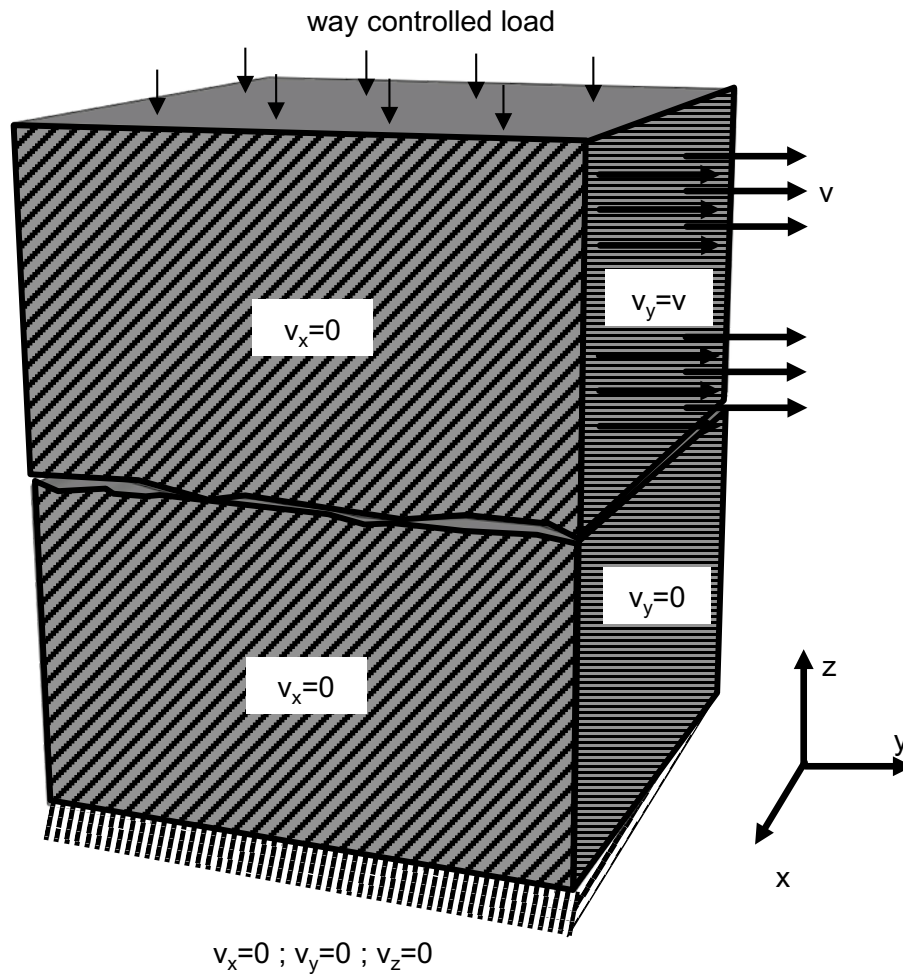


Figure 5.20: Dry running model with boundary conditions

To build this model up, materials and geometries need to be as simple as possible in order to master attempted tribological phenomena. As for lubricated model, three different orientations are used for the dry running model, as displayed on Figure 5.21.

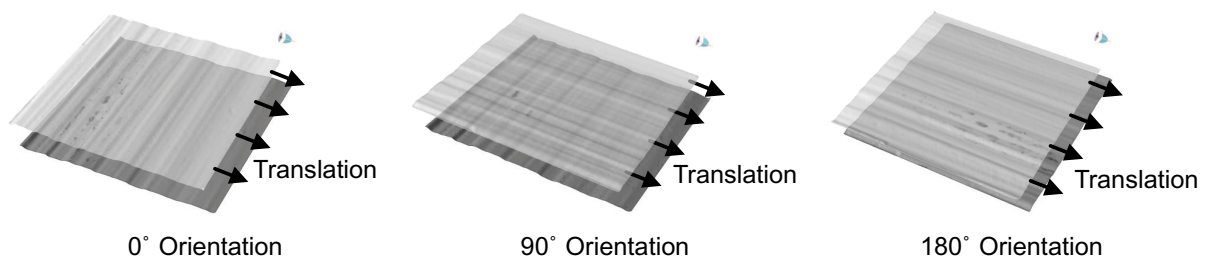


Figure 5.21: Three model configurations

Boundary conditions applied to the model are following:

- Sliding velocity applied on the bottom with $v = 1\text{m/s}$
- bottom fixed on the ground
- tangential contact interfaces managed by means of critical shear stress algorithm (critical shear stress calculated with yield strength technique)
- normal contact managed by means of hard contact technique

This model is used to verify the Bowden and Tabor criterion, a step done in next chapter where experimental results are compared to numerical simulation results.

6 First Steps for the Micro-Models Verification

This chapter proposes a validation of the dry contact model and a numerical verification of the mixed lubrication model. The difference between verification and validation is following: verification consists in checking if the assumptions listed in chapter 4.3 are adapted or not. This task belongs to a usual model validation step.

First part treats the convergence of dry running model (see chapter 5.4). This model is used both to evaluate accuracy of the Bowden and Tabor model and to deliver results relevant for studies at the macroscopic scale. Additionally, this enables it also to determine mesh setup as well as geometry to be used to model solid-solid contacts on the microscopic scale. A second step gives a comparison between numerical calculations with experimental measurements, with a view to determine the deviation to be expected between model and experiment.

Last step treats convergence of mixed lubrication model. Especially the applicability of mesh properties originally defined in the dry model and applied to the lubrication model is verified. Here only a numerical verification is possible.

6.1 Demonstrator for Dry Running Model

Dry running model combining two rough profiles was described in subsection 5.4. In order to minimize physical error, chemical inert materials are considered for the model validation: pairing is composed of an aluminum oxide sphere and a structured titan profile. Configuration is shown on Figure 6.1, on which a sphere of 30 mm is taken as indenter on the structured surface.

To avoid stochastic roughness effects, structured profiles are used, leading to an ideal regular profile, as displayed on Figure 6.3. This enables it to have reproducible contact pairings, as roughness has less impact when investigating such profiles. Surface machining is achieved as follows: a lapped surface is used on which laser generates a “structured” profile by means of interferometry technique. This leads for example to topographies in which maximal distance between a peak and a valley is of 1.31 μm . In the simulation used to establish a relationship between material properties and friction coefficient, computational time is the main limitation for following reasons:

- Low load induce low friction areas and so implies using small elements (a direct consequence is a huge number of DoF)
- Low sliding velocities induce long investigation steps leading to huge transient simulations

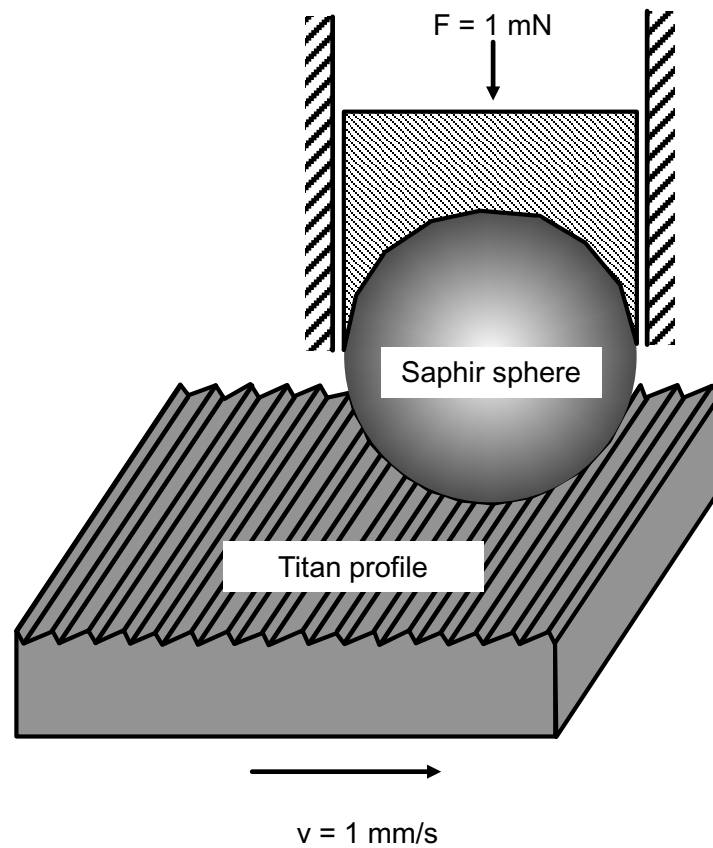


Figure 6.1: Experimental setup of dry friction model

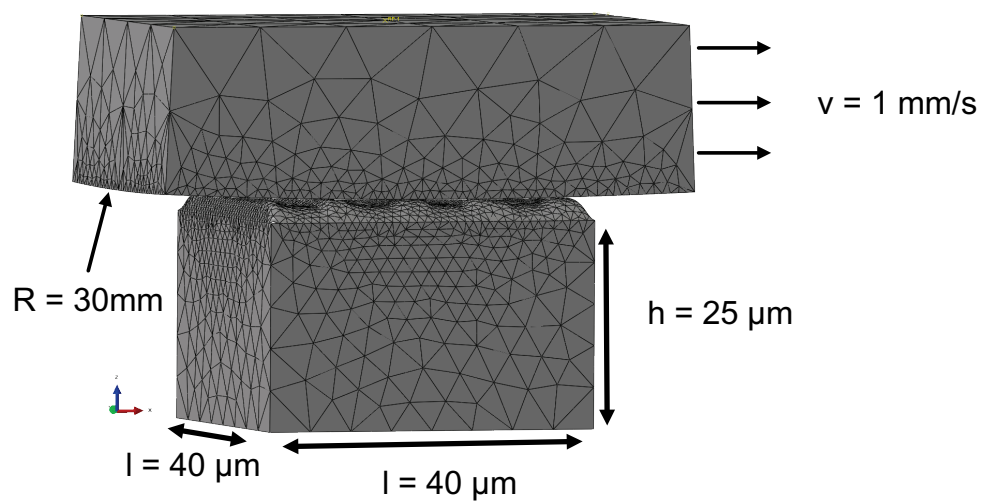


Figure 6.2: Numerical dry friction model

To limit calculation time, the simulation model is reduced as displayed on Figure 6.2. An extract of the indenter is taken, whose radius is of 30 mm: $10^\circ \times 10^\circ$ are used with a thickness of 25 μm . An extract of titan part is also kept small (40 $\mu\text{m} \times 40 \mu\text{m} \times 25 \mu\text{m}$). Material parameters considered here are displayed in Table 6.1.

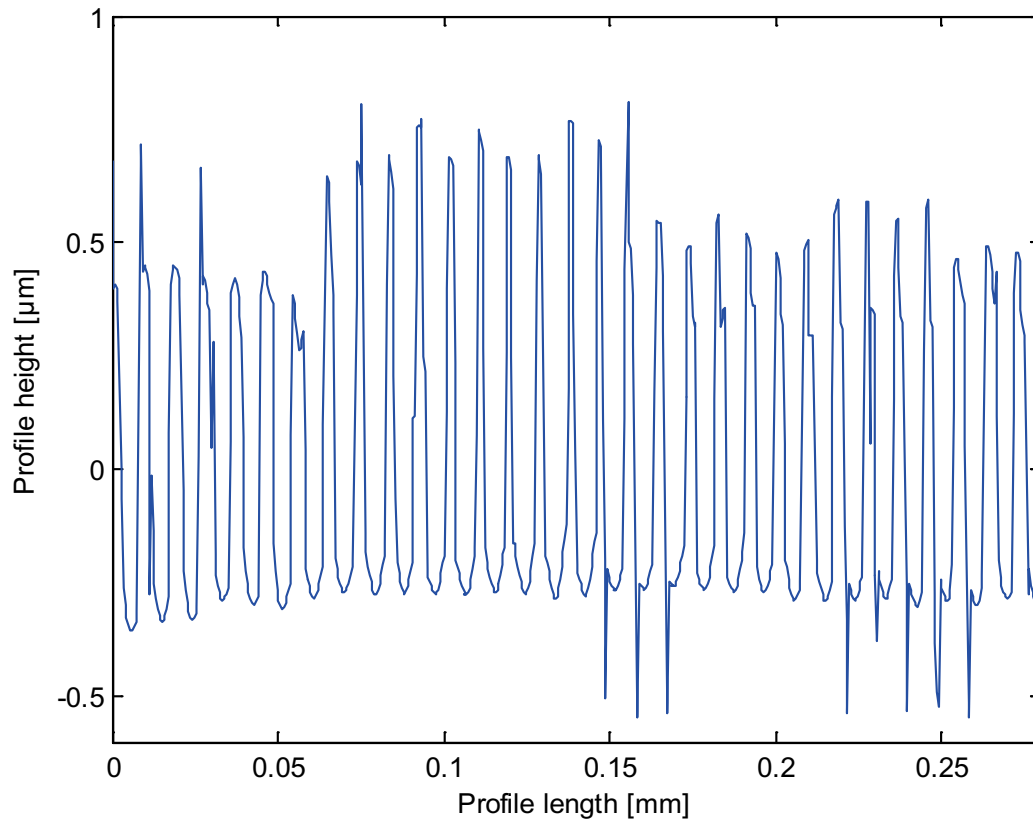


Figure 6.3: Titan profile

Table 6.1: Material properties of the dry model

Symbol	Quantity	Aluminum oxide (Al_2O_3)	Titan (Ti-6Al-4V)
ρ	Density	4000 kg/m^3	4900 kg/m^3
E	Young coefficient	$329 \cdot 10^9$ Pa	$121,58 \cdot 10^9$ Pa
ν	Poisson coefficient	0.33	0,338
R_e	yield stress	$700 \cdot 10^6$ Pa	$334 \cdot 10^6$ Pa

6.2 Convergence Verification and Validation of the Dry Running Model

Convergence studies are first done to verify if equations are solved correctly and then to check if correct equations are solved. A validation is achieved by comparing numerical results to experimental results. Convergence study consists in varying mesh parameters to see if results are converging to a fixed value. First study investigates impact of the mesh on contact pressure whereas second investigation checks its influence on whole friction coefficient. The reason for that is that friction coefficient is the parameter used for the parameter study.

6.2.1 Shear stress

Mesh is varied here only in the contact zone, going from an element characteristic length of 0,75 μm up to 1,75 μm . Convergence study is displayed on Figure 6.4.

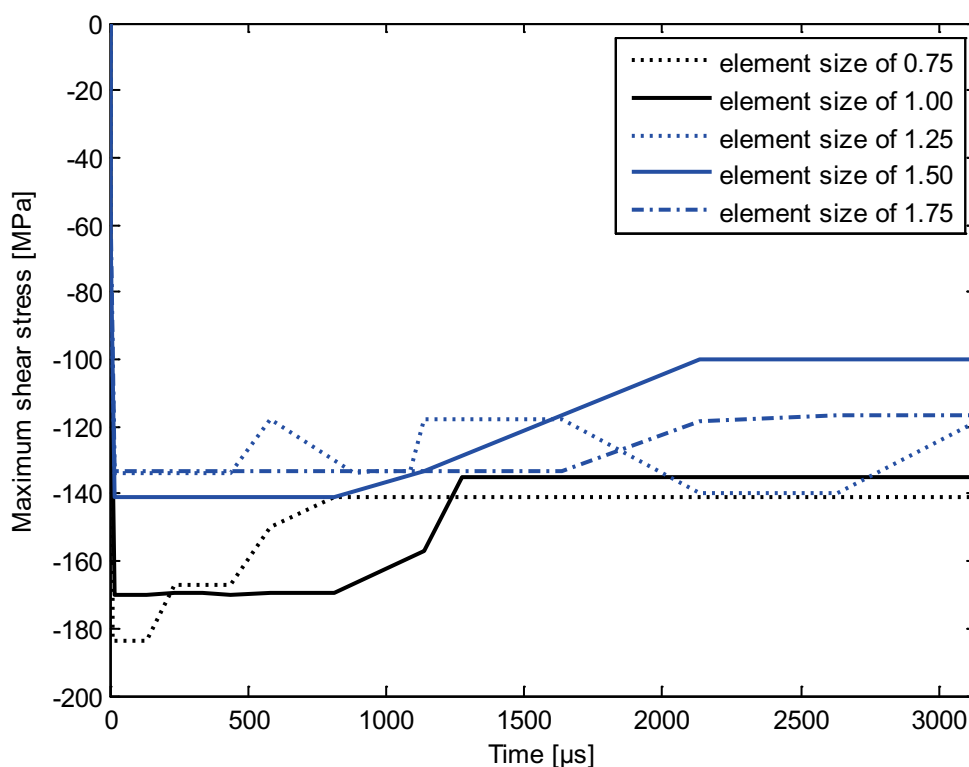


Figure 6.4: Impact of contact element size on maximal shear stress

Analysis shows that maximal shear in the contact, which is according to Bowden and Tabor theory by circa 200 MPa, is not reached with a mesh refinement of 0,75 μm . Reached value are of 180 MPa and relatively near to the model with 1,00 μm as element refinement. When considering the finest mesh as reference, worse result reaches an error of 25,5 % for the roughest mesh which element size of 1,75 μm .

This error becomes important when analyzing precise contact behaviors and has a high impact especially for calculation of friction coefficient. Nevertheless, conventional convergence investigations are more complex for contact models, as pinball regions has also a huge importance on contact reaction force. The parameter of contact reaction force has not been modified in order not to interfere on results: normal contact was kept as “hard contact” all during investigations.

6.2.2 Friction

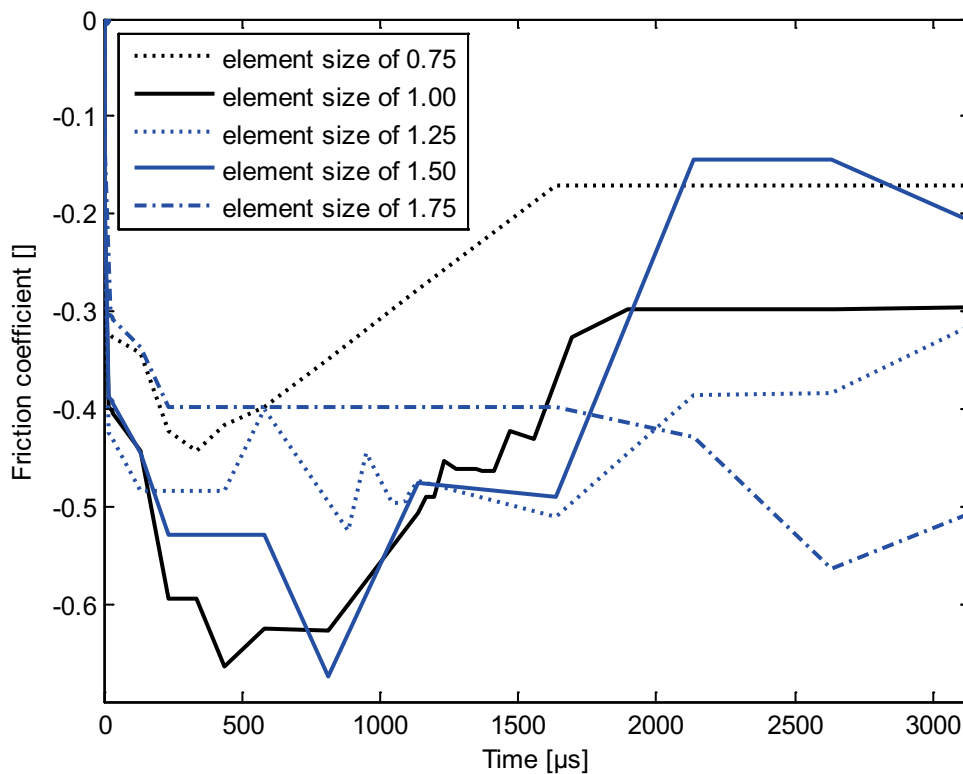


Figure 6.5: Impact of mesh refinement on friction coefficient

Defined friction behavior also takes into account also tangential component of the friction force. Mesh refinement shows that contact area can change. This has a direct impact on frictional shear that occur in the contact. Analyzing the evolution of the friction coefficient in function of mesh refinement, reveals that conventional convergence behavior in contact modeling is not observed. For friction coefficient studies, convergence is tested for the maximum contact pressure or friction coefficient directly and not the Von Mises stresses. As a consequence, the friction coefficient is displayed on Figure 6.5 where mesh refinement remains the same than on previous figure (see Figure 6.4).

Usually, the trend related to the convergence behavior shows data which are converging to the final value calculated by the finest mesh as previously stated with

the shear stress. Such a clear trend can hardly be observed in contact modeling as it depends not only on the mesh but also on the contact tolerance (penetration depth occurring at the contact). The finest mesh shows here a stabilized behavior of friction coefficient over the sliding time. Nevertheless a dispersion of 50 % is observed between the finest and the three upcoming meshes. Once this numerical convergence is verified, validation is done with experimentations as displayed in next subsection. In this analysis no simple convergence can be observed, it can only be stated that lowest friction coefficient is reached with the finest mesh whereas the highest friction coefficient is observed for the coarsest mesh. This correlates with shear stress analysis which showed the highest stress value for the finest mesh and the lowest value for the coarsest. An explanation for present results resides in the Bowden and Tabor theory. Applied normal load initiates shear stress in the contact, which is facilitating sliding. This is explained as less tangential load is required to reach critical contact shear stress defined by the Bowden and Tabor theory until which sliding is initiated. On this account, friction coefficient is lower for the finest meshed model as maximal shear stress is also the highest observed from all mesh configurations. Considering mesh refinement, the one which offers the best compromise between CPU time and error corresponds to a contact element length of 1 μm , as summarized in Table 6.2. In this table the finest model is taken as reference to calculate the error.

Table 6.2: Comparison mesh refinement and CPU time

Contact element size (μm)	CPU Time (s)
0,75	84811
1,00	39229
1,50	20453

After an analysis of the non-lubricated model, the mixed lubrication model needs now to be verified.

6.2.3 Validation of the Dry Running Model with the Ball-On-Disk Experiment

In the framework of cooperation, the University of Saarland with the Institute of Material Sciences of Prof. Mücklich delivered experimental results of contacts between titan and Al_2O_3 materials with a view to validate the use for the Bowden and Tabor theory of both contact models (dry and lubricated models).

The experimental test consists in taking the profile displayed in Figure 6.3 for the rotating titan (Ti-6Al-4V) disk. The setup displayed in Figure 6.1 consists in applying

a load of 1 mN on the Al_2O_3 ball and in measuring the friction occurring between the ball and the disk. Material parameters are those displayed in Table 6.1. When comparing both the simulations (see Figure 6.5) and the experimentations (see Figure 6.6), it was found that dispersion is much higher for experimental tests. Consequently, having a friction coefficient of circa 0.2 with the numerical models belongs to the interval of experimental measures. As a consequence, numerical model can be considered as valid.

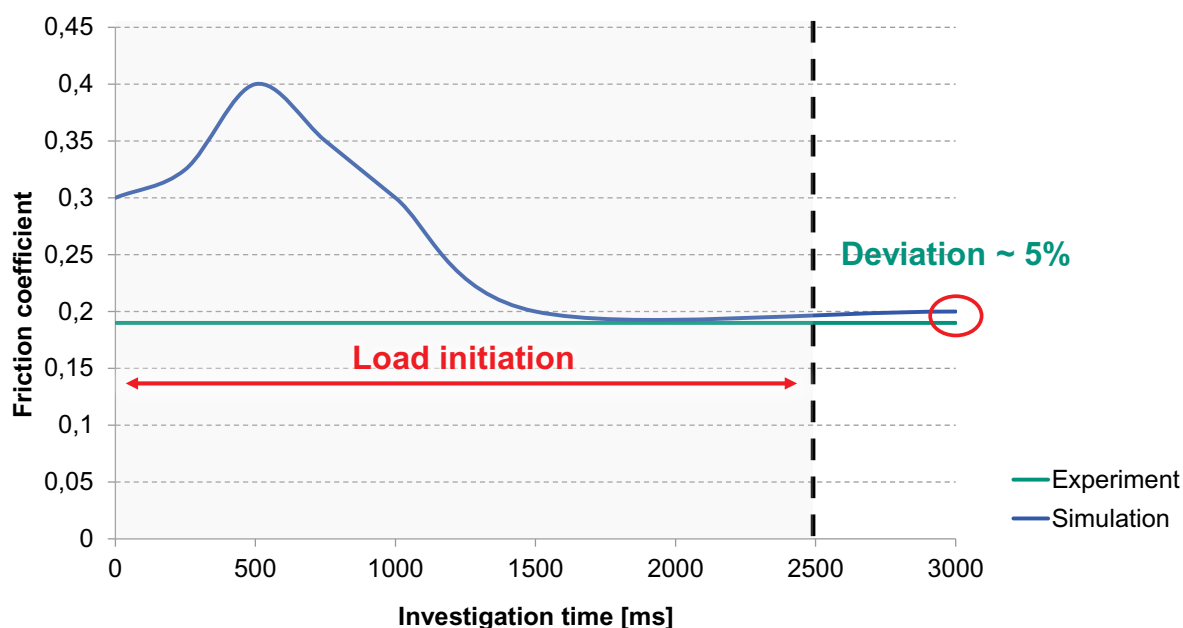


Figure 6.6: Experimental results (ball-on-disk experiment)¹⁶⁰

6.3 Convergence of the Mixed Lubrication Model

As this model is made of two meshes, present subsection has two parts dealing with impact of both meshes on the model convergence.

6.3.1 Convergence Study on Fluid Mesh

Fluid mesh modeled as eulerian part was displayed on Figure 5.18 and meshed with hexahedron elements. Three variants of mesh are considered here to investigate which impact element length have on normal load (see Figure 6.8): coarsest elements with a size of $4.5\ \mu\text{m}$, then $4.0\ \mu\text{m}$ and then the finest one with $3.5\ \mu\text{m}$. In this analysis, reference solid elements have a length of $4\ \mu\text{m}$.

¹⁶⁰ Lorentz / Rosenkranz (2013)

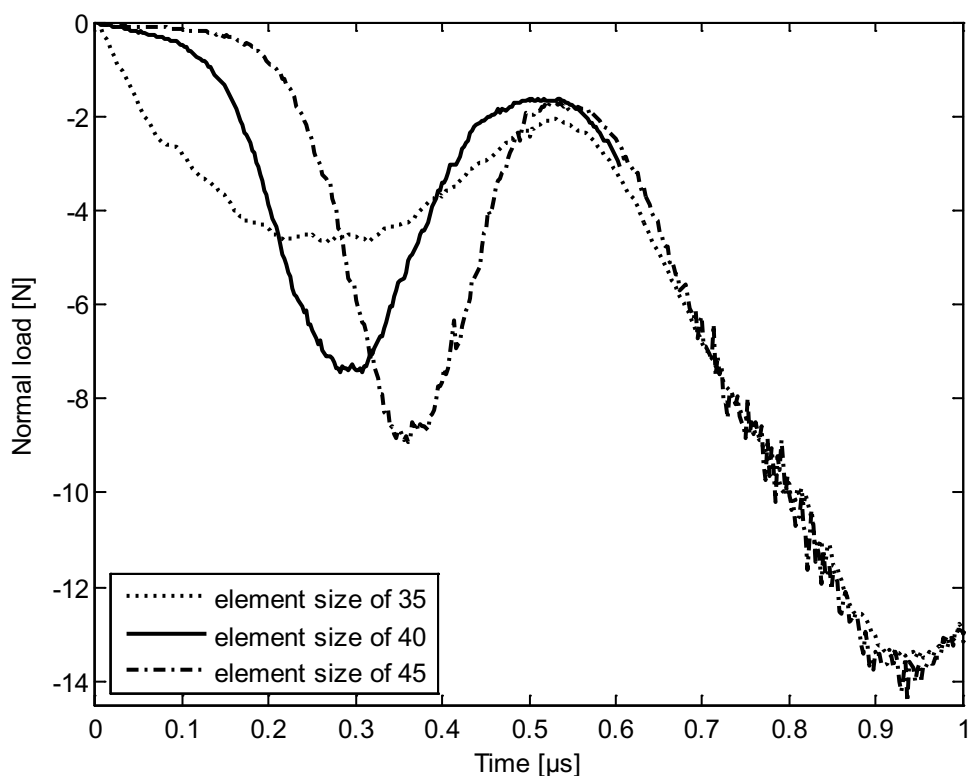


Figure 6.7: Normal load in function of fluid mesh element size

Analysis shows a significant impact of fluid element size on the dynamic load during first compression phase (between 0 and 0.5 μs). The smaller the element size is, the smaller the normal load is. This is due to a better accuracy in the contact between fluid and solid. When a fluid element is smaller, a higher number of elements are active in the contact. As a consequence, pressure repartition is better and fluid leakage occurs less frequently. This has a direct impact on the resultant forces which are comparable to “impulsions” or “shocks” when mesh is too coarse.

An additional effect is the fluid pressure oscillations occurring during load phase: during the compression phase, when elements are too coarse, higher fluid volume leaves the domain. In combination with applied boundary conditions, the fluid is “refilled”. As a result, coarse elements induce more oscillations or higher oscillation amplitudes as shown on the diagram on Figure 6.7 in the second compression phase (0.5 until 1 μs). Main problems resulting from artifact are simulation interruptions calculation errors.

Another major observation is that final load is not really impacted by the fluid mesh itself. An explanation to this is that final load concerns the step when both solids are in contact and so when fluid support has less impact than solid-solid contacts. As the fluid-solid contact is not the main focus of present investigation, an element size of 3.5 μm was finally defined to be sufficient for the accuracy (fluid friction represents

less than 10% of the overall friction coefficient). After fluid mesh convergence studies, solid mesh is set under investigation.

6.3.2 Impact of Solid Element Size on Normal Load

In this investigation, four element lengths are used for tetrahedrons present at the contact interface: 3.5, 4.0, 4.5 and 5.0 μm . Figure 6.8 displays the impact of solid elements on the normal load.

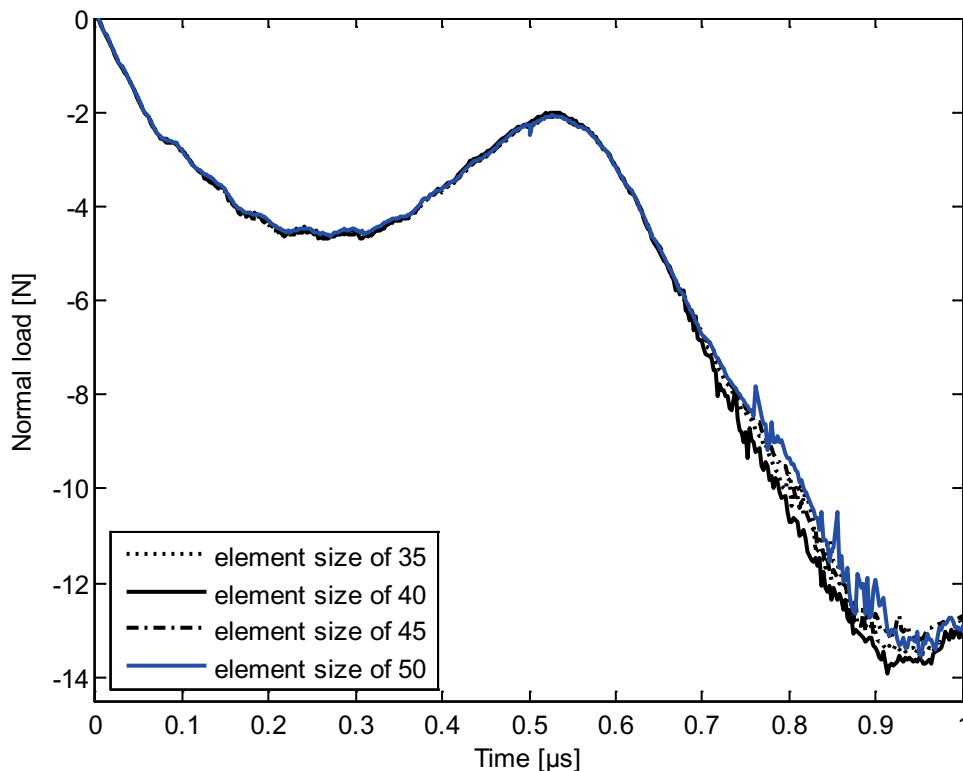


Figure 6.8: Normal load in function of solid element size

Convergence study shows that solid elements have a low impact on the normal load. All results are within a window of 5 % around final average load. Figure 6.9 zooms on the final load phase and shows the impact of element size on the normal load.

As already observed for the dry model, the finest meshes lead to highest loads whereas both coarsest lead to the lowest normal forces. Moreover, deviations are here low, enabling it to take as refinement the coarsest one (50 μm). Unfortunately, this case leads to fluid leakages into the solids and so to unrealistic solid deformations. This is also the case for the 45 and 40 μm ones. As a consequence, a refinement of 3.5 μm needs to be used. For the normal load, mainly due to solid-solid contact, this has no impact as the oscillations observed for the coarsest model are reaching 2.5 % of the final value.

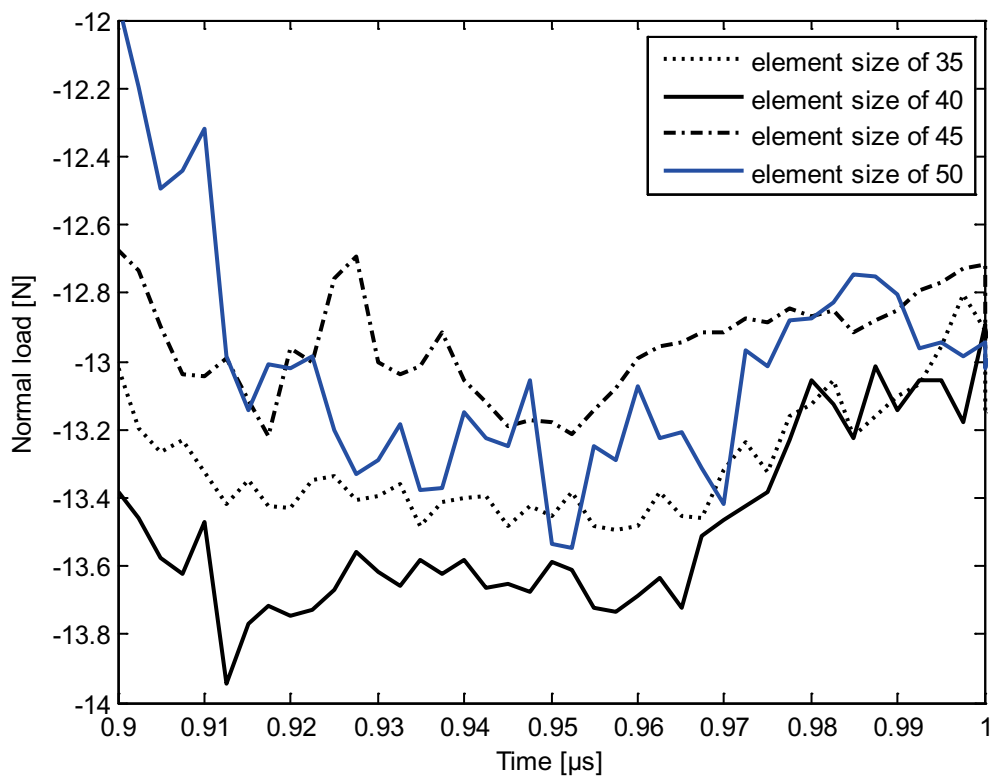


Figure 6.9: Focus on final contact load

After convergence analyses, a numerical validation of the fluid flow is made between CEL and CFD in order to check if used investigation time does not lead to unrealistic results.

6.4 Comparison of CFD and CEL for Full Hydrodynamic Conditions

For comparison, a hydrodynamic model has been built and is based on CFD code ANSYS Multiphysics itself using FVM. This model considers rigid interfaces, also boundary conditions remain the same as those presented in Figure 5.19. Basically, the fluid part exposed in section 5.3.4 is used here for the fluid part displayed on Figure 6.10.

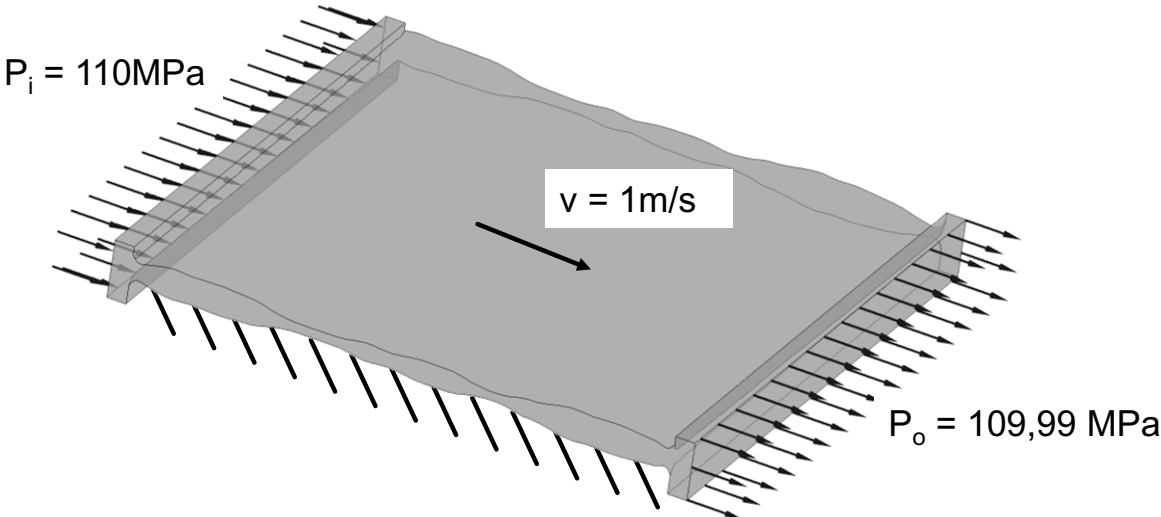


Figure 6.10: Fluid part with boundary conditions used for the CFD model

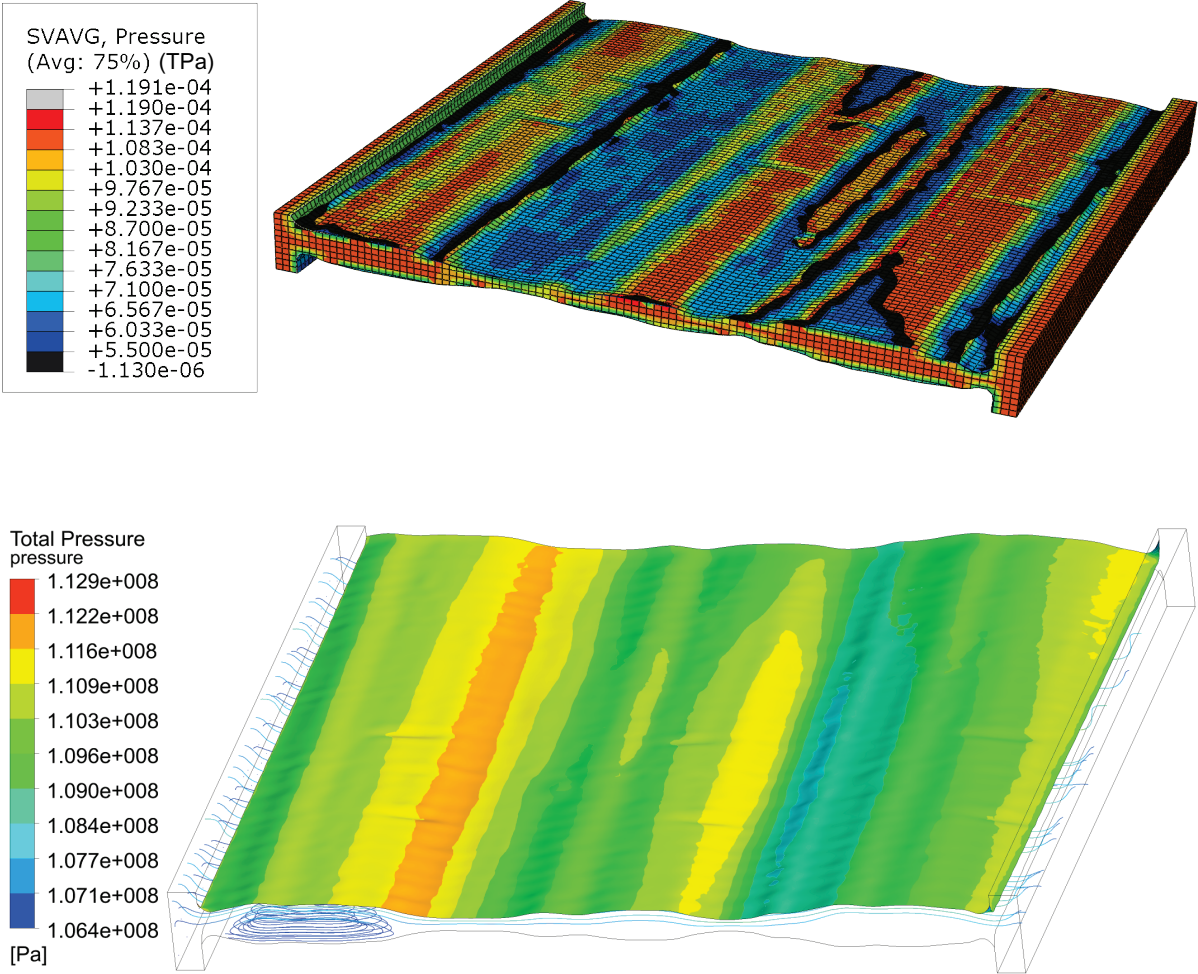


Figure 6.11: Comparison of both contact pressures: FEM (top) in TPa and CFD (bottom) in Pa

Lubricated FE-model is a dynamic model, however working condition are chosen to reproduce a quasi-static regime with a constant sliding velocity. As a consequence, CFD investigation is a static simulation used to generate a similar quasi-static flow.

Comparative results displayed on Figure 6.11 show a relative small deviation of the pressure field between both solving methods. Negative pressure occurs in the dynamic FE-model on the whole contour where fluid-solid contacts take place. This effect is due to the local contact where small low negligible leakage phenomena are occurring. In both cases pressure field varies from 100 to 120 MPa in the whole domain.

This comparison attests that the FEM can be used to model fluid flow in mixed lubrication models instead of using a conventional CFD method. Advantage of first method towards the second one in modeling mixed lubrication has been argued in section 2.7.

Next comparison concerns hydrodynamic friction: both models have an average lubricant film thickness of 5.8 μm , a sliding velocity of 1 m/s and same inlet resp. outlet pressures. When comparing both methods, CEL and CFD, normal load is the same (less than 1% difference) whereas tangential force issuing from the wall shear has 50 % deviation when taking the CFD model as reference. A plausible cause of this problem resides probably in the no slip condition which is not accurate with the CEL method as solid and fluid meshes are not directly coupled. This lack of accuracy impacts the resulting hydrodynamic friction coefficient. In present work, this will not affect highly the resulting calculated friction coefficient as hydrodynamic part takes only a low part (see section 7.3).

6.5 Impact of the Boundary Conditions

In order to get acceptable CPU time, different boundary conditions are applied. These are mainly boundary pressures resulting from analytical models of macroscopic systems. Then comes the time during which normal load is initiated and finally the solid height contributing to both computing time and model accuracy.

6.5.1 Pressure

As the mixed lubrication model is a dynamic model, pressure need to be built up in a first phase. To achieve this, different solutions are available:

- Pressure build up through sliding velocity and conventional no-slip condition (so called wedge effect)
- Building up the pressure by means of an initial fluid flow induced by fluid velocity field
- Defining initially the lubricant film between both solids and applying a pressure gradient on both sides in combination with the normal load

Among all three solutions, first one is the most used and accurate one, CPU time would be too high to use this method. On this account, the second one could be used but is also not adapted as the fluid velocity is highly tangential to solids at some places and leads then to too important leakage effects. As a result, only the last solution remains realistic as the pressure build up is realized in combining normal load to application of the boundary pressure (see 5.3.5).

Two tasks have to be executed when verifying the impact of applied pressure boundary conditions on friction. The approach consists in keeping the pressure gradient constant and varying maximal pressure. On the other hand, the impact of pressure gradient needs to be investigated in keeping maximal pressure constant. These verifications were realized with the model composed of turned surfaces, with parallel machining direction and sliding velocity of 1 m/s. Configuration noted as “reference” in next diagrams has following properties:

- Average film thickness is here of 2,8 μm .
- Viscosity: 0,588 Pa/s
- R_a : 0,901 μm
- Sliding Velocity: 1 m/s
- P_{Inlet} : 110 MPa
- P_{Outlet} : 109,9 MPa

First results showing the impact of the inlet pressure on the friction are displayed on Figure 6.12. Each model has the same pressure gradient and the trend shows increasing friction coefficient when overall fluid pressure decreases. This phenomenon is due to the overall load which is mainly supported by the lubricant when boundary pressures are higher.

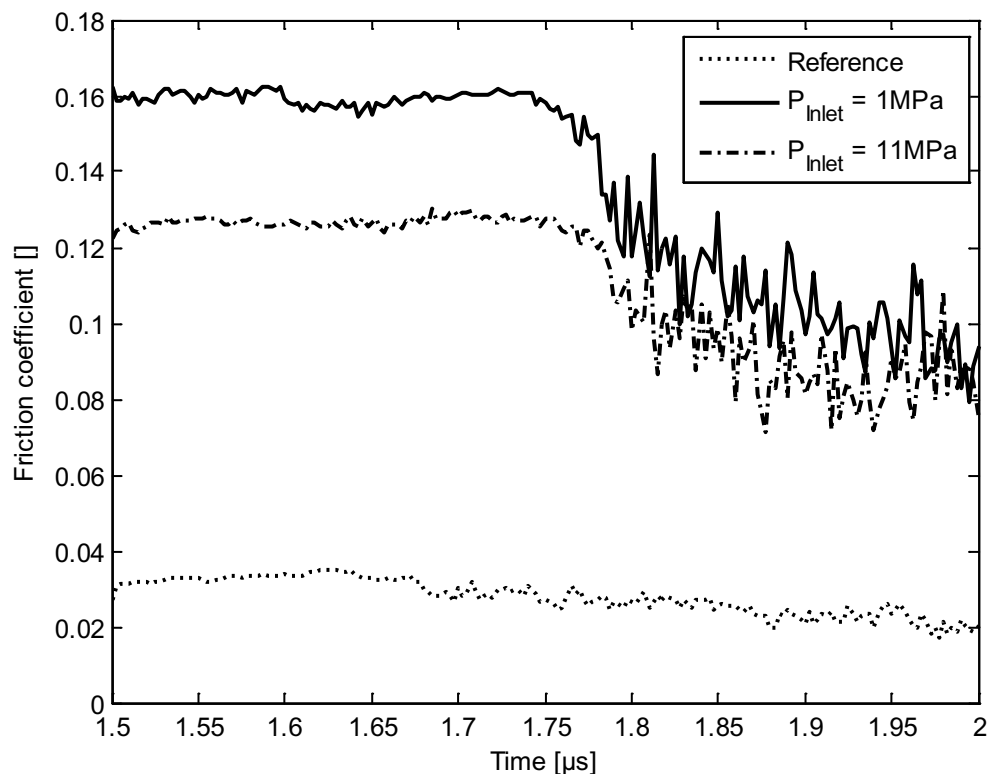


Figure 6.12: Impact of the inlet pressure on the friction coefficient

Boundary pressure has a high impact on friction. This is explained by its impact on local asperity pressure. For high pressures such as those applied in the reference model, fluid pressure induces higher asperity deformations as for both other models. As a consequence, contact shear induced by to contact pressure is more important for high fluid pressures. Additionally, less shear forces are necessary to initiate a sliding. This explains why a lower friction force and so a lower friction coefficient is observed for higher fluid pressures in Figure 6.12. Such observations underline the fact that the detection of mixed lubrication cannot be limited to the measurement of friction coefficients between two surfaces.

Next figure shows which impact pressure gradient has on friction. In this case, inlet pressure was kept to 110 MPa. As in preceding test pressure gradient has been kept on 0.1 MPa for the reference model. Pressure gradient is varied from 0.1 until 100 MPa (see Figure 6.13).

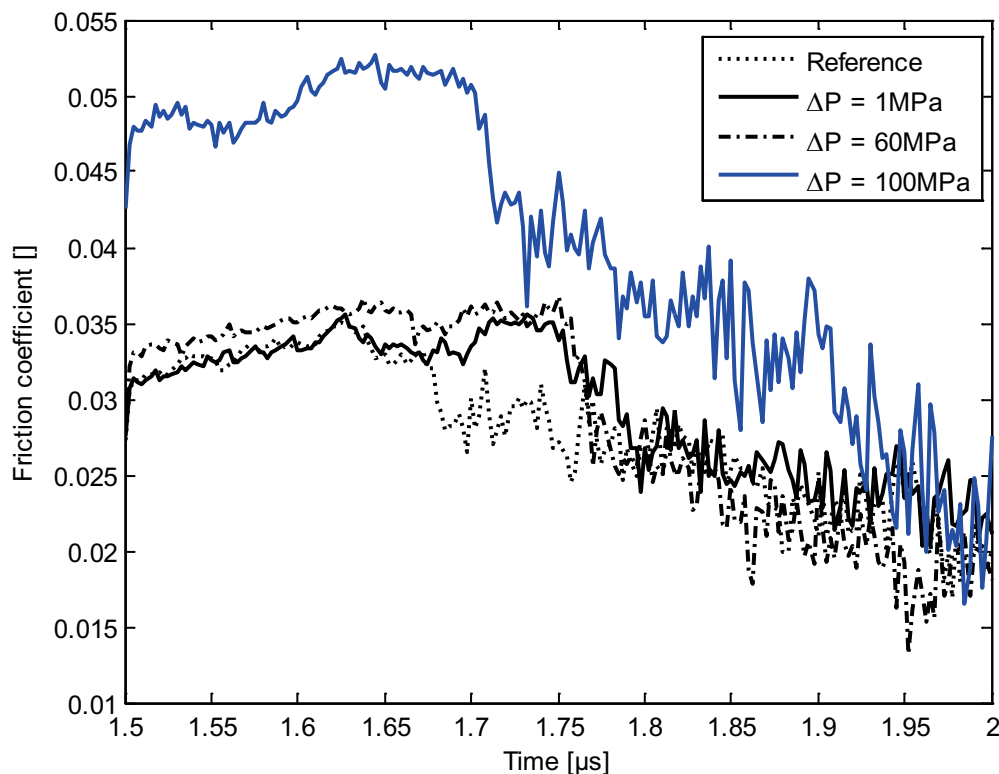


Figure 6.13: Impact of applied boundary pressure gradient on friction

Trend observed for pressure gradient investigation shows a similar trend as for the conventional pressure investigation. This phenomenon is governed partially by the minimal pressure: if this minimal pressure is low, friction force necessary to initiate a sliding is high. Nevertheless, this trend is not as important as in previous analysis as minimal pressure is kept constant. Observed phenomenon is mainly governed by average pressure: when the pressure gradient ΔP is equal to 100 MPa, the friction coefficient is only half as high as when P_{Inlet} is of 11 MPa in Figure 6.11.

A further parameter that cannot be visualized on last both diagrams is that low pressure gradients combine to high pressures decrease pressure build up phase. This phase is described and analyzed in next subsection.

6.5.2 Loading Velocity

Described in chapter 5.3.5, whole process requires phase in which fluid pressure is built up. Three loading velocities were chosen for the analysis, displayed on Figure 6.14. Loading time has a range going from 1 μs for the reference model (having the same properties than previous reference model) up to 2 μs .

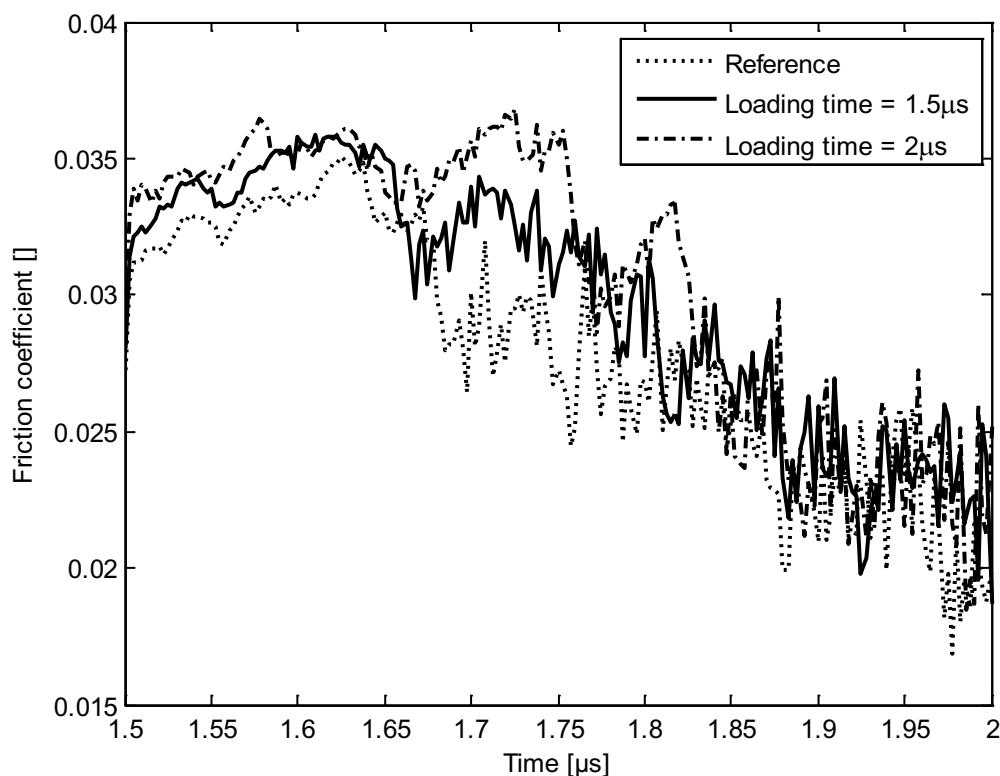


Figure 6.14: Impact of the load velocity on friction

Present analysis underlines that impact of pressure built up velocity is not high enough to influence the calculated friction coefficients once the model is in a quasi-static condition. That means that the time used to stabilize the contacts pressure is high enough. A further parameter likely to influence the results is the height of the model. This parameter is further explained in next part.

6.5.3 Model Height

This parameter remains important as it impacts directly the boundary conditions. If applied loads are too close to the contact zone, contact stresses can be higher than the real ones. On this account, height variation has been done to check the condition of maximal height for which the von Mises stresses are not present on the location where load application takes place (see Figure 6.15).

Diagram shows that a convergence is present for 85-100 μm , a region where stress is half as high as when height is set to 30 μm (60 MPa instead of 110 MPa).

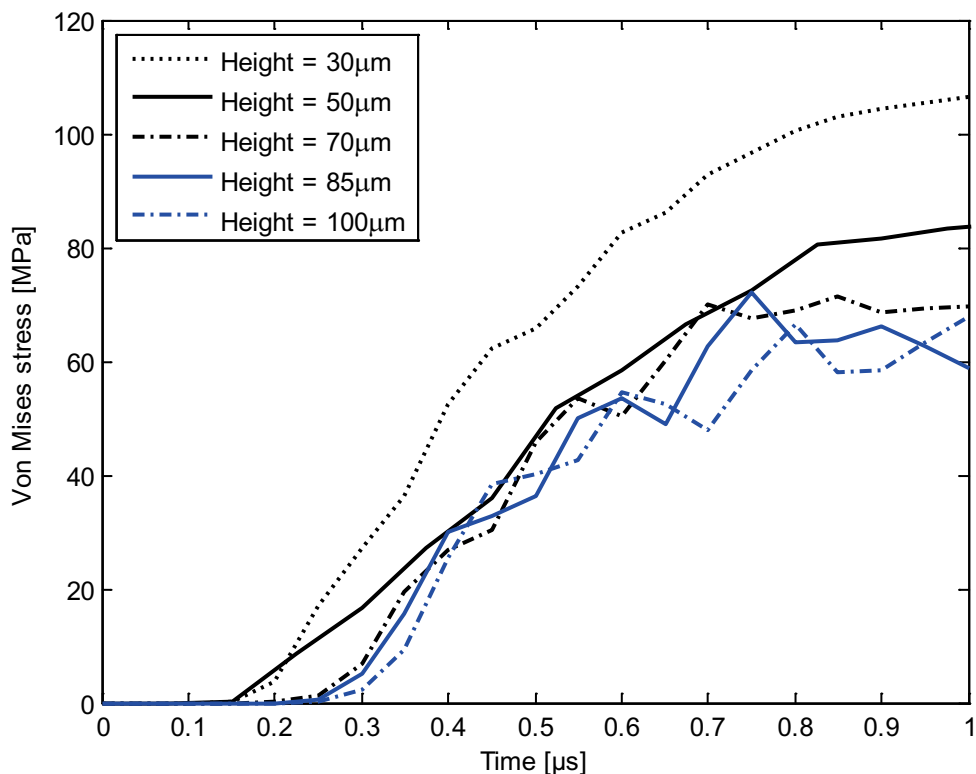


Figure 6.15: Von Mises stress in function of the body height

6.6 Summary

The dry friction numerical model has been verified. For that purpose, the convergence behavior of the model has been studied by means of several analyses. After this successful investigation, a validation of the dry running model has been achieved. Comparison of the numerical dry friction model with real ball-on-disk experiments has been done to validate the results. This step showed that experimental results can deliver results where interpretation remains complex because of their dispersion. Nevertheless, it led on the validation of the Bowden and Tabor contact model which is accurate enough for the present studies.

Next point concerned the convergence abilities of lubricated model showing that loads were lightly impacted by the selected mesh refinement (see 0). This analysis was completed with a successful numerical validation of the lubricated model. This consisted in comparing it with a similar hydrodynamic model built in CFD (see section 6.3).

Then, the impact of boundary conditions on the calculated results was verified. Different investigations showed, that these boundaries had no or only a small influence on relevant results.

An experimental validation of the lubricated model is impossible yet with pin-on-disk facilities. The difficulty resides in the application of boundary conditions present in studied tribological systems that cannot be applied on such facilities for microscopic contacts. After validation and verification activities, both models are utilized to perform parametrical study:

- Fluid properties
- Thermal properties
- Operating conditions (load and velocity)
- Roughness

7 Results and Investigations on the Micro Scale for Lubricated Conditions

Different parameter variations are carried out at the microscopic scale to analyze which impact these parameters have on friction. First parameters are physical parameters characterizing fluid and solid whereas last parameters concerns topography properties. Present chapter considers only the lubricated microscopic model. Results of the dry running model are published in the master thesis from Savio⁴⁸ who showed the impact of machining direction and roughness on the friction coefficient.

7.1 Influence of the Fluid Viscosity on the Friction Behavior

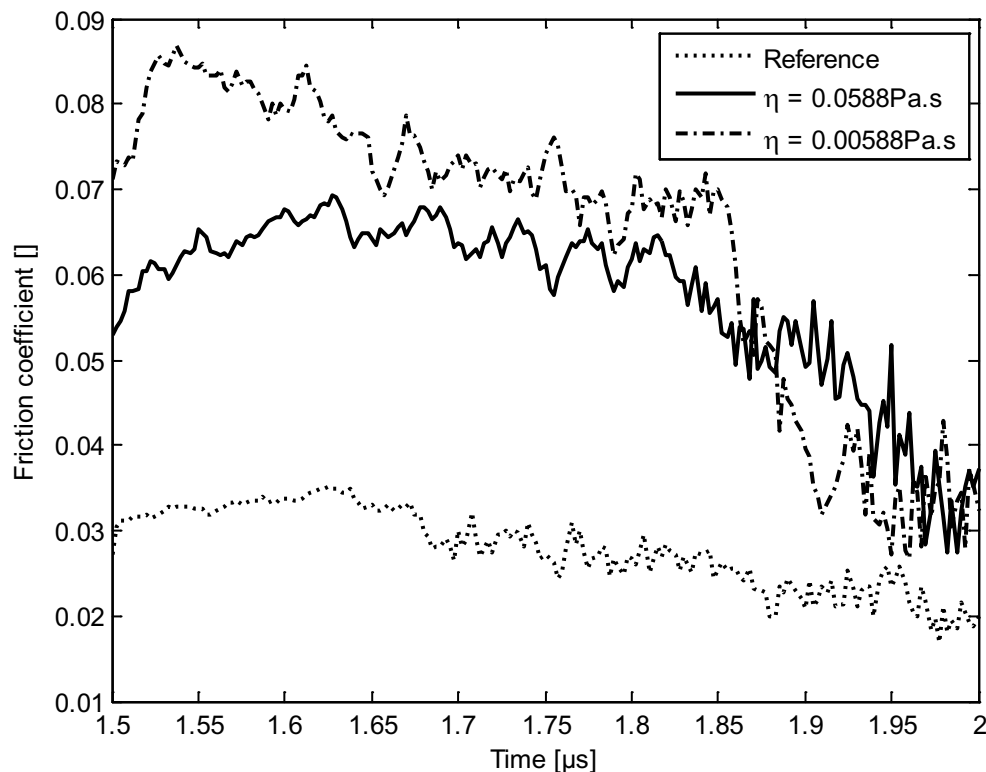


Figure 7.1: Impact of the viscosity on friction coefficient in present model

Fluid properties can highly interfere with friction behavior. Depending on how the lubrication regime is behaving. Fluid viscosity plays an essential role in case of full hydrodynamic conditions. On the other hand, when solid-solid interface is occurring, solid friction takes the main part of friction forces. This section aims at investigating influence of lubricant viscosity on friction behavior displayed in Figure 7.1. Reference model is the same reference model as in section 6.3.

Average pressure occurring in simulated contacts can vary between 80 MPa and 1 GPa. Following the theory of piezo-viscosity, viscosity used in present models, was from 0.088 Pa.s is then in reality of 0.588 Pa.s and so nearly of a factor 10 higher when pressure goes up to 300 MPa. On this account different pressures were calculated with factors 10 and 100 smaller in order to check the impact of such viscosity differences and to remain in the real range of pressure to be expected. Results displayed on Figure 7.1 show a significant difference between the reference model and the non-actualized viscosity. Friction coefficient is half as low for the model with actualized viscosity (reference) than the model having a viscosity of 0.0588 Pa.s. Temperature impact on viscosity is also taken under investigation. Due to the short investigation time, oil temperature does not increase highly. Average temperature increases observed in subsection 7.4.3 are between 20 and 100°C with initial temperature is of 25°C. This corresponds to a viscosity increase of a factor three, in this case, less than for the pressure impact. Viscosity is then adapted for an average temperature of 65°C and average pressure of 300 MPa.

7.2 Impact of Solid Properties on Friction

Two main parameters are observed here with regard to their influence on friction: plasticity and elasticity. Plasticity is taken into account in the solid models as well as friction parameters. Additionally, these material properties are considered here temperature dependent in order to verify the temperature impact on friction. First part of this section treats impact of temperature on both the elasticity and yield strength on friction behavior. Second part evaluates the importance of taking a real elastic-plastic model instead of an ideal elastic-plastic model.

7.2.1 Impact of Temperature on Solid Properties and Friction Coefficients

Conventional construction steel A537 is studied here, characterized by Rothman and Maykluth.¹⁶¹ A set of four models has been calculated in which reference case uses neither thermal dependent plasticity nor thermal dependent elasticity:

¹⁶¹ Maykuth (1981) / Rothman (1988)

- Reference: temperature has no impact on material properties
- Only elastic modulus is temperature dependent
- Only plasticity is temperature dependent (not the critical shear stress)
- Each parameter is temperature dependent (even critical shear stress)

The whole analysis of these models is displayed on Figure 7.2.

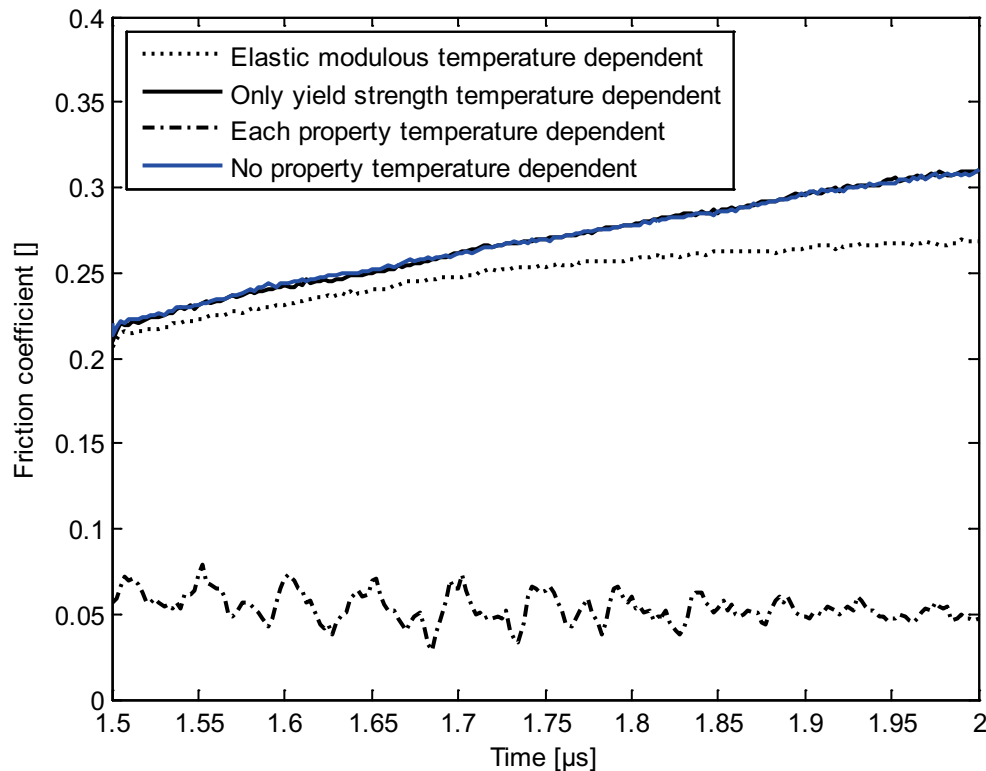


Figure 7.2: Impact of temperature on the friction coefficient in non-lubricated conditions

Results displayed in Figure 7.2 shows a huge difference between models that have no temperature dependent critical shear stress and the others. Taking a temperature dependent elastic modulus has also a higher impact than taking only the plastic stresses temperature dependent. A discussion of these results is proposed at the end of this subsection.

7.2.2 Impact of Elastic Modulus and Yield Strength on Friction

In the study shown on Figure 7.3 only elastic deformations are defined for solid properties. Friction criterion (critical shear stress) is kept constant like in previous models based on critical shear stress theory. The diagram represents a comparison between two models (Young modulus temperature dependent) and the reference which is temperature independent. Both material models investigated here are on

mechanical properties of steel A537 and Ti-6Al-4V having an elastic modulus of 198 and 115 GPa respectively. Both models have a strict elastic behavior (temperature independent).

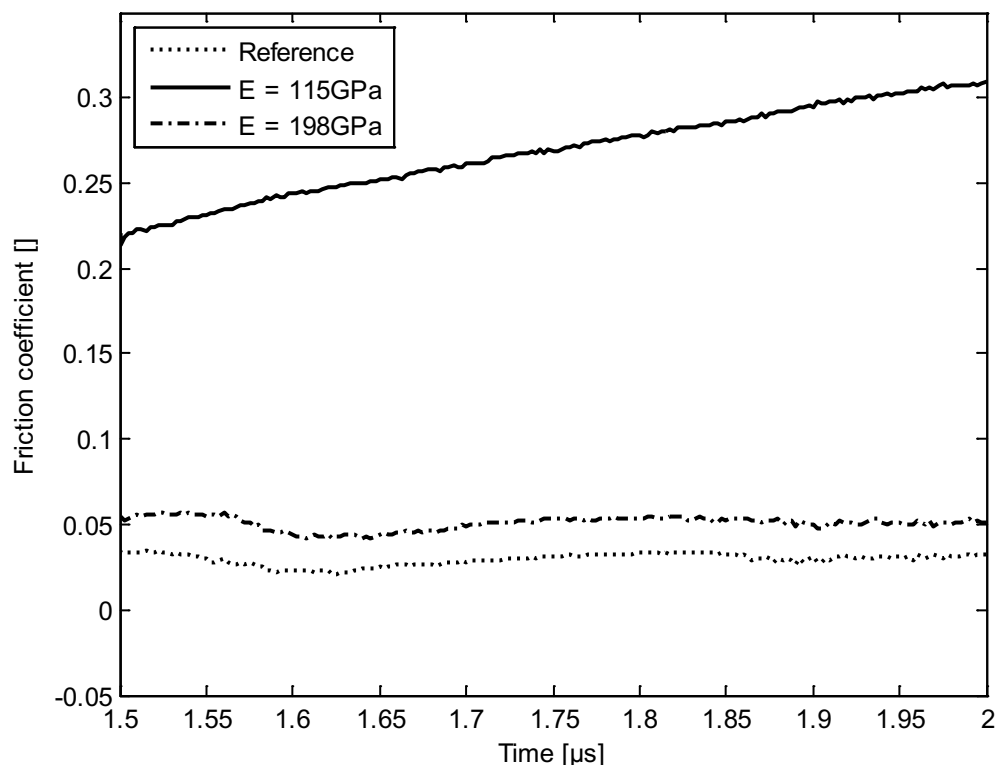


Figure 7.3: Impact of elastic modulus on friction coefficient

Results demonstrate as expected that a strict elastic model is insufficient to model friction behavior on the microscopic scale as resulting normal loads are much higher than for the reference model considering plastic deformations. These high loads are then impacting much more contact shear stress and finally lead to lower friction coefficients.

The friction force, can be broken down into three main components: interaction forces (Bowden and Tabor shear), elastic and plastic forces. First component can be calculated by an integration of shear stress over the solid-solid contact area. Numerically, this consists in averaging shear stresses occurring at nodes which are in solid-solid contact and multiply it with solid-solid contact area.

Friction forces are composed of different forces: elastic forces, plastic forces and adhesion forces and lubricant shear forces. Plastic deformations induce a change in contact area. On this account their calculation cannot be simplified as the resulting contact shear is directly dependent from the contact area. Higher friction observed when taking into account plasticity is coming from the resulting deformations. When only elasticity is taken into account, local pressure increases much more as no

maximal stress has been defined. This results locally to high stress concentrations and so to a higher local shear stress. As a consequence, critical shear stress used as sliding criterion in the Bowden and Tabor theory is met much earlier in strict elastic model than when also plasticity is taken into account. As a consequence, the friction coefficient is smaller for strict elastic models than for models possessing an elastic-plastic material model. This effect can also be correlated with the changes occurring in real solid-solid contact area which is quite smaller in case of use of pure elastic material models, as displayed on Figure 7.4. For a given normal force, friction increases proportionally to contact area. Contact area is calculated considering the following criterion: the nodes of both surfaces are separated by less than 1 nm then the contact is considered to be closed.

Contact area is calculated as follows: overall surface is of $19133.6 \mu\text{m}^2$ and corresponding to a total number of 19881 nodes set as 141×141 . As a consequence, each node represents a surface of $0,96 \mu\text{m}^2$.

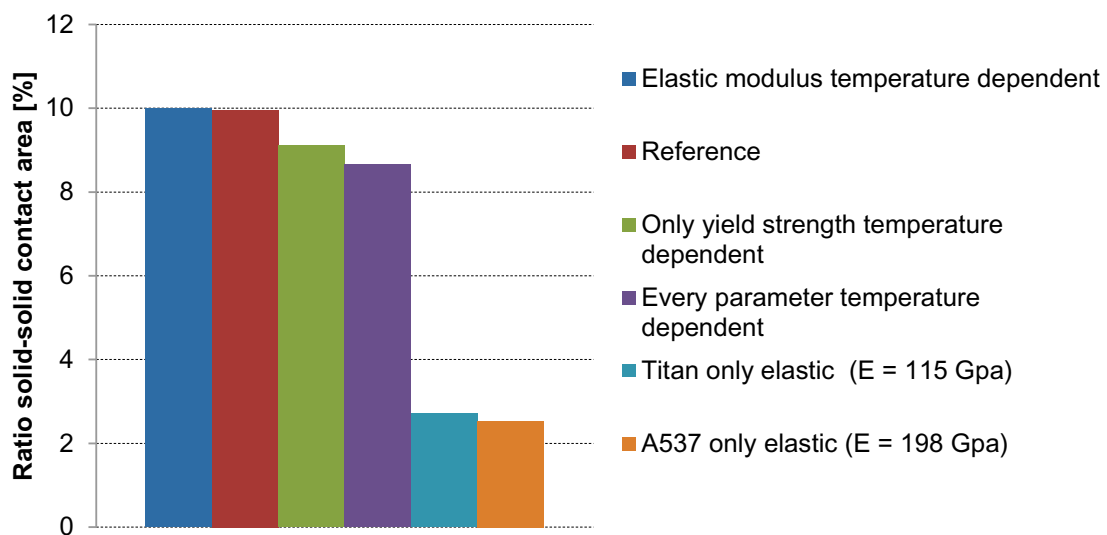


Figure 7.4: Solid-solid contact area ratios of thermal tests

There is no need to do an analysis with different yield strengths as the strict elastic models can be considered as having infinite yield strength. Nevertheless, critical shear stress is kept constant (tangential contact property) for the elastic trials and each of investigated 4 material models also are kept different as proposed in section 7.2.1.

This part underlines the fact that the plasticity must be taken into account in microscopic tribological analyses. Additionally, in combination with the results displayed in Figure 7.2 temperature impact on material properties has to be taken into account in future analyses. The reason for that is related to contact pressures are so high that heat generation impact material properties. After thermal investigations, focus is set on impact of normal load and velocity on friction behavior.

7.3 Impact of Loads and Sliding Velocity Applied on the Friction Coefficient

Loads and sliding velocity are both boundary conditions which are expected to have a direct impact on the friction coefficient. The load impacts the solid-solid contact shear whereas the velocity impacts fluid shear. Both conditions are taken under investigation in present section.

7.3.1 Normal Load

Present load conditions are applied for turned rough surfaces, and machining directions which are parallel to the sliding velocity (0° configuration, see Figure 5.21). Parameter variations are summarized in the next table.

Table 7.1: Model setup

Machining	Turning
Film thickness	5.8, 4.3, 2.8 and 1.3 μm
Sliding velocity	1, 2 and 3 m/s
Average roughness	0.800, 0.816, 0.820, 0.833, 0.900 μm
Machining configuration	0°

Trials are done with one defined velocity, roughness, machining type and direction. The result is displayed in Figure 7.5 illustrating friction coefficient in function of average pressure.

Evolution of friction coefficient is visible on Figure 7.5 and studied in function of contact pressures calculated during the constant sliding phase for a set of different film thicknesses.

Configurations in which 4.3 resp. 5.8 μm average film thickness are defined, represents a fully hydrodynamic regime. In this case, a very low dispersion is observed. Transition between mixed and hydrodynamic regime is present between 4.3 and 2.8 μm as average lubricant film thickness. Once solid-solid contact occurs, dispersion of friction coefficient and contact pressure during the sliding becomes higher.

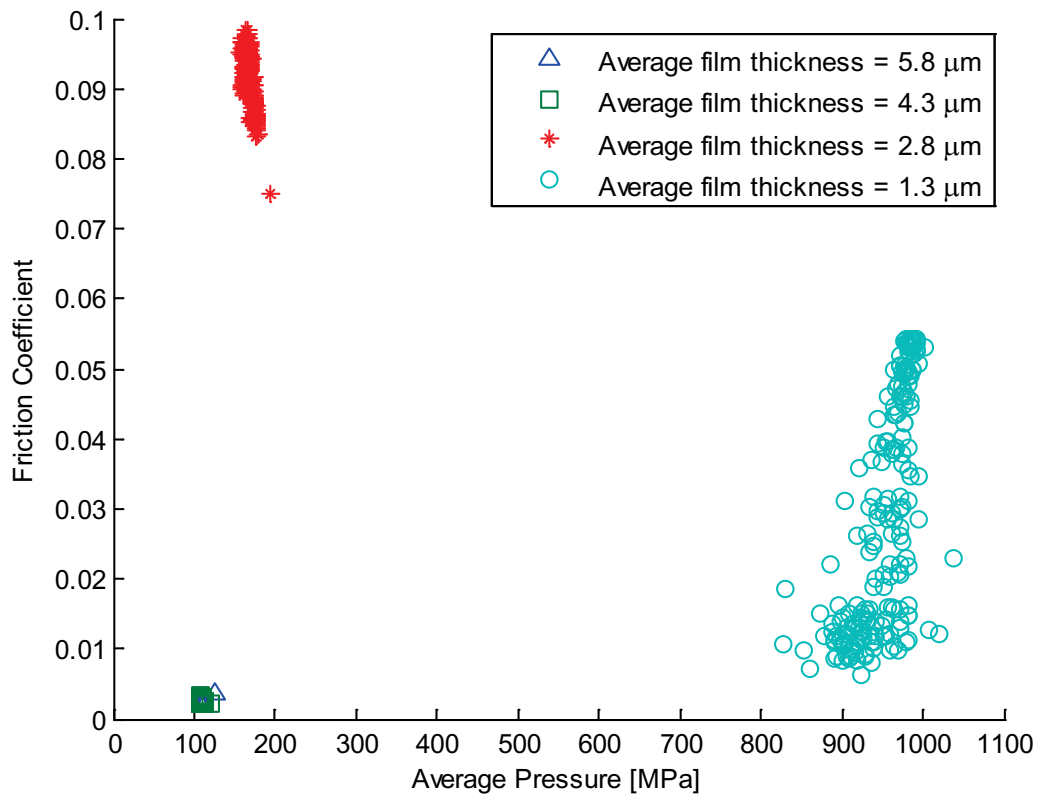


Figure 7.5: Example of impact of film thickness on friction coefficient and load (sliding velocity of 2 m/s and Ra of 0.800 μm)

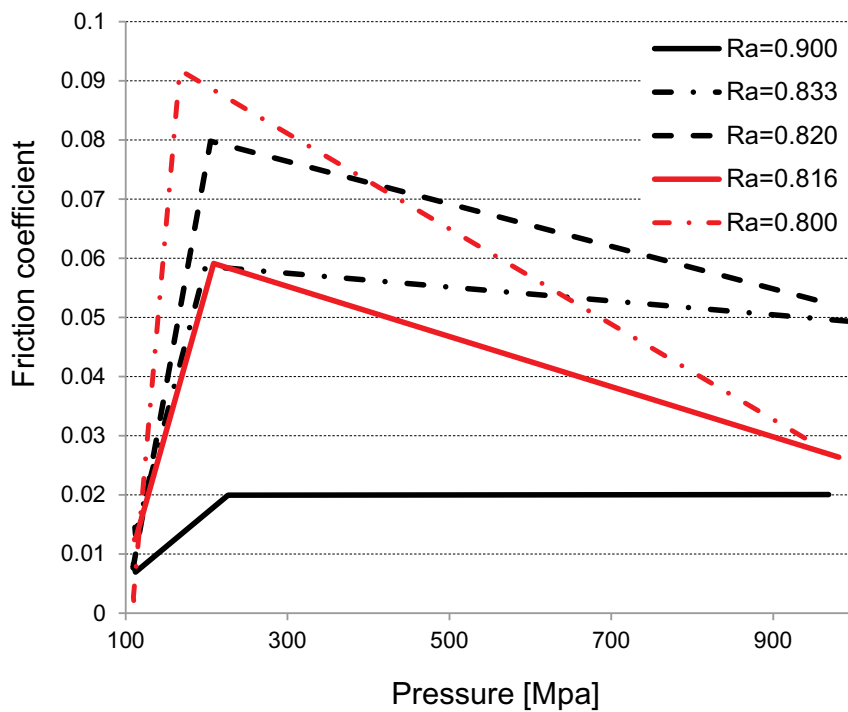


Figure 7.6: Impact of the average normal pressure on friction for five different rough surfaces

After averaging friction coefficients of five rough profiles for each of the four film thicknesses chosen, a diagram can be displayed in Figure 7.6 gives an overview of the friction coefficient in function of roughness and pressure. For this measurement, sliding velocity is set to 2 m/s.

Each of the five calculated profiles displays a similar behavior with a transition between hydrodynamic and mixed lubrication appearing nearly to an average pressure of 200 MPa. Highest friction coefficient is reached for the lowest average roughness profile whereas the lowest friction coefficient is reached with the profile having the highest roughness. This firstly confirms that the average roughness cannot be used to deliver a fixed tribological behavior. A hypothesis can be made that high roughness leads to smaller contact areas leading directly to high local contact pressures on the contrary to profiles with a low R_a . This thesis has to be verified in subsection 7.4.

7.3.2 Sliding Velocity

After different load simulations, three sliding velocities are selected to check their impact on friction under mixed lubrication conditions: 1, 2 and 3 m/s. Material properties are defined here as isothermal, so solid-solid friction is not impacted by the sliding velocity. Nevertheless, when both solids are running in a strictly hydrodynamic condition, a higher sliding velocity should lead to higher friction coefficients (in general but especially for Newtonian fluids that have a linear relationship between shear rate and velocity). Next diagram (see Figure 7.7) displays an example of a hydrodynamic regime of turned solids with an average lubricant film thickness of 5.8 μm .

Among the 200 calculated data points of the simulated models exhibit one point from 200 completely out of range from all other calculated points. Results displayed in last diagram are in accordance with the hydrodynamic theory. The behavior corresponding to the outer points is due to local leakage phenomena but does not have any consequences on whole analysis. In case of solid contact, this effect is not expected to have as much impact as for hydrodynamic conditions (see Figure 7.8) where average lubricant film thickness is of 2.8 μm .

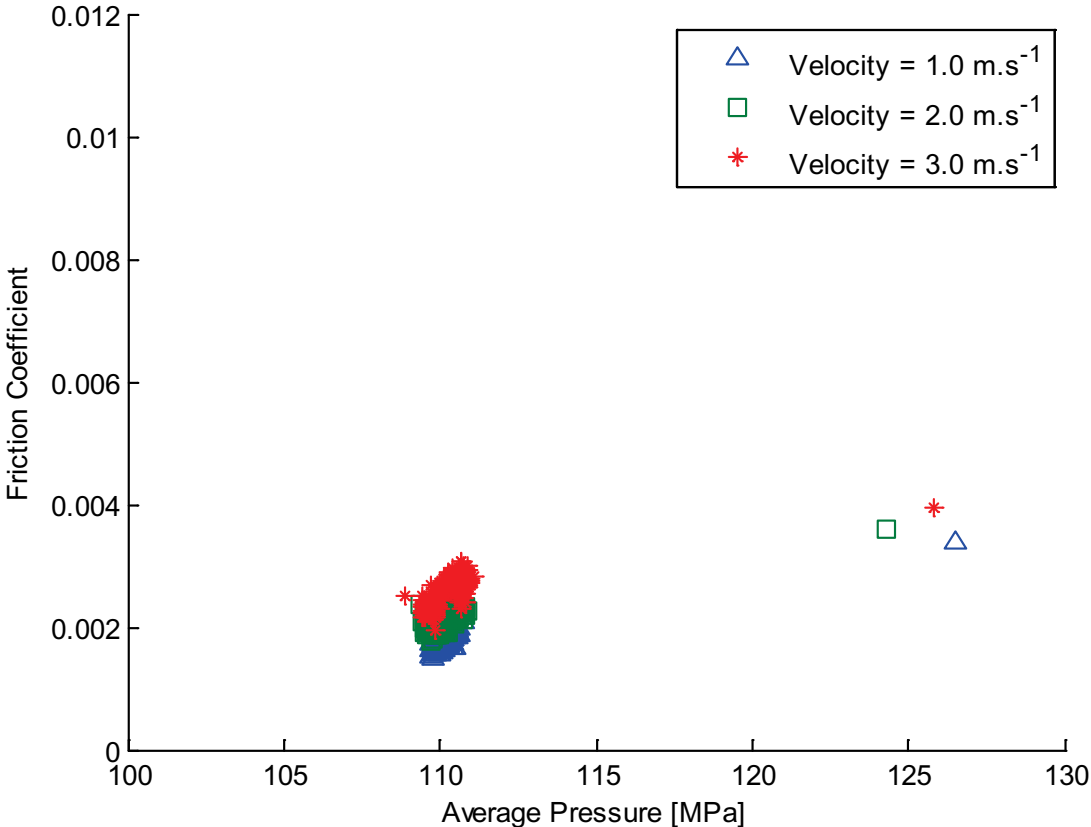


Figure 7.7: Turned surfaces running in hydrodynamic conditions ($R_a = 0,800 \mu\text{m}$)

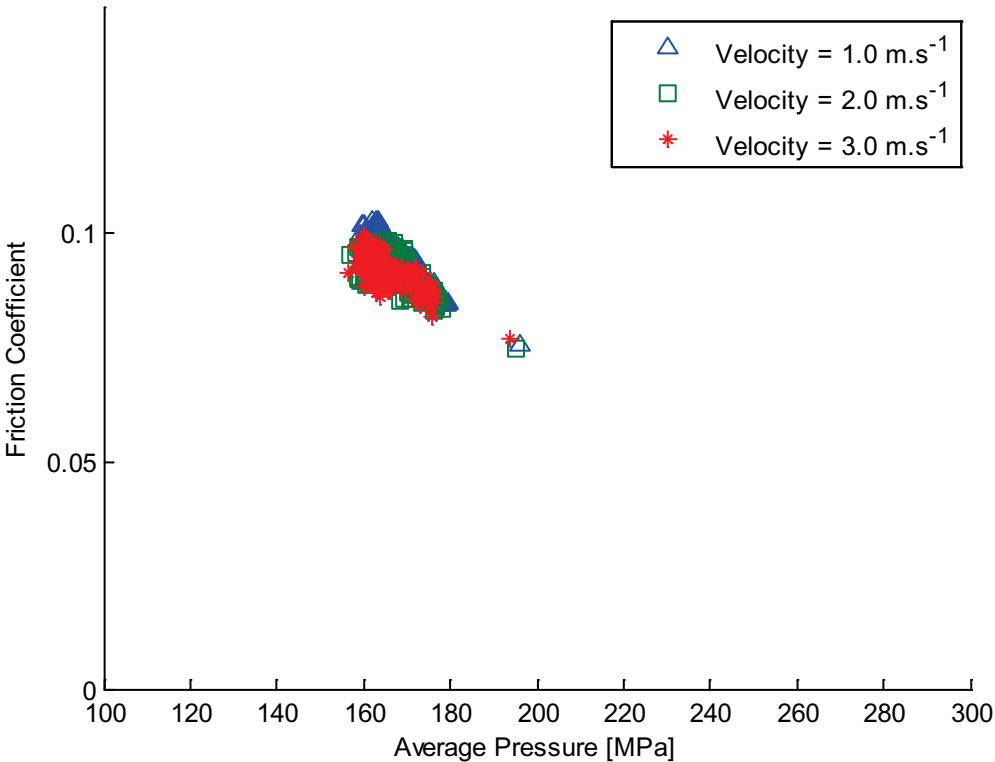


Figure 7.8: Impact of the velocity on mixed lubrication regime ($R_a = 0,800 \mu\text{m}$)

According to the prediction from simulation, sliding velocity has neither impact on friction nor on average contact pressure. Corresponding solid-solid contact areas are calculated they represent the area for which film thickness is less than 6 nm (Table 7.2).

Table 7.2: Contact areas and corresponding ideal tangential force

Variable	Solid-Solid area [μm^2]	Corresponding tangential force [μN]	Overall tangential force [μN]	% of solid-solid friction [%]
Velocity 1 m/s	651.84	0.263	0.3127	84.1
Velocity 2 m/s	605.76	0.245	0.3005	81.5
Velocity 3 m/s	570.24	0.230	0.2978	77.2

Corresponding tangential force displayed in Table 7.2 is calculated by multiplying solid-solid contact area with critical shear stress. For all three velocities, part of solid friction represents more around 80 % of the overall friction. With an increasing velocity, friction area decreases as the configuration is in a contact opening phase for each of the three velocities. As a consequence, contact status is not the same for each measurement. Opening phase is reached when the sliding velocity becomes faster. Trend observed for this present profile ($R_a=0,800 \mu\text{m}$) is also taking place for the other profiles. After investigating impact of working conditions: investigation of the machining impact on friction behavior is exposed in the coming section.

7.4 Influence of the Surface Machining

In addition to boundary conditions, influence of geometrical parameters on friction behavior has to be analyzed in order to check the impact machining conditions on the friction behavior as well as on the finale topography.

7.4.1 Impact of Machining Type

Results are displayed here for two rough profile types: turned and grinded surfaces. Operating conditions are the same for both surface topographies. Next graph (see

Figure 7.9) compares grinded and turned surfaces in full hydrodynamic conditions (film thickness of 5.8 μm) and minimal film thickness of 1.3 μm .

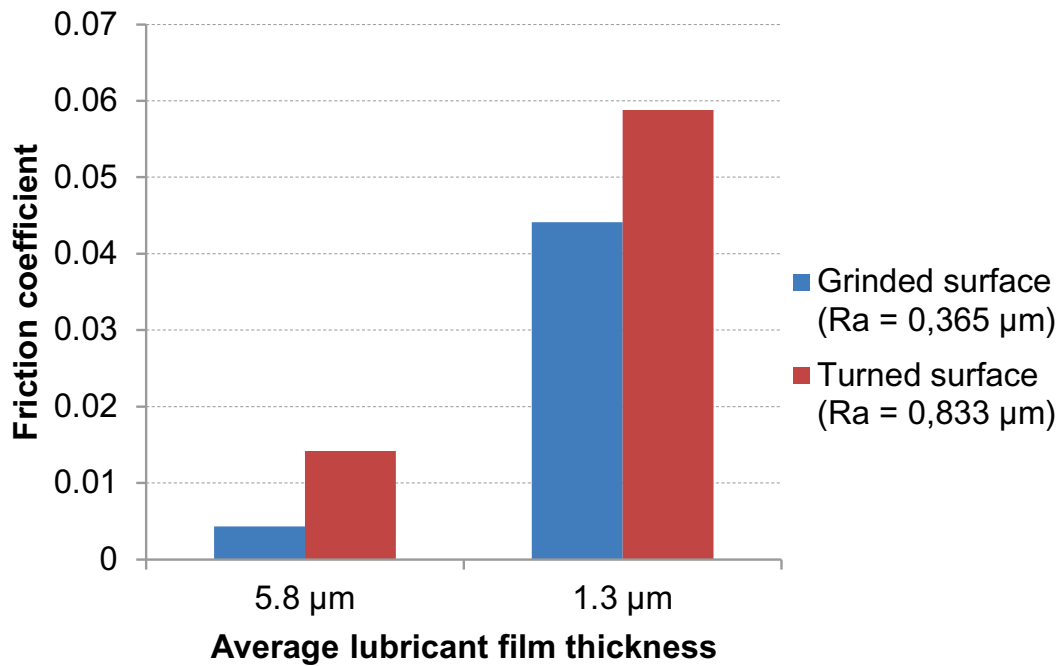


Figure 7.9: Comparison between turned and grinded surfaces running in hydrodynamic and mixed lubrication regimes (0° configuration)

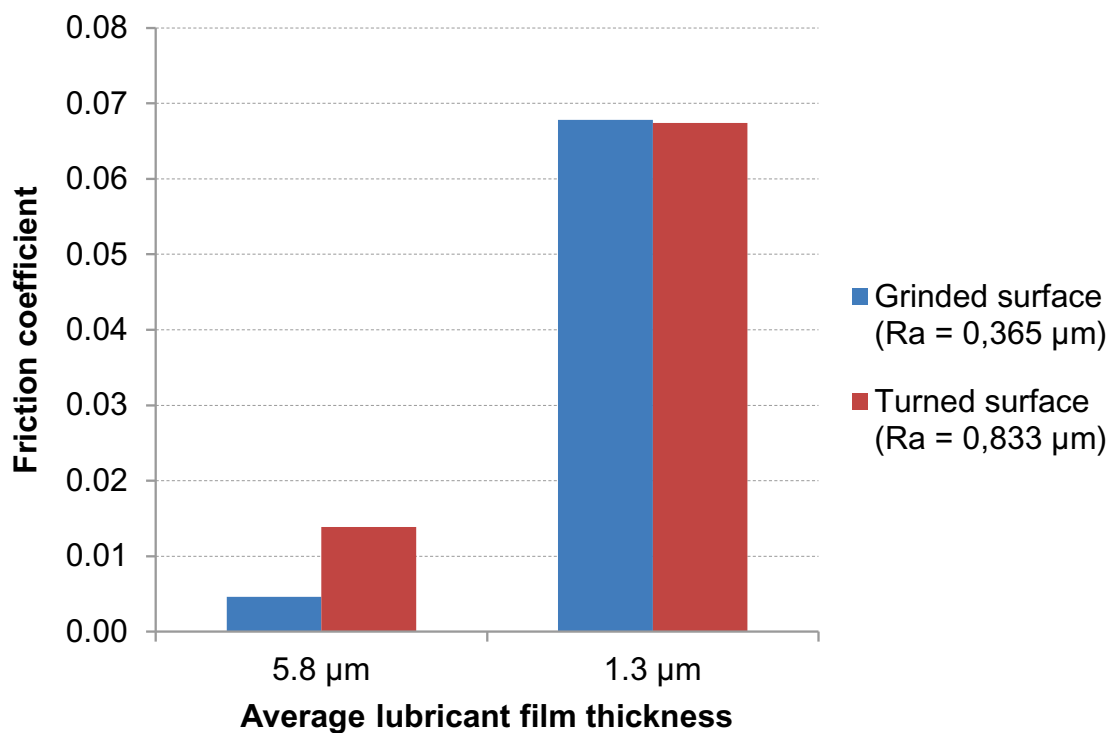


Figure 7.10: Comparison of the friction between grinded and turned surfaces in hydrodynamic and mixed lubrication regimes for the 90° configuration

Each test was achieved with a sliding of 1 m/s. Sliding direction was taken here perpendicular to both profiles. Test shows a lower friction coefficient for the grinded surfaces in both hydrodynamic and mixed lubrication conditions. In comparison with next diagram (Figure 7.10) where profiles have a 90° configuration (see Figure 5.21), friction is lower (only for 1.3 μm). This is explained as solid-solid contact pressure is lower in the second configuration, which thus induces a lower contact shear.

For both machining directions when solids are under full hydrodynamic conditions, turned surfaces induce higher friction coefficients than grinded surfaces. This is explained by the presence of larger valley leading to higher fluid shear forces. On the other hand, when mixed lubrication condition is met, differences between turning and grinding become more complex: in the case presented on Figure 7.10, turned surfaces offer lower friction than grinded surfaces. Solid-solid contact for grinded surfaces is of 70,1 μm^2 whereas solid-solid contact area is of 141,9 μm^2 for turned surfaces. Differences observed between pressure fields of grinded (Figure 7.11) and turned surfaces (Figure 7.12) confirms why friction coefficients are comparable for both trials: on the one hand, contact pressures are low what is also observed for the solid-solid contact area. On the other hand, high pressures are combined with a larger contact area. Additionally, for a same average lubricant film thickness, contact zone is significantly different, extreme peaks are higher for turned surfaces than for grinded surfaces. This trend is confirmed when analyzing film thickness profile for both machining types (Figure 7.13 and Figure 7.14).

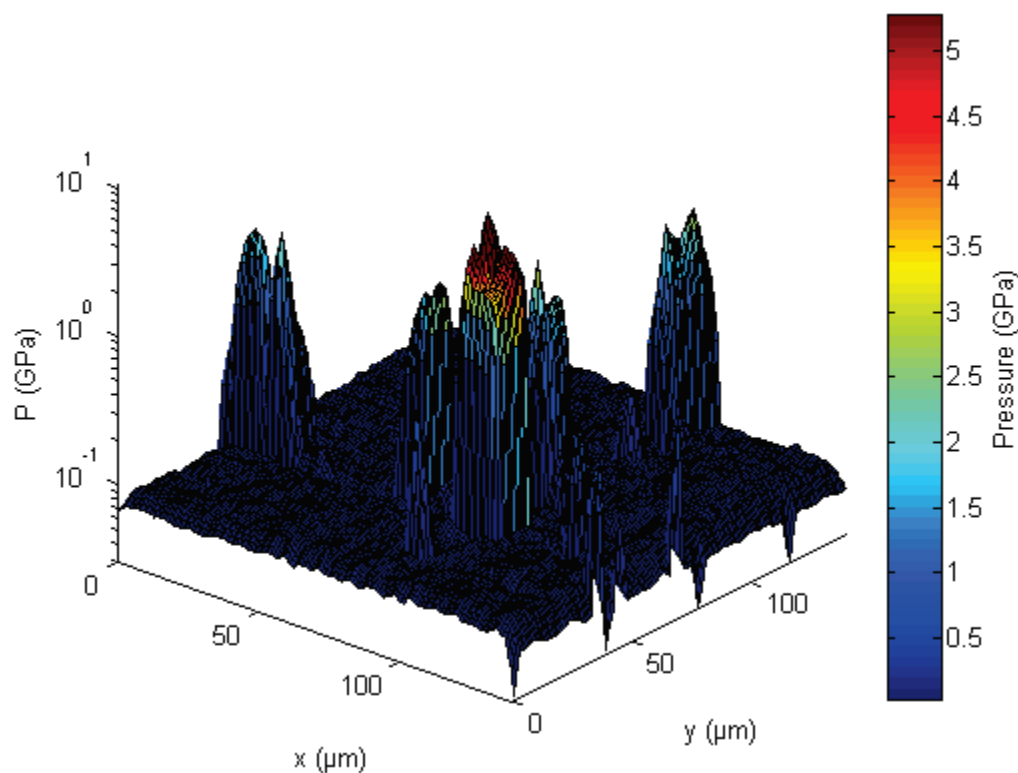


Figure 7.11: Pressure field for grinded profile in the 90° configuration ($R_a = 0.365 \mu\text{m}$)

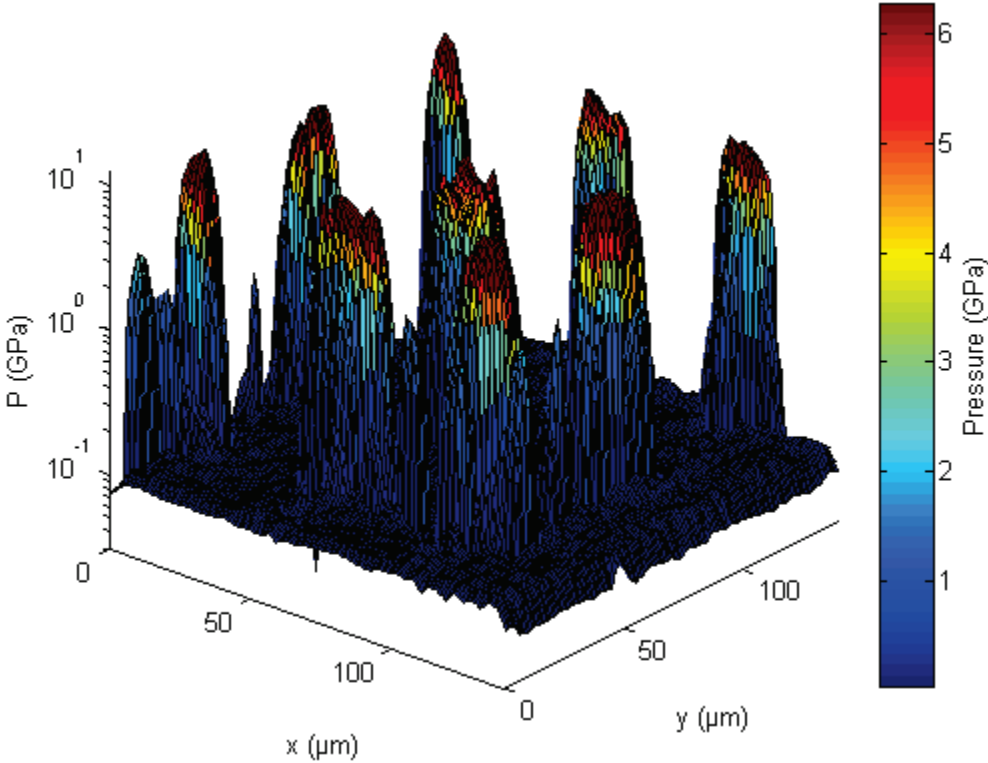


Figure 7.12: Pressure field for turned profile in the 90° configuration ($R_a = 0.833 \mu\text{m}$)

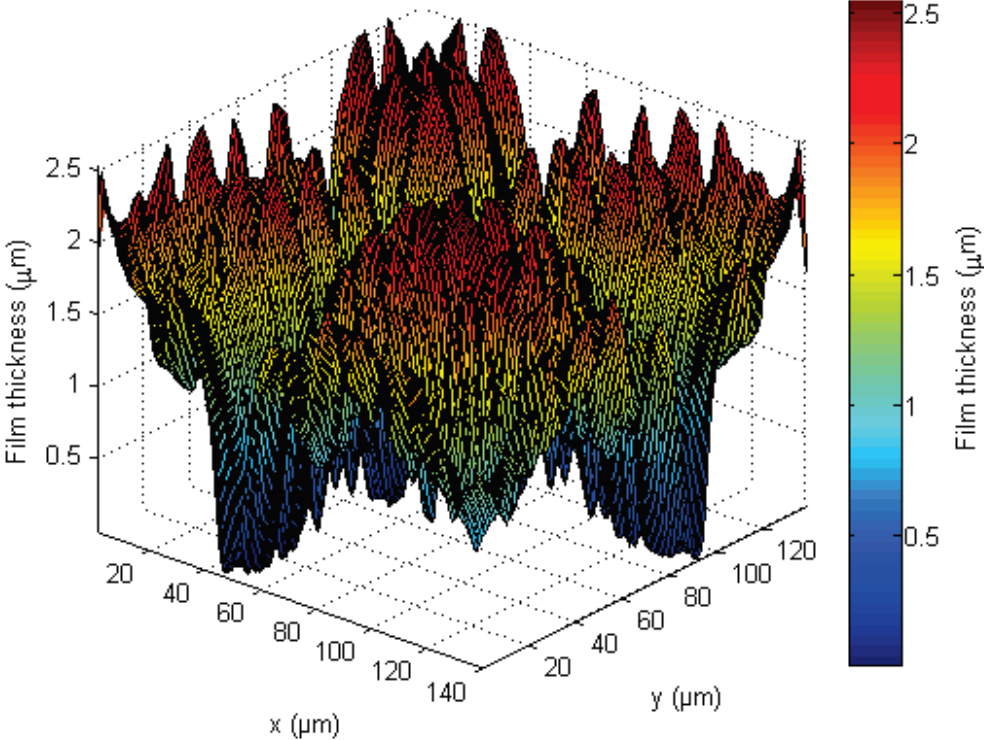


Figure 7.13: Lubricant film thickness for grinded profile in the 90° configuration ($R_a = 0.365 \mu\text{m}$)

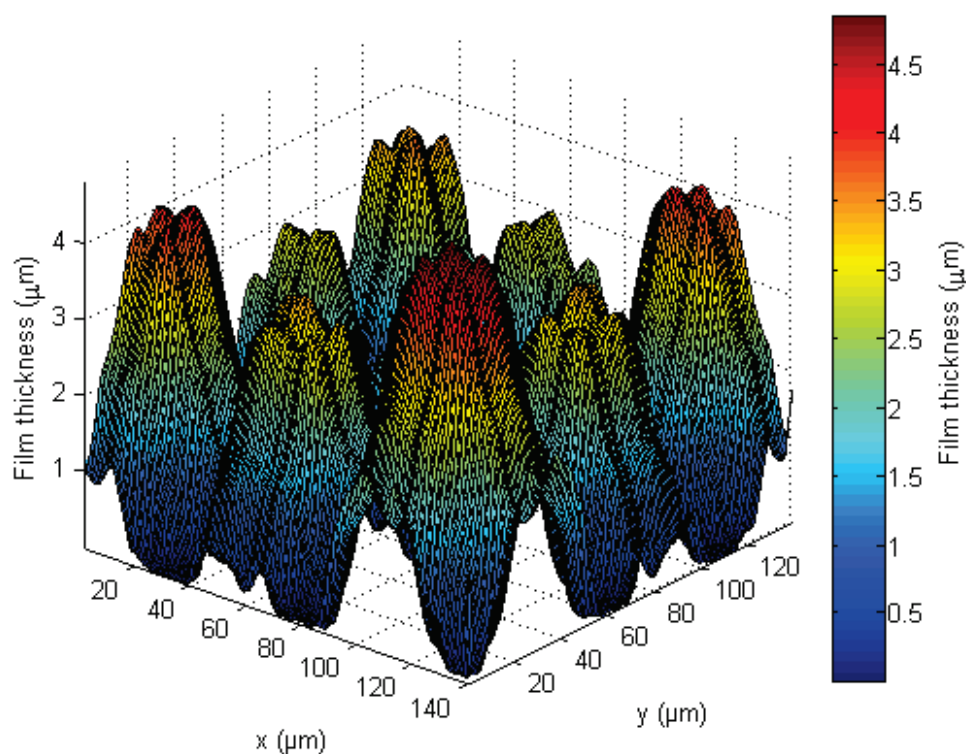


Figure 7.14: Lubricant film thickness for turned profile in the 90° configuration
($R_a = 0.833 \mu\text{m}$)

Such effects show that an easy correlation between roughness and contact pressure is non-intuitive. Knowing the solid-solid contact area enables it, in combination with contact pressure information, to explain of occurring tribological phenomena. Present investigation done for two different machining directions is deepened in next subsection.

7.4.2 Machining Directions

In this section, diagrams are representing friction coefficient in function of the average contact pressure. To achieve what, friction coefficients established for a whole sliding phase are averaged to get only one mean value for a given lubricant film thickness. First diagram presented on Figure 7.15 displays an averaged friction coefficient. This is itself an average value of five experimentally tested identical machined profiles. Although these are machined with the same process and parameters, they do not have exactly the same topography. Next tests display the friction coefficient in function of the average contact pressure for three different machining directions all corresponding to turned surfaces.

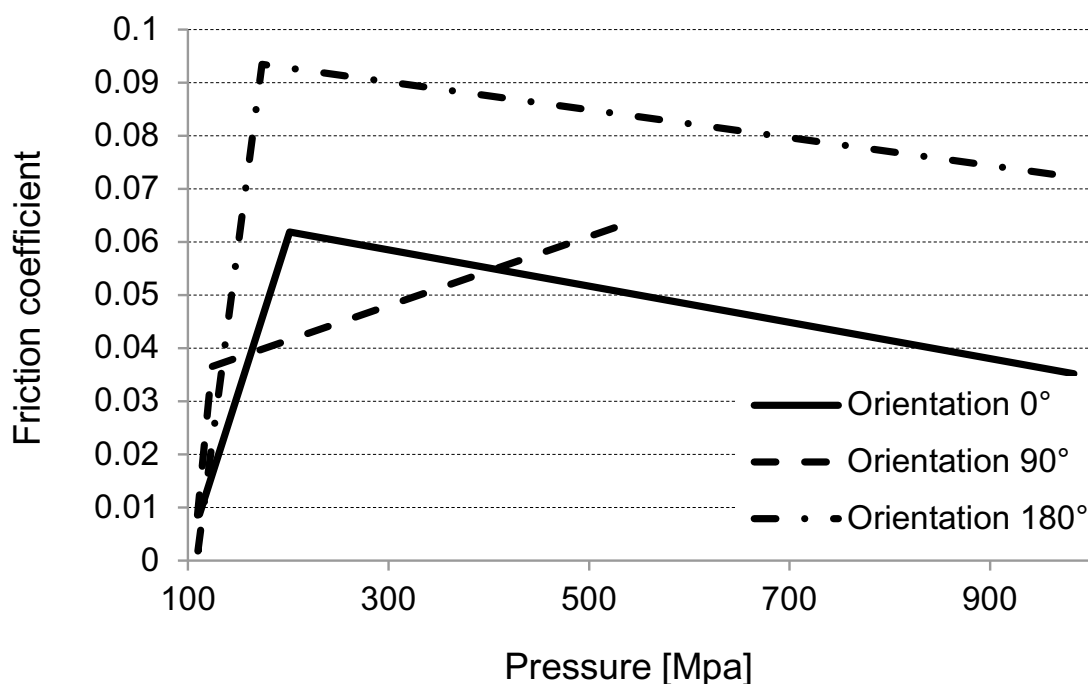


Figure 7.15: Friction coefficient in function of average contact pressure for turned surfaces

For turned surfaces, the friction coefficient begins with a hydrodynamic regime and changes into a mixed lubrication regime. Once a maximal value of friction coefficient is reached, friction decreases when the normal load continues to increase, this corresponds to a phenomenon described with the Bowden and Tabor theory and detailed previously. Comparison between parallel (0° and 180°) and perpendicular profiles shows that for same average pressure, friction coefficient is behaving totally differently. This is due to totally different contact surfaces inducing totally different contact behaviors (compare Figure 7.12 and Figure 7.17).

The same diagram has been generated for grinded surfaces, where the observed trend looks similar: friction coefficient increases when evolving from a full hydrodynamic regime to mixed lubrication (see Figure 7.16).

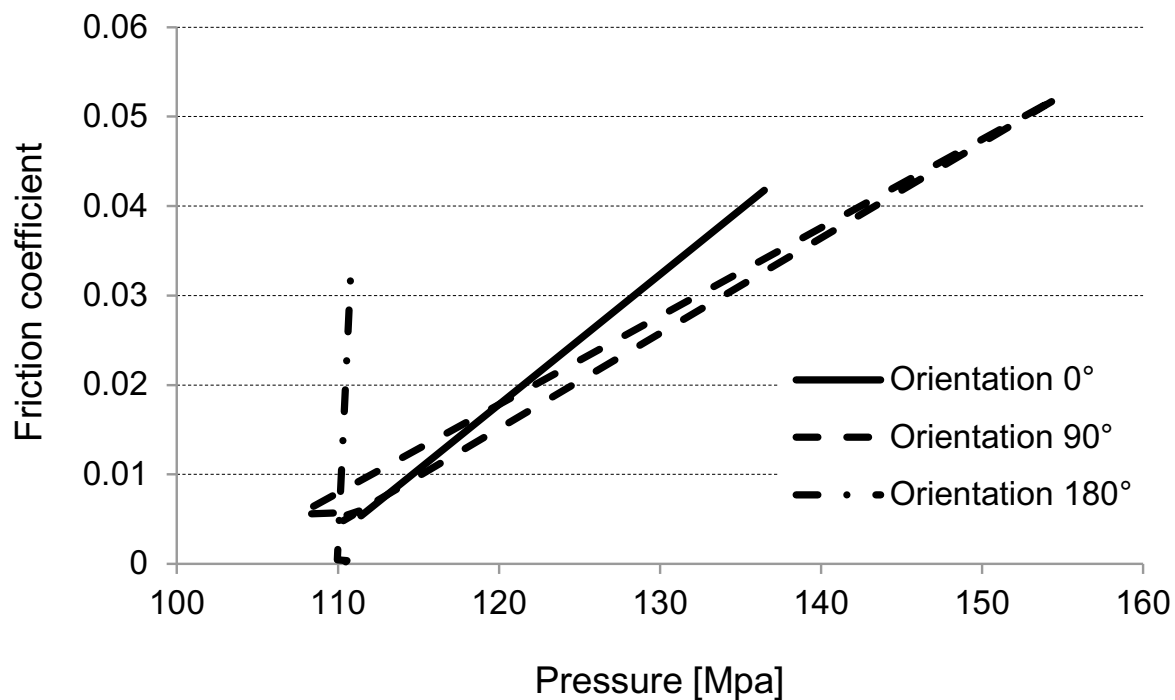


Figure 7.16: Friction coefficient in function of average contact pressure for grinded surfaces

First part observed for turned surface (transition between hydrodynamic and mixed lubrication) is also observed for grinded surfaces. Nevertheless, a main difference is observed for grinding: for tested lubricant film thicknesses, solid-solid contact takes a smaller part than for turned surfaces. As a consequence, friction coefficient is also smaller for grinded surfaces as in mixed lubrication regime, solid-solid contact is smaller same average film thicknesses.

When comparing both profile types, trend shows that machining combined to the fluid film thickness has a high impact on the friction coefficient. Friction coefficient is globally minimal for perpendicular machining configuration (90°). This is the case for grinded and turned surfaces. This results from lower solid-solid contact areas – for perpendicular configurations – although maximal pressures are nearly the same. Then, when comparing both parallel machining directions (0 and 180°), friction coefficient is higher when the sliding direction is parallel to the machining direction. This is due to the ratio solid-solid contact area vs average load. For a given 0° configuration, local pressure is higher than for the 180° configuration. In this last configuration, the lubricant can leave easily solid cavities whereas for the other configuration, it initiate a higher local pressure implying also a lower friction forces. These lower friction forces are explained by the fact that the critical shear which is reached faster when pressures are higher. This hypothesis is confirmed in next figures representing both pressure fields for grinded surfaces (see Figure 7.17 and Figure 7.18).

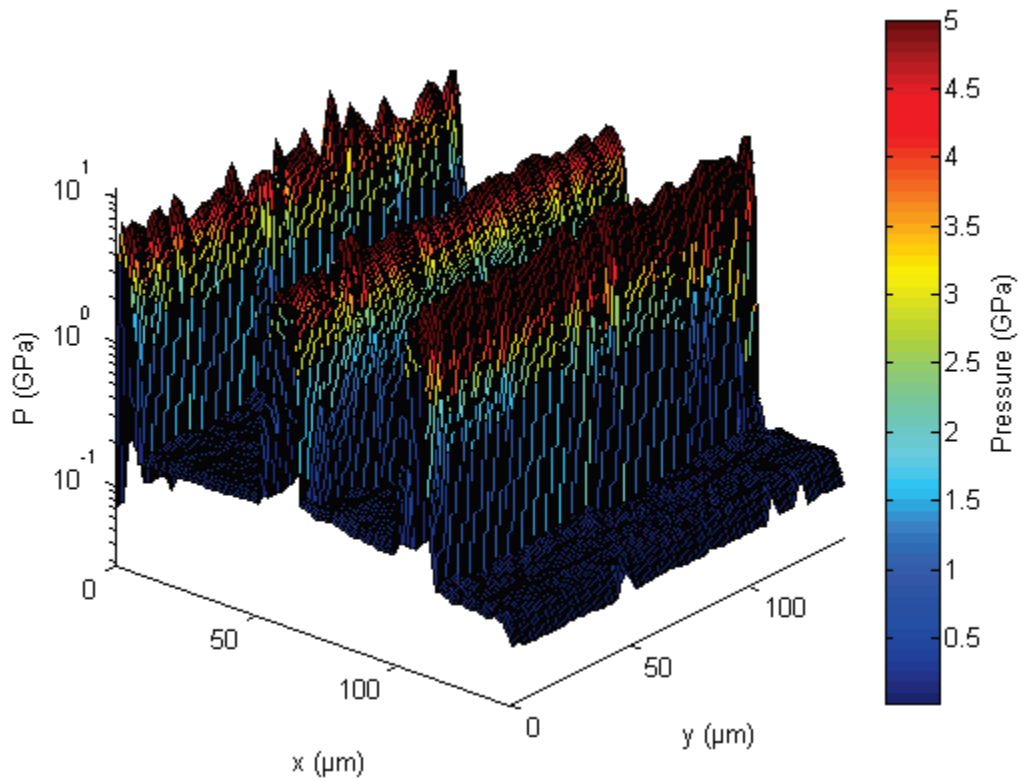


Figure 7.17: Pressure profile for grinded pairing (0° configuration and $R_a = 0.800 \mu\text{m}$)

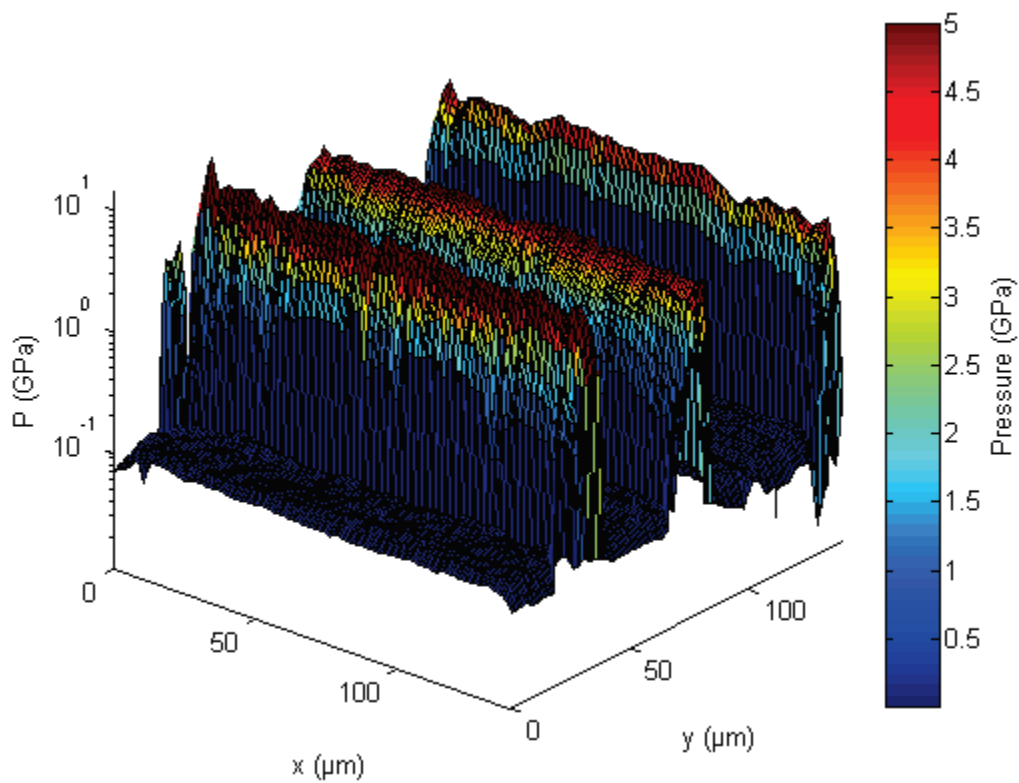


Figure 7.18: Pressure in the grinded pairing (180° configuration and $R_a = 0.800 \mu\text{m}$)

Another parameter gives an indication on frictional behavior between solids: contact temperature. Heat generation is displayed in next subsection in order to see which temperature gradient and rising velocity can be reached in such contacts.

7.4.3 Impact of Roughness on Contact Temperature

For all tests performed, temperature is displayed in the last sliding frame of the calculation. It is expected that, contact temperatures are the highest for the lowest oil film thickness configurations and for the configurations where local pressures are the highest. Next figures plot temperature profiles observed in average, minimal and maximal temperature for turned and grinded surfaces in all three configurations.

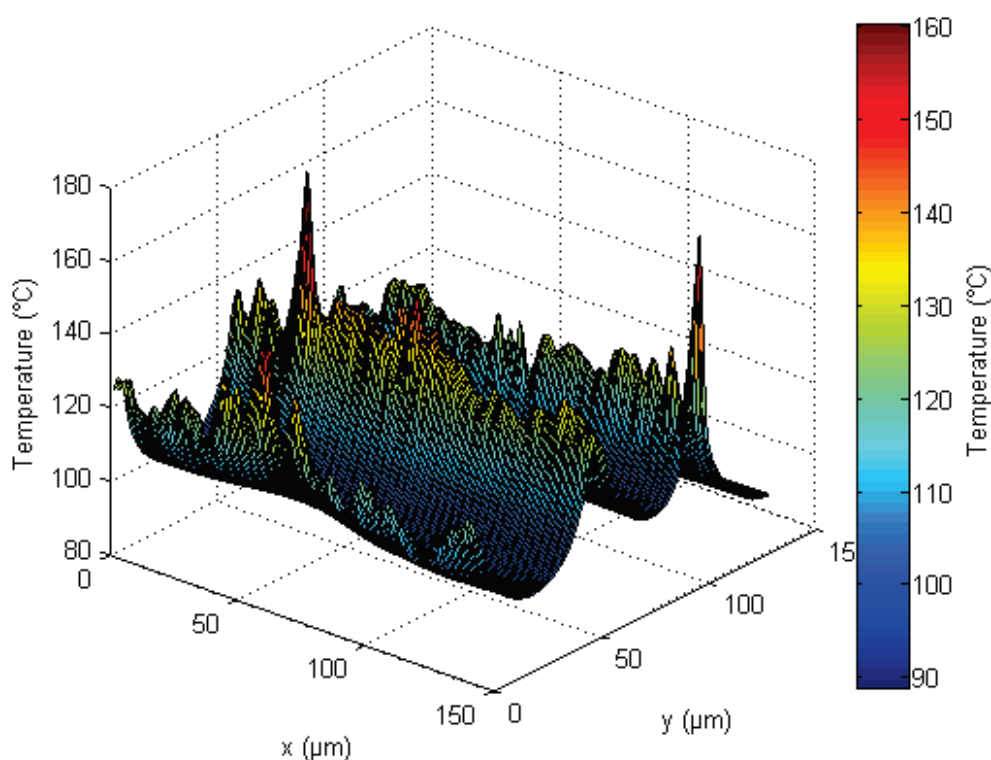


Figure 7.19: Contact temperature profile for turned surfaces (configuration 0°, film thickness = 1,3 μm and $R_a = 0.800 \mu\text{m}$)

Investigations done with different machining directions and minimal oil film thickness show some influences but no direct relationship between contact temperature and average roughness is existing. A summary of these investigations are displayed in next figures (see Figure 7.21, Figure 7.22 and Figure 7.23).

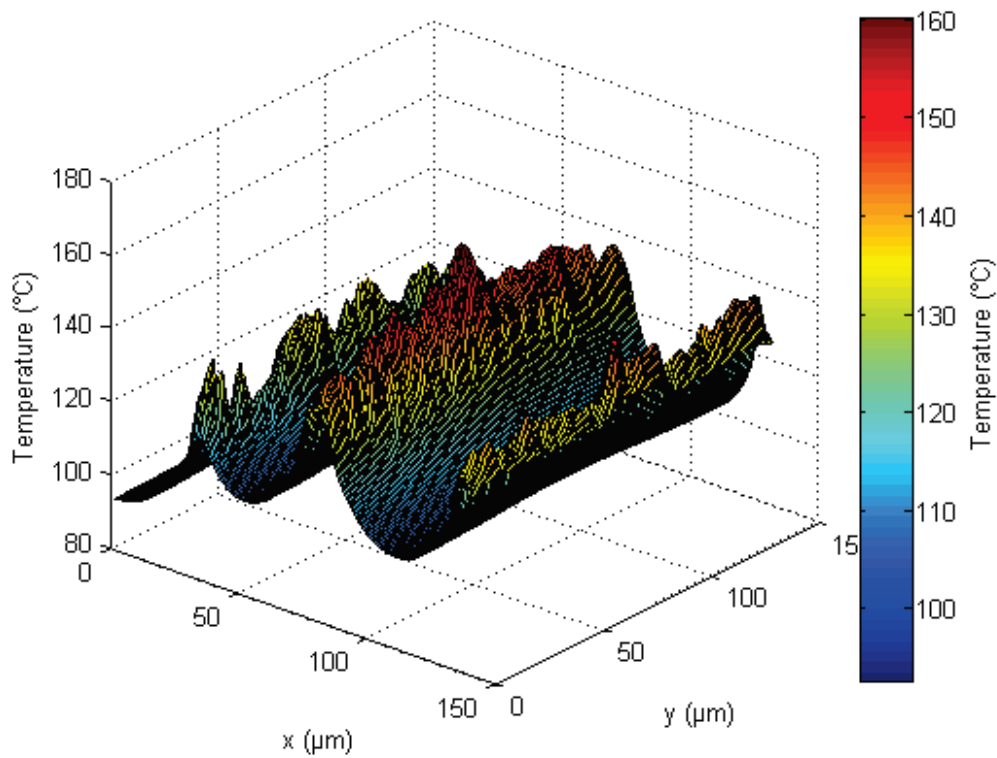


Figure 7.20: Contact temperature profile for grinded surfaces (configuration 180°, film thickness = 1.3 μm and $R_a = 0.800 \mu\text{m}$)

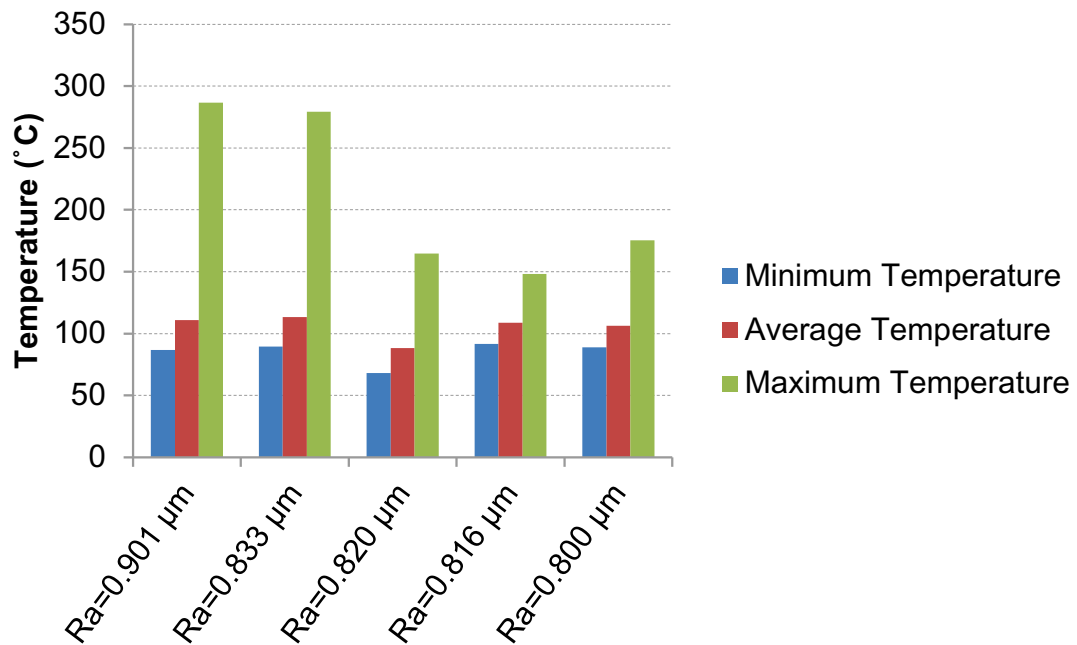


Figure 7.21: Contact temperature for five calculated turned surfaces (0° configuration and 1.3 μm lubricant film thickness)

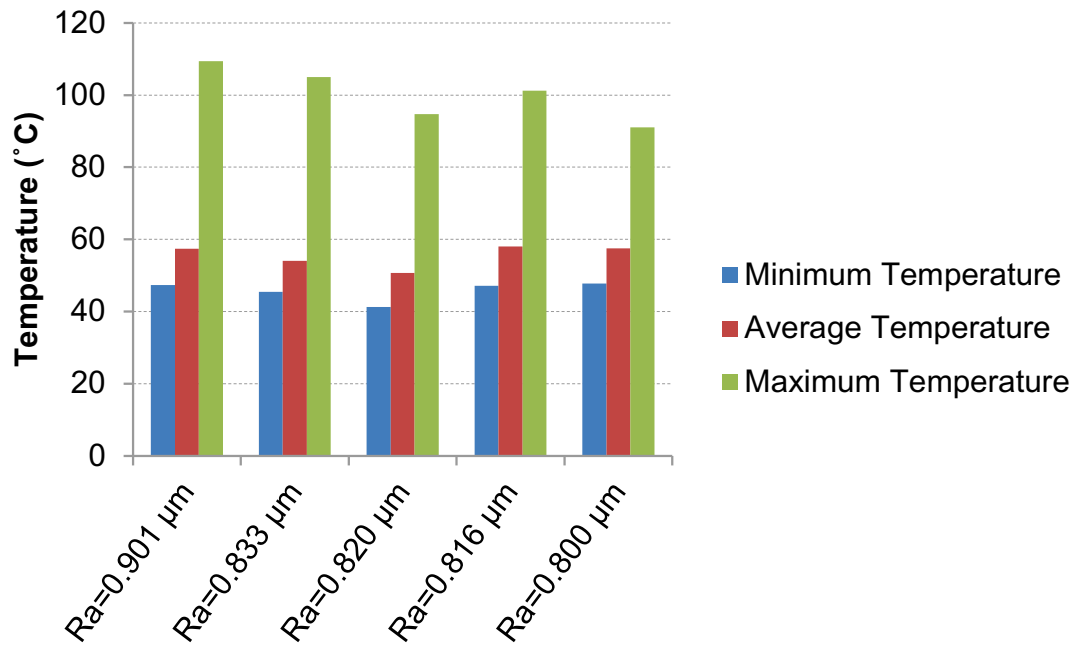


Figure 7.22: Contact temperature for five calculated turned surfaces (90° configuration and 1.3 μm lubricant film thickness)

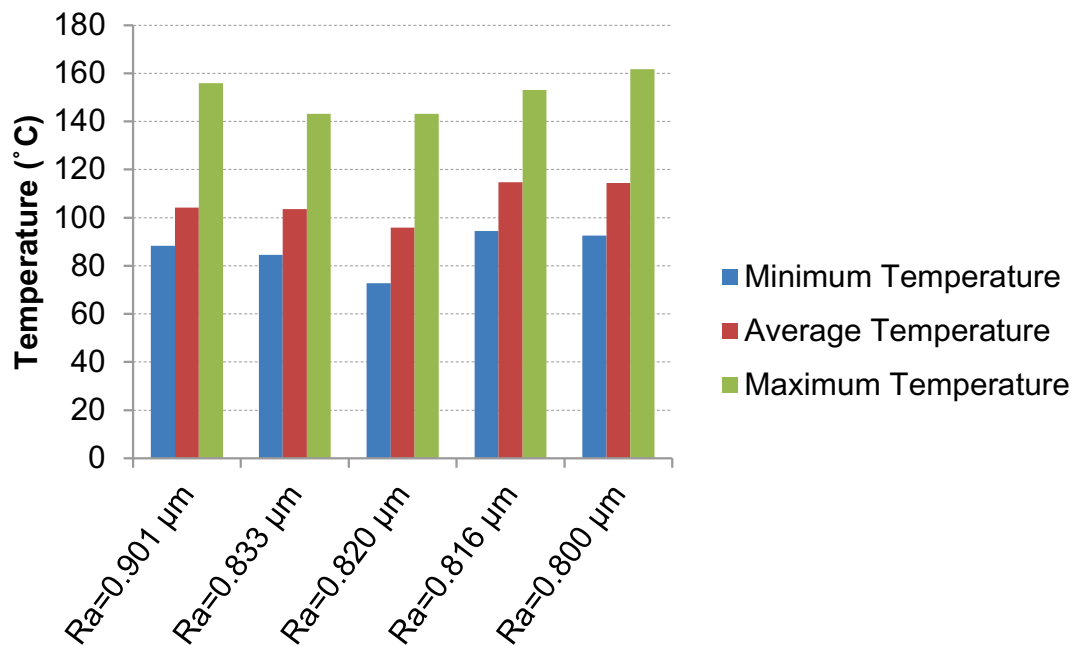


Figure 7.23: Contact temperature for five calculated turned surfaces (180° configuration and 1.3 μm lubricant film thickness)

7.5 Classification of the Most Influencing Parameters

Previous parameters need to be classified in order to know which one has the most influence on friction. These investigations provide relationships existing between varied parameters and friction coefficients. Present subsection is composed of two parts, impact of roughness parameters (topography) on friction and impact of working conditions (loads and sliding velocity) on friction.

7.5.1 Classification of Roughness Parameters on Friction

This part compares different impacts of interacting parameters on following parameters:

- Min, max and mean Friction coefficient
- Min, max and mean contact temperature
- Min, max and mean contact pressure
- Min, max and mean real lubricant film thickness

Interacting parameters are listed as follows:

- R_p , R_v , R_a , R_q , R_t S_k and K are kept constant
- Sliding velocities
- Normal load (theoretical lubricant film thickness)
- Machining direction

To reach this objective, a full automatized post processing tool was developed with the software MATLAB in order to deliver a result file containing a summary of relevant parameters (see Figure 7.24).

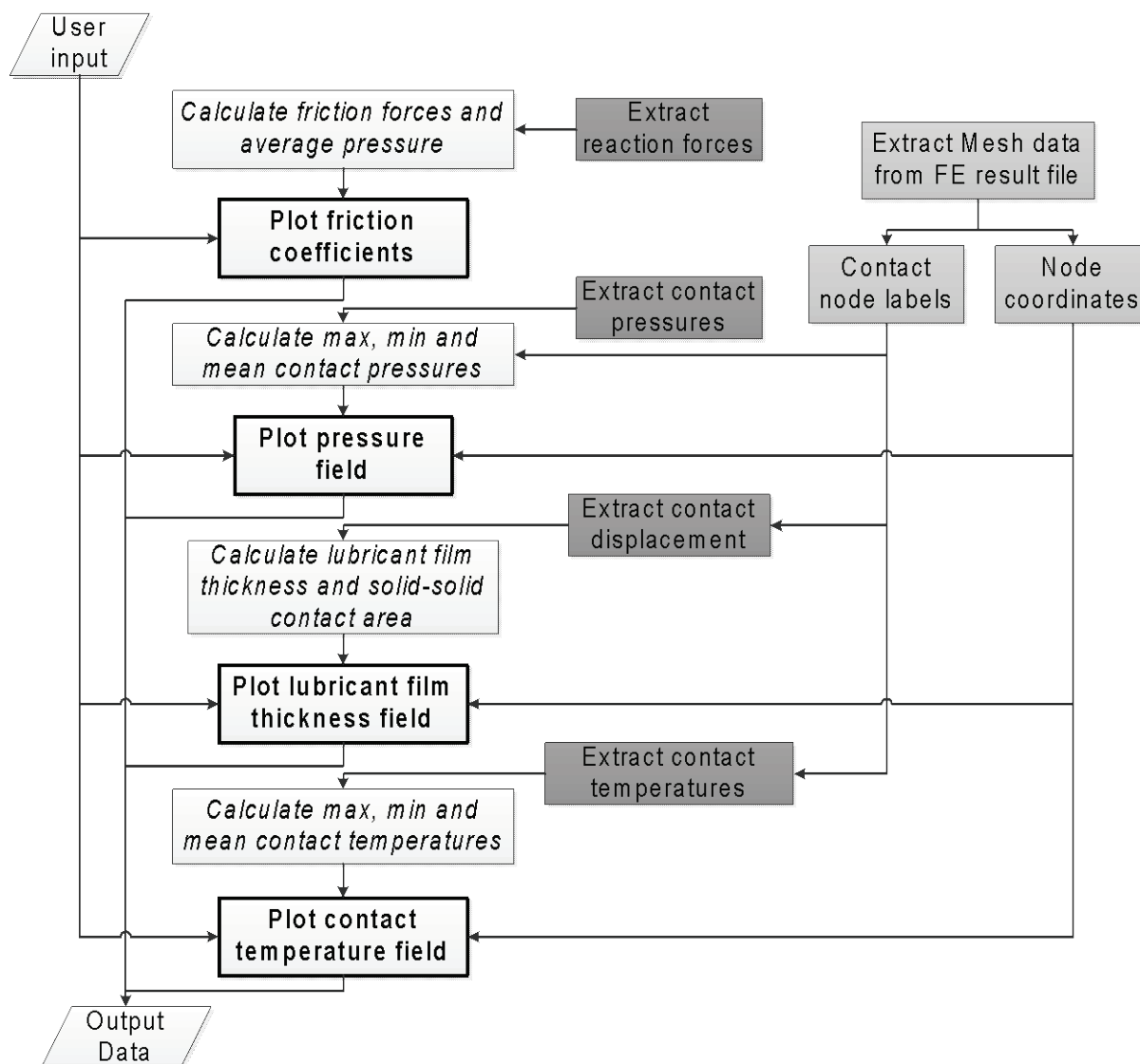


Figure 7.24: Post processing process

The use of past tool focuses here on the identification of influencing interacting parameters for the analysis of the friction behavior. After getting the output data, an interaction analysis is performed to firstly see which of cited roughness parameters have the most impact on friction under different lubrication conditions (see Figure 7.25). In this diagram, roughness parameters are normalized with their respective maximum value according to next operation:

$$X_{i_{norm}} = \frac{X_i}{\max(X_i)} \quad (7.1)$$

in order to compare each parameter (noted here X_i) equally for giving an overview of the sensitivity of each parameter. Ten samples were chosen, five grinded and five turned ones and only the sliding velocity was taken as constant (1 m/s).

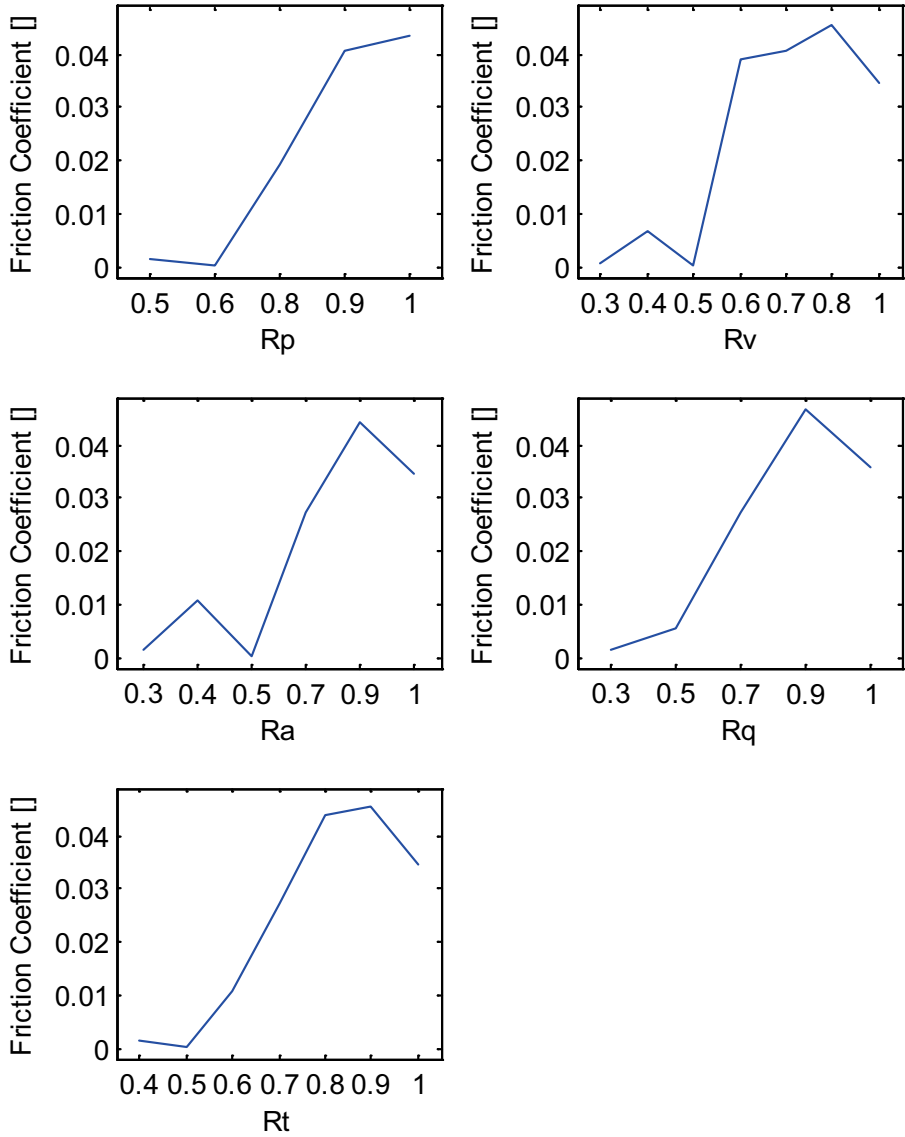


Figure 7.25: Influence of different roughness parameters on friction coefficient (each roughness parameter is normalized)

Results displayed in Figure 7.25 shows that for rising values of tested parameters is increasing, friction coefficient increases too. Statistic regroupes both the hydrodynamic and mixed lubrication conditions and main trend is in accordance with the theory:

- in hydrodynamic conditions, main factor impacting on friction force should be the maximal peak height (R_p) as it limits minimal lubricant film thickness. This hypothesis is verified in the diagram in which R_p factor shows the most significant influence on the friction coefficient (when varying from only 50 % friction increases from 200 %)
- in mixed lubrication conditions, higher roughness leads to higher solid-solid contact areas and so higher friction coefficients

According to diagram of Figure 7.25, R_p value is the most impacting roughness factor, followed directly by R_t . Then come R_v which is the valley depth and has no real impact on solid-solid contact, R_a and R_q , average and quadratic roughnesses is not sufficient and less important than R_p to characterize the tribologic behavior of a lubricated contact. This analysis is completed with the coming study examining the effect surface kurtosis and skewness on friction (see Figure 7.26).

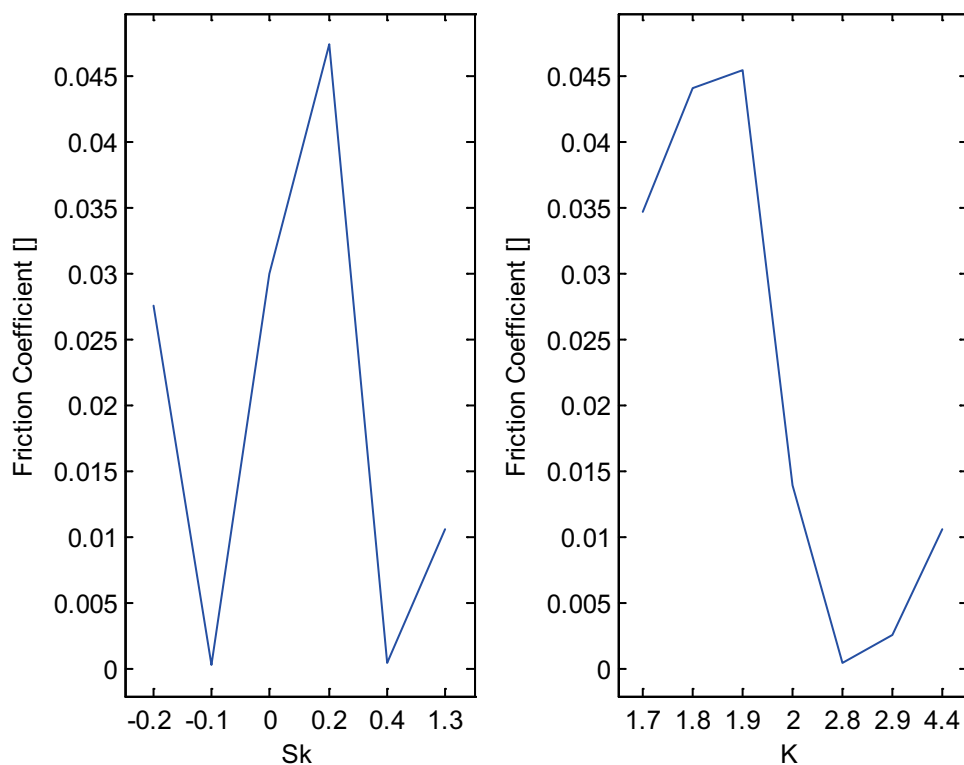


Figure 7.26: Friction coefficient in function of surface Skewness and Kurtosis

A skewness of 0 means Gaussian dispersion, a negative one means that there are more “plateaux” than valleys in the profile, whereas a positive skewness means the contrary. No explicit trend can be concluded from of last diagram, except that a Gaussian repartition leads to a friction maximisation.

Moreover, kurtosis shows a clear impact on friction. Friction is higher for low kurtosis values whereas low friction rates are reached when kurtosis is near to 5. High kurtosis means also low standard deviation and so relative regular profiles. This last point is typically a characteristic of grinded surfaces having in present case a lower friction coefficient for given film thicknesses, which explains why low kurtosis leads here to lower friction coefficients. High kurtosis leads to lower solid-solid contact area and so to lower friction coefficients as displayed in Figure 7.27. This trend has to be validated by means of statistical tests.

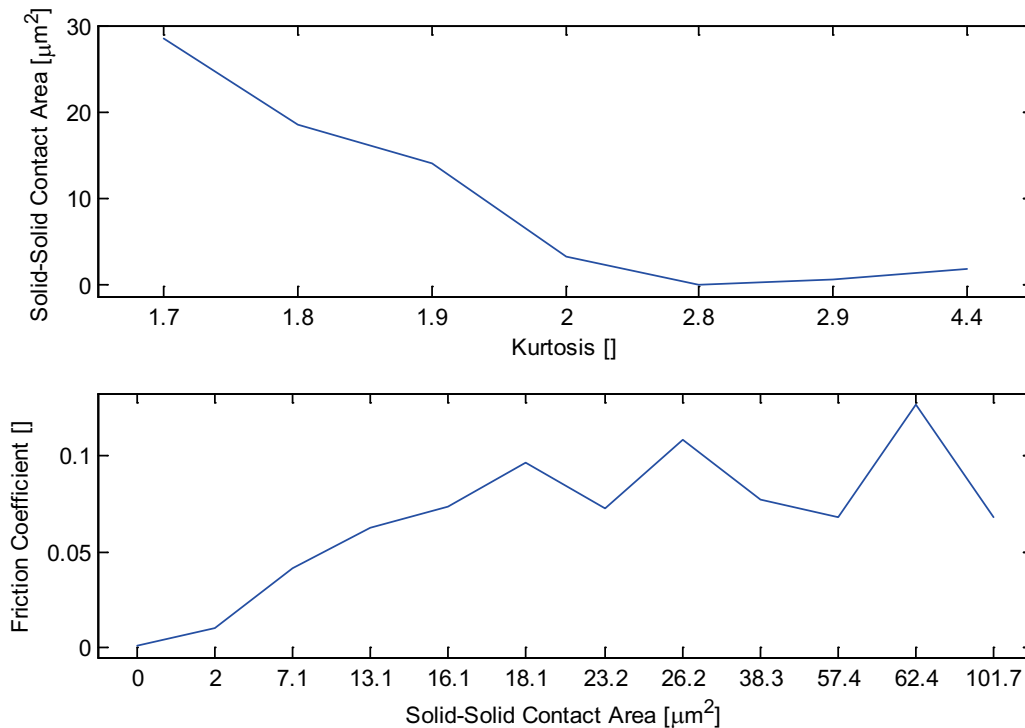


Figure 7.27: Contact area in function of kurtosis (on the top) and friction coefficient in function of the solid-solid contact area (on the bottom)

After classification of roughness parameters on friction, operating conditions are investigated with a view to identify the conditions influencing mainly friction.

7.5.2 Classification of the Operating Conditions

Each of the operating conditions is integrated here in a whole analysis in order to classify the relevance of each condition on the friction. Two cases are considered: full and hydrodynamic and mixed lubrication conditions. Sample used for this analysis has characteristics displayed in Table 7.3.

Table 7.3: Sample characteristics for operating condition analysis

Sample	Rp	Rv	Ra	Rq	Rt	Sk	K
Grinding	0.99	-0.70	0.26	0.33	1.70	0.35	2.81
Turning	1.84	-1.45	0.80	0.92	3.29	0.19	1.78

Varied parameters are listed below:

- Sliding velocity: 1, 2 and 3 m/s (slidVel)
- Theoretical lubricant film thickness: from 1.3 until 5.8 μm (thFt)
- Machining direction: 0, 90, 180° configurations (machDir)
- Machining type: turning (1) and grinding (2) (machType)

The first diagram illustrates impact of all parameters in hydrodynamic lubrication conditions (see Figure 7.28).

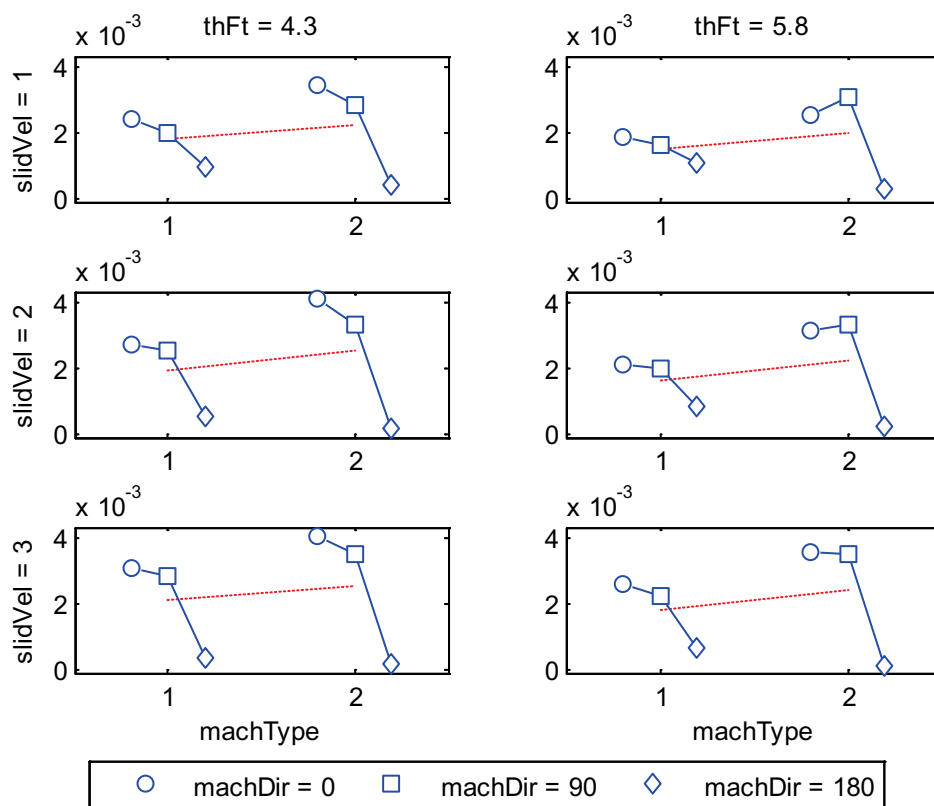


Figure 7.28: Impact of operating conditions on the friction coefficient for full hydrodynamic conditions

In full hydrodynamic condition, most important parameter is the machining direction. When the orientation is 180° , friction reaches a minimum for all configurations. Sliding velocity impacts less friction coefficient: a light increase is observed for increasing velocities. In hydrodynamic conditions, difference between grinded and turned surfaces is quite low. This is due to the profiles which have more asperities leading in sum to higher lubricant shear. This confirms also that in the case of the 180° configuration, fluid is flowing parallel to the profile asperities, leading to lower lubricant shear and so lower friction coefficients.

Next diagram (Figure 7.29) displays also the sensitivity of each of four parameters on friction behavior in mixed lubricated contacts.

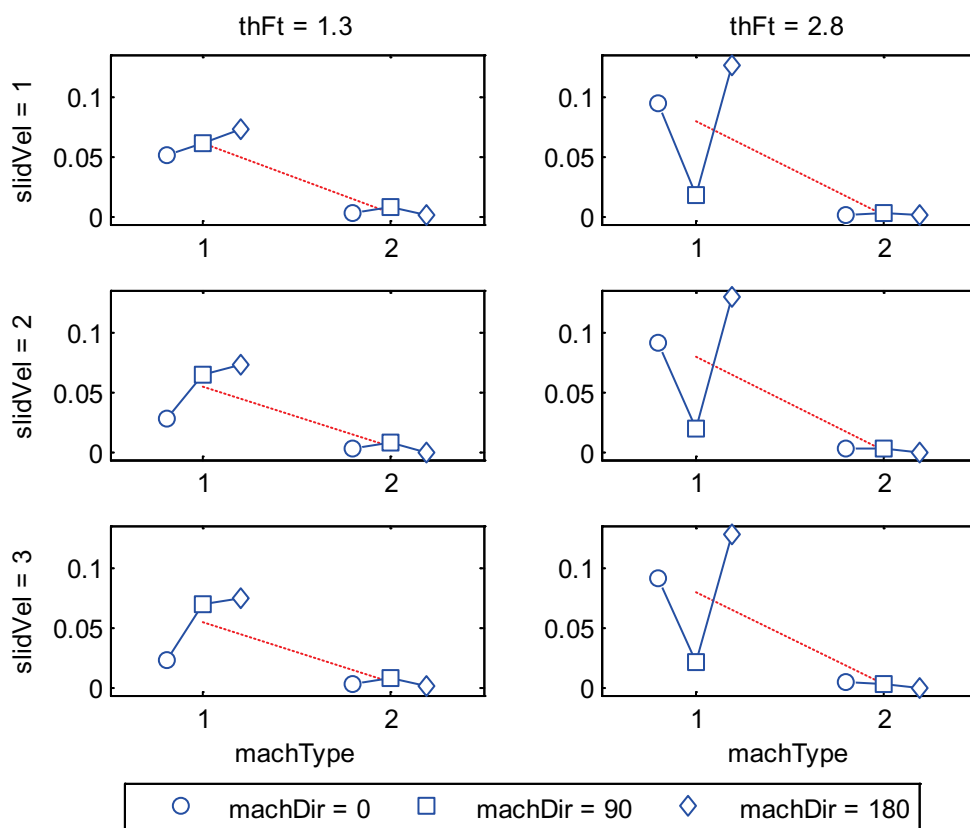


Figure 7.29: Impact of operating conditions on the friction coefficient for mixed lubrication conditions

Machining direction has the highest impact on friction behavior also for mixed lubrication conditions. This is well observed when theoretical lubricant film thickness is of $2.8 \mu\text{m}$. In this specific lubrication condition, turned surfaces offer a lower friction coefficient for the 90° configuration than for parallel machining. This is due to a lower solid-solid contact area, phenomenon which is not reproduced when the film thickness decreases ($\text{thFt} = 1.3 \mu\text{m}$). This last phenomena is explained by the fact that solid-solid contact does not change highly between all three configurations. For each three different sliding velocities, the contact location has a high impact on the

friction for the lowest film thickness configuration. These analyses show that for a higher velocity, the solid-solid contact changes faster than for the lowest sliding velocities. This happens for the turned configuration. The average friction is lower as the solid-solid interface is in a contact-opening phase. To override this phenomenon, present studies need to be extended taking into account a contact surface configuration where the contact interface interfere less friction coefficient: large contact surfaces need to be taken into account.

In comparison with turned surfaces and running with the same boundary conditions, grinded surfaces are not significantly impacted by solid-solid friction. For a same theoretical film thickness, turned surfaces are fully under mixed lubrication whereas grinded surfaces are in low mixed lubrication conditions. The explanation for that is the average roughness which is lower as well as the R_p : there are less peaks in contact for grinded surfaces. Additionally, conclusion underlines that, machining and especially R_p factor has the highest impact on mixed lubrication conditions.

7.5.3 Summary of Parameters Impact on Friction Behavior

From all parameters varied in present analysis, two main classes were distinguished:

- roughness characteristics
- operating conditions

Operating conditions underlined that most impact was first coming from machining type then machining orientation followed by lubricant film thickness. Sliding velocity has only a low impact can be neglected in present investigations. Concerning roughness characteristics, main interacting parameters are first maximum roughness peak height followed by average roughness, quadratic roughness and kurtosis parameters. Same investigation was achieved in dry conditions resulting on similar ranking:

- Machining type
- Machining direction
- Film thickness was replaced with normal load

These relationships will then be used to describe frictional behavior of macroscopic systems. On this account, next chapter will test the impact of different machining types and directions as well as the normal load on the frictional behavior of a dry running technical system. A frictional law established at the microscopic scale is used in this macroscopic tribological system. Present results are valid only in chosen working window. This means that impact of chosen parameter can be totally different once working and machining conditions are out of here chosen working window.

8 Extension of the Investigations to the Macroscopic Scale

Present chapter proposes an example of extension of the present investigation to the macro scale. This is done in order to give a qualitative overview on the impact of machining system's behavior. To achieve this, a dry running tribological system is studied. The reason for this is that the application of boundary conditions established at the macroscopic scale can be directly applied to microscopic model. This is not the case for lubricated tribological systems as lubrication boundaries are different between scales.

8.1 Demonstrator of the Tribological System

Demonstrator is an extract of an intelligent lifting system (ILS), airplane recovery system. Lifting function is achieved by means of three hydraulic cylinders interconnecting upper and lower platforms (see Figure 8.1). To avoid the rotation of the upper platform, an additional mechanical telescopic cylinder is used to absorb the torque resulting from the lifting.

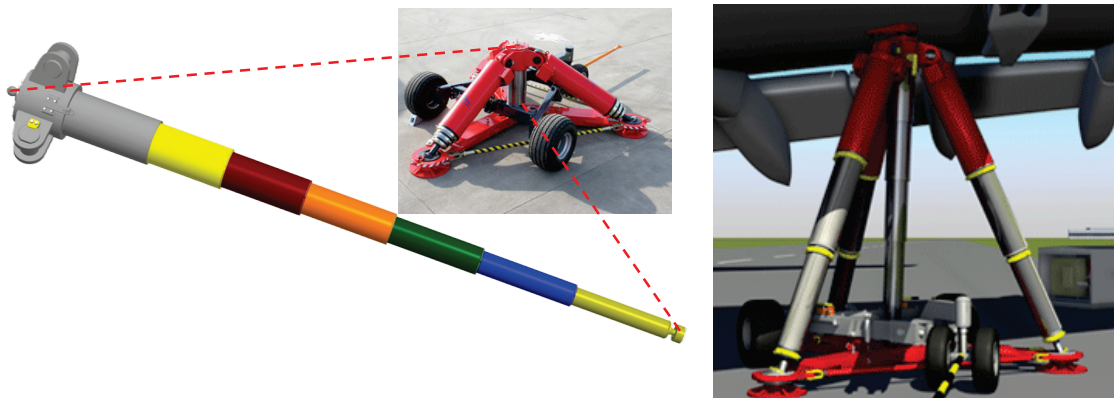


Figure 8.1: Overview of the ILS and focus on the telescopic cylinder

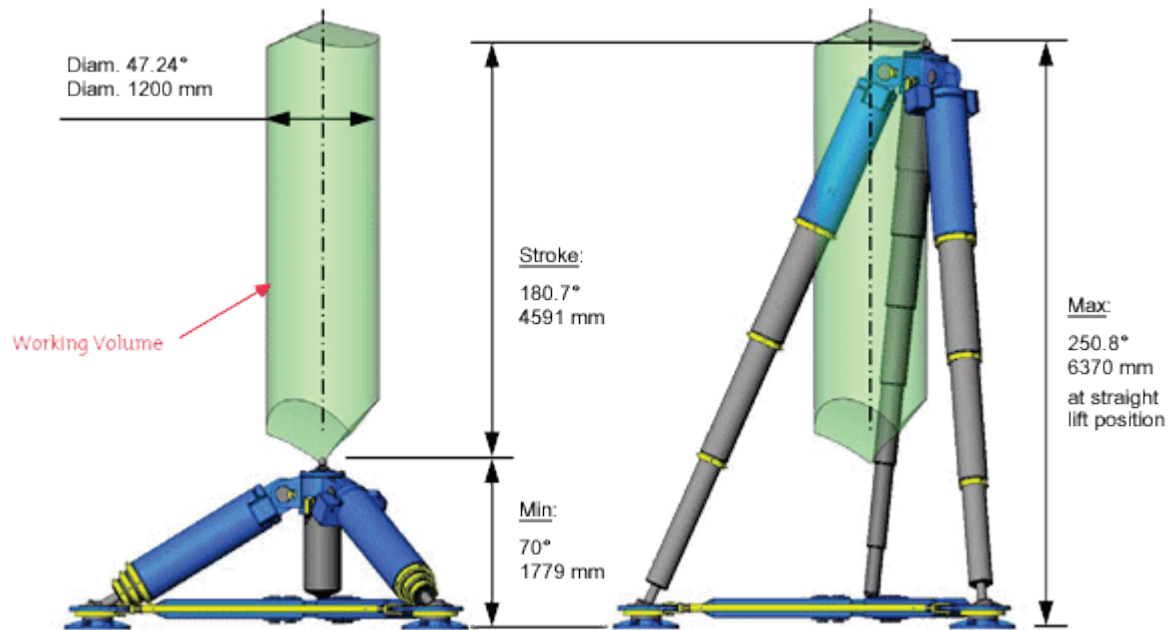


Figure 8.2: Working window of the ILS

The working window corresponding to lifting separation is illustrated in Figure 8.2. Stick-slip effects are initiated in the mechanical cylinder (displayed in Figure 8.1) due to the differences between sticking and sliding friction as well as loading conditions. To reproduce this phenomenon, a numerical model of the mechanical telescopic cylinder is built and helps to investigate the impact of the machining direction on this effect.

8.2 Extension to the Macroscopic Scale: Macro-Model

This part allows a better understanding of the impact of roughness, and machining direction on this disturbing effect. To achieve this, a multi-body system – MBS – is developed in the software ADAMS (see Figure 8.3), in which macroscopic frictional contacts are managed by rules established at the microscopic scale. Extension to macroscopic scale consists in establishing both the sticking and sliding friction coefficients at the microscopic scales and to use them in the MBS.

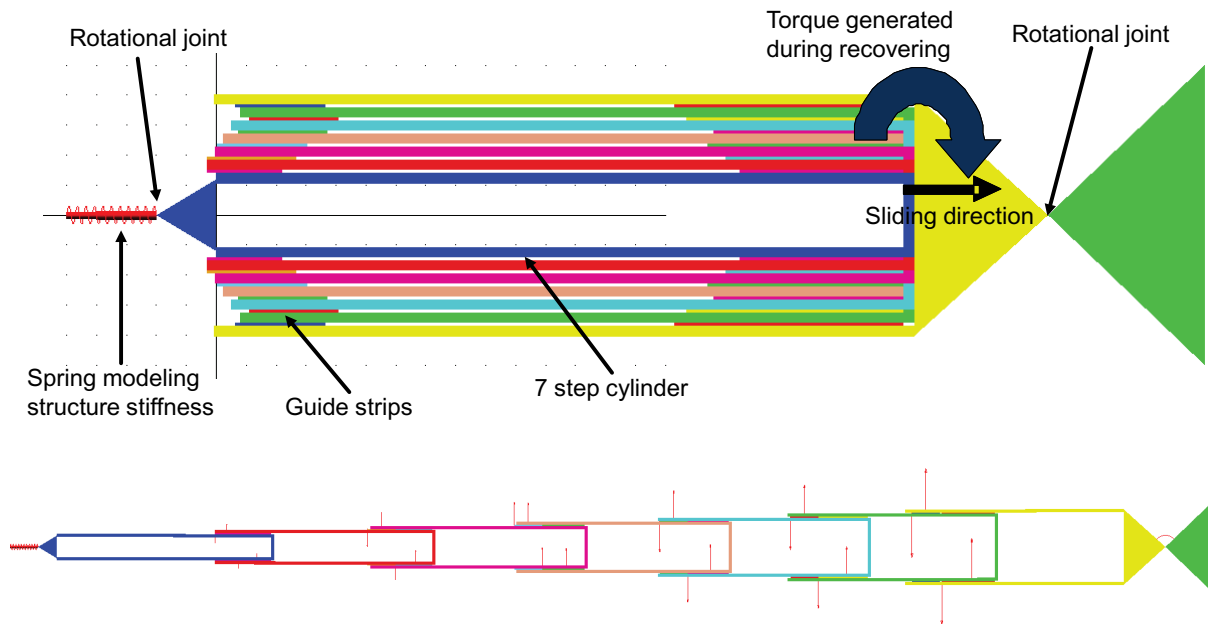


Figure 8.3: 2D-macroscopic MBS of the ILS (on the top),
scheme of the extension process (on the bottom)

In order to generate the required friction coefficients, same boundary conditions are applied to the microscopic model. For each of the three machining configurations, a model used previously for micro scale investigations calculates the static and dynamic friction coefficient. After simulation of these wanted configurations, out coming results are used as input for the response surface method. This method generates then a friction coefficient curve in function of the sliding velocity used in the MBS model. The advantage of this method is that there is no need to re-compute the microscopic model for each of the sliding velocity.

8.3 Establishment of the Frictional Rule at the Microscopic Scale

Materials used for the extension is a structural steel with the same properties than the ones displayed in Table 5.5. Three machining directions are taken into account and for each the minimal resp. maximal friction coefficient is displayed in Table 8.1.

Table 8.1: Relevant calculated influence variable on the micro scale

Machining direction	Slip friction coefficient	Stick friction coefficient
0°	0.1	0.32
90°	0.1	0.24
180°	0.14	0.32

The three friction rules presented in Table 8.1 are included in the MBS model. Results of simulation corresponding to these different rules are displayed in Figure 8.4.

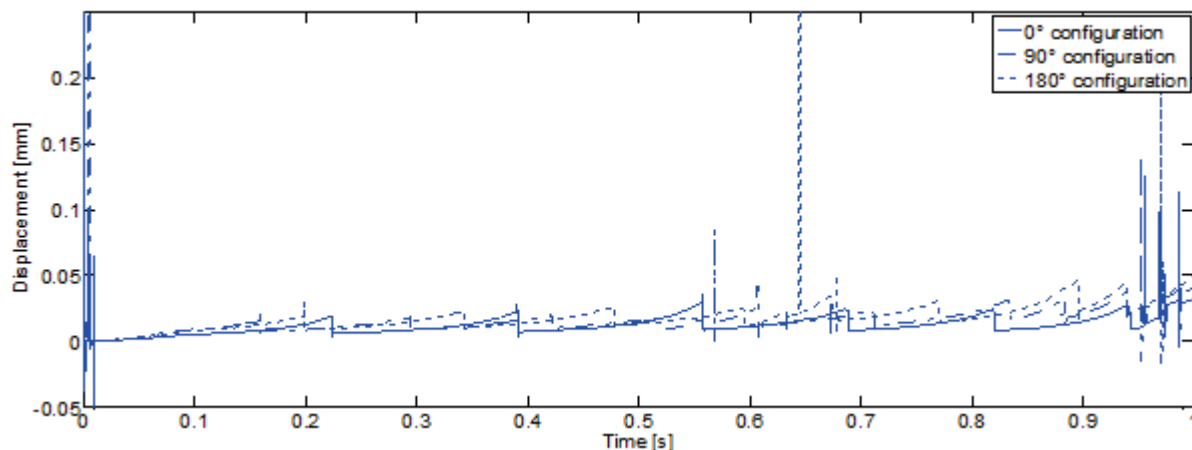


Figure 8.4: Simulation process at for the macro model

Last diagram shows the displacement of the point of the structure which is attached to the spring (see rotational joint in Figure 8.3). As a consequence, measured displacement is characterizing the stick-slip effect: when the displacement is huge and fast this corresponds to a shock that is not wanted in the system.

Results displayed in Figure 8.4 shows that the 0° configuration delivers the lowest shocks (lower maximal displacement) in comparison with both others configurations. On the other hand, shock occurrence is also lower as displayed in Table 8.2.

Table 8.2: Comparison of shock occurrence and maximum shock amplitude for all three configurations

Configuration	Shock occurrence	Maximum amplitude (mm)
0°	8	0.1262
90°	12	0.1426
180°	10	0.2136

Shock occurrence and their maximum amplitudes are usually linked together. If numerous shocks are occurring, their amplitudes are low. On the other hand, if only a few shock are taking place, their amplitudes are high.

This trend is observed between 90° and 180° configurations but is not confirmed with the 0° configuration offering the lowest amplitude combined with low occurrences. This configuration has the largest difference between stick and slip friction coefficient

a setup which is considered as the best of three tests: the one with the less shocks and shock amplitude.

This chapter shows the importance of a multi-scale investigation as different machining setups are leading to different system behavior. Taking arbitrary friction rule is insufficient to optimize a system if each relevant interacting variable is not taken into account for the optimization resp. investigation.

9 Conclusion and Outlook

Present part gives an overview of the whole method developed in this work. Advantage and limitations of this method are discussed and further steps required to improve and extend it are also proposed.

9.1 Synthesis of the Results

Presentation of the state of the art underlined the lack of knowledge with respect to the impact of roughness impact on tribological behavior of tribological systems. Such investigations are mainly carried out by means of experimental tests which require costly resources and are often subjected to physical limitations. This is the case for lubricated as for non-lubricated systems. Because of the previous enounced reason, present thesis has been defined to set bases by means of numerical investigation method on impact of roughness on friction. This has been achieved for non-lubricated systems and this has been further extended especially for complex cases not treated with same detail level until now: mixed lubrication regime. This developed method aims at modeling phenomena occurring in such types of contacts by means of numerical tools (FEA, CFD).

Method development consisted in setting firstly an analysis framework in order to define which parameters were required to build a reliable numerical model. Once this environment was defined, working conditions were set and the machining type was characterized with several parameters. Next step of this method was the modeling realized at the microscopic scale for dry friction problems as well as for mixed lubricated friction problems. Main challenge of this work was to combine solid-solid and fluid-solid interaction in a whole transient model able to deliver realistic results.

After setting framework and building the model, used models were verified numerically, and contact theory was validated with experimental ball-on-disk tests. This resulted in a full parameter variation in order to define which of the tested parameters had the highest influence on the friction coefficient.

This model confirmed experimentations performed in the past, which demonstrated, that the R_p value was the most impacting parameter on the friction coefficient and wear rates. Point not treated until now was the influence of machining direction. Having a significant impact on real solid-solid contact areas, this parameter reveals the importance in having adapted machining in function of the working conditions: high loads, low loads, sliding velocities, etc. It also attested the possibility to model

this type of complex friction problem by means of numerical models in order to deliver realistic results and get more information on the contact itself (temperatures, local pressures, and plasticization).

Although the proposed investigation approach focused mainly on the microscopic scale, a multi-scale investigation showed the importance of taking into account more realistic parameters. Limiting the analysis to the application of an empiric constant friction coefficient is not acceptable to get information on the friction behavior of any tribological system. Following part gives an overview on the advantage and limitations of the presented method, as well as on the cases of applications.

9.2 Discussion of the Method

Present method enables to deliver results on the state of mixed lubrication, friction coefficient in function of load cases, sliding velocities, lubricant types and machining conditions. Such investigations can be very efficient if material parameters are known. It can also be taken as basis for optimization activities such as finding optimal topographies for lubricated mixed contacts.

In addition, when material or topography data are not present, they need to be measured, a task which can be more expensive than measuring directly what happens in the contact. Furthermore, measuring process can be realized by means of automatized processes suitable for a calculation friction coefficient in function of many different working conditions. Another advantage of this method resides in its high level of details: it offers the possibility to calculate the profile changes (wear, plastic deformation). Unfortunately, main problem resides in the necessity to measure real surface topography for both contact solids.

An essential parameter to master is the working window of the model that needs also to be known in order to deliver valid results. Further points for discussion concern the robustness of the whole method and the representativeness of delivered friction information in correspondence with tested surfaces.

Nevertheless, this method has also limitations concerning the simulation of lubricated rough surfaces. These were not present for dry running systems as such systems have the same boundary conditions for micro- and macroscopic scales. These limitations are issuing from the refinement necessary for fluid solid contact. Consequently, lots of DoF are generated in this case which leads to huge memory requirements. Additionally, the element size chosen induce also low time increments and so high parallelization to keep acceptable CPU time (~ one Day calculation duration with 32 CPU for one lubricated microscopic model). Last disadvantage is linked with the previous one, high CPU resources imply short investigation times

($\sim 1 \mu\text{s}$). This leads to difficulties to reach a quasi-static regime necessary to establish friction rules.

Finally, results presented in this study showed clearly the potential of presented approach. Although its development is in an early phase, it provides a modeling of the physical the behavior of mixed lubrication by means of the finite element method. Some limitations need to be overridden as it is displayed in next subsection.

9.3 Future Development and Requirements

Potential of present approach has been established and its ability in taking into account real profiles has been proven. Next step is to validate the model by comparing it to experimental tests using regular structured profiles. This validation considers following aspects:

- Comparing pressure field and friction coefficient of experimental and numerical setup
- Checking the impact of model's dimensions on the results. This gives an overview on the size to be defined for the microscopic model to keep acceptable result dispersion

Last point is possible only if a multi-scale dimension is taken into account as microscopic structures cannot be tested with experimental facilities. This is more complex for lubricated conditions (because of the lubricant boundary conditions) and requires a loop function to check the whole investigation convergence before realizing any validation.

Once this validation is realized, second aspect concerns different improvements leading to new analysis abilities for the microscopic model such as:

- Abrasive wear modeling
- Adhesive wear modeling
- Using thermal dependent material data
- Modeling Thermal interactions between fluid and solid
- Using non-newtonian lubricants

Such extensions will enable to model wear phenomena happening in such contacts, as well as durability simulations in order to predict wear rate in powertrain components.

A further point would consist in extending this approach with non-isotropic structures, for instance plastics or other composites. The reason for this is that the actual trend

consists in using lightweight materials also for designing tribological systems for following reasons:

- Better thermal abilities
- Higher pressure resistance
- Higher resistance against corrosion

10 References

- Abbott / Firestone 1933** ABBOTT, E.J., FIRESTONE, F.A. *Specifying surface quality: a method based on accurate measurement and comparison*, Mechanical Engineering, 55, p. 569–572, 1933
- Achanta et al. 2009** ACHANTA, S., LISKIEWICZ, T., DREES, D., CELIS, J.-P. *Friction mechanisms at the micro-scale*, Tribology International, 4211-12, p. 1792–1799, 2009 <http://linkinghub.elsevier.com/retrieve/pii/S0301679X09001030> accessed, August 9, 2010
- Albers / Bernhardt / et al. 2010** ALBERS, A., BERNHARDT, J., OTT, S. Ceramic Engineering and Science Proceedings *Mechanical Properties and Performance of Engineering Ceramics and Composites V* eds, Dileep Singh, Jonathan Salem, Sanjay Mathur, and Tatsuki Ohji, Hoboken, NJ, USA: John Wiley & Sons, Inc., , 2010 <http://doi.wiley.com/10.1002/9780470944127> accessed, April 29, 2012
- Albers / Braun 2011** ALBERS, A., BRAUN, A. *A generalized framework to compass and to support complex product engineering processes*, International Journal Of Product Development, 151, p. 6–25, 2011
- Albers / Braun / et al. 2011** ALBERS, A., BRAUN, A., SADOWSKI, E. *System Architecture Modeling in a Software Tool based on the Contact and Channel Approach*, Journal of Mechanical Design, 133, 2011
- Albers / Lorentz 2010 a** ALBERS, A., LORENTZ, B. *A numerical approach to investigate mixed friction systems in the micro scale by means of the Coupled Eulerian-Lagrangian method*, Proceedings of the ASIM-Treffen STS/GMMS Workshop, Ulm: Proceedings of the, p. 1–7, 2010
- Albers / Lorentz 2012** ALBERS, A., LORENTZ, B. *A Numerical Method for Investigating Mixed Lubrication Phenomena*, Proceedings of TMCE 2012, p. 1–12, 2012
- Albers / Lorentz 2011** ALBERS, A., LORENTZ, B. *A Numerical Model for investigating Mixed Lubricated Systems taking into Account Adhesion Effects and Surface Roughness*, Ecotrib 11, 3rd European Conference on Tribology, Vienna, p. 1–6, 2011
- Albers / Lorentz 2010 b** ALBERS, A., LORENTZ, B. *An approach to investigate mixed lubricated systems in the micro scale by means of the Coupled-Eulerian-Lagrangian method*, Proceeding of the ASME IMECE 2010, p. 1–9, 2010
- Albers / Lorentz 2010 c** ALBERS, A., LORENTZ, B. *Numerical investigations of mixed lubricated systems taking into account surface roughness*, Proceedings of the GFT Fachtagung, p. 1–10, 2010
- Albers / Lorentz / et al. 2010** ALBERS, A., LORENTZ, B., NOWICKI, L. *Numerical investigations in mixed friction systems*, International Journal of Multiphysics, 41, p. 95–106, 2010

- Albers / Martin / et al. 2011** ALBERS, A., MARTIN, P., LORENTZ, B. *Modeling and Design of Contacts in electrical Connectors*, ICED 2011, , 2011
- Albers / Nguyen / et al. 2011** ALBERS, A., NGUYEN, H.T., BURGER, W. *Energy-efficient hydrodynamic journal bearings by means of condition monitoring and lubrication flow control*, *Insight*, 538, p. 431–433, 2011 <http://cat.inist.fr/?aModele=afficheN&cpsidt=24468562> accessed, April 29, 2012
- Albers / Savio / et al. 2010** ALBERS, A., SAVIO, D., LORENTZ, B. *A model to investigate the influence of surface roughness on the tribological behavior of dry friction systems*, *Proceedings of the GFT Tribologie Fachtagung*, p. 1–10, 2010
- Almqvist et al. 2011** ALMQVIST, A., FABRICIUS, J., SPENCER, A., WALL, P. *Similarities and Differences Between the Flow Factor Method by Patir and Cheng and Homogenization*, *Journal of Tribology*, 1333, p. 031702, 2011 <http://link.aip.org/link/JOTRE9/v133/i3/p031702/s1&Agg=doi> accessed, September 22, 2011
- Andersson et al. 2007** ANDERSSON, S., SODERBERG, A., BJORKLUND, S. *Friction models for sliding dry, boundary and mixed lubricated contacts*, *Tribology International*, 404, p. 580–587, 2007 <http://linkinghub.elsevier.com/retrieve/pii/S0301679X05003154> accessed, August 9, 2010
- ASTM 2012** ASTM *Standard Specification for High-Yield-Strength, Quenched and Tempered Alloy Steel Plate, Suitable for Welding*, 2012 <http://enterprise.astm.org/SUBSCRIPTION/NewValidateSubscription.cgi?A514/A514M-HTML>
- Attanasio et al. 2011** ATTANASIO, A., CERETTI, E., GIARDINI, C. *3D FEM Simulation of Flank Wear in Turning*, *Industrial Engineering*, 5611, p. 561–566, 2011 <http://link.aip.org/link/APCPCS/v1353/i1/p561/s1&Agg=doi> accessed, April 9, 2012
- Attanasio et al. 2008** ATTANASIO, A., CERETTI, E., RIZZUTI, S., UMBRELLO, D., MICARI, F. *3D finite element analysis of tool wear in machining*, *CIRP Annals - Manufacturing Technology*, 571, p. 61–64, 2008 <http://linkinghub.elsevier.com/retrieve/pii/S0007850608000930> accessed, April 9, 2012
- Aurich et al. 2008** AURICH, J. C., BIERMANN, D., BLUM, H., BRECHER, C., CARSTENSEN, C., DENKENA, B., KLOCKE, F., KRÖGER, M., STEINMANN, P., WEINERT, K. *Modelling and simulation of process: machine interaction in grinding*, *Production Engineering*, 31, p. 111–120, 2008 <http://www.springerlink.com/index/10.1007/s11740-008-0137-x> accessed, November 8, 2010
- Ayel 1974** AYEL, J. *Les différentes formes tribologiques d'usure des surfaces métalliques*, *Revue I.F.P.*, 313, 1974
- Bakolas 2003** BAKOLAS, V. *Numerical generation of arbitrarily oriented non-Gaussian three-dimensional rough surfaces*, *Wear*, 254, p. 546–554, 2003 <http://linkinghub.elsevier.com/retrieve/pii/S0043164803001339> accessed, October 27, 2011
- Barink et al. 2005** BARINK, M., KAMPEN, A V., MALEFIJT, M. DE W., VERDONSCHOT, N. *A Three-Dimensional Dynamic Finite Element Model of the Prosthetic Knee Joint: Simulation of Joint Laxity and Kinematics*, *Proceedings of the Institution of Mechanical Engineers, Part H: Journal of*

- Engineering in Medicine, 2196, p. 415–424, 2005
<http://journals.pepublishing.com/openurl.asp?genre=article&id=doi:10.1243/095441105X34437>
accessed, November 10, 2010
- Bartel et al. 2011** BARTEL, D., BOBACH, L., ILLNER, T., DETERS, L. *Simulation des Langzeitverhaltens von mischreibungsbeanspruchten Radialgleitlagern*, GFT Tribologie-Fachtagung, , 2011
- Benra et al. 2011** BENRA, F.-K., DOHMEN, H.J., PEI, J., SCHUSTER, S., WAN, B. *A Comparison of One-Way and Two-Way Coupling Methods for Numerical Analysis of Fluid-Structure Interactions*, Journal of Applied Mathematics, 2011, p. 1–16, 2011
<http://www.hindawi.com/journals/jam/2011/853560/> accessed, March 11, 2012
- Berry / Lewis 1980** BERRY, M.V., LEWIS, Z.V. *On the Weierstrass-Mandelbrot fractal function*, Proc. R. Soc. London, Ser. A, p. pp. 459–484, 1980
- Bhushan 2002** BHUSHAN, B. *17 Introduction to Tribology* John Wiley and Sons, , 2002
- Bielsa et al. 2010** BIELSA, J.M., CANALES, M., MARTÍNEZ, F.J., JIMÉNEZ, M.A. *Application of finite element simulations for data reduction of experimental friction tests on rubber–metal contacts*, Tribology International, 434, p. 785–795, 2010
<http://linkinghub.elsevier.com/retrieve/pii/S0301679X09003211> accessed, February 5, 2012
- Bosseler et al. 2009** BOSSELER, M., GBR, B.K., LANFRIT, M., REESE, H., PETER, H., LOREMO, H. *Zeitschrift für numerische Simulationsmethoden und angrenzende Gebiete*, Nafems Magazine, 121, p. 1–76, 2009
- Bowden / Tabor 1950** BOWDEN, F.P., TABOR, D. 432 *The friction and lubrication of solids* Oxford University Press, , 1950 <http://books.google.de/books?id=OQ7FCKNixK0C>
- Broster et al. 1974** BROSTER, M., PRITCHARD, C., SMITH, D.A. *Wheel/Rail Adhesion: Its Relation to Rail Contamination on British Railways*, Wear, 29, p. 309–321, 1974
- Bucher et al. 2006** BUCHER, F., DMITRIEV, A. I., ERTZ, M., KNOTHE, K., POPOV, V. L., PSAKHIE, S. G., SHILKO, E. V. *Multiscale simulation of dry friction in wheel/rail contact*, Wear, 2617-8, p. 874–884, 2006 <http://linkinghub.elsevier.com/retrieve/pii/S0043164806000780> accessed, February 1, 2012
- Butt et al. 2003** BUTT, H.-J., GRAF, K., KAPPL, M. *Physics and Chemistry of Interfaces* Weinheim, FRG: Wiley-VCH Verlag GmbH & Co. KGaA, , 2003 <http://doi.wiley.com/10.1002/3527602313> accessed, March 22, 2012
- Cai / Bhushan 2006** CAI, C., BHUSHAN, B. *Three-Dimensional Dry/Wet Contact Analysis of Multilayered Elastic/Plastic Solids With Rough Surfaces*, Journal of Tribology, 128, 2006
- Chang 1995** CHANG, L. *Deterministic modeling and numerical simulation of lubrication between rough surfaces—a review of recent developments*, Wear, 1842, p. 155–160, 1995
<http://linkinghub.elsevier.com/retrieve/pii/0043164894065705>

- Cheng 2003** CHENG, K. *Modeling and simulation of the tool wear in nanometric cutting*, *Wear*, 2557-12, p. 1427–1432, 2003 <http://linkinghub.elsevier.com/retrieve/pii/S0043164803001789> accessed, November 8, 2010
- Crouch / Cameron 1961** CROUCH, F.R., CAMERON, A. *Viscosity-Temperature Equations for Lubricants*, *Journal of the Institute of Petroleum*, 47, p. 307–313, 1961
- Dassault-Simulia 2011 a** DASSAULT-SIMULIA *Abaqus Analysis User's Manual, 12.2.1 ALE adaptive meshing: overview*, 2011
- Dassault-Simulia 2011 b** DASSAULT-SIMULIA *Abaqus Analysis User's Manual, 35.1.5 Frictional behavior*, *Abaqus Analysis User's Manual*, 2011
- Debler 2005** DEBLER, C. *Bestimmung und Vorhersage des Verschleißes für die Auslegung von Dichtungen*, 2005
- Dickerhof 2011** DICKERHOF, M. *Potentiale der Schallemissionsanalyse zur Überwachung und Diagnose tribologischer Systeme*, 2011
- DIN EN ISO 12085 2002** DIN EN ISO 12085 50 458 *Oberflächenbeschaffenheit: Tastschnittverfahren Motifkenngrößen*, 2002 <http://www.oldenbourg-link.com/doi/abs/10.1524/auto.2002.50.9.458>
- DIN EN ISO 13565-1 1998** DIN EN ISO 13565-1 *Oberflächenbeschaffenheit: Tastschnittverfahren, Oberflächen mit plateauartigen funktionsrelevanten Eigenschaften, Teil 1: Filterung und allgemeine Meßbedingungen*, 1998
- DIN EN ISO 3274 1997** DIN EN ISO 3274 *Oberflächenbeschaffenheit: Tastschnittverfahren, Nenneigenschaften von Tastschnittgeräten*, 1997
- DIN EN ISO 4287 2009** DIN EN ISO 4287 12 152–152 *Geometrische Produktspezifikation (GPS) – Oberflächenbeschaffenheit: Tastschnittverfahren – Benennungen, Definitionen und Kenngrößen der Oberflächenbeschaffenheit*, 2009
- DIN EN ISO 4288 1998** DIN EN ISO 4288 *Oberflächenbeschaffenheit: Tastschnittverfahren, Regeln und Verfahren für die Beurteilung der Oberflächenbeschaffenheit*, 1998
- Dmitriev et al. 2008** DMITRIEV, A., OSTERLE, W., KLOB, H. *Numerical simulation of typical contact situations of brake friction materials*, *Tribology International*, 411, p. 1–8, 2008 <http://linkinghub.elsevier.com/retrieve/pii/S0301679X07000709> accessed, October 14, 2010
- DoITPoMS - TLP Library The Stiffness of Rubber - Lennard-Jones potential** <http://www.doitpoms.ac.uk/tlplib/stiffness-of-rubber/lennard-jones.php> accessed, March 21, 2012
- Donea et al. 1982** DONEA, J., GIULIANI, S., HALLEUX, J.P. *An Arbitrary Lagrangian-Eulerian Finite Element Method for Transient Dynamic Fluid-Structure Interactions*, *Computer Methods in Applied Mechanics And Engineering*, 33, p. 689–723, 1982

- Dong et al. 1994** DONG, W P, SULLIVAN, P J, STOUT, K J *dimensional surface topography properties*, Wear, 178, p. 29–43, 1994
- Dowson 1979** DOWSON, D. *History of Tribology*, Longman Group Limited, p. 1, 1979 http://www.wiley-vch.de/books/sample/3527320571_c01.pdf accessed, January 27, 2012
- Dowson / Higginson 1977** DOWSON, D., HIGGINSON, G.R. SI Edn. Chapter 6. Pergamon Press. Oxford SI Edn. Chapter 6. Pergamon Press. Oxford *Elastohydrodynamic Lubrication*, 1977
- Du 2010** DU, Y. 1–136 *Numerical simulation of mechanical and thermal fluid-structure interaction in labyrinth seals*, 2010
- Düser 2010** DÜSER, T. 242 *X-in-the-Loop – an integrated validation framework for vehicle development using powertrain functions and driver assistance systems*, 2010
- Eyre 1979** EYRE, T.S. *Treatise on Materials*, Technology, 13, 1979
- Fang et al. 2005** FANG, L, CEN, Q, SUN, K, LIU, W, ZHANG, X, HUANG, Z *FEM computation of groove ridge and Monte Carlo simulation in two-body abrasive wear*, Wear, 2581-4, p. 265–274, 2005 <http://linkinghub.elsevier.com/retrieve/pii/S0043164804002704> accessed, September 22, 2010
- Federal Information Processing Standards Publications 1993** FEDERAL INFORMATION PROCESSING STANDARDS PUBLICATIONS Public Law *Integration Definition for Function Modeling (IDEF0)*, 1993
- Finnie 1965** FINNIE, I. *Some observations on the erosion of ductile metals*, Wear, 1965
- FVA 2003** FVA Referenzöle - Datensammlung -, 2003
- Gao et al. 2002** GAO, H., BARBER, G. C., SHILLOR, M. *Numerical Simulation of Engagement of a Wet Clutch With Skewed Surface Roughness*, Journal of Tribology, 1242, p. 305, 2002 <http://link.aip.org/link/JOTRE9/v124/i2/p305/s1&Agg=doi> accessed, August 9, 2010
- Garcia et al. 1999** GARCIA, A.L., BELL, J.B., CRUTCHFIELD, W.Y., ALDER, B.J. *Adaptive Mesh and Algorithm Refinement Using Direct Simulation Monte Carlo*, Journal of Computational Physics, 1541, p. 134–155, 1999 <http://linkinghub.elsevier.com/retrieve/pii/S0021999199963052>
- Goncalvès 2005** GONCALVES, E. *Resolution numerique, discretisation des EDP et EDO*, 2005
- Gras 2009** GRAS, R. *TribologieI: Principes et Solutions Industrielles*, 2009
- Greenwood 1972** GREENWOOD, J. A. *An extension of the Grubin theory of elastohydrodynamic lubrication*, Journal of Physics D: Applied Physics, 5, 1972
- Greenwood / Williamson 1966** GREENWOOD, J. A., WILLIAMSON, J. B. P. *Contact of Nominally Flat Surfaces*, Proceedings of the Royal Society A: Mathematical, Physical and Engineering Sciences, 2951442, p. 300–319, 1966 <http://rspa.royalsocietypublishing.org/cgi/content/abstract/295/1442/300> accessed, August 16, 2011

- Hamrock / Dowson 1975** HAMROCK, B.J., DOWSON, D. *sothermal elastohydrodynamic lubrication of point contacts*, American Society of Mechanical Engineers and American Society of Lubrication Engineers, Joint Lubrication Conference, p. 6, 1975 <http://md1.csa.com/partners/viewrecord.php?requester=gs&collection=TRD&recid=A7614865AH&q=Hamrock+and+Dowson+ehl+numerical&uid=1280740&setcookie=yes> accessed, March 5, 2012
- Hertz 1881** HERTZ, H. *Über die Berührung fester elastischer Körper*, Journal für die reine und angewandte Mathematik, 92, p. 156–171, 1881
- Hilber et al. 1977** HILBER, H.M., HUGHES, T.J.R., TAYLOR, R.L. *Improved numerical dissipation for time integration algorithms in structural dynamics*, Earthquake Engineering & Structural Dynamics, 53, p. 283–292, 1977 <http://doi.wiley.com/10.1002/eqe.4290050306> accessed, March 10, 2012
- Hirt 1971** HIRT, C.W. *An arbitrary Lagrangian-Eulerian computing technique*, Proceedings of the second international conference on numerical methods in fluid dynamics, p. 350–355, 1971
- Hirt / Nichols 1981** HIRT, C.W., NICHOLS, B.D. *Volume of fluid (VOF) method for the dynamics of free boundaries*, Journal of Computational Physics, 39, 1981
- Hishda / Fujiwara 2003** HISHDA, K., FUJIWARA, A. *1–10 Measurements of Turbulent Micro-Structure in Bubbly Flows Using Combined PIV / LIF / IST Technique* Keio, , 2003
- Hu / Zhu 2000** HU, Y.-Z., ZHU, D. *A Full Numerical Solution to the Mixed Lubrication in Point Contacts*, Journal of Tribology, 1221, p. 1, 2000 <http://link.aip.org/link/JOTRE9/v122/i1/p1/s1&Agg=doi>
- Hübner et al. 2010** HÜBNER, B, SEIDEL, U, ROTH, S *Application of fluid-structure coupling to predict the dynamic behavior of turbine components*, IOP Conference Series: Earth and Environmental Science, 12, p. 012009, 2010 <http://stacks.iop.org/1755-1315/12/i=1/a=012009?key=crossref.6651c3c1a4f65c1651102dba7ffc7eb0> accessed, March 11, 2012
- IGES/PDES Organization 1996** IGES/PDES ORGANIZATION *IGES*, 1996 http://www.uspro.org/documents/IGES5-3_forDownload.pdf
- Institute SAS 2005** INSTITUTE SAS *Design of Experiments*, 2005
- Jackson 2011** JACKSON, R.L. *A model for the adhesion of multiscale rough surfaces in MEMS*, IEEE 43rd Southeastern Symposium on System Theory, Ieee, p. 257–262, 2011 <http://ieeexplore.ieee.org/lpdocs/epic03/wrapper.htm?arnumber=5753817>
- Jackson / Green 2008** JACKSON, R.L., GREEN, I. *The Thermoelastic Behavior of Thrust Washer Bearings Considering Mixed Lubrication, Asperity Contact, and Thermoviscous Effects*, Tribology Transactions, 511, p. 19–32, 2008 <http://www.informaworld.com/openurl?genre=article&doi=10.1080/10402000701739271&magic=crossref||D404A21C5BB053405B1A640AFFD44AE3> accessed, August 9, 2010

- Jackson / Streator 2006** JACKSON, R.L., STREATOR, J. *A multi-scale model for contact between rough surfaces*, *Wear*, 26111-12, p. 1337–1347, 2006
<http://linkinghub.elsevier.com/retrieve/pii/S0043164806001359> accessed, September 29, 2011
- Jhurani / Higgs 2010** JHURANI, S.M., HIGGS, C.F. *An elastohydrodynamic lubrication (EHL) model of wear particle migration in an artificial hip joint*, *Tribology International*, 438, p. 1326–1338, 2010
<http://linkinghub.elsevier.com/retrieve/pii/S0301679X0900406X> accessed, April 3, 2012
- Jiang et al. 1999** JIANG, X Q, BLUNT, L, STOUT, K J *Three-dimensional surface characterization for orthopaedic joint prostheses.*, *Proceedings of the Institution of Mechanical Engineers. Part H, Journal of engineering in medicine*, 2131, p. 49–68, 1999
<http://www.ncbi.nlm.nih.gov/pubmed/10087904> accessed, February 20, 2012
- Johnson / Cook 1985** JOHNSON, G.R., COOK, W.H. *FRACTURE CHARACTERISTICS OF THREE METALS SUBJECTED TO VARIOUS STRAINS , STRAIN RATES , TEMPERATURES AND PRESSURES*, *Engineerin Fracture Mechanics*, 211, p. 31–48, 1985
- Johnson 1998** JOHNSON, K.L. *Mechanics of adhesion*, *Tribology International*, 318, p. 413–418, 1998
<http://linkinghub.elsevier.com/retrieve/pii/S0301679X98000607>
- Kamp et al. 2004** KAMP, N., PARRY, M.R., SINGH, K.D., SINCLAIR, I. *Analytical and finite element modelling of roughness induced crack closure*, *Acta Materialia*, 522, p. 343–353, 2004
<http://linkinghub.elsevier.com/retrieve/pii/S1359645403005494> accessed, February 1, 2012
- Kcharik et al. 2007** KCHARIK, M., LISKA, R., VÁCHAL, P., SHASHKOV, M. *Arbitrary Lagrangian-Eulerian (ALE) Method in compressible fluid dynamics*, *Applied Mathematical Sciences*, p. 1–6, 2007
- Khruschov 1974** KHRUSCHOV, M.M. *Principles of abrasive wear*, *Wear*, 281, p. 69–88, 1974
<http://linkinghub.elsevier.com/retrieve/pii/0043164874901021>
- Knoll et al. 2000** KNOLL, G., LECHTAPE-GRÜTER, R., SCHÖNEN, R., TRÄBING, C., LANG, J. 1–18 *Simulationstools für strukturdynamisch/elastohydrodynamisch gekoppelte Motorkomponenten*, 2000
- Knoll et al. 2007** KNOLL, G., SCHLEREGE, F., BRANDT, S., BUSCHE, E., LONGO, C. *Kolbenringreibung (Simulationstechniken zur Berechnung der Reibungsverluste von Kolbenringen bei Mischreibung und hydrodynamischer Schmierfilmbildung)*, *GFT Tribologie-Fachtagung*, , 2007
- Kogut / Etsion 2004** KOGUT, L., ETSION, I. *A Static Friction Model for Elastic-Plastic Contacting Rough Surfaces*, *Journal of Tribology*, 1261, p. 34, 2004
<http://link.aip.org/link/JOTRE9/v126/i1/p34/s1&Agg=doi> accessed, July 15, 2011
- Kubiak / Mathia 2009** KUBIAK, K.J., MATHIA, T.G. *Influence of roughness on contact interface in fretting under dry and boundary lubricated sliding regimes*, *Wear*, 2671-4, p. 315–321, 2009
<http://linkinghub.elsevier.com/retrieve/pii/S0043164809001628> accessed, August 9, 2010

- Larsson 2009** LARSSON, R. *Modelling the effect of surface roughness on lubrication in all regimes*, Tribology International, 424, p. 512–516, 2009
<http://linkinghub.elsevier.com/retrieve/pii/S0301679X0800145X> accessed, August 9, 2010
- Le et al. 2005** LE, H. R., SUTCLIFFE, M. P. F., WILLIAMS, J. A. *Friction and material transfer in micro-scale sliding contact between aluminium alloy and steel*, Tribology Letters, 181, p. 99–104, 2005
<http://www.springerlink.com/index/10.1007/s11249-004-1762-y> accessed, August 9, 2010
- Ledoux et al. 2011** LEDOUX, Y., LASSEUX, D., FAVRELIERE, H., SAMPER, S., GRANDJEAN, J. *On the dependence of static flat seal efficiency to surface defects*, International Journal of Pressure Vessels and Piping, 8811-12, p. 518–529, 2011
<http://linkinghub.elsevier.com/retrieve/pii/S0308016111000603> accessed, February 6, 2012
- Lee et al. 2008** LEE, S, KIM, J, SUNG, H *PIV measurements of turbulent boundary layer over a rod-roughened wall*, International Journal of Heat and Fluid Flow, 296, p. 1679–1687, 2008
<http://linkinghub.elsevier.com/retrieve/pii/S0142727X08001434> accessed, July 29, 2010
- Leslabay 2009** LESLABAY, P.E. *Robust optimization of mechanical systems affected by large system and component variability*, 2009
- Leu 2009** LEU, D.-K. *A simple dry friction model for metal forming process*, Journal of Materials Processing Technology, 2095, p. 2361–2368, 2009
<http://linkinghub.elsevier.com/retrieve/pii/S0924013608004445> accessed, November 18, 2011
- Lin / Chou 2002** LIN, J.F., CHOU, C.C. *The response surface method and the analysis of mild oxidative wear*, Tribology International, 3511, p. 771–785, 2002
<http://linkinghub.elsevier.com/retrieve/pii/S0301679X02000300>
- Lorentz / Rosenkranz 2013** LORENTZ, BENOIT, ROSENKRANZ, ANDREAS *Validation of a numerical model by means of pin-on-disk tests for low loaded dry contacts (Al₂O₃ -Titan Alloy)*, World Tribology Congress 2013, p. 1–6, 2013
- Majumdar / Bhushan 1990** MAJUMDAR, A., BHUSHAN, B. *Role of Fractal Geometry in Roughness Characterization and Contact Mechanics of Surfaces*, Journal of Tribology, 1122, p. 205, 1990
<http://dx.doi.org/10.1115/1.2920243> accessed, January 12, 2012
- Mäki 2005** MÄKI, R. 1–143 *Wet Clutch Tribology - Friction Characteristics in Limited Slip Differentials*, 2005
- Mansot et al. 2009** MANSOT, J. L., BERCIÓN, Y., ROMANA, L. *Nanolubrication*, Brazilian Journal of Physics, 391A, p. 186–197, 2009
- Marklund / Larsson 2008** MARKLUND, P., LARSSON, R. *Wet clutch friction characteristics obtained from simplified pin on disc test*, Tribology International, 419-10, p. 824–830, 2008
<http://linkinghub.elsevier.com/retrieve/pii/S0301679X07001995> accessed, August 9, 2010
- Marklund et al. 2007** MARKLUND, P., MAKI, R., LARSSON, R., HOGLUND, E., KHONSARI, M., JANG, J. *Thermal influence on torque transfer of wet clutches in limited slip differential applications*,

- Tribology International, 405, p. 876–884, 2007
<http://linkinghub.elsevier.com/retrieve/pii/S0301679X06003124> accessed, August 9, 2010
- Maykuth 1981** MAYKUTH, D. J. *Structural Alloys Handbook* ed, Mechanical Properties Data Center, , 1981
- Merchant et al. 1973** MERCHANT, H. D., MURTY, G. S., BAHADUR, S. N., DWIVEDI, L. T., MEHROTRA, Y. *Hardness-temperature relationships in metals*, Journal of Materials Science, 83, p. 437–442, 1973 <http://www.springerlink.com/index/10.1007/BF00550166>
- Mihailidis et al. 1999** MIHAILIDIS, A., RETZEPIS, J., SALPISTIS, C., PANAJIOTIDIS, K. *Calculation of friction coefficient and temperature field of line contacts lubricated with a non-Newtonian fluid*, Wear, 2322, p. 213–220, 1999 <http://cat.inist.fr/?aModele=afficheN&cpsidt=1997977> accessed, February 5, 2012
- Moatamedi et al. 2006** MOATAMEDI, M., KHAN, M. U., ZEGUER, T., SOULI, M. *A New Fluid Structure Coupling Method for Airbag OOP*, Lecture Notes in Computational Science and Engineering, 53, p. 101–109, 2006
- Netherwood / Tauber 1972** NETHERWOOD, P.H., TAUBER, D. *The shock Hugoniot of mineral oil*, 1972
- Newmark 1959** NEWMARK, N.M. *A method of computation for structural dynamics*, ASCE 85 EM3, p. pp. 67–94, 1959
- Nikas 2012** NIKAS, G. K. Proceedings of the Institution of Mechanical Engineers, Part J: Journal of Engineering Tribology *An experimentally validated numerical model of indentation and abrasion by debris particles in machine-element contacts considering micro-hardness effects*, 2012 <http://pij.sagepub.com/lookup/doi/10.1177/1350650111434358> accessed, April 9, 2012
- NIST 2012** NIST *Engineering Statistic Handbook*, NIST/SEMATECH e-Handbook of Statistical Methods, 2012 <http://www.itl.nist.gov/div898/handbook/pri/section3/pri339.htm> accessed, April 29, 2012
- Nowicki 2008** NOWICKI, L. 81 *Raue Oberflächen in geschmierten Tribokontakten* Karlsruhe Institute of Technology, , 2008
- Ozdemir et al. 2009** OZDEMIR, Z., MOATAMEDI, M., FAHJAN, Y.M., SOULI, M. *ALE and Fluid Structure Interaction for Sloshing Analysis*, The International Journal of Multiphysics, 33, p. 307–336, 2009 <http://multi-science.metapress.com/openurl.asp?genre=article&id=doi:10.1260/175095409788922257>
- Özel et al. 2011** ÖZEL, T., THEPSONTHI, T., ULUTAN, D., KAFTANO LU, B. *Experiments and finite element simulations on micro-milling of Ti–6Al–4V alloy with uncoated and cBN coated micro-tools*, CIRP Annals - Manufacturing Technology, 601, p. 85–88, 2011 <http://linkinghub.elsevier.com/retrieve/pii/S0007850611000886> accessed, February 3, 2012

- Parry et al. 2000** PARRY, M.R., SYNGELLAKIS, S., SINCLAIR, I. *Numerical modelling of combined roughness and plasticity induced crack closure effects in fatigue*, Materials Science and Engineering A, 291, p. 224–234, 2000
- Patir 1978** PATIR, N. *A NUMERICAL PROCEDURE FOR RANDOM GENERATION OF ROUGH SURFACES*, Wear, 47, p. 263–277, 1978
- Patir / Cheng 1978** PATIR, N., CHENG, H.S. *An average flow model for determining effects of three-dimensional roughness on partial hydrodynamic lubrication*, ASME, Transactions, Journal of Lubrication Technology, 100, p. 12–17, 1978
<http://md1.csa.com/partners/viewrecord.php?requester=gs&collection=TRD&recid=A7823351AH&q=cheng+and+patir+flow+factor&uid=1280740&setcookie=yes> accessed, March 5, 2012
- Patir / Cheng 1979** PATIR, N., CHENG, H.S. *Application of Average Flow Model to Lubrication Between Rough Sliding Surfaces*, Journal Of Lubrication Technology, 101April, 1979
- De Pellegrin / Stachowiak 2004** DE PELLEGRIN, D.V., STACHOWIAK, G.W. *Evaluating the role of particle distribution and shape in two-body abrasion by statistical simulation*, Tribology International, 373, p. 255–270, 2004
<http://linkinghub.elsevier.com/retrieve/pii/S0301679X03001804> accessed, March 5, 2012
- Peng / Kirk 1997** PENG, Z., KIRK, T.B. *Two-dimensional fast Fourier transform and power spectrum for wear particle analysis*, Tribology International, 308, p. 583–590, 1997
<http://linkinghub.elsevier.com/retrieve/pii/S0301679X97000261>
- Plackett / Burman 1946** PLACKETT, R.L., BURMAN, J.P. *The design of optimal multifactorial experiments*, Biometrika, 33, 1946
- Podsiadlo / Stachowiak 2002** PODSIADLO, P., STACHOWIAK, G.W. *Hybrid fractal-wavelet method for characterization of tribological surfaces — a preliminary study*, Tribology Letters, 134, p. 241–250, 2002
- Podsiadlo / Stachowiak 2000** PODSIADLO, P., STACHOWIAK, G.W. *Scale-invariant analysis of tribological surfaces*, Tribology Series, 38, p. 747–757, 2000 [http://dx.doi.org/10.1016/S0167-8922\(00\)80177-7](http://dx.doi.org/10.1016/S0167-8922(00)80177-7) accessed, February 20, 2012
- Podsiadlo / Stachowiak 1998** PODSIADLO, P., STACHOWIAK, G.W. *The development of the modified Hurst orientation transform for the characterization of surface topography of wear particles*, Tribology Letters, 4, p. 215–229, 1998
- Popov / Psakhie 2001** POPOV, V. L., PSAKHIE, S. G. *Theoretical principles of modeling elastoplastic media by movable cellular automata method . I . Homogeneous media*, Physics, 1, p. 15–25, 2001
- Ray 2006** RAY, S. *RSM: A statistical tool for process optimisation*, Indian Textile Journal, 2006
<http://www.indiantextilejournal.com/articles/FAdetails.asp?id=393> accessed, April 29, 2012

- Redlich 2002** REDLICH, A. C. *Simulation von Punktkontakten unter Mischreibungsbedingungen* Doktoringenieur, 2002
- Reichelt et al. 2006** REICHELT, M., WEIRICH, T.E., MAYER, J., WOLF, T., LOOS, J., GOLD, P.W., FAJFROWSKI, M. *TEM and nanomechanical studies on tribological surface modifications formed on roller bearings under controlled lubrication conditions*, Journal of Materials Science, 4114, p. 4543–4553, 2006 <http://www.springerlink.com/index/10.1007/s10853-006-0147-z> accessed, April 29, 2012
- Ren et al. 2010** REN, N., ZHU, D., CHEN, W.W., WANG, Q.J. *Plasto-Elastohydrodynamic Lubrication (PEHL) in Point Contacts*, Journal of Tribology, 1323, p. 031501, 2010 <http://link.aip.org/link/JOTRE9/v132/i3/p031501/s1&Agg=doi> accessed, March 10, 2012
- Renouf et al. 2011** RENOUF, M., MASSI, F., FILLOT, N., SAULOT, A. *Numerical tribology of a dry contact*, Tribology International, 447-8, p. 834–844, 2011 <http://linkinghub.elsevier.com/retrieve/pii/S0301679X11000491> accessed, June 15, 2011
- Resource Engineering Inc.** RESOURCE ENGINEERING INC. *Types of DOE's/Design of Experiments* http://www.qualitytrainingportal.com/resources/doe/doe_types.htm accessed, April 29, 2012
- Rimai et al. 1995** RIMAI, D. S., DEMEJO, L. P., MITTAL, K. L. 296 *Fundamentals of adhesion and interfaces*, 1995 <http://books.google.com/books?hl=fr&lr=&id=xPISbDPJMaAC&pgis=1> accessed, March 25, 2012
- Robbe-Valloire 2001** ROBBE-VALLOIRE, F. *Statistical analysis of asperities on a rough surface*, Wear, 249, p. 401–408, 2001
- Ropohl 2009** ROPOHL, G. 120 *Allgemeine Technologie Eine Systemtheorie der Technik*, 2009
- Ross 1985** ROSS, D. T. *Applications and Extensions of SADT*, ComputerApril, 1985
- Rothman 1988** ROTHMAN, M.F. *High-Temperature Property Data: Ferrous Alloys*, ASM International, 1988
- Sadeg 1996** SADEG, B *Quelques transparents de cours sur la méthode SADT (Structured Analysis and design Technics)*, 1996
- Savio 2010** SAVIO, D. *Numerische Untersuchung der Einflüsse der Oberflächenrauheit auf das Reibverhalten bei trockener Reibung*, 2010
- Schäfer et al. 2008** SCHÄFER, MI., BECKER, C. G., HECK, M., SACHS, S., STERNEL, D. C., YIGIT, S. *Numerical Simulation of Coupled Fluid-Structure Systems*, FSI Summer School, p. 1–13, 2008
- Schulze 2006** SCHULZE, A. *Virtual Engineering STEP*, 2006
- Sedlacek et al. 2011** SEDLACEK, M., PODGORNIK, B., VIŽINTIN, J. *Correlation between standard roughness parameters skewness and kurtosis and tribological behaviour of contact surfaces*,

- Tribology International, 2011 <http://linkinghub.elsevier.com/retrieve/pii/S0301679X11003215> accessed, November 18, 2011
- Seeton 2006** SEETON, C.J. *Viscosity–temperature correlation for liquids*, Tribology Letters, 221, p. 67–78, 2006 <http://www.springerlink.com/index/10.1007/s11249-006-9071-2> accessed, March 10, 2012
- Sellgren 2003** SELLGREN, U *A finite element-based model of normal contact between rough surfaces*, Wear, 25411, p. 1180–1188, 2003 <http://linkinghub.elsevier.com/retrieve/pii/S0043164803003326> accessed, August 31, 2011
- Simulia 2011** SIMULIA *Rate-dependent yield*, p. 22.2.3, 2011
- Singh et al. 2006 a** SINGH, K.D., KHOR, K.H., SINCLAIR, I. *Roughness- and plasticity-induced fatigue crack closure under single overloads: Analytical modelling*, Acta Materialia, 5417, p. 4405–4414, 2006 <http://linkinghub.elsevier.com/retrieve/pii/S1359645406003053> accessed, February 1, 2012
- Singh et al. 2006 b** SINGH, K.D., KHOR, K.H., SINCLAIR, I. *Roughness- and plasticity-induced fatigue crack closure under single overloads: Finite element modelling*, Acta Materialia, 5417, p. 4393–4403, 2006 <http://linkinghub.elsevier.com/retrieve/pii/S1359645406003041> accessed, February 1, 2012
- Söderberg / Andersson 2009** SÖDERBERG, A., ANDERSSON, S. *Simulation of wear and contact pressure distribution at the pad-to-rotor interface in a disc brake using general purpose finite element analysis software*, Wear, 26712, p. 2243–2251, 2009 <http://linkinghub.elsevier.com/retrieve/pii/S0043164809005316> accessed, December 1, 2010
- Stachowiak / Podsiadlo 1999** STACHOWIAK, G.W., PODSIADLO, P. *Surface characterization of wear particles*, Wear, 225-229, p. 1171–1185, 1999 <http://linkinghub.elsevier.com/retrieve/pii/S0043164898003974>
- Straffelini 2001** STRAFFELINI, G. *A simplified approach to the adhesive theory of friction*, Wear, 249January, p. 79–85, 2001
- Tezduyar et al. 2006** TEZDUYAR, T.E., SATHE, S., KEEDY, R., STEIN, K. *Space–time finite element techniques for computation of fluid–structure interactions*, Computer Methods in Applied Mechanics and Engineering, 19517-18, p. 2002–2027, 2006 <http://linkinghub.elsevier.com/retrieve/pii/S0045782505001957> accessed, March 11, 2012
- Tzeng / Saibel 1967** TZENG, S.T., SAIBEL, E. *Surface Roughness Effect on Slider Bearing Lubrication*, ASLE Transaction, 10, p. 334–338, 1967
- Vanlaere et al. 2004** VANLAERE, W., VAN IMPE, R., LAGAE, G., BELIS, J., BUFFEL, P., DE BEULE, M. *Inclusion of Real Material Behaviour in the Numerical Model for Stringer Stiffened Cylinders*, Key Engineering Materials, 274-276, p. 691–696, 2004 <http://www.scientific.net/KEM.274-276.691> accessed, February 22, 2012

- Vanloon et al. 2007** VANLOON, R., ANDERSON, P., VANDEVOSSE, F., SHERWIN, S. *Comparison of various fluid–structure interaction methods for deformable bodies*, Computers & Structures, 8511-14, p. 833–843, 2007 <http://linkinghub.elsevier.com/retrieve/pii/S0045794907000181> accessed, August 9, 2010
- Wang et al. 2008** WANG, J., AQUELET, N., TUTT, B., DO, I., CHEN, H., SOULI, M. *Porous Euler-Lagrange Coupling: Application to Parachute Dynamics*, 9th International LS-DYNA Users Conference, p. 11–22, 2008
- Wang et al. 2012** WANG, L. F., RONG, W. B., SHAO, B., SUN, L. N. *Influence of the Tabor Parameter on the Roughness-Induced Adhesion Hysteresis*, Applied Mechanics and Materials, 157-158, p. 1233–1237, 2012 <http://www.scientific.net/AMM.157-158.1233> accessed, March 25, 2012
- Wang / Hsu 1998** WANG, Y., HSU, S.M. *Lubricated friction and wear simulation of multi-scratches in asperity-asperity contact*, Ceramics, 217, p. 104–109, 1998
- Wiersch 2006** WIERSCH, P. *Berechnung thermoelastohydrodynamischer Kontakte bei Mischreibung* Technische Universität Clausthal, , 2006
- Wriggers 1996** WRIGGERS, P. *Finite element methods for contact problems with for friction*, Tribology International, 298, p. 651–658, 1996
- Yastrebov et al. 2011** YASTREBOV, V.A., DURAND, J., PROUDHON, H., CAILLETAUD, G. *Rough surface contact analysis by means of the Finite Element Method and of a new reduced model*, Comptes Rendus Mécanique, 3397-8, p. 473–490, 2011 <http://linkinghub.elsevier.com/retrieve/pii/S163107211100091X> accessed, February 1, 2012
- Zhai 2001** ZHAI, X *Some insights into asperity temperatures in mixed-film lubrication*, Tribology International, 346, p. 381–387, 2001 <http://linkinghub.elsevier.com/retrieve/pii/S0301679X01000275>
- Zhang et al. 2011** ZHANG, J.Q., GUAN, P., SU, C., WANG, W.S. *Simulation of Vitrified CBN Grinding Wheel Abrasive Wear Based on SPH*, Advanced Materials Research, 317-319, p. 498–502, 2011 <http://www.scientific.net/AMR.317-319.498> accessed, April 9, 2012
- Zhao et al. 2009** ZHAO, S., HILMAS, G.E., DHARANI, L.R. *Numerical simulation of wear in a C/C composite multidisk clutch*, Carbon, 479, p. 2219–2225, 2009 <http://linkinghub.elsevier.com/retrieve/pii/S0008622309002334> accessed, April 9, 2012
- Zhu et al. 2006** ZHU, W., HOUT, R., LUZNIK, L., KANG, H. S., KATZ, J., MENEVEAU, C. *A comparison of PIV measurements of canopy turbulence performed in the field and in a wind tunnel model*, Experiments in Fluids, 412, p. 309–318, 2006 <http://www.springerlink.com/index/10.1007/s00348-006-0145-6>

Curriculum Vitae

Personal information

Name: Benoît Lorentz
Date of birth: 05. Mai 1983
Location of birth: Obernai (France)
Nationality: french
Civil status: single

Education

1989 – 1994 Basic school (Dorlisheim)
1994 – 1998 Secondary college (Molsheim)
1998 – 2001 Highschool (Molsheim)
2001 – 2003 “Classes préparatoire aux grandes écoles” to prepare engineering highschool
2003 – 2007 Engineering highschool of Bourges, France (risks management)
University of Poitiers master of science, France (solid mechanics)

Industrial experience

2004 Internship at Brabus, Bottrop, Germany
2005 Internship at Siemens AG, München, Germany
2006 Internship at Siemens AG, München, Germany
2007 Master Thesis at Bosch GmbH, Gerlingen-Schillerhöhe
2007-2012 Academic scientist at IPEK - Institute Product Engineering at Karlsruhe Institute of Technology (KIT)
Since 2013 Leader of the research field “Tribological systems”